Combinatorial ink-jet printing for ceramic discovery

Wang, Jian

COMBINATORIAL INK-JET PRINTING FOR CERAMIC DISCOVERY

JIAN WANG

Thesis submitted for the degree of

Doctor of Philosophy

Department of Materials
Queen Mary,
University of London

2006

Abstract

An aspirating and dispensing printer established inside a robot gantry equipped with furnace and measurement table is used to prepare thick-film combinatorial libraries. Implementation of series of screening tests for ceramic inks that address stability against sedimentation, evaporation and particle segregation during drying, has provided a series of calibration inks can be used for calibration of this printer. The instrument can assemble ceramic mixtures with compositional accuracy of 1-3 wt %. By changing the amount of dispersant used in the inks or by printing onto a porous substrate, the geometry of residues from dried ceramic ink droplets can be modified to facilitate property measurements and uniform composition, as planned, can be achieved. The same material prepared in three ways, in the form of dried ink, ink-jet printed as for a combinatorial sample and by conventional compaction gave similar dielectric measurements. A combinatorial system has been developed so that combinatorial libraries can be printed, fired and screened automatically. A ternary Al_2O_3-TiO_2-ZrO_2 system was first studied using the developed combinatorial method.

The particle segregation during drying of multi-component ceramic ink drops is not due to preferential sedimentation unless dispersant addition is restricted. The segregation is due to the partitioning of particles between the growing peripheral 'foot' that develops during drying and the diminishing liquid pool which contains vigorous recirculation flows. Better dispersed particles remain in the pool and hence are found in excess on the upper surface of residues. Less well dispersed particles join the 'foot' earlier in the drying process.

The contact angle and height of droplets containing large amounts of dispersant steadily reduced during drying until a minimum value was reached; the contact diameter being almost unchanged during drying. These droplet residues retained a dome shape. Droplets of suspensions containing small additions of dispersant terminated in a 'doughnut' shaped residue.

Contents

List of Tables

List of Figures

Chapter 1 Introduction

1.1 Aims and objectives of the research

The aim of this research is to develop a new combinatorial method for the discovery of new ceramics. The method is first thoroughly calibrated and then applied to discovery of ceramic dielectrics although it can be used to study various properties of ceramics. The following sub-objectives of the research lead to this goal.

(1) The development and characterisation of several water-based ceramic inks that can be used in direct ceramic ink-jet printing.

(2) The investigation of procedures for creating ceramic compositions using an aspirating-dispensing printer for the combinatorial method. The study is intended to affirm that the printed compositions are those that the user wanted to produce and to account for errors.

(3) The investigation of compositional distribution of residue from droplets of water-based multi-components ceramic inks. The study is intended to find solutions to the problem of producing droplet residues with uniform planned composition.

(4) The investigation of the drying behaviour of water-based ceramic ink droplets.

(5) The investigation of the dielectric properties of ink-jet printed ceramics. This includes the design, implementation and calibration of the automated instruments, principally their sample probes and electroding procedures used to measure dielectric properties of ceramic libraries.

(6) Implementation of the automation of the combinatorial method so that ceramic libraries can be printed, sintered and screened by robot with minimum human intervention.

(7) The application of the combinatorial method so developed to study dielectric properties of the Al_2O_3-TiO_2-ZrO_2 system in order to discover new ceramic dielectrics and examine performance and functionality of the combinatorial method.

1.2 Combinatorial methods

In the 19th century, William Whewell of Cambridge responded with the name "Dielectric" when Michael Faraday asked him to give a word for materials that would "convey the electric force"[1]. Today, dielectric materials (dielectrics) have various applications in industry as, inter alia, insulators, capacitors and ferroelectric devices. There is tremendous interest in finding new and better dielectrics to meet requirements raised by current applications. For example, the continuing drive towards miniaturisation of capacitors is motivating the search for new dielectrics. Computer simulation techniques are being used to optimise dielectrics and have produced promising results[2-4]. However, due to the limitation of predictive theories, there are limited opportunities for users to design the structure of dielectrics for enhanced properties, and then build the target materials. The traditional method of discovering dielectrics remains a time-consuming and rather unpredictable trial-and-error process. Hence there is a need for a more efficient and systematic ways to search through the largely unexplored ternary, quaternary and higher order compounds that the periodic table provides in order to discover new dielectrics. With the advent of computers, automated techniques and analytical instruments, an automated approach to discovering materials, the combinatorial method, may fit this need[5-7].

The combinatorial method may be described as a method that can create large libraries of different samples with high-efficiency, and screen those libraries for specific properties of interest. The method involves the process of (1) the experimental design; (2) the creation of sample libraries; (3) the high-throughput

measurement of the libraries; (4) the modelling of the measurement results in the form of composition-structure-property relationships[5, 6].

In the pharmaceutical industry, automation of the creation of multivariate specimen arrays, screening and analysis techniques have dramatically accelerated the development of new drugs. There are a number of reviews of the combinatorial method used in the pharmaceutical industry[8-9]. Given this success, the combinatorial method has been adopted in other scientific fields such as metallurgy[10] and polymer synthesis[11]. One of the earliest attempts to realise this approach in the ceramic field was conducted at the GEC Hirst Research Centre UK, in the early 1990s in a quest for new ceramic superconductor compositions. In this pioneering approach, a robot was used to mix up to nine aqueous chelated solutions of oxide precursors over the full composition range[12]. The robot synthesised over 18,000 samples and successfully generated a range of new cuprate superconductors[12, 13].

X.-D. Xiang et al.[14], 1995, reported the application of the discrete combinatorial synthesis (DCS) technique[14, 15] for the discovery of new solid state materials with novel properties. The method uses the fact that in many materials systems, it is possible to grow stoichiometric compounds by means of controlled thermal diffusion of precursors. The DCS technique can generate a spatially defined library of thin films by sequentially depositing the individual precursors of target materials through a series of precisely positioned shadow masks, which allow spatially selective deposition on a substrate. Each sample can be varied with respect to elemental composition, the sequence in which the layers are deposited, and the thickness of each layer. The thin films were sputtered using an RF magnetron-sputtering gun. After the library was sintered at 840 °C in air, the resistance of each sample was automatically measured as a function of temperature using specially developed instruments. BiSrCaCuO and YbaCuO super-conducting films were identified within the library[14]. Their method can synthesize combinatorial libraries with samples as small as 200 μm × 200 μm in size and spacing of 50 μm between samples, corresponding to library densities of 1.55×10^7 sites per square metre[14].

X.-D. Xiang and his colleagues at Lawrence Berkeley National Laboratory continued to improve the DCS technique, for example by developing the Pulsed Laser Deposition technique[15] to efficiently deposit film and extended the combinatorial method to discover or optimise luminescent materials, magnetic materials, ferroelectrics and dielectrics [14-18].

Van Dover et al.[19], 1998, at Bell Laboratory reported the first application of the continuous composition-spread (CCS) technique[19-22] for the discovery of useful amorphous dielectrics. The CCS technique employed three magnetron-sputtering guns, which have been arranged in the 90° off-axis configuration around a substrate, to form a spread two-dimensional ternary composition of oxide dielectric materials. The Zr, Ti and Sn guns run at different radio frequency power providing the desired Zr/Ti/Sn composition at the substrate midpoint. Rutherford Backscattering Spectroscopy was used for obtaining the mapping of positions and compositions. The capacitance and current-voltage characteristics of the resulting films were automatically measured using a scanning Hg-probe instrument. $Zr_{0.2}Sn_{0.2}Ti_{0.6}O_2$ was identified as a promising dielectric[22]. They typically synthesize and evaluate 4,000 samples in a ternary composition in one day[20]. The CCS technique was also adopted for the combinatorial method of discovery of new hard coating materials[23].

In previous work on the combinatorial method for the discovery of solid-state materials, samples are often prepared in thin-film form. The phosphors used in industry are usually in powder form and it could be suggested that there may be some difference in results observed in a thin-film library and those from the corresponding powdered sample. X. Sun et al.[24, 25], 2002, at Berkeley lab have developed and applied a chemical ink-jet liquid-dispensing system for the combinatorial method of discovery of advanced phosphors. The system can quantitatively deposit the volume range from 10nl to 250μl and mix a stoichiometric volume of different chemical solutions and bake them to make a powdered phosphor library on a ceramic multiple-well template. As reported[24], a library with 128 different solution-mixing precursors of powdered phosphors can be generated in a matter of minutes.

Ikuo Yanase et al. [26], 2002, reported a combinatorial robot system that was developed for measuring, mixing, and moulding liquid samples and producing sample libraries for ceramic powders on the reaction pallet. In their study, slurries that consist of metal oxide nano-particles suspended in water and inorganic solutions were used as starting raw materials. Mixing was performed by repetition of aspirating from vials that contain raw slurries and injecting into the mix vials using a micropipette. A platinum pallet with 16 holes of 5mm diameter and 2mm in depth was positioned on a hot plate. Slurry mixtures were distributed in the holes one–by-one for modelling, drying and heat treatment. The products on the pallet were studied by using powder XRD. As reported, $LiMn_2O_4$ was successfully synthesised by using either of two different combinations of raw materials: LiOH and $Mn(CH_3COO)_2$ aq. solution and LiOH aq. solution and Mn_3O_4 slurry.

Reichenbach and McGinn[27], 2003, reported the application of the Pechini process in conjunction with ink jet deposition for the combinatorial method to study catalytic activity of the $LaMO_3$ (M = Cr, Co) system. Most of the catalytic activity was found in the cobalt-rich regions. Pechini process[27-29] is a solution-polymerisation route to produce single-phase mixed oxide powders, wherein the metal ions are suspended in solution with organic acids (e.g., citric acid) and polyhydroxyl alcohol (i.e., ethylene glycol). The metal ions are chelated by citric acid and are evenly distributed throughout the solution; upon heating, the solvent evaporates, the ethylene glycol undergoes polyesterification resulting in a polymer resin that has the various cations distributed uniformly in stoichiometric proportions. After higher temperature heating, the resin decomposed and formed the oxide powders. Because Pechini process is a liquid mixing process, metal ions are mixed on a molecular level, thereby requiring shorter processing time and lower processing temperatures than those needed by solid state processes. A probable disadvantage of the process is the ratio of citric acid to ethylene glycol and the ratio of organic material to metal. These need to been re-investigated to guarantee the success of the process.

1.3 Combinatorial ink-jet printing

Ink-jet technology has been used extensively in biotechnology[30-32] and polymer[33] research to make arrays of compositions. The use of direct ink-jet printing in ceramics is well advanced and 3-D ceramic architectures[34-36] including functionally graded structures[37] are produced. Ink-jet technology is compatible with micro-scale and high speed. Not surprisingly, this technique has been applied to the preparation of combinatorial libraries.

Combinatorial libraries can be prepared using ink-jet printing of ceramic precursor solutions. For instance, as discussed in section 1.2, H. M. Reichenbach et al. applied the Pechini process coupled with ink-jet deposition for combinatorial study of catalytic activity. X. Sun et al.[24, 25] applied a drop-on-demand ink-jet printer for the combinatorial discovery of advanced phosphors. Soichiro Okamura et al[38]. 2002, reported $Pb(Zr,Ti)O_3$ (PZT) thin films with various Zr/Ti ratios can be fabricated by overlapped ink jet printing. In these methods, the composition and structure of the material synthesized are either known by X-ray diffraction (XRD) or by reliance on the Pechini process.

The combinatorial library also can be prepared using direct mixing of powder suspensions. The composition and structure of members of a combinatorial library can be established as planned before screening and analysis of the library. Ink-jet printers can mix ink in three ways. In conventional colour printers, separate coloured droplets are placed adjacent; colour mixing actually occurs in the observer's brain. Applied to ceramic powders, this discrete printing approach involves large diffusion distances during sintering. Thus it is unlikely to be a promising approach for mixing ceramic powders.

Mixing can also take place in the pipe-work behind the nozzles[37,39]. A drop-on-demand printer was developed to create combinatorial libraries and functionally graded ceramics. In this printer, ceramic inks from multiple reservoirs pressurised with nitrogen are supplied via electromagnetic valves to a manifold. Variation in the opening times of the electromagnetic valves provides precise composition while a solenoid micro-pump provides circulation and mixing. After mixing, the

ink is printed through an electromagnetic valve-nozzle assembly[39,40]. Three ceramic mixtures in the Al_2O_3–TiO_2–Y_2O_3 system were prepared from alcohol-based ceramic inks. Initial analysis of ceramic mixtures showed systematic deviations from programmed compositions. Energy Dispersive X-ray Spectrometry (EDS) analysis of the cross sections of printed droplet residues revealed segregation of some oxides to the upper surfaces. When libraries of thicker samples were printed, this compositional deviation decreased to below 1 wt. % which is comparable with the error of the analysis method (EDS).[41] The segregation effect is associated with particle dynamics during slow droplet drying and fast drying by absorption of the vehicle into the porous lower layers eliminated the effect. In this method, the number of ceramics that can be mixed is dependent on the number of reservoirs but the device can deposit large quantities and build functionally graded components.

The third approach, used in this research, is to mix inks ahead of the nozzle by reformatting well plates. Stepper driven syringes control aspiration and dispensing of ceramic suspensions. Miniature electromagnetic valves provide ink-jet printing. This approach allows a very large number of components to be mixed limited only by the well number while retaining the patterning capability of the printer. The research work reported in this thesis pioneers the combinatorial method for the discovery of new ceramic dielectrics. The work is based on an aspirating-dispensing ink-jet printer that is integrated with a large-scale combinatorial robot. There are two features of this research: (1) the samples of the combinatorial libraries are prepared in powdered form by using the ink-jet ceramic printing technique, corresponding to the fact that many dielectrics used in the industry are prepared in powdered form. (2) The ceramic libraries can be printed, sintered, tested and analysed by robot. The idea of the work is to develop a powerful combinatorial system, which can perform unlimited operations with minimum human intervention and thus generate a large amount of dielectric information that is stored in the database for further data mining and analysis.

1.4 Dielectrics

Dielectrics can be defined as materials with high electrical resistivities[42]. When an electric field is applied to an ideal dielectric material, there is no long-range

transport of charge but only a slight shift in the balance of charge within the material to form electrical dipoles, a process known as *polarisation*[43, 44]. Polarisation and the dynamics of electric charges in dielectrics are often described in terms of macroscopic properties such as permittivity, dielectric loss and dielectric strength.

1.4.1 Electric permittivity, dielectric loss and dielectric strength

Coulomb's law[45, 46] states: (1) like charges repel and opposite charges attract each other, (2) the force between the charges is

(a) inversely proportional to the square of the distance between them
(b) proportional to the product of the charge magnitudes
(c) dependent on the medium in which they are embedded
(d) acts along the line joining the charges.

This is summarised in Coulomb's law that may be stated as:

$$F = A.\frac{q_1 q_2}{\varepsilon r^2}, \tag{1.1}$$

where F is defined as the force between the charges; q_1 and q_2 are two charges; r is the distance between the charges; A is a constant whose value depends on the units used for charge, distance and force; ε is a property of the medium in which charges are embedded called its *permittivity*[42-50].

Permittivity may be also defined as a property of a material that describes the electric flux produced when the material is excited by an electromotive force[44, 46]. *Absolute permitivity* is the ratio of electric flux density produced to the electric field strength. The unit of absolute permitivity is farad per meter. The absolute permittivity of free space[46] is equal to approximately 8.85×10^{-12} Fm^{-1}. In engineering applications, permittivity is often expressed in *relative permittivity* or *relative dielectric constant*, that is

$$k' = \frac{\varepsilon'}{\varepsilon_0}, \tag{1.2}$$

where k' is relative permittivity of a substance; ε' is the absolute permitivity of the substance; ε_0 is the absolute permittivity of free space.

Early researchers such as Faraday, Maxwell, and Lord Kelvin found dielectric materials can increase the charge-storage capacity of a condenser[47]. When an air condenser is connected to a battery, the air condenser charges until the free charges on each plate produce a potential difference equal and opposite to the battery voltage. Due to polarisation, a dielectric increases the charge-storage capacity of a condenser by neutralising some of the free charges, which would otherwise contribute to the potential difference opposing the battery voltage as visualised in Figure 1.1. By neglecting fringing effects, the increased storage capacity is

$$C = k'C_0, \tag{1.3}$$

where C is the increased storage capacity; C_0 is the original capacity in air; k' is relative permittivity of the dielectric material. Thus, the degree of polarisation or charge storage capability of a material is identified by relative permittivity.

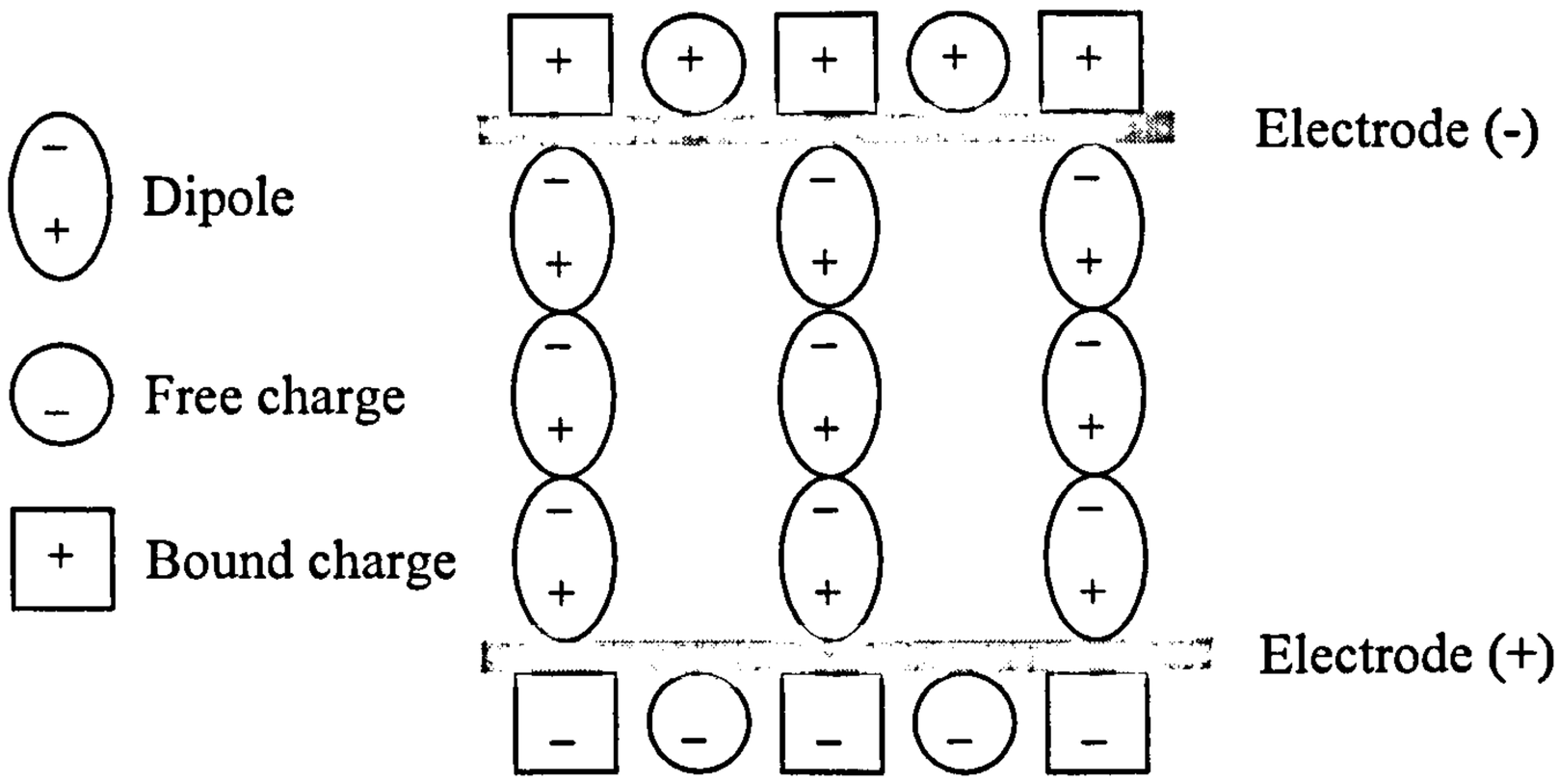

Figure 1.1 Schematic representation of the polarisation effect in the capacitor involving a dielectric material (Adapted from reference [48], p. 54).

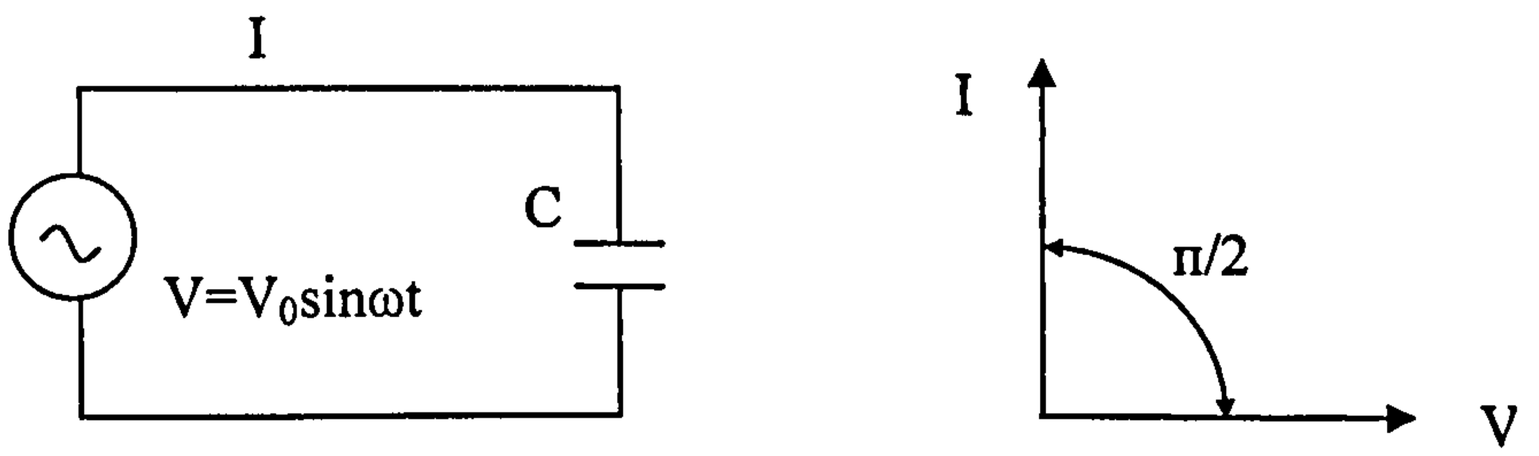

Figure 1.2 The current-voltage relation in the circuit with an ideal capacitor.

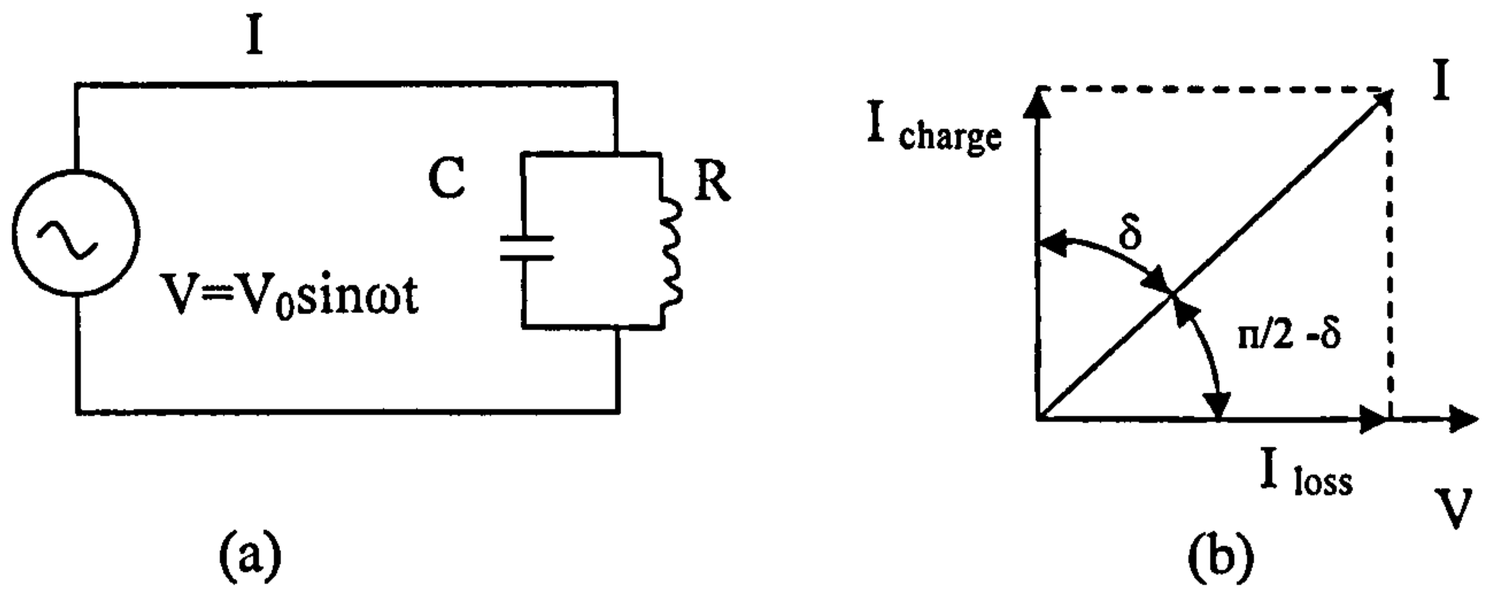

Figure 1.3 Representation of the loss in capacitor. (a) Parallel resistance models of a lossy capacitor. (b) Phase diagram for a real capacitor.

When connected to a sinusoidal voltage source, an ideal capacitor would have zero loss, because during one half–cycle the capacitor is charged and during the

next it releases its charge reversibly back (without loss of energy) into the source. Under this circumstance, an alternating current **I** would lead voltage **V** by a phase angle of π/2 as illustrated in Figure 1.2. A real capacitor does dissipate energy because of lead and electrode resistance, DC leakage resistance, and most importantly, dielectric losses of real materials. There is a loss component $\mathbf{I}_{loss}$ of the current **I** that is in phase with the voltage **V**. The component $\mathbf{I}_{loss}$ may be related not only to the electric current flowing through the dielectric material and hence related to ohmic resistance but also to other energy consuming processes such as dipole orientation[48]. Therefore, the phase angle between **V** and **I** is not exactly π/2. The current **I** lags slightly behind what it would be in a perfect capacitor as shown in Figure 1.3 (b). The angle of lag is defined as δ. The dielectric loss is characterised by tanδ, named as the *loss tangent* or *dissipation factor*[42-44, 46]. By introducing a *complex relative permittivity*[46, 48] (the concept of complex quantities can be found in reference 48, p. 48-50.)

$$k^* = k' - jk'', \tag{1.4}$$

where k' and k'' denote the real and the imaginary components of the complex relative permittivity, respectively; j is equal to $\sqrt{(-1)}$. The loss tangent is

$$\tan\delta = \frac{k''}{k'}, \tag{1.5}$$

where k' is relative dielectric constant and k'' is defined as relative loss factor. When the dielectric medium is loss-free, k'' will be zero. It is sometimes convenient to regard the "lossy" capacitor as an ideal capacitor shunted by a resistance R as shown in Figure 1.3 (a), which gives rise dissipation of energy by dipole orientation.

The insulating properties of dielectrics can be described in the terms of *dielectric strength* [43, 44, 46], which is defined as the electric field just sufficient to initiate an uncontrollable current to flow through or across dielectric. The unit of dielectric

strength is voltage per unit of thickness of the materials. For example, dielectric strength as high as 200 MVm^{-1} has been measured for a mica material[44].

1.4.2 Mechanisms of polarisation

There are several different mechanisms of polarisation[43, 44, 46, 48, 49], which may overlap one another or take place independently:

(1) Electronic polarisation.

When a field is applied, electrons shift very slightly to the positive electrode and nuclei shift very slightly to the negative electrode, causing the atoms to acquire an induced dipole moment. This is named electronic polarisation and occurs in all dielectrics.

(2) Dipole polarisation

Dipole polarisation occurs in non-symmetrical molecules that contain permanent electric dipoles. Taking H_2O as an example, the dipole arises because the electro-negative oxygen depletes the electron density around the hydrogen. The covalent bonds between the hydrogen and oxygen atoms are directional such that the two hydrogens are one side of the oxygen. Under an electric field, H_2O molecules align the positive side (the hydrogen side) facing the negative electrode and the negative side (the oxygen side) facing positive electrode. This is an example of dipole polarisation.

(3) Atomic or Ionic polarisation

The field may cause the atoms or ions within a crystal structure to be displaced, altering the distance between them and hence changing the dipole moment of the crystal. This is called atomic or ionic polarisation.

(4) Space charge polarisation

The space charge polarisation is due to defects in real crystals such as lattice vacancies, dislocation and interfaces such as grain bound or phase boundaries. When an applied field drives free charge carriers, these migrate through the

crystal and may be trapped or pile up against the defects, resulting in a localised accumulation of charge which gives a dipole moment.

Temperature affects the permittivity of the material[43, 44]. Electronic polarisation is relatively insensitive to temperature. Space charge and orientation polarisation are strongly temperature dependent. Dipole polarisation decreases as the temperature increases because increasing the temperature increases the random fluctuations of the system. Atomic or ionic polarisation tends to increase with temperature due to an increase in ion mobility.

Because charges have inertia, the polarization requires time to respond to an applied field[43, 48, 50]. Electronic polarisation responds very rapidly and no lag of the polarization contribution occurs up to 10^{17} Hz. Ionic polarizations have a slower and hence lower frequency response because ions are larger and less mobile when being displaced within the crystal. The ionic displacement begins to lag the field reversal at about 10^{13} Hz, increasing the loss factor and contributing less to the dielectric constant. Dipole polarisation and space charge polarisation only occur at low frequency. At very high frequencies, none of these mechanisms is able to follow the field, and the relative dielectric constants approaches one. The polarization process is accompanied by energy dissipation. At every frequency where relative dielectric constant varies rapidly, the relative loss factor tends to be maximum.[44, 49] The total net effect is illustrated in Figure 1.4.

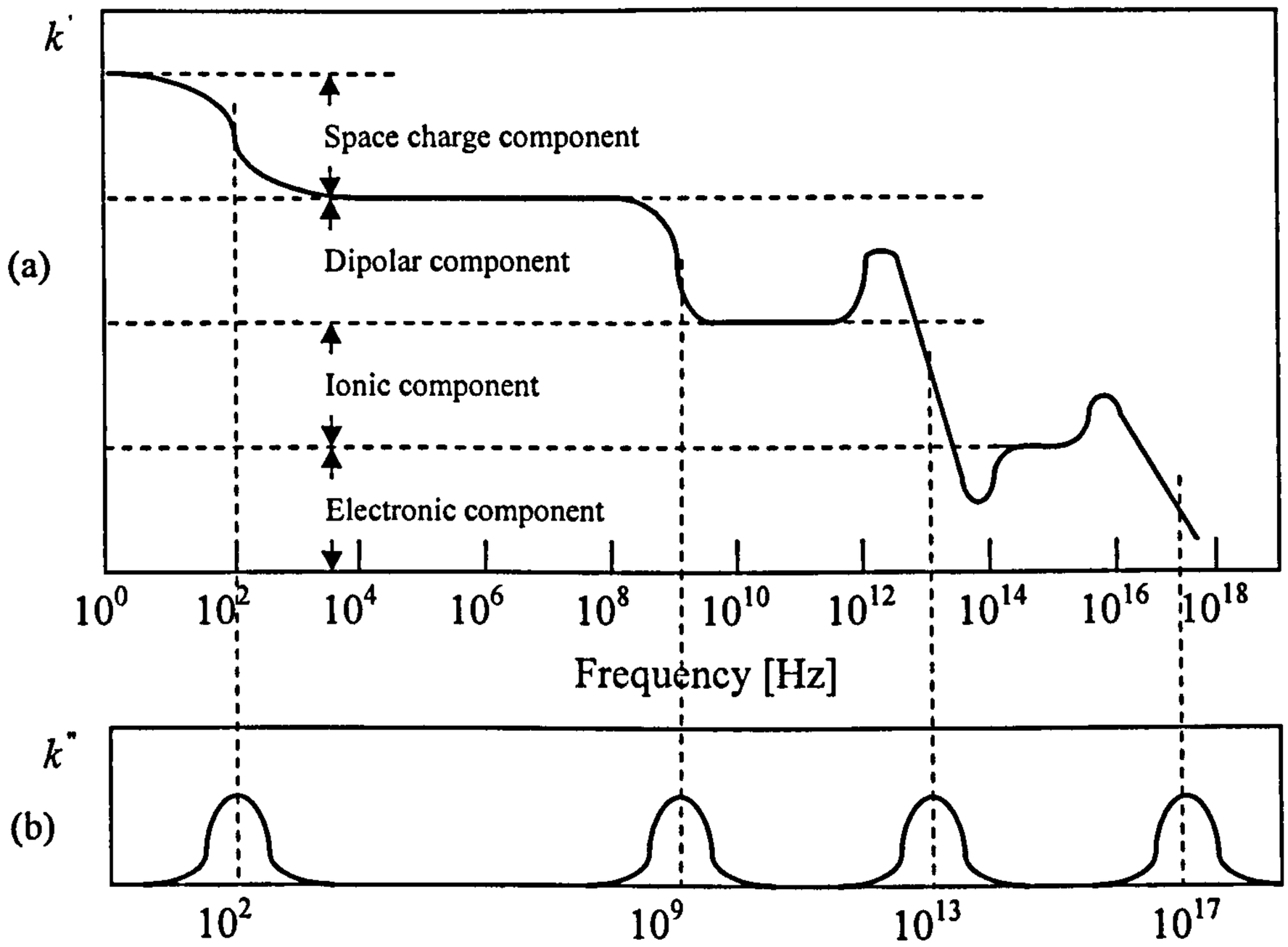

Figure 1.4 Variation of (a) relative dielectric constant and (b) dielectric loss with frequency (Modified from Reference 51, p. 543).

The Debye equations[46, 47] describe how materials with dipole polarisation behave with frequency. If a steady field is applied to align the molecules and is then switched off, the polarisation and hence the internal field diminish. By assuming that it decays exponentially with a time constant τ, the real and imaginary parts of complex relative permittivity and the loss tangent are

$$k' = \varepsilon_\infty + \frac{\varepsilon_s - \varepsilon_\infty}{1+\varpi^2\tau^2} \tag{1.6}$$

$$k'' = \frac{\varpi\tau}{1+\varpi^2\tau^2}(\varepsilon_s - \varepsilon_\infty), \tag{1.7}$$

$$\tan\delta = \frac{k''}{k'} = \frac{(\varepsilon_s - \varepsilon_\infty)\varpi\tau}{\varepsilon_s + \varepsilon_\infty\varpi^2\tau^2} \tag{1.8}$$

where ε_∞ is the relative permittivity (representing electronic polarization) when the applied frequency is much greater than the reciprocal of the alignment time of the molecule; For much lower frequencies it becomes ε_s, named the static relative permittivity; ϖ is an angular velocity, $\varpi = 2\pi\nu$ (radians per second), where ν is the frequency of the applied field. Equations (1.6)-(1.8) are known as the Debye equations and agree well with experimental results.

The purpose of dielectric theory should be to permit calculation of the macroscopic properties of a dielectric from its atomic and molecular structure. In practice, the calculation of explicit values of permttivity from an atomic or molecular model and its temperature and frequency dependence is beset by considerable difficulties. For example, in the case of electronic polarisation, no calculation could be made unless the precise configuration of their electron clouds were known, and is the case for only a limited number of relatively simple examples[46].

1.4.3 Piezoelectricity and ferroelectricity

Some materials produce dielectric polarisation when under mechanical strain, This effect is referred to as *piezoelectricity*[43, 44, 46]. The application of stress separates the effective centre of the positive charges from the effective centre of the negative charges, producing a dipole moment (polarisation). For a centro-symmetrical crystal, no combination of uniform stresses produces the necessary separation of the centres of the charges. Piezoelectricity can occur only in crystals with no centre of symmetry.

Heating of certain crystals produces dielectric polarisation. This effect is known as *pyroelectricity*[43, 46]. Pyroelectric crystals are a special class of piezoelectric crystals. When heated, the crystal expands and there may be deformation due to thermal expansion. Due to the piezoelectric effect it acquires dielectric polarisation by virtue of the deformation. The change of temperature has a direct effect on the form of polarisation in certain portions of the crystal[46].

Ferroelectric crystals (Ferroelectrics) are a subclass of pyroelectric crystals. There are three characteristics of ferroelectrics[43, 44, 46]:

(1) Ferroelectrics can retain a dipole even after an applied voltage has been removed. This is known as *spontaneous polarisation.*

(2) The direction of the polarisation can be reversed by application of an electric field showing a *hysteresis loop* as illustrated in Figure 1.5 (b);

(3) Ferroelectrics have a *Curie temperature* that is defined as the temperature of transformation from *paraelectric* material to ferroelectric. Paraelectric materials[50], such as TiO_2, don't have spontaneous polarisation and shown linear response of polarisation versus voltage as illustrated in Figure 1.5 (a).

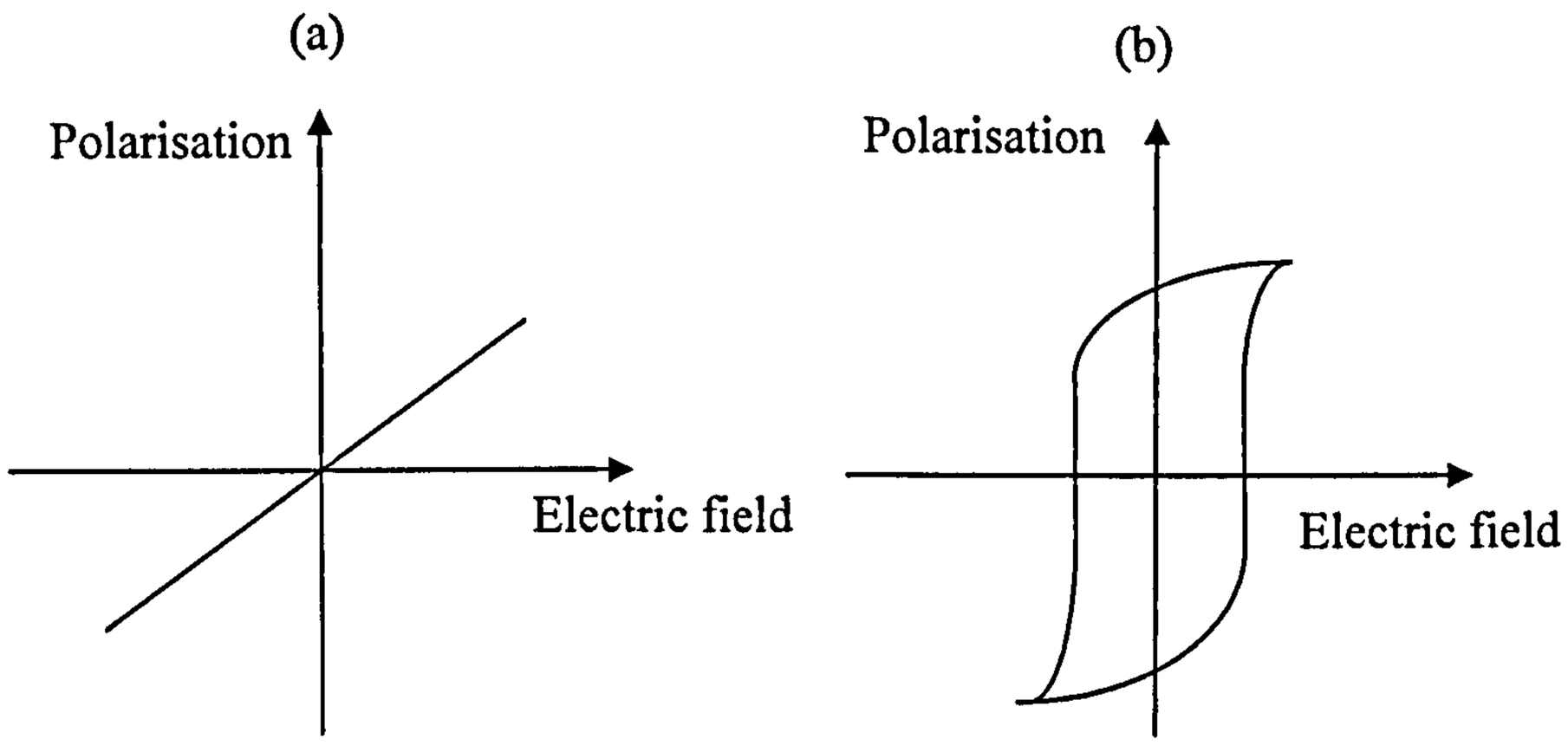

Figure 1.5 (a) Paraelectric behaviour has a linear response of polarisation to voltage. (b) A ferroelectric shows a hysteresis loop.

Ferroelectric crystals must contain alternate atom positions or molecular orientations to permit the reversal of the dipole and a spontaneous polarization[43]. Taking $BaTiO_3$ as a sample[43, 44, 48], $BaTiO_3$ has the perovskite structure as illustrated in Figure 1.6. There are minimum-energy positions off-centre in the direction of each of the six oxygen ions surrounding the Ti ions[27]. The Ti ions adopt positions randomly in one of these six possible minimum-energy sites. From 120°C to 1460°C, $BaTiO_3$ has a cubic structure. The Ti^{4+} ion does shift

position when an electric field is applied, but it returns to its stable central position once the field is removed. There is no spontaneous polarisation and no ferroelectric behaviour. From 120°C to 0°C the structure of $BaTiO_3$ shifts from cubic to tetragonal. The Ti^{4+} ion moves off-center toward one of the two oxygen ions of the long axis, resulting in a spontaneous increase in positive charge in this direction. An electric field opposite to the original dipole causes the Ti^{4+} ion to move through the centre of the octahedral site and to an equivalent off-centre position as illustrated in Figure 1.7. This is referred to as ferroelectric behaviour. 120°C is the Curie temperature of $BaTiO_3$.

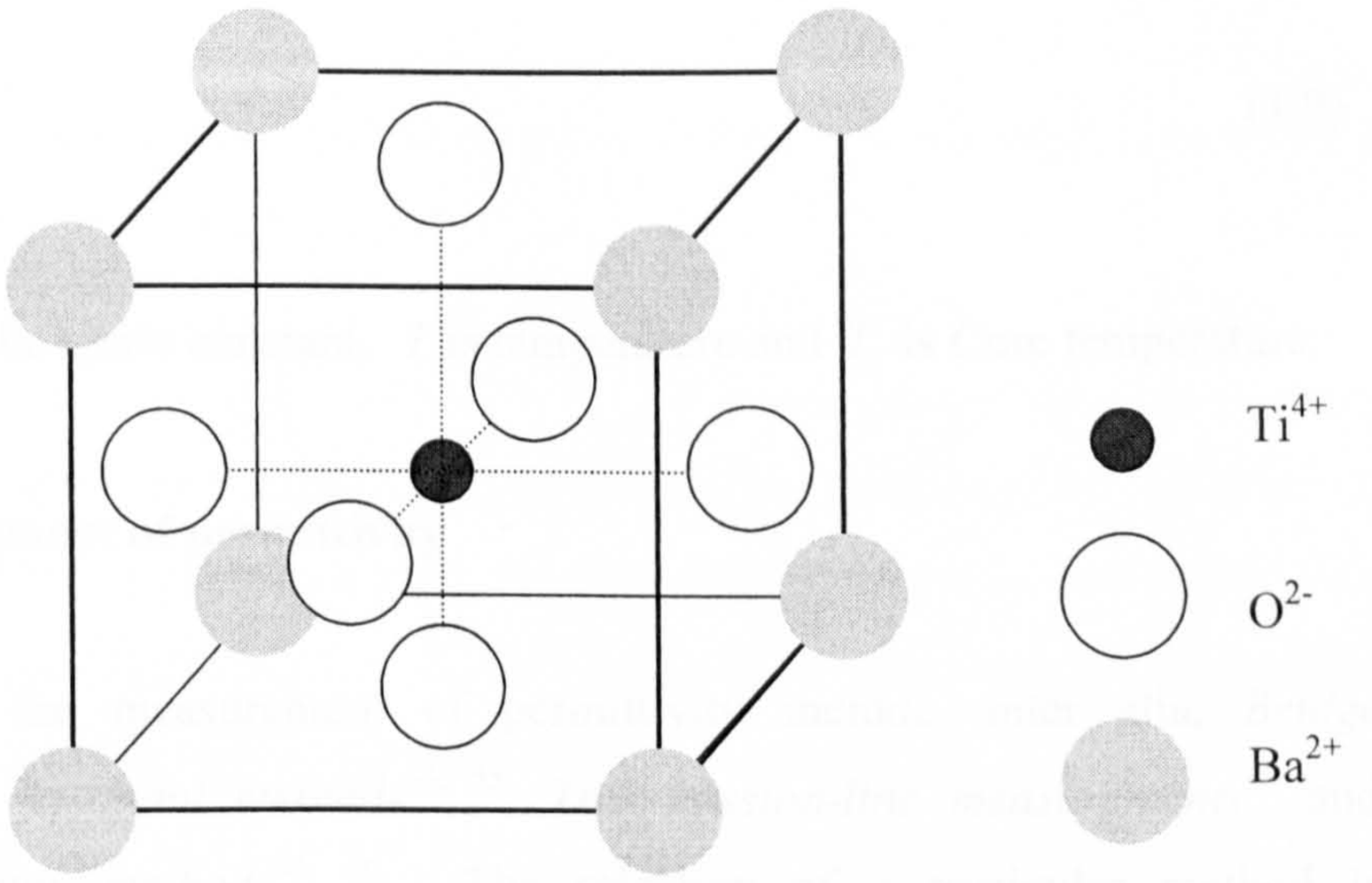

Figure 1.6 Schematic of the perovskite structure of $BaTiO_3$.

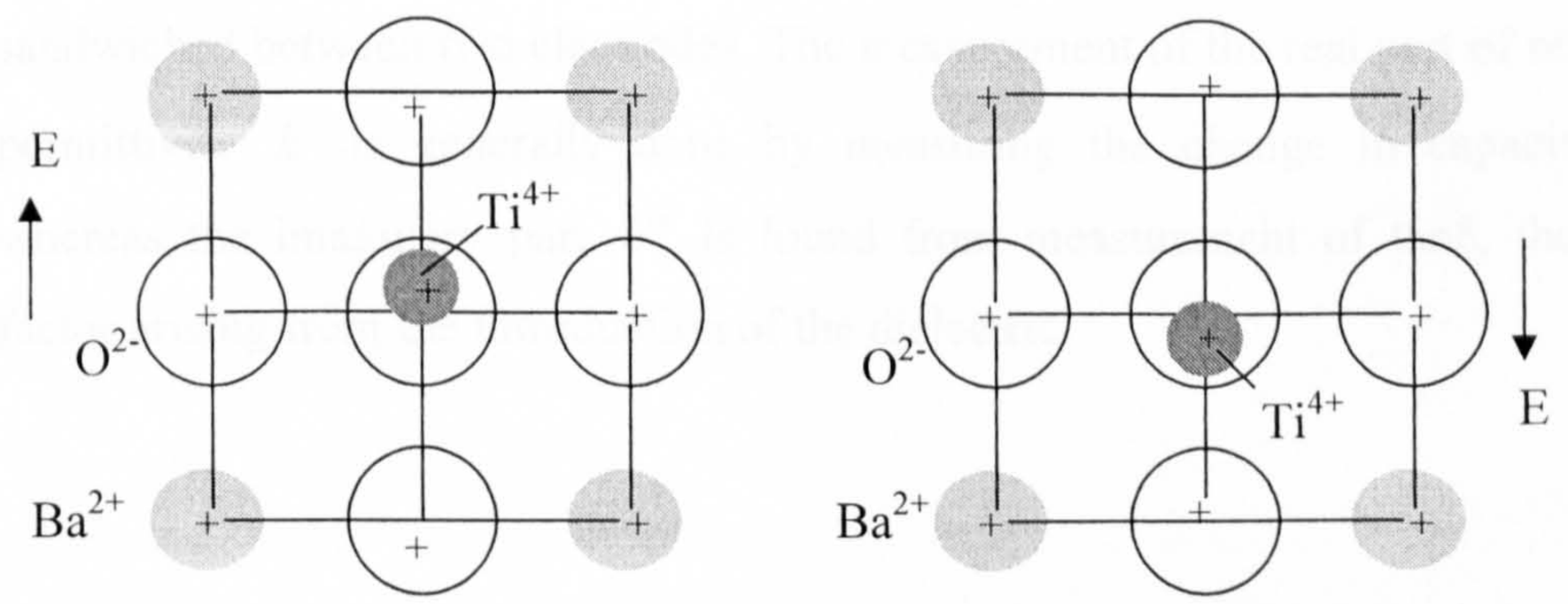

Figure 1.7 Reversal in the direction of spontaneous polarisation in $BaTiO_3$ by reversal of the direction of the applied electric field (from reference 43, p.274).

A spontaneously polarised, ferroelectric crystal forms domains to minimise its electrostatic energy[43, 46]. The domain is a region of the crystal in which the dipoles are all aligned parallel to each other. Such domains can be rendered visible by suitable techniques e.g., Transmission electron microscopy (TEM) which are used to study mechanisms of ferroelectric behaviour[52, 53]. The permittivity of a ferroelectric has a sharp maximum at the Curie temperature and thereafter falls further as temperature decreases. Above the Curie temperature, the dielectric susceptibility χ follows the Curie-Weiss law[45, 46]

$$\chi = \frac{C}{T - T_c}, \tag{1.9}$$

where C is the Curie constant, T is temperature and T_c is Cure temperature.

1.4.4 Measurement of permittivity

Methods for the measurement of permittivity include, inter alia, *Bridge methods*[46, 54], *Resonant methods*[46, 55], *Transmission-line measurements*[46] and *Cavity resonator methods*[46, 56]. The selection of a particular method is determined by factors such as the nature of the specimen, frequency coverage and ease of operation. To measure permittivity, a dielectric material is assembled as a capacitor. The basic structure of a capacitor is a dielectric material sandwiched between two electrodes. The measurement of the real part of relative permittivity k' is generally done by measuring the change in capacitance, whereas the imaginary part k'' is found from measurement of tanδ, the loss factor arising from the introduction of the dielectric.

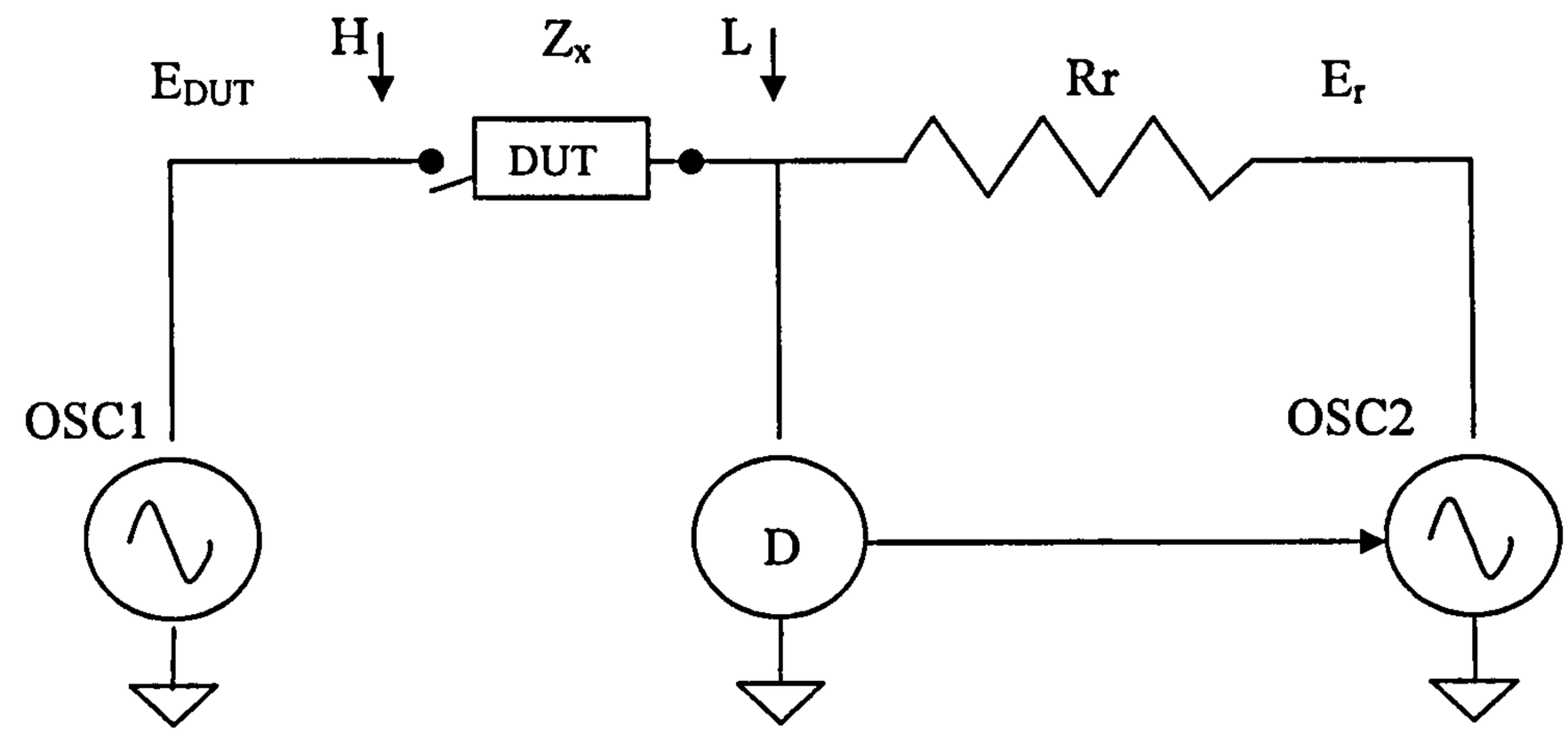

Figure 1.8 The simplified block diagram of the auto balancing bridge method (modified from reference 54, p. 2-7).

The auto balancing bridge method[54, 57, 58] is commonly used in modern impedance measurement instruments. Its operational frequency ranges from 20 Hz to 110 MHz. Figure 1.8 shows the simplified block diagram of the auto balancing bridge method used in the Agilent 4294A precision impedance analyser. The current flowing through the Device under Test (DUT), also flows through a range resister R_r. The detector D detects potential at the point "L" and controls both magnitude and phase of the OSC2 output, so that the potential at the point "L" is maintained at zero volts and so [54]

$$\frac{E_{DUT}}{Z_x} + \frac{Er}{R_r} = 0, \tag{1.10}$$

$$Z_x = R_r \times (\frac{E_{DUT}}{E_r}), \tag{1.11}$$

Where Z_x is the impedance of the DUT; E_{DUT} and E_r are voltages across the DUT and the range resistor R_r, respectively. Both E_{DUT} and E_r are measured and R_r is known. Z_x is calculated from Equation [1.11]. An impedance vector consists of a real part (resistance, $R = |Z|\cos\theta$) and an imaginary part

(reactance, $X = |Z|\sin\theta$) as shown in Figure 1.9. For a capacitor (by excluding its parasitic inductance), the reactance X is

$$X = \frac{1}{2\pi fC}, \tag{1.12}$$

where f is the applied frequency and C is the capacitance of the capacitor. The capacitance C can be calculated using Equation (1.12) if the reactance X is known from the impedance Z. The real part of relative permittivity k' is calculated from[58, 59]

$$k' = \frac{D \times C}{A \times \varepsilon_0}, \tag{1.13}$$

where D is thickness of the test material; A is the area of electrode of capacitor; C is the measured capacitance of the DUT; ε_0 is the permittivity of air 8.854×10^{-12} farads/metre. The imaginary part of relative permittivity k'' is found from measurement of tanδ [54].

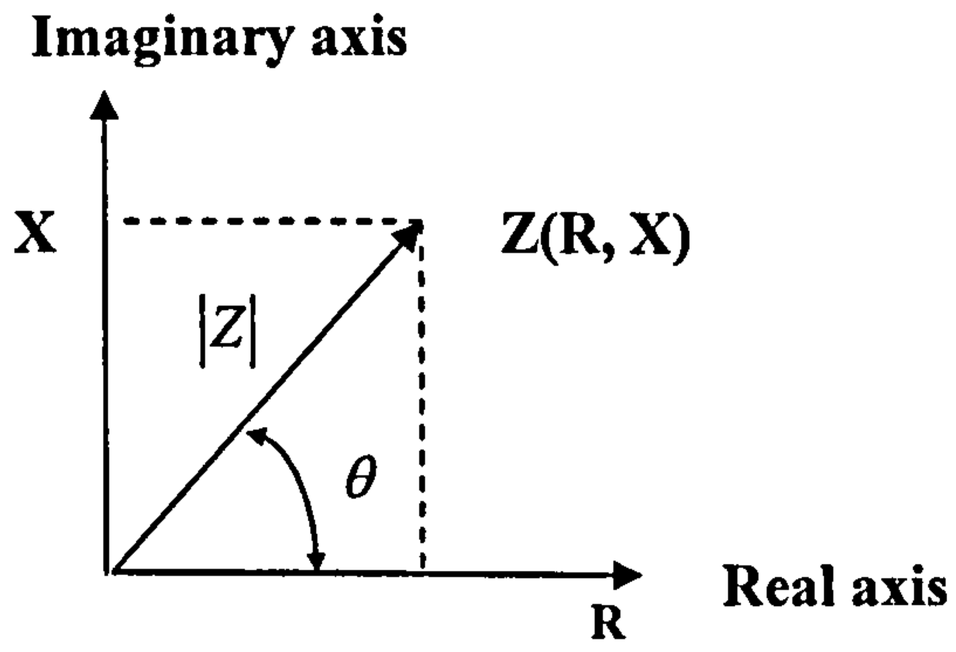

Figure 1.9 Impedance (Z) consists of a real part (R) and an imaginary part (X).

Once a particular measurement method is selected, the accuracy of measurement of permittivity depends critically on the measuring cell in which the specimen is mounted and how the specimen is prepared. Errors are associated with the inductance and resistance of the leads to the electrodes, stray capacitance from these leads to earth and fringe fields at the edges of the electrodes, etc[46, 59].Von

Hippel[42] has given a full discussion of types of measuring cell and corrections. An ultimate accuracy of approximately 0.2% in the measurement of capacitance and 2% in the measurement of tanδ can be quoted. Various standards exists for the measurement of permittivity such as, ASTM D150, British Standard (BS) 99/243524 DC.

1.5 Ceramic dielectrics

Ceramics can be defined as non-metallic, inorganic solids that experience high temperature in fabrication or use. Suyama and Yamaguchi has defined three features of advanced ceramics that distinguished them from their traditional counterparts such as bricks, sanitary wares and household porcelain[60]:

1. High purity raw materials with controlled composition and particulate properties are used.
2. Processing is subject to precise control of both forming and firing.
3. Products have a well-controlled microstructure, which ensures high performance.

Ceramic dielectrics may be classified in three groups[42,61]: (1) Ceramics with a relative permittivity below 12; (2) Ceramics with a relative permittivity above 12; (3) Ceramics with piezoelectric and ferroelectric properties.

(1) Ceramics with a relative permittivity below 12

The ceramics of this group are widely used for applications requiring insulation. Insulators are used principally to hold conductive elements in position preventing electrical conduction. In this case their mechanical properties are as important as their dielectric properties. When required in large quantities, they must also be based on a low-cost material.

(a) Low-tension and high tension electrical porcelain

Porcelain was the first ceramic insulating material to be used by the electrical industry[61]. A typical porcelain composition would lie in the following ranges:

clays, 40-60wt%; flux, 15-25wt%; filler, 30-40wt%. Kaolinite, with the composition $Al_2(Si_2O_5)(OH)_4$, is the most common clay mineral. The common fluxes are feldspars, having the general formula, $[K_xNa_{1-x}(ALSi_2)O_8]$. The common fillers are quartz (SiO_2) in the form of sand or flint. When high mechanical strength is required, bauxite ($Al_2O_3.2H_2O$) is substituted for quartz to given aluminous porcelain. Table 1.1 gives typical physical properties of electrical porcelains. To reduce corona on high-tension (or high-voltage) insulators and eliminate interference with electronic devices, high-voltage insulators are frequently equipped with semi-conducting glazes or coatings over areas which are in contact with metallic conductors[42, 44]. There are also many low-tension applications for electrical porcelain as, inter alia, switch bases and fuse holders.

Table 1.1 Physical properties of electrical porcelains (From reference 28, P. 208)

Property	Siliceous	Aluminous
Density/Mgm^{-3}	2.4	2.8
Flexural strength/MPa	125	185
Coefficient of linear expansion /MK^{-1}	6.0	5.0-6.0
Dielectric strength /MVm^{-1}	25	25
Volume resistivity /Ωm at 20 °C	~ 10^{10}	~ 10^{10}
Tanδ/10^{-4} at 20 °C	~150	~150

(b) High-temperature and high-frequency insulation

When selecting insulators for electrical heating elements or resistor wires, the important properties are free from deformation under mechanical load, resistance to thermal shock and high insulation resistance at operating temperature. The convention electrical porcelains are not satisfactory because they contain a glassy phase that may cause deformation. Cordierite ceramics ($Mg_2Al_2Si_5O_{15}$) are best known for excellent thermal shock resistance combined with high insulation resistance at high temperature. Steatite ceramics have low dielectric losses that are desired for high frequency application and can be made to close tolerances with high mechanical strength. Steatite ceramics are widely used in electronic

applications. A typical composition is about 85wt% talc ($Mg_3Si_4O_{11}.H_2O$), 15wt% clay and 2wt% calcium carbonate (chalk). When lower dielectric losses are required, forsterite ceramics (Mg_2SiO_4) are used. Alumina ceramics[44, 62] are widely used for spark-plug insulators, thick-film circuit substrates and integrated circuit packaging because of their excellent combination of mechanical, thermal, chemical and electrical properties. Table 1.2 gives typical properties of some low-permittivity ceramic dielectrics.

Table 1.2 Typical properties of low-permittivity ceramic dielectrics (Adapted from reference 44, p. 209)

Material	Dielectric Constant	Tan δ /10^{-4} at 1 MHz	Thermal conductivity $Wm^{-1}K^{-1}$ at 25°C	Linear expansion coefficient MK^{-1} at 20- 1000 °C
Steatite	6.1	7	3	8.9
Cordierite	5.7	80	2	2.9
Forsterite	6.4	2	3	10.7
96% Al_2O_3	9.7	3	35	8.2

(2) Ceramics with a relative permittivity above 12

The ceramics in this group, also called high dielectric constant ceramics, are mainly used for capacitors. Electronic Industries Association[50, 63] (EIA) has classified these dielectrics for capacitors by the capacitance temperature coefficient (T.C.). Two basic groups (Class I and Class II) are used in the manufacture of ceramic chip capacitors. Class III identifies the reduced barium titanate barrier-layer materials used in the production of disc capacitors[50]. The T.C. is determined by measurement of the capacitance change at various temperatures from the reference room temperature. The T.C. is expressed in parts per million per degree (ppm/°C) for Class I dielectrics and as percent capacitance change (%ΔC) for Class II. The method of calculation of T.C can be found in reference [50]. EIA has developed a series of codes that define the temperature coefficients[50]. For example, the most common Class II dielectric for chip

capacitors is the X7R designation, which means ±15% maximum ΔC from 55°C to 125 °C.

(a) Class I dielectrics

This group identifies the dielectrics showing a linear relation of polarisation to voltage as shown in Figure 1.5 (a). These materials are based primarily on TiO_2, with dielectric constants under 150. With addition of other (ferroelectric) oxides[50], such as $CaTiO_3$ or $SrTiO_3$, compositions display near-linear and predictable temperature characteristics with dielectric constants ranging up to 500. Class I dielectrics are used in circuits requiring stability of capacitor, i.e. negligible aging, low loss, negligible change in capacitance and dielectric loss with voltage or frequency, and predictable linear behaviour with temperature within prescribed tolerances. The most common Class I dielectric for chip capacitors is the COG designation, which means 0 ppm/°C with ±30% ppm/°C tolerance of temperature coefficient.

(b) Class II dielectrics

Class II dielectrics comprise the ferroelectric formulations with much higher dielectric constant than Class I dielectrics, but with less stable properties with temperature, voltage, frequency and time. They are useful where changes in capacitance with temperature are not too critical, for examples, as by-pass and coupling capacitors[55]. Most of these compositions are based on barium titanate. By various oxide additions to barium titanate[64-67] or by changing the ratio of BaO to TiO_2 from the stoichiometric ratio[44], it is possible to shift the Curie temperature and change the T.C. value to meet application requirements. Class II dielectrics can be subclassified into two categories[34] by T.C. characteristics: (1) "stable Mid-K" Class II, which typically have dielectric constants in the range of 600 to 4000, and meet EIA X7R characteristics (± 15% maximum ΔC from –55°C to 125°C); (2) "High K" Class II dielectrics, which display dielectric constants from 4000 to 18,000 and typically have Z5U characteristic (+ 22% to – 56% maximum ΔC from +10°C to +85°C) or Y5V (+22% to –82% maximum ΔC from -30°C to +85°C).

(3) Piezoelectric and ferroelectric ceramics

Piezoelectric and ferroelectric ceramics are important and widely used in modern technology. Table 1.3 lists four main uses of piezoelectric ceramics.[44,68] Ferroelectric ceramics are mainly used in various switch applications such as binary memory devices[69]. The first piezoelectric ceramic to be developed commercially was $BaTiO_3$ whose ferroelectric model has been discussed earlier. By the 1950s, the solid solution system Pb(Ti, Zr)O_3 (PZT), which also has the pervoskite structure, was found to be ferroelectric. PZT compositions are now widely used in piezoelectric applications owing to its excellent electromechanical properties[44, 70, 71]. Great efforts have been made by researchers to discover other novel piezoelectric and ferroelectric ceramics[72-77].

Table 1.3 Main description of uses of piezoelectric ceramics

Main uses	Main properties' requirements	Application examples
The generation of charge at high voltages by means of a compressive stress	High g coefficients* with resistance to damage of either electrical or mechanical properties by high mechanical stress.	Gas igniter
The detection of mechanical vibrations	High g coefficients combined with low permittivity	Actuator
The control of frequency	Properties stable with both time and temperature, with minimal losses and a high coupling coefficient	Quartz clocks, Wave filters
The generation of acoustic and ultrasonic vibrations	Low losses when the high fields necessary to generate vibrations of useful amplitude are applied.	Various ultrasonic devices.

* In this table, g is voltage output coefficient, indicating piezoelectric field strength per applied mechanical stress. The piezoelectric body vibrating at a resonant frequency can absorb considerably more energy than at other frequencies.[44] This fact provides a basis for the application of the control of frequency and the generation of acoustic and ultrasonic vibrations.

1.6 Advanced Ceramics processing

The objective of ceramic processing is to produce a material with specific properties, required shape and size at an economic cost. The ceramic properties are basically controlled by the composition but also affected by the grain size and porosity of the sintered ceramic, which are affected by the method of processing. Because ceramics have relatively high melting point, it is difficult to use the melting–casting method employed for metals and plastics to form ceramic products. The brittle and high hardness of ceramics also make machining of final shape commercially prohibitive except in a few cases. Most advanced ceramics processing starts with powder as the precursor. This is formed into an assembly with a shape close to the final product and a larger size to allow for shrinkage on firing.

(1) Powder processing

Improvement in the dielectric properties of ceramics can be achieved by carefully controlling the characteristics of the initial powders[48, 78]. Ceramic powders are traditionally prepared via mixed-oxide processes[48]. This involves milling the component metal oxides or blending their acid salts to achieve mixing. The mixed powders are subject to heat treatment (calcination) to promote the inter-diffusion of constituent cations, the solid state reaction and the formation of the required compound. The commonly used method of mixing is ball milling[43, 44]. Ball milling involves placing the powder in a closed cylindrical container with grinding media (balls, short cylinders, or rods) and rotating the cylinder horizontally on its axis so that the media cascade. Ball milling can be conducted either dry or wet[43]. There are also other mixing methods such as attrition milling[43] and vibratory milling[43, 44] each used with great success.

In recent years, various novel preparation routes such as hydrothermal synthesis[43, 79], oxalate route[48, 80] and Sol-Gel processing[48, 81, 82] have emerged in an attempt to produce powders more suitable for processing of high relative density fine grain size ceramics[48]. These preparation routes are often called wet chemical processes. Most of the techniques take advantage of reactions that take place in the liquid phase (as opposed to the solid-state) so that more intimate

mixing of cations is achieved initially and in turn the optimum homogeneity of the powder can be expected. A flowsheet describing the essential steps for both the mixed oxide and wet chemical processes is given in Figure 1.10. Ball milling of the calcined materials is necessary for both types of powders to produce fine powders.

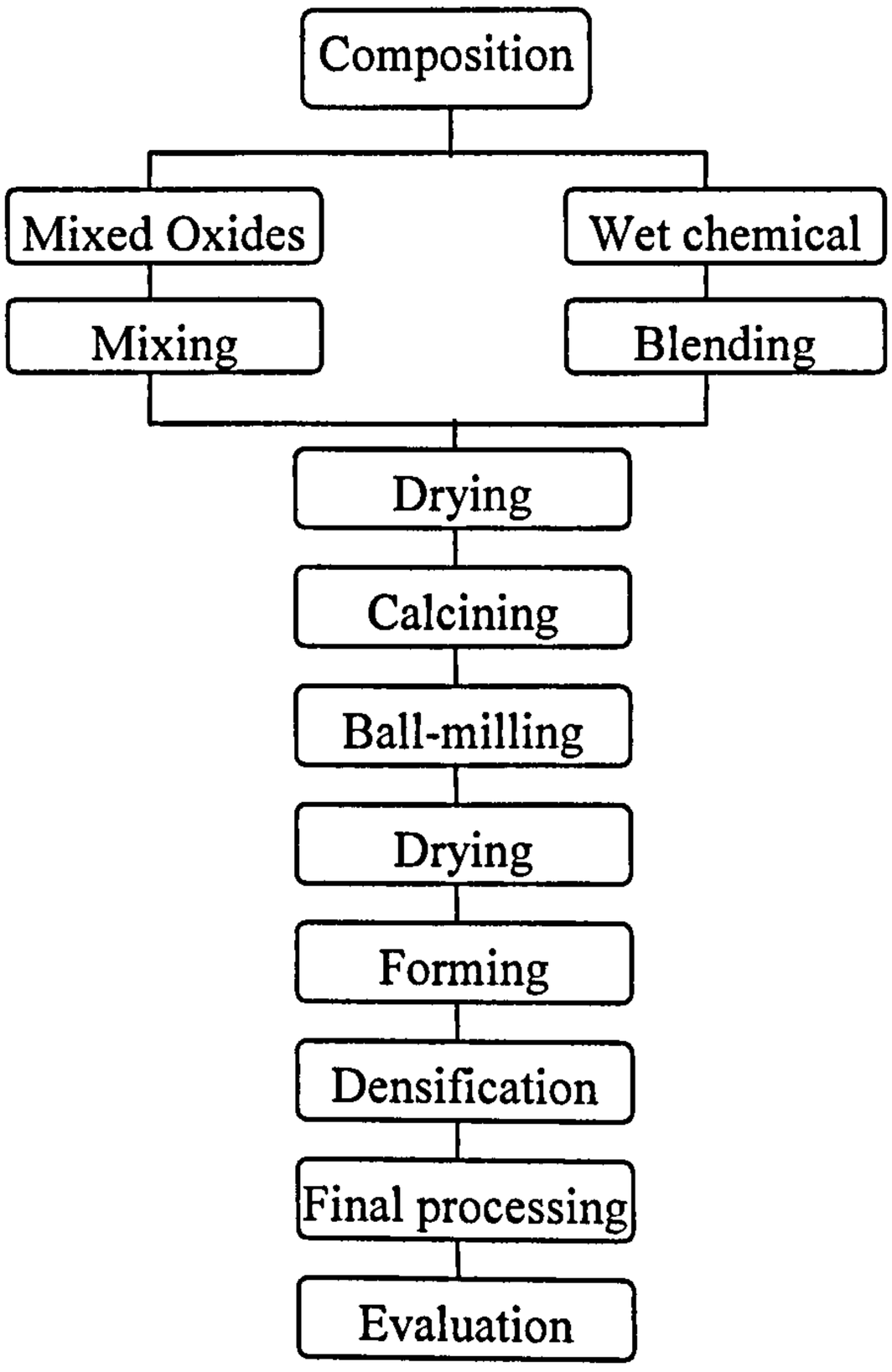

Figure 1.10 Flow sheet for ceramics processing (adapted from reference 56)

(2) Forming and Firing (Densification)

Various forming methods exist to compact the powders to a specific form or shape prior to densification. Cold pressing is, perhaps, oldest and most economical of these methods. Two types of cold pressing are available: Uniaxial pressing - the powder, mixed with a very small amount (1-2%) of fluid or organic additives, is compacted into a rigid body by applying pressure along a single axis through upper and lower pistons; Isostatic pressing – the powder is normally sealed in a rubber mould of the required shape and immersed in a hydraulic fluid through which applied pressure is transmitted in all directions

during all stages of compaction. For example, spark plug insulators are commonly produced using cold isostatic pressing. There are many other forming methods including extrusion[43, 83], slip casting[43, 44, 84], tape casting[44, 85], roll compaction[86], screen printing[43, 87] and injection moulding[43, 44] currently used for a wide range of ceramic powders.

Powders assemblies are then subject to densification in an attempt to produce a pore-free, fully dense ceramic by sintering. Complex–shaped components can be densified easily by this method if appropriate powder processing and pro-forming have been accomplished. Generally, sintered density increases with rising temperature although the full density is rarely achieved unless special techniques are used to assist the sintering processing. Taking Pb(Ti, Zr)O_3 (PZT) as an example[71], with an air atmosphere, densities of ~96% of theoretical can be achieved, but the use of excess PbO during sintering to compensate for PbO loss (volatilisation), the sintered density can approach 99%. Hot pressing[43] is commonly used to produce piezoelectric ceramics. It involves compacting powders under uniaxial pressure in a die at a high enough temperature that the powder can densify. With the simultaneous application of pressure and temperature, the formation of fully dense ceramics can be achieved. For example, tiles of PLZT as large as 150mm in diameter and 25mm in thickness are regularly hot-pressed to full density and high transparency[71]. Other densification methods that have been proved to be successful for dielectric ceramics in more recent years includes hot istostatic pressing[43, 44, 71] and vacuum sintering[88, 89].

After densification, ceramics are subject to final processing that is product-depended. For example, the final steps involved in processing of ferroelectric ceramics are (1) slicing, (2) lapping of the slices, (3) polishing of the plates for electro-optic elements, (4) electroding and (5) evaluation of the parts for further assembly to components[71].

(3) Thin- and thick-film processing

Piezoelectric and ferroelectric films have wide electronic applications such as non-volatile memory, light modulator and switches[44, 87]. Thin films are often made by vapour deposition, typically no more than a few micrometers thick.

Vapour deposition involves the condensation of an element or a compound from the vapour state onto a substrate as a thin film. In chemical vapour deposition (CVD), a vapour of the source materials is thermally decomposed or reacted with other gases or vapours to produce a non-volatile reaction product that is deposited on a heated substrate. Physical vapour deposition (PVD) involves the removal of the vapour phase of a target material and its deposition as a thin film on a substrate.

Rather thicker films with thickness typically in the range 10-22 μm are commonly made by screen printing techniques[44]. In screen printing, the screens that define the printed pattern are meshes of either nylon or stainless steel. The screen is held taut in a frame that is fixed 1-3mm above the surface to be printed. A thick paste is swept across the screen by a hard rubber 'squeegee' with sufficient pressure to extrude paste through the non-masked areas. The consistency of the paste is such that, as the screen rises from the surface, it flows over the spaces left by the threads or wires of the screen so that there is only a small variation in the thickness of the deposit.

The wet chemical solution deposition techniques (sol-gel and metal-organic decomposition) have been quite successful and extensively used in producing thin and thick films of ferroelectrics, dielectrics and many other materials[71]. Sol-gel processing begins with a colloidal dispersion of particles in a liquid, which is the definition of a sol. Through subsequent chemical cross-linking, electrostatic destabilisation, evaporation or some combination these of, the fluid sol may be transformed into a rigid gel that is a substance containing a continuous solid skeleton enclosing a continuous liquid phase. This sol-gel transition allows the solid phase to be shaped into films.

Metal organic decomposition[45] involves metallic species introduced as gaseous organic complexes in epitaxial growth. For examples, trimethyl indium vapour is mixed with hydrogen and phosphine and passed over a heated substrate where deposition of indium phosphide occurs.

1.7 Ceramic Solid freeforming

There is a close relationship between Solid Freeforming Processes (SFF) that have acquired the capability to make functional gradients and combinatorial methods; SFF devices that can make three dimensional (3D) functional gradients can also produce combinatorial libraries. The direct ceramic ink-jet printing process used in this research was initially developed for solid freeforming of ceramics. SFF, also sometimes referred to as Rapid Prototyping (RP), is a computerized fabrication technique that can produce complex three-dimensional physical objects from a computer file by point, line or planar addition of material rather than abstracting material from a blank. SFF was initially used in the plastics industry and has extended to metals and ceramics. The two main advantages of SFF are (1) it can create complex 3D objects with lower cost and shorter time compared with the conventional fabrication technology; (2) different parts of an object can be fabricated using different materials as required to produce functional gradient materials. The following sub-sections describe several main SFF methods used in the fabrication of ceramics including: stereolithography[90-92], fused deposition modelling (FDM)[93-95], selective laser sintering (SLS)[96-98], laminated object manufacturing (LOM)[99-101], three dimensional printing (3DP)[102-105]and direct ceramic ink jet printing (DCIJP)[37,39,40]. The common feature of these techniques is that 3D computer images of components generated by CAD software are sliced to produce two dimensional (2D) layers, and then sent sequentially to a peripheral device that fabricates a real component layer by layer.

1.7.1 Stereolithography

Figure 1.11 illustrates the stereolithography process. A laser beam scans the surface of a monomer containing a photo-polymerization initiator. The monomer is polymerized and hence solidified when exposed to ultraviolet light. Once the first layer is solidified, the elevator moves downwards, deeper into the pool of resin, by a distance equivalent to the layer thickness. Resin is deposited on top of the previously cured layer. The next layer is scanned by laser and so forth, the self-adhesive property of the materials causes the layers to bond to one another

and eventually form a 3D object. For objects having overhanging areas, support structures are commonly used and cut off after the completion of fabrication. For ceramic applications, the photopolymers are charged with powder. In order to achieve high density upon sintering, the monomer is filled with typically 50-65vol.% of solids. The cured resin serves only as a binder for ceramic particles and is removed by slowly heating to 250-500°C, followed by high temperature sintering.

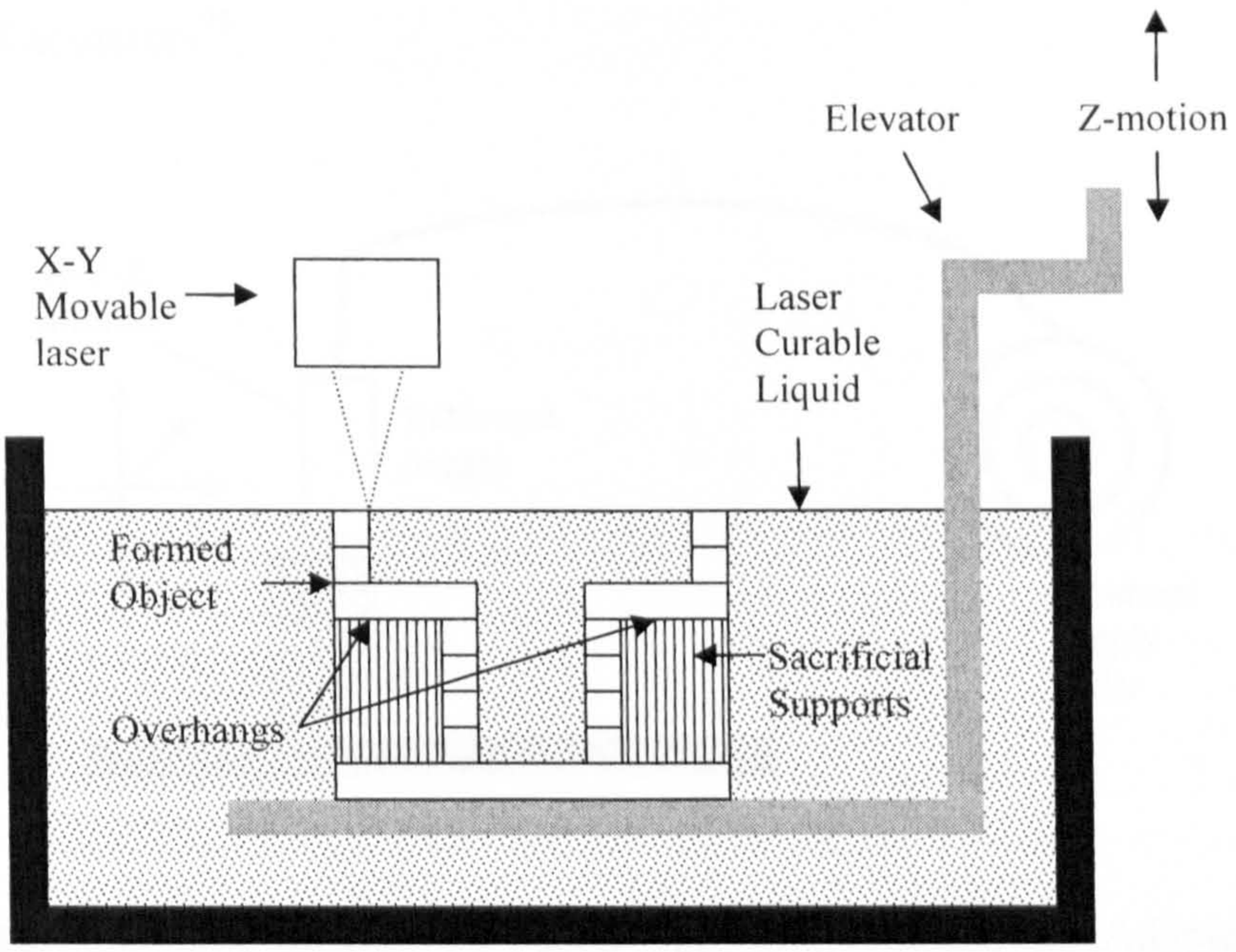

Figure 1.11 Schematic principle of Stereolithography (from reference 92)

1.7.2 Fused Deposition Modelling (FDM)

Figure 1.12 illustrates the process of FDM. The FDM machine builds the part by extruding a semi-molten filament through a temperature controlled nozzle in a prescribed pattern onto a platform. A second nozzle may extrude a second material in order to build support structures for the part where needed. When the first layer is completed, the platform lowers by one layer thickness and the process is repeated until the entire object is formed. Support structures are later removed. A water-soluble support material which can be washed away is also available. For ceramic applications, the starting materials for FDM are filaments

of ceramic powder mixed with thermoplastic polymer or wax binder. The starting materials are mixed, granulated and extruded to produce continuous lengths of flexible filament. The filament is typically 0.5-2mm nominal diameter and fed into a movable head with a heated nozzle where it softens to just above its melting point at the exit. A significant advantage of FDM is that materials are delivered on demand and the process does not require a large reservoir of expensive feedstock at the start. Piezoelectric ceramics and polymer-ceramic composites with functional gradients have been prepared using the FDM for sensors and actuators[93].

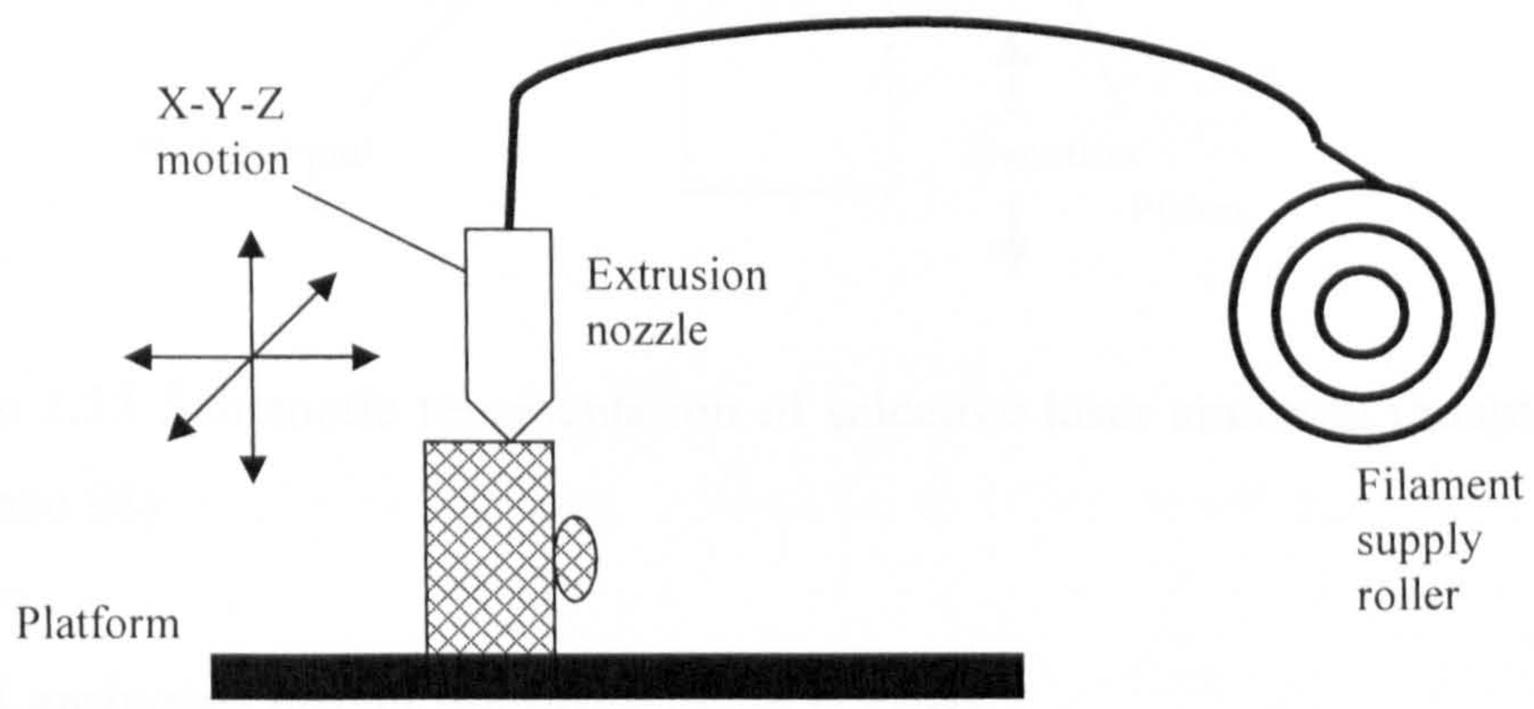

Figure 1.12 Schematic drawing of Fused Deposition Modelling (Adapted from reference 91)

1.7.3 Selective laser sintering (SLS)

The SLS process (as illustrated in Figure 1.13) involves depositing a uniform layer of powder on a building platform. A laser then selectively scans and sinters the forming areas of the powder in a defined pattern. The non-forming areas are left as free powder to support subsequent layers. The platform is then lowered and the next layer of powder is dispensed. The process is repeated until a 3D object is built directly from a CAD file. The unsintered powder is removed and may be reused. The laser energy also fuses consecutive layers together. The building chamber is commonly purged with inert gas and is often heated to reduce the additional laser energy required to heat the powder to its fusion temperature. Recent advances include methods to deposit multiple powder

patterns onto the building platform to produce 3D functional gradient and the use of the same device to produce combinatorial libraries[98].

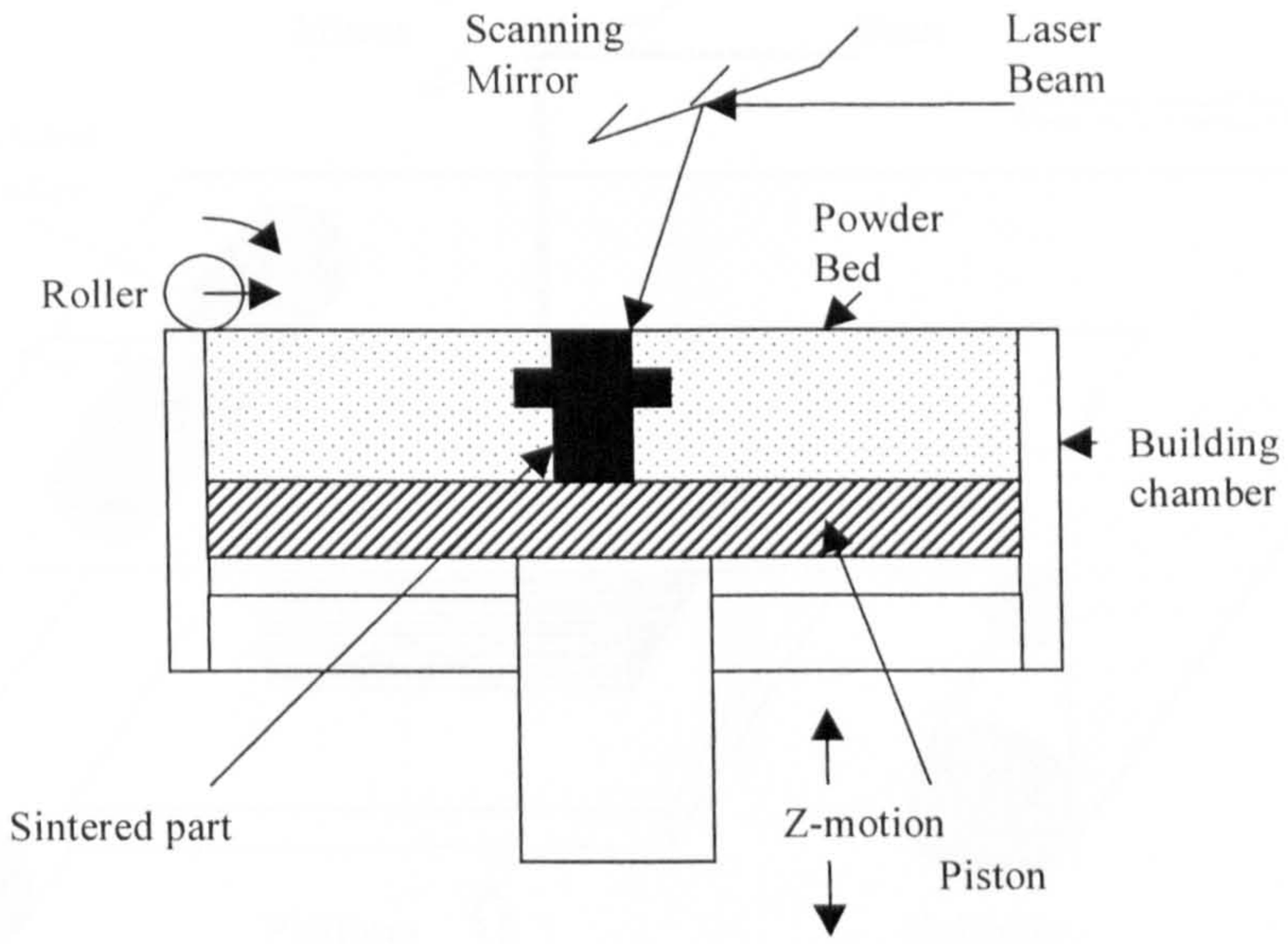

Figure 1.13 Schematic representation of selective laser sintering (adapted from reference 98)

1.7.4 Laminated object manufacturing (LOM)

The LOM process is illustrated in Figure 1.14. The LOM produces 3D components through laser cutting 2D sheets of material in CAD defined contours and by laminating the layers to obtain the 3D shape. The under-surface of the sheet has a binder that when pressed and heated by the roller causes it to adhere to the previous sheet. To help the removal of the excess material once the parts have been built, the exterior of the slice is heavily cross-hatched with the laser. The waste material is left in place during fabrication to serve as a support. After all layers have been stacked, the part block is removed from platform. The excess material is eliminated and then the part produced is subject to binder removal[99] and densification. LOM using ceramic tapes as feed materials is currently employed to make ceramic functional components. Thin (typically around 100 μm) ceramic tapes are pre-processed by mixing ceramic powder with an appropriate binder through tape casting, roll compaction or an extrusion process.

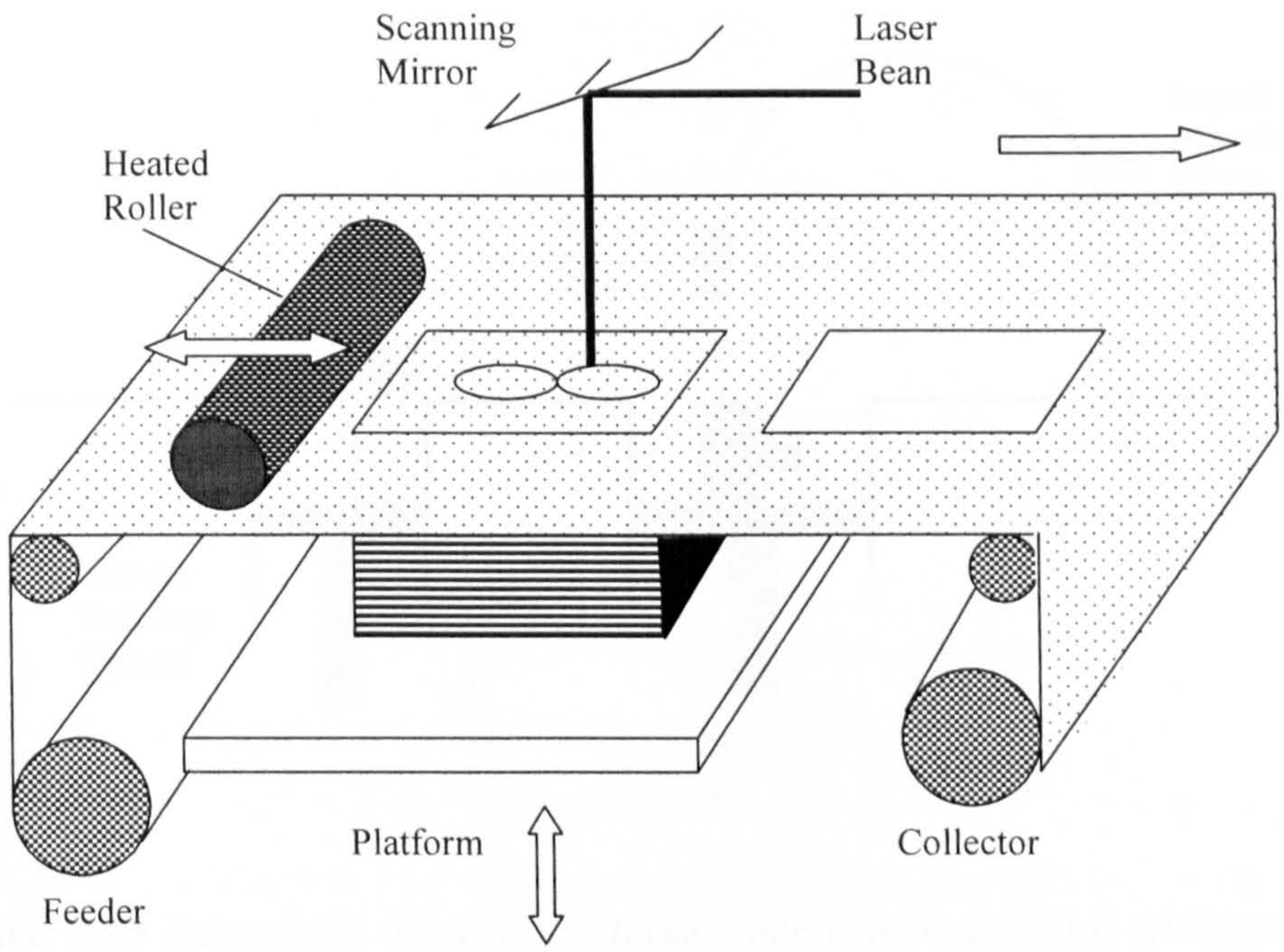

Figure 1.14 Schematic drawing of laminated object manufacturing (Adapted from reference 91)

1.7.5 Three dimensional printing (3DP)

Figure 1.15 illustrates the 3DP. The process starts by depositing a measured quantity of powder at the top of a fabrication chamber. The roller then distributes and compresses the powder at the top of the fabrication chamber. The multi-channel jetting head subsequently deposits a liquid adhesive in a 2D pattern onto the layer of the powder. The powder becomes bonded in the areas where the adhesive is deposited to form a layer of the object. Once a layer is completed, the fabrication piston moves down by the thickness of a layer, and the process is repeated until the entire object is formed. The object then is elevated and the excess powder brushed away leaving a powder assembly in the shape demanded by the computer file. This assembly is oven-cured and excess powder is removed by immersion in a water bath before sintering. No external supports are required during fabrication because overhangs are supported by the free powder. By using multiple print heads, additives may be deposited in a prescribed fashion to create gradients in composition, for example, 3DP has been used for the

fabrication of functionally graded reaction infiltrated SiC-Si composite ceramic[105].

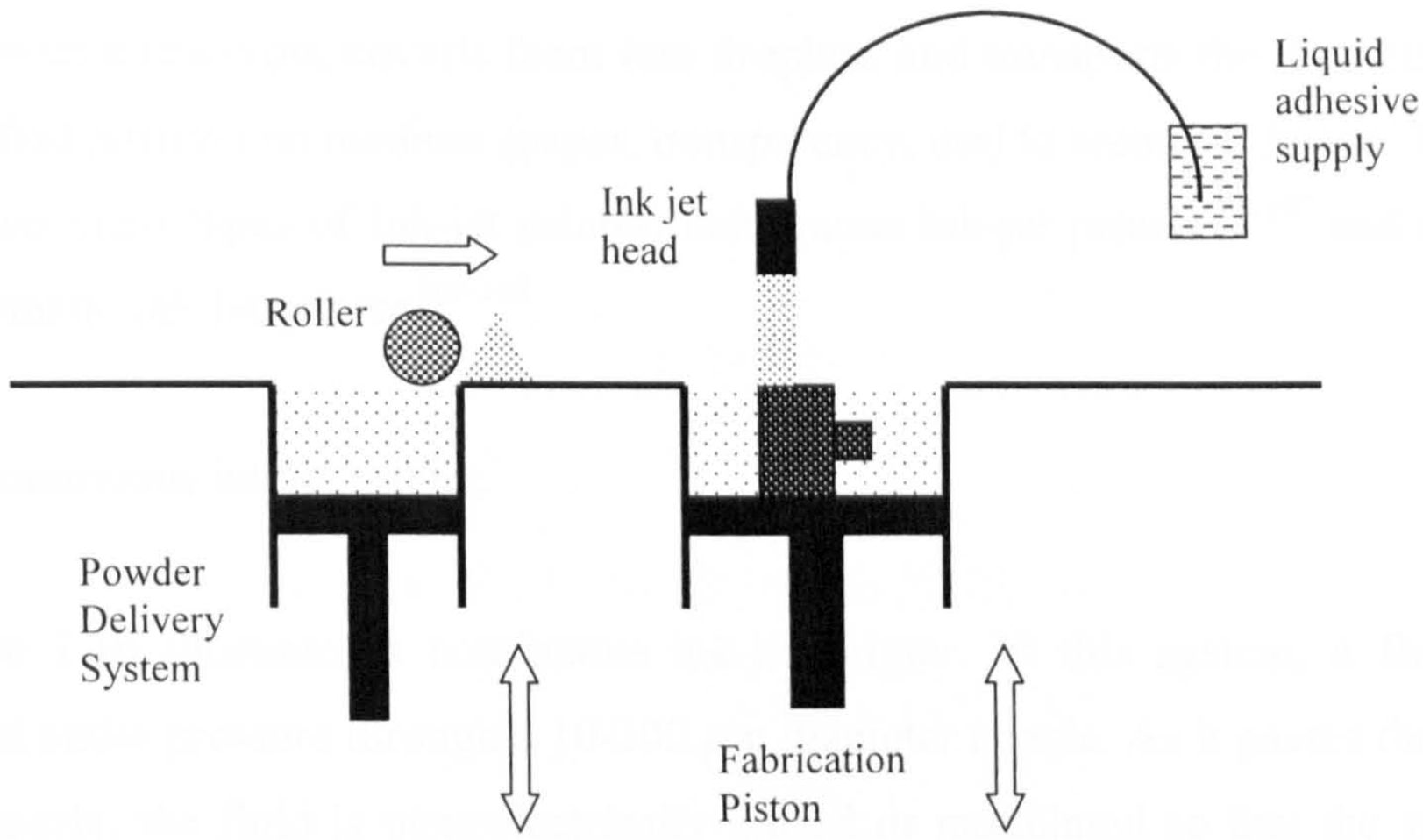

Figure 1.15 Schematic drawing of three dimensional printing (Adapted from reference 91)

1.8 Direct ceramic ink jet printing (DCIJP)

DCIJP is distinguished from 3DP in that a ceramic-powder containing ink is dispensed directly instead of the binder. The basic process of DCIJP involves the following steps: A ceramic suspension is passed through a printer nozzle and layer upon layer of ink is deposited according to a computer model until the part is built. The printed ceramic part is then subjected to conventional binder removal and sintering to produce a dense ceramic component. The application of multi-nozzle printing heads allows different inks from separate reservoirs to be printed at the same time, thus it is possible to change the composition from point-to-point. Therefore, DCIJP gives the materials engineer not only control over the shape but also the composition of ceramic parts via a computer interface. DCIJP has been successfully applied to form ferroelectric film[38] and zirconia/alumina functionally graded materials[37]. DCIJP is built upon two fundamental principles: (1) Freeforming via ink-jet printing and (2) Ceramic inks prepared via colloidal processing.

1.8.1 Ink–jet printing technology

Ink-jet is a non-impact dot-matrix technology which takes small quantities of inks from a reservoir, coverts them into droplets, and transports the droplets to a specified position on medium (paper, transparency, etc) to create an image. There are two main types of ink-jet printer: continuous ink-jet printer[106-107] and drop-on-demand ink-jet printer [106-108].

(1) Continuous ink jet printer

Figure 1.16 illustrates a continuous ink-jet printer. In this system, a fluid is forced under pressure through a 10-200 μm diameter nozzle. As it passes through the nozzle, the fluid is piezoelectrically pulsed or modulated so that the stream breaks up into a continuous series of droplets. These droplets are selectively charged as they pass through a charging electrode. The charged drops when passing through a high-voltage deflection electrode are deflected and directed to the substrate. Uncharged drops that are undeflected continue in their flight. A gutter collects the droplets that do not reach the substrate for recirculation. Continuous ink-jet printers form droplets continuously even when there is no printing. It is normally used for high-speed printing of bar codes and for date labelling of food packages.

(2) Drop-on-demand (DOD) ink jet printer

In the DOD printer, ink droplets are formed only when required. Depending on the mechanism used in the drop formation process, the technology can be categorized into four major methods: thermal, piezoelectric, electrostatic and acoustic ink-jet. Thermal ink-jet DOD printer is the most successful method on the market today. The thermal ink-jet printer normally uses a disposable ink-jet printer-head that contains a liquid ink supply, several nozzles and their associated droplet formation systems. Figure 1.17 illustrates the droplet formation process in a thermal ink jet printer. Droplets of ink are forced out of the nozzle by heating a resistor, which causes an air bubble to expand. When the bubble collapses, the ink droplet breaks off and is transferred to the substrate. Capillary

force causes the ink chamber to refill with ink and the process is ready to begin again. Compared with the continuous ink-jet method, the DOD principle is less useful for printing on curved surfaces or where the ink droplet must transverse a long distance[106]. It is used mainly in home and office printing.

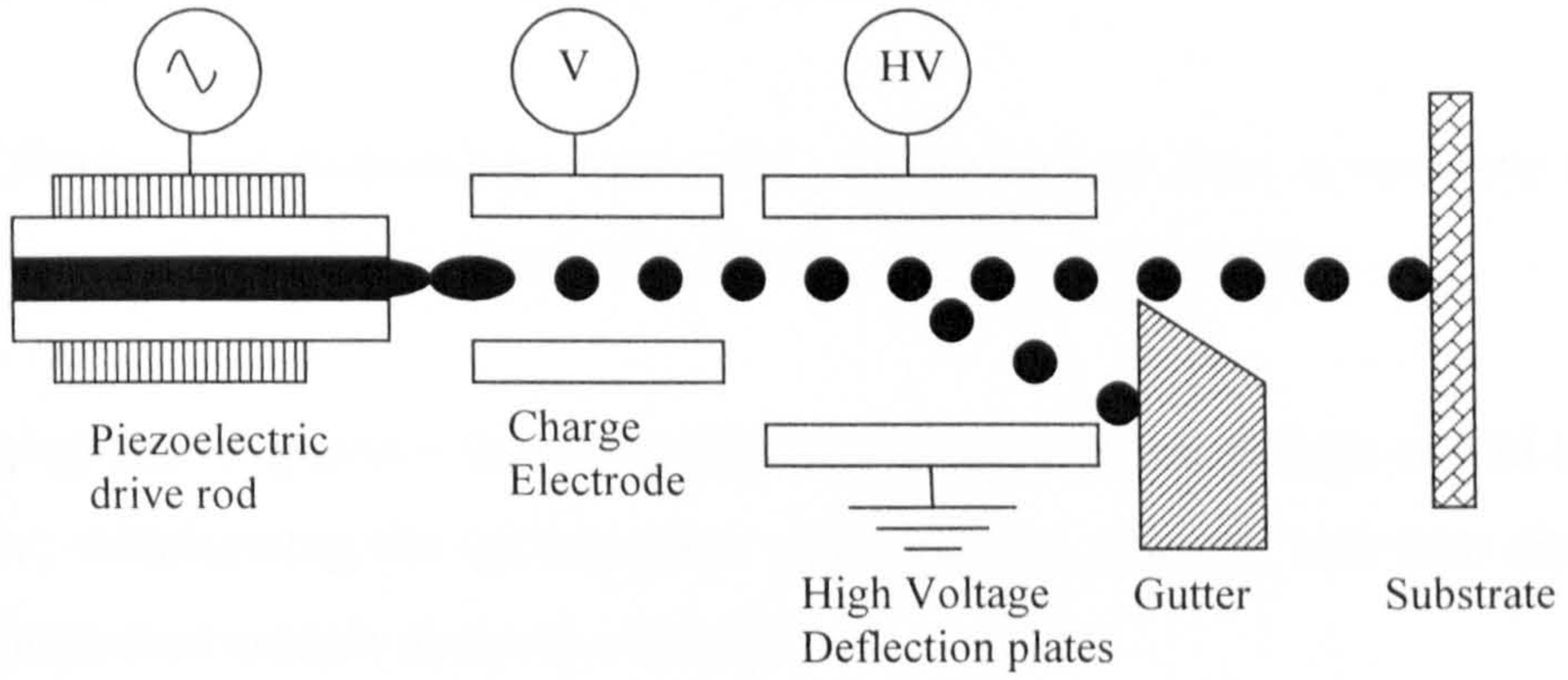

Figure 1.16 Schematic drawing of continuous ink-jet (modified from reference 107).

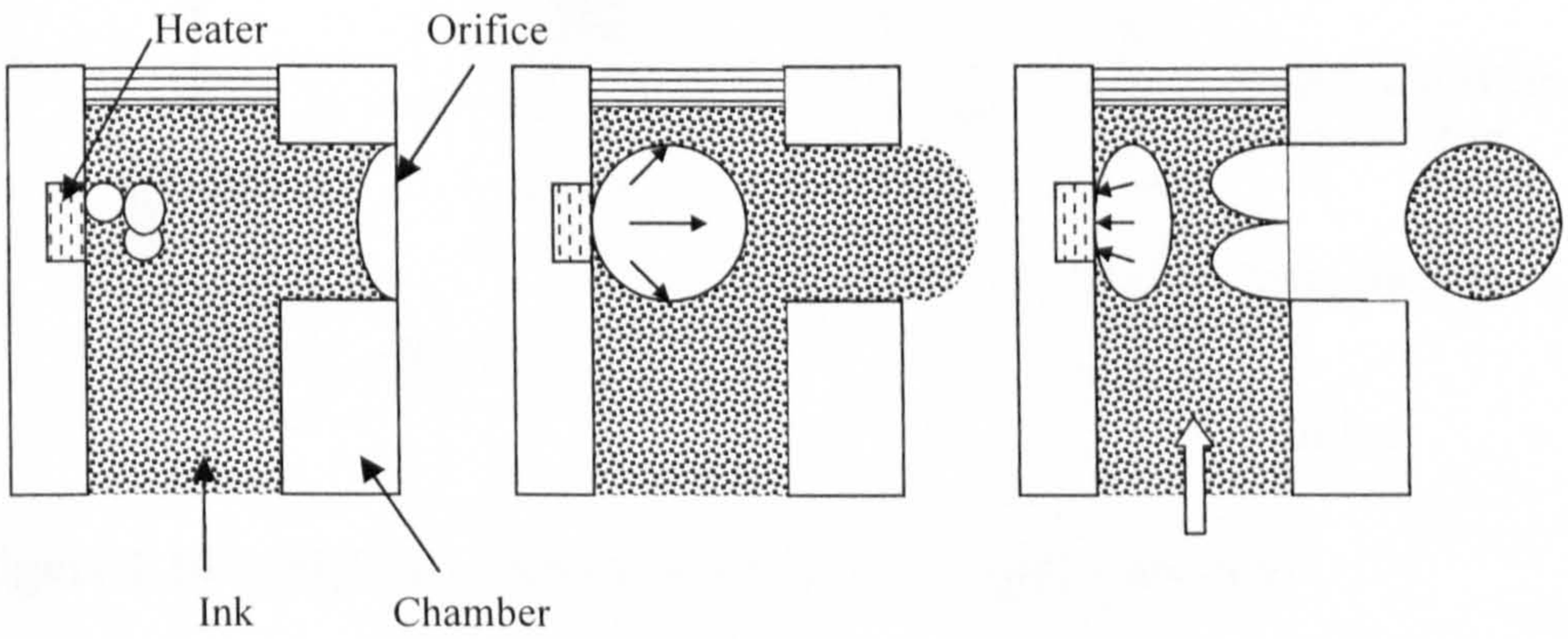

Figure 1.17 Droplet formation process in a thermal ink-jet printer (modified from reference 108).

(3) SynQUAD™ dispensing technology

The printer used in this research is based on SynQUAD dispensing technology[109] allowing non-contact dispensing of nanoliter volumes. The dispensing system (Figure 1.18) is a hydraulically driven system and requires a fluid medium to be present from the syringe to the microsolenoid valve. Two modes of liquid handling of SynQUAD techniques are possible:

(1) Continuous dispensing – involves pulling liquids from a reservoir into the syringe and then dispensing it through the micro solenoid valve.

(2) Aspirate/dispense – involves dipping the tip of the valve into a fluid in a well plate, withdrawing the syringe after aspirating the sample, and then dispensing the aspirated sample at another location.

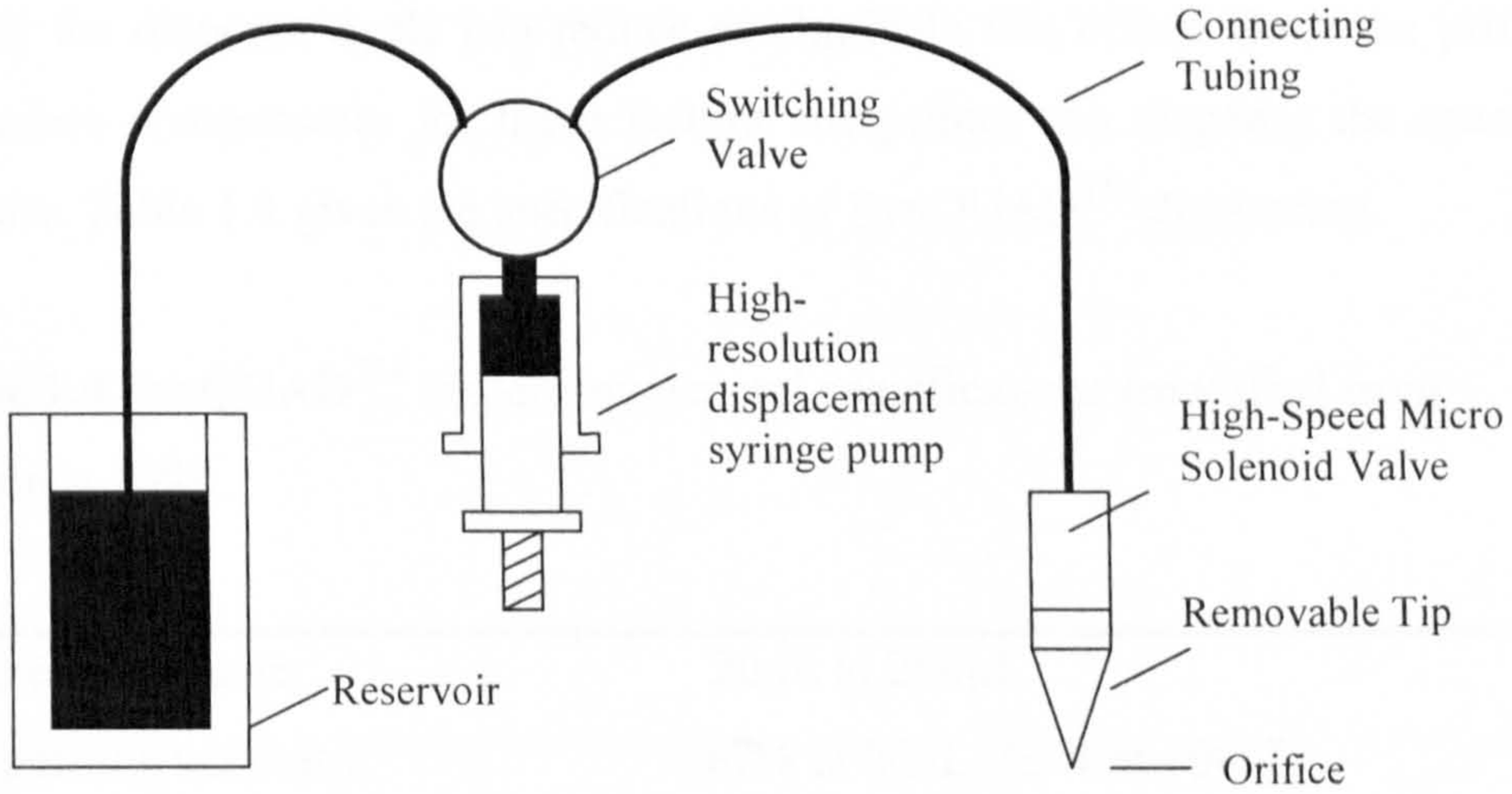

Figure 1.18 SynQUAD dispensing system (from reference 109)

Dispensing the specified volume is achieved by a 192000 step syringe that displaces a given amount of fluid. The amount of fluid displaced by the syringe pump equals the amount dispensed. The micro solenoid valve is opened for a short period of time (i.e., milliseconds). The fluid is released from the valve and travels to the tip. The fluid increases its linear velocity as it passes through the tip orifices and ejects as a drop (or stream if the amount of fluid is large). The co-

ordination of the syringe pump and micro solenoid valve is embedded in proprietary software.

Several factors may influence achieving the desired dispense volume: (1) Gas bubbles in the dispensing system can cause variation in dispensed volumes. Bubbles can be removed by purging the system with isopropanol and using degassed solvents. (2) When the sample is aspirated, the syringe pump draws fluid through the tip orifice. The resistance to flow from the tip and valve creates a negative pressure which must first be overcome. Venting (i.e aspirating zero volume) can bring the system to a known (zero/ambient) pressure. To prevent the introduction of air, venting is typically done with tips in the sample to prevent the introduction of air. If an air gap is not used, dilution occurs at the interface of the aspirated sample and system fluid. As a general rule, 3 to 4 times the dispense volume must be aspirated to produce a series of undiluted dispenses. (3) The interaction of ejected drops with fluid on the tip orifice can lead to loss of control of dispense volumes. Vacuum drying of the tips at appropriate times during the dispense cycle can reduce or eliminate this effect. Once the printing procedure compensates for these factors, the printer can dispense the specified volume. Table 1.4 gives the specifications of SynQUAD™ dispensing.

Table 1.4 SynQUAD™ dispensing general specifications (modified from reference 109).

Dispensing range:	20nL to 250μL
Dispensing accuracy:	±7% at 20nL, ±5% at 100nL
Dispense to Dispense precision*:	<10% CV at 20nL, <7% CV at 100nL <5% CV at 1μL
Minimum aspiration volume:	5μL

*CV stands for coefficient of variation.

1.9 Ceramic inks

The properties of ceramic inks are important to the functioning of ink-jet printing and quality of the printed sample. A ceramic ink normally comprises the ceramic powder, solvent, dispersant, binder and other additives as shown in Table 1.5. Each component has to been carefully selected and accurately controlled to give the ink the desired properties and to ensure its compatibility with others. There are two basic requirements for ceramic inks. One is stability and homogeneity of the suspension that is achieved via colloidal processing. The other is that physicochemical properties of ceramic inks should meet the requirements of the ink-jet printer, for example, solvents should not damage valves and tubing. A third requirement arises when combinatorial ink-jet printers create mixtures of ceramic inks. The inks must mix without causing instability in each other. Flocculation, sedimentation or separation should be prevented.

Table 1.5 Components of ceramic inks

Components	Function
Ceramic powders	Building the green part.
Solvent	Impart fluidity and as a vehicle for the dissolution and uniform distribution of all additives and ceramic particles.
Dispersant	Distribute the powder homogeneously in the solvent; Promotes deflocculation and stability; Enables effective total wetting of the solid by the solvent.
Binder	Provides strength to the green part for handling and storage.

1.9.1 Colloidal processing of ceramics.

A colloidal dispersion[110, 111] can be defined as a system in which particle having diameters between 1-1000 nm of any state (solid, liquid or gas) are dispersed in a continuous phase of a different composition or phase. In colloidal dispersions, the contact area between particles and the dispersing media is large. As a result, inter-particle forces (or surface forces) strongly influence suspension behaviour.

The gravitational force often can be ignored. The dominating inter-particle forces in most ceramic colloidal systems are van der Waals forces, electrostatic forces and steric forces associated with adsorbed dispersant molecules. Preparation of the ceramic ink essentially involves dispersing the powder in a liquid, achieving stability by adjusting pH or adding dispersant and then preventing sedimentation during storage. Bell and Crowl[112] described the dispersion process as "Incorporation of a dry powder into a liquid medium in such a way that the individual particles of the powder become separated from one another, or form small clusters, evenly distributed throughout the entire liquid medium".

Various inter-particle forces such as, van der Waals forces, electrostatic forces, bonding due to moisture and gravitation forces, are responsible for the formation of agglomerates in a dry powder[110]. These forces must be overcome before the powder can be incorporated in the liquid where powder-air and powder-powder interfaces are replaced by powder-liquid interface. Breakdown of agglomerates (de-agglomeration) is usually achieved mechanically by either shear or impact. Ultrasonic disruption[113] and high energy bead mills[40] have been employed to break down agglomerates during ceramic ink processing. After de-agglomeration, the entire surface of each particle is available for wetting. Wetting refers to the spreading of a liquid over a solid surface whereby the adsorbed air and other contaminants on the particle surface are replaced. Surface active agents can be used to assist the wetting of liquid over the powder surface.

The breakdown of agglomerates is a dynamic process in which re-agglomeration (flocculation) is constantly in competition with de-agglomeration as the attractive van der Waals forces are always present in the dispersion. To create a stable suspension[111] (i.e., dispersed, weakly flocculated or strongly de-flocculated states), the repulsive electrostatic force and/or steric force can be manipulated by pH or surface-active agents or both to overcome the attractive van der Waals forces.

Electrostatic stabilisation refers to the stability of the powder suspension due to the repulsive interaction of charged particles of equal sign. Solid oxides in aqueous suspension are generally electrically charged. Ions can be attracted from

the liquid to the particle surface or preferential dissolution of ions from the solid surface takes places. Both effects produce a net charge on the surface. As illustrated in figure 1.19, Ions are distributed between two regions. In the Stern layer the ions are close against the surface; Beyond the Stern layer the ions are distributed in a diffuse 'atmosphere'. They have a high concentration near the surface and gradually decrease with distance, until an equal density of positive and negative ions is reached. If direct current passes through a colloidal solution, according to the sign of the charge, particles move either to the positive or negative electrode. This phenomenon is called electrophoresis. For spherical particles the electrophoretic mobility u (unit $m^2v^{-1}s^{-1}$) is[114]

$$u = \frac{(\frac{E}{l})\zeta D}{6\pi\eta}, \tag{1.14}$$

where E/l is the potential gradient which means the volts E applied and on the distance l between the electrodes; The zeta potential ζ is the electrokinetic potential of the particle ; D is the dielectric constant of the medium and η is the viscosity of the medium. In general, a high absolute zeta potential value indicates the presence of a well-dispersed colloid by electrostatic repulsion. The zeta potential value can be determined from equation (1.14) by measuring the mobility u at a definite voltage gradient, dielectric constant D and the viscosity of the medium must be known as well. By adding electrolytes or adjusting the pH value of a colloidal solution, the zeta potential may either increase or decrease. Isoelectric point[110] is the pH value at which zeta potential is zero. At this point, there is no repulsion between particles and they flocculate under van der Waals attraction. DLVO theory[111] explains the interaction of electrostatic forces with van der Waals forces.

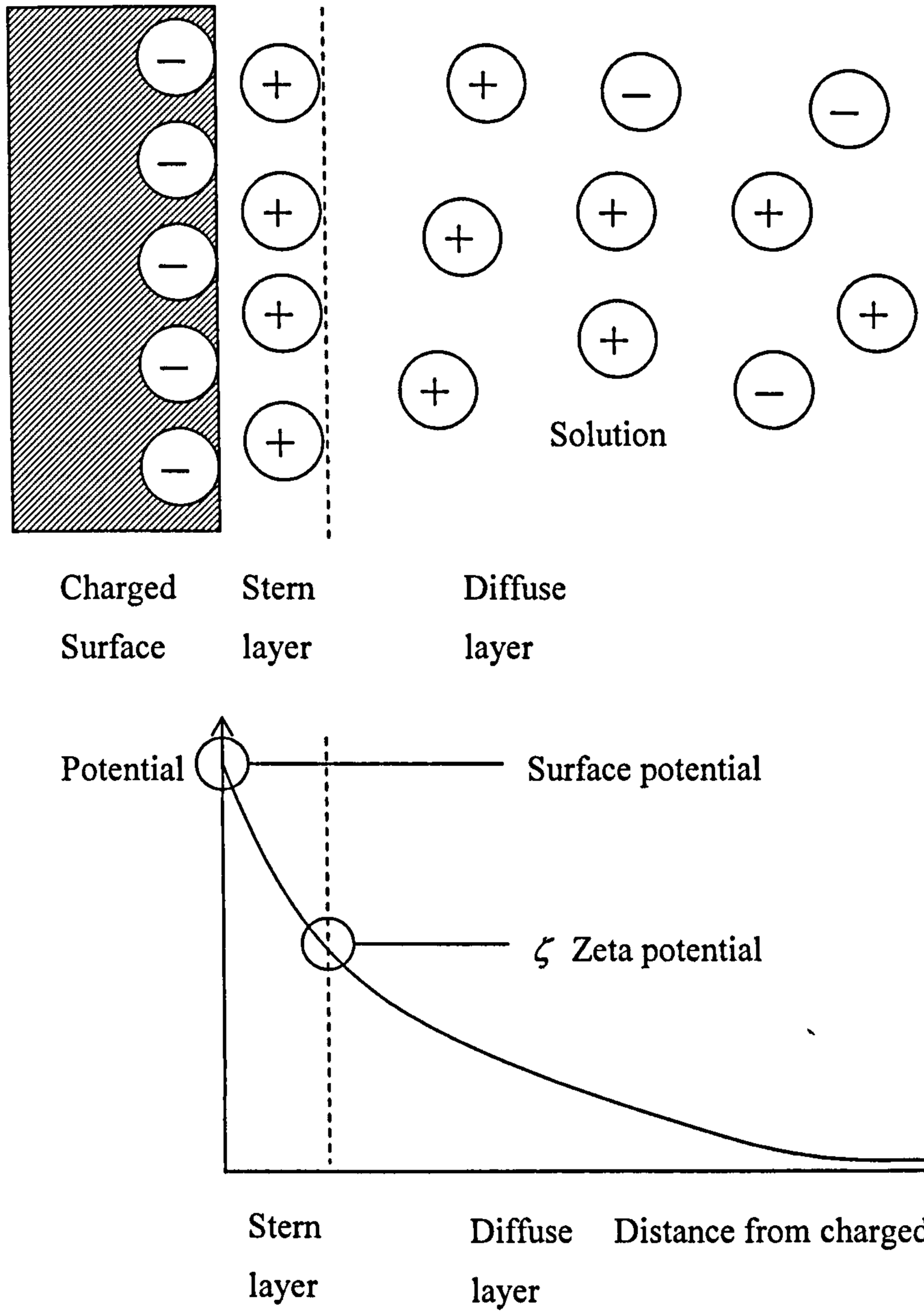

Figure 1.19 Double layers describe ion attached to charged particles in the colloid.

Steric stabilisation[111] arises from the repulsive interaction between absorbed polymer chains at the particle surfaces. When particles approach each other, these adsorbed polymeric chains intermingle, they lose degrees of freedom which they would otherwise possess. In thermodynamic terms, this involves a reduction in entropy, which leads to a higher free energy and provides an opposing force to prevent further attraction. As chains intermingle, solvent is forced out from

among particles, which causes a counter-force to separate particles, known as osmotic repulsion. When the polymer dissolves in the solvent, it is flexible and can fold in different ways. A well dispersed suspension requires the polymer chains to be in an extended configuration so that the steric repulsion can be established when the chains interact. Many factors determine the adsorption of polymers onto the ceramic particles such as, compatibility with solvent, molecular architecture and active surface site density[115]. The third stabilisation mechanism is known as electrosteric stabisation[111], which is combination of a pure electrostatic repulsion and a steric force. Non adsorbing, smaller species (e.g., polymers, electrolyte or fine colloidal particles) in the solution also form structural barriers to separate large colloidal particles. Colloidal systems are complicated, and much work has still to be done to clarifying numerous theoretical and practical problems.

There are various methods of assessment of dispersion stability such as measurements of light scattering[110], the measurement of zeta potential and viscosity of suspension as a function of pH value[116, 117] and the measurement of changes in flow behaviour in response to an applied stress or strain[118]. Sedimentation testing is possibly the simplest method of studying the behaviour of dispersion. It is often performed in a cylinder to follow the evolution of particle agglomeration by monitoring the rise of sediment level formed at the bottom under the influence of gravity until the sediment is constant or the collapse of the turbid region from the top of the tube. The dispersion stability may be inferred form the observation of ceramic inks during a sedimentation test. The time that it takes for an apparently homogenous ceramic ink to develop layers or sediments is a guide to the stable working time for this ink.

1.9.2 The properties of ceramic inks

The ceramic ink properties relevant to functioning of a jet printer and quality of the printed sample are the viscosity, surface tension and in some printers, electrical conductivity or boiling point (for thermal jet printers).

Viscosity[45, 119] is the property of a liquid that resists shear forces, and hence flow. Shear is the orderly movement of layers of liquid relative to parallel adjacent layers. In steady shear, the rate of relative movement of layers is known as the rate of shear, and the tangential force per unit area applied to the layers to sustain the motion is the shear stress. Dynamic viscosity, η, is the shear stress divided by the rate of shear for steady flows of liquid. The SI unit is pascal second (i.e., Pa s). Kinematic viscosity, ν, is:

$$\nu = \frac{\eta}{\rho}, \tag{1.15}$$

$$\eta = \nu.\rho, \tag{1.16}$$

where both dynamic viscosity, η, and the density of the liquid, ρ, are measured at the same temperature. When the viscosity is measured using a U-tube viscometer, Kinematic viscosity is calculated from[119]:

$$\nu = Ct, \tag{1.17}$$

where C is the calibration constant for the viscometer given in its calibration certificate, t is the mean flow time (in s) of liquid of a given volume between the etched rings. Dynamic viscosity, η, is calculated from kinematic viscosity using equation 1.16. The detailed procedure of measuring viscosity using the U-tube viscometer can be found in British Standard 188:1977 *Methods for determination of the viscosity of liquids* (i.e., reference 119).

A liquid is said to exhibit Newtonian flow when its viscosity is independent of the rate of shear at constant temperature and pressure. For non-Newtonian fluids, their viscosities are dependent on the rate of shear, such as polymer melts, whose viscosities decrease with increasing shear rate. The viscosity requirements of ceramic inks may vary with machine types but ideally the flow should be Newtonian. A value of 1-3 mPa s is normally chosen for continuous jet printers but this is lower than for a DOD printer[107].

Surface tension[120, 121] is due to unbalanced molecular cohesive force near the surface and is measured by the force acting perpendicular to unit length of a line drawn in the surface. Units of measurement are Nm^{-1}. The surface tension of water is 72.8 mNm^{-1} at 20 °C, but this value may decrease significantly when blended with additives. The formation of droplets during ink-jet printing and their subsequent dispersal after impact on a substrate is dependent on the surface tension of ceramic inks[107,108]. A drop of liquid placed on a smooth and solid surface has 3 phase boundaries and there are 3 tensions acting at the 3 interfaces (Figure 1.20). In the case of equilibrium, by the Young's equation:

$$\sigma_1 - \sigma_{1,2} = \sigma_2 \cos\phi \qquad (1.18)$$

The pull $\sigma_1 - \sigma_{1,2}$ tends to spread the liquid over the whole surface of the solid. Wetting, therefore, occurs if $\sigma_1 - \sigma_{1,2} > \sigma_2 \cos\phi$. The wetting is perfect, if at contact angle $\phi = 0$ $(\cos\phi = 1)$, and $\sigma_1 - \sigma_{1,2} > \sigma_2$. The wetting is imperfect if $\sigma_1 - \sigma_{1,2} < \sigma_2$, because in this case, it is always possible to satisfy Young's equation 1.18 as the contact angle increases and $\cos\phi$ decreases. There are various methods of measuring surface tension such as the ring-detachment method, the Wilhelmy plate method and the bubble pressure method (the details of each method can be found in reference 121).

The DC conductivity of ink is critical to the printer that makes use of electrostatic force[108]. For continuous jet printers, the ink droplet has to be charged for the duration of the charging pulse so that it can be deflected and deposited on the printing substrate. Polar solvents such as water can yield high conductivity but present the problem of slow drying rate comparing with non-polar solvent such as benzene (C_6H_6).

High volume fraction of ceramic powder of the ink is often wanted to provide efficient ink-jet printing - deliver more powder to the building platform using less vehicle and time. However, increasing the volume fraction of ceramic powder in ink often means increasing viscosity, decreasing the dispersion

stability and affecting conductivity. To use DCIJP, ceramic inks must have a careful balance of the volume fraction of ceramic powder in the ink, viscosity, surface tension, DC conductivity and other properties as the application specifies.

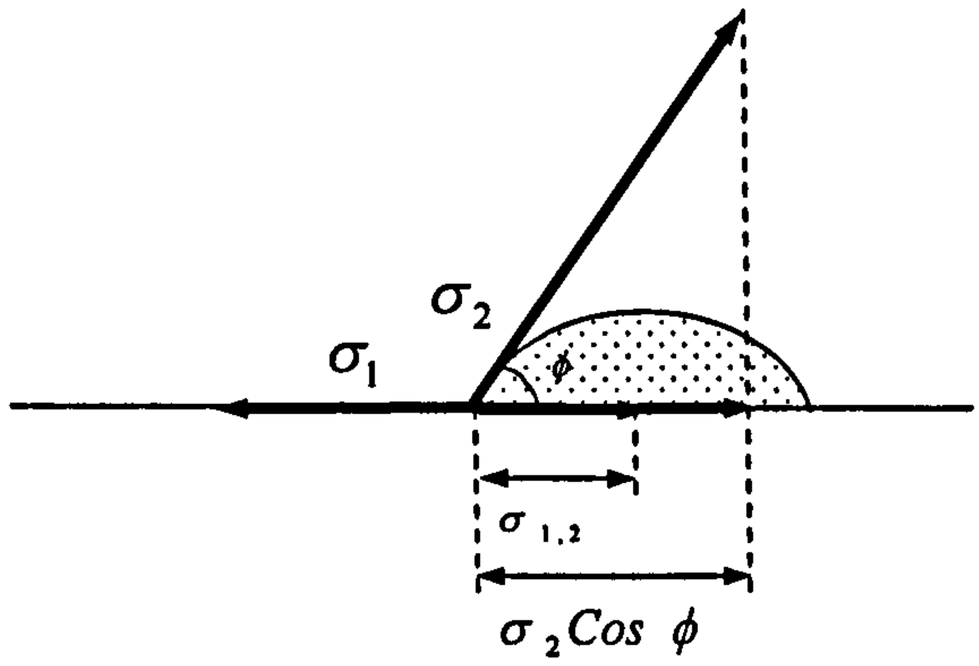

Figure 1.20 The spreading of a liquid over the surface of a solid. Surface tension: σ_1- solid/gas, σ_2- liquid/gas, $\sigma_{1,2}$ - solid/liquid. (modified from reference 120).

1.9.3 The drying behaviour of ceramic ink droplets

The powder assembly produced by DCIJP is built from residues of ceramic ink droplets. It is important to study the drying behaviour of such droplets because the drying process influences the compositional distribution and geometry of the residues of droplets.

In general, the drying of ceramic suspensions can be divided into two stages[111,122]. In the initial constant-rate period, fluid is transported to the external surfaces at a rate that matches evaporation. Then, in the falling-rate period, the fluid can no longer get to the surfaces at this rate and experimentally, there are two falling rate periods. In the first (linear) period, fluid menisci retreat into the body (the funicular state). Moisture migration is controlled by capillary flow. As further evaporation occurs, fluid resides in isolated pockets (the pendular state), marking the transition to a second non-linear falling rate period. The remaining liquid is removed from the body by vapour-phase diffusion.

There have been many studies of the drying of unsupported droplets of ceramic slurries, the better to understand spray drying[123-126]. Spray drying is one of the ways to convert ceramic slurries into a free-flowing powder. In the spray drying process, a slurry containing ceramic powder is atomised into tiny droplets, which are mixed with hot drying gas, typically air, which dries the individual droplets into clusters of solid particles. Geoff and Red[124] have found droplets from well-dispersed slurries in which particles retain mobility during drying, form irregular shaped agglomerates with a central hole. Suspensions with a tendency to flocculate, form dense spherical agglomerates.

On the other hand, the drying of drops of liquid deposited on a horizontal non-porous substrate is affected by (1) the wetting characteristics of the substrate[127] (2) the temperature and atmospheric conditions[128], and (3) the properties of the liquid and solids it may contain. Shannahan and Bourges[128] showed that in a dry environment, a pure water droplet placed on a smooth polymer surface, experienced three stages of drying. First, the contact diameter remained constant whilst both drop height and contact angle decreased. Second, both the drop height and diameter decreased concomitantly while maintaining a small contact angle. Finally, height, diameter and contact angle all decreased sporadically as the droplet volume diminished to zero.

There is general agreement that unlike a sessile drop of pure liquid, for which the contact radius decreases during drying, presenting a receding contact angle, the three-phase boundary of a droplet of suspension is pinned by the rapid deposition of particles at the boundary[129]. The pinning is generally attributed to surface irregularities and can be eliminated by using smooth Teflon™ as the substrate[129]. The consequence is that while the radius remains constant, either the drop shape ceases to be a spherical cap, the cap recedes to the centre leaving a foot or the contact angle decreases. In some cases, a series of concentric rings is formed as the droplet dries rather than one peripheral ring[130].

Guo and Lewis (1999)[131], characterized the microstructure of dried films prepared from aqueous SiO_2 suspensions stabilized by electrolyte (NH_4Cl). Non-uniformities developed in the spatial distribution of colloidal particles and

precipitated salt. SiO_2 films were cast onto (001) silicon substrates. The salt concentration decreased substantially from the film edge to its centre as evident in EDS analysis. Such features resulted from capillary-induced transport of free colloidal particles and dissolved salt species.

Parisse & Allain (1997)[132] demonstrate that a 'foot' becomes fixed around the edge of the droplet where particles build up as drying proceeds. The remaining drop, treated as part of a spherical cap recedes into the centre and they calculate its shape based on the radial flow of liquid to the periphery resulting from the higher relative proportion of liquid-air interface there. For their experiments, the drops were of an aqueous silica colloidal sol containing 24 vol.% solids deposited on cleaned glass. Maenosono et al. (1999) reported[133] a system in which two types of particles, CdS and CdSe/CdS(core/shell) were suspended in pyridine and water respectively. A drop of suspension was placed on a solid substrate and the solvent was allowed to evaporate in a nitrogen atmosphere. A ring-shape multilayer formed at the drop periphery, with the ring width depending on the particle volume fraction. Such lateral transport of carrier liquid has been observed directly by magnetic resonance microscopy during the drying of emulsion paints[134]. This process, modeled by Routh and Russel[135] shows how a front of closely packed particles advances from the drying edge as solvent recedes into the film.

The full story of droplet drying and of the effects reported here, cannot be told until it is recognized that another factor is at play. The splendid observational work presented in a paper by Haw et al.[136] tells us that as the more densely packed particle assembly at the droplet periphery grows, vertical circulation flows are present in the undried central region of the droplet: "aggregates in the cap are seen to continuously circulate in the vertical plane" and so " we can expect *macroscopic* inhomogeneity in the final residue". Later, convection-like cells form in the horizontal plane. The packing of particles in the 'foot' does not become fully dense until the liquid-rich cap has dried. The radial flow of liquid continues to supply the foot to replace the liquid lost there by evaporation. Only when the cap disappears and no replacement is available does the foot become well-packed. Very recently (2005), the circulation flows have been analysed by

Hu and Larson[137] in terms of the Marangoni stresses that result from surface tension gradients in an evaporating droplet.

Although the drying of drops of colloidal suspension is an important step in a diverse range of applications including protective coatings, DCIJP, etc. there has been relatively little effort directed towards the fundamental understanding of the shape and compositional changes that take place in the drying process. These matters are relevant to the properties of combinatorial libraries made by ink-jet printing and are explored in more detail in this thesis.

1.10. Platinum coated substrates

In combinatorial ink jet printing, combinatorial libraries are printed on platinum coated substrates. The platinum coating has two functions: (1) Due to its high melting point (1768.3 °C), the platinum layer serves as a barrier to prevent ceramic samples reacting with alumina substrates during firing. (2) Due to its low resistance, the platinum layer also serves as an electrode when measuring the electrical properties.

For thin doped layers such as platinum coatings, resistivity is a strong function of thickness. In modern electrical engineering, it is often convenient to work with a parameter called the "Sheet resistance"[45].

Considering the resistance (R) of a rectangular block of uniform material (Figure 1.21), the resistance is given by:

$$R = \frac{\rho \times L}{A}, \tag{1.19}$$

where ρ is the resistivity of the sample and L and A are its length and cross-section area. If W is the width of the sample and t is its thickness (i.e., $A = W \times t$), then the equation (1.19) can be written as

$$R = (\frac{\rho}{t})(\frac{L}{W}) = R_S\ (\frac{L}{W}) \tag{1.20}$$

Where $R_S = \frac{\rho}{t}$ is the sheet resistance of a layer of this material, strictly speaking, the unit for sheet resistance is the ohm (since L/W is unitless). To avoid confusion between R and Rs, however, sheet resistance is specified in unit of "ohms per square." indicating that a square of any side which has the same resistance.

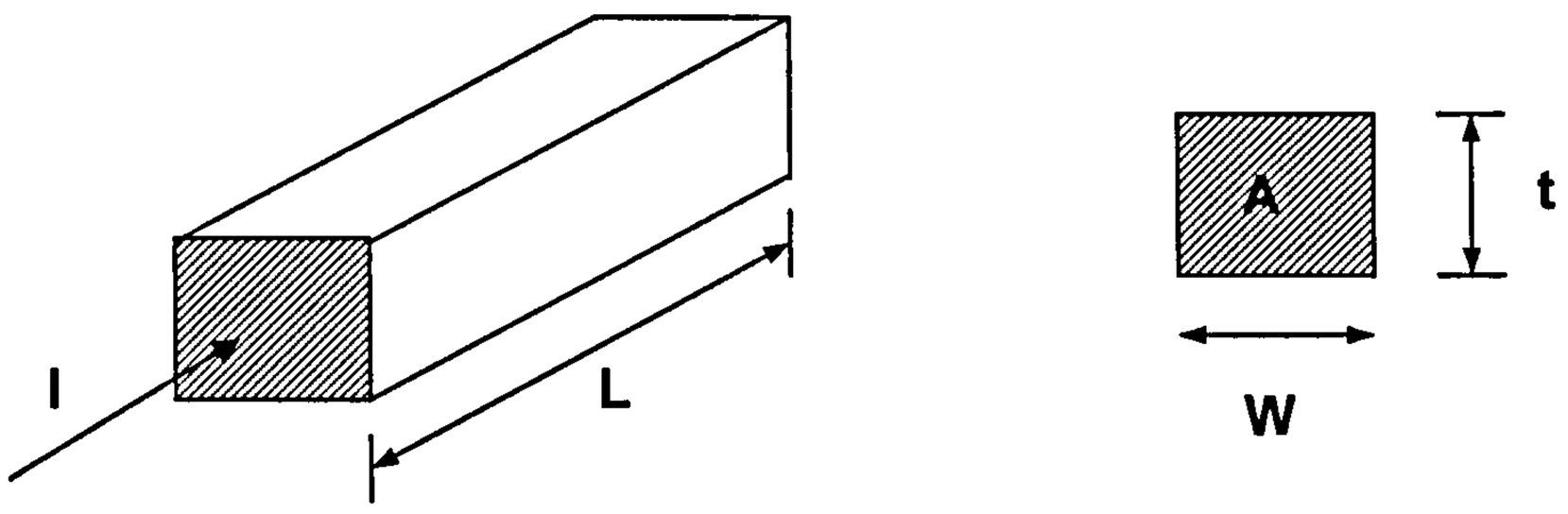

Figure 1.21 The figure used to describe the concept of sheet resistance.

Chapter 2 Experimental details

2.1 Materials

Table 2.1 describes the materials used in these experiments and lists their sources. The alumina is a fine milled submicron powder which is widely used in industry. The TiO_2 is an anatase pigment used in paint formulations. The zirconia, selected for calibration using EDS is additive-free to avoid the confounding effects of dopant oxides. High purity barium titanate is crystallographically cubic and suitable for use in formulating X7R (reference page. 35) compositions. The dispersant is a solution of an ammonium salt of a polyacrylate widely used to stabilise oxides in aqueous media.

2.2 Equipment

The equipment used for these combinatorial experiments includes an aspirating-dispensing ink-jet printer, a furnace, an impedance analyzer and its accessories and a two-axis measurement table fitted with a hotplate. These are combined within a gantry robot and described in detail in what follows. Other equipment used in the experiments described in this chapter is listed in Table 2.2.

2.2.1 The aspirating-dispensing ink jet printer

The printer (ProSys 4510, Cartesian Ltd, Huntingdon, Cambridge) is based on SynQUAD^{TM} dispensing technology described in section 1.8.1. The specification of dispensing and aspirating abilities of the printer was described in Table 1.4. Figure 2.1 is a photograph of the printer. The printer head is fitted with eight nozzles each having an independent dispensing system. The nozzles can automatically visit a cleaning station for purging, external washing, ultrasonic cleaning and air drying. The printer head can move with 1μm resolution in x-y-z directions on a 425 mm × 540 mm table holding one hundred 76mm x 25mm ceramic substrates. The printer is controlled by AxSys^{TM} software that is used to program complex tasks involving aspirating-dispensing of solutions to precise

locations. AxSys™ software runs in a Personal Computer (PC) (Pentium 3, Windows 95).

Table 2.1 Materials and their sources

Material	Suppliers	Grade	Purity	Density / kgm^{-3}	Average particle diameter / μm
Al_2O_3 powder	Alcoa, Ludwigshafen, Germany	A16-SG	99.8%	3987	0.5
TiO_2 Powder	Tioxide Europe SA, Calais Cedex, France	A-HR	99.0%	3850	0.15
ZrO_2 powder	PI-KEM LTD, Wem Shropshire, England	_	99.5%	5750	0.9
$BaTiO_3$ Powder	TPL Inc, NE Albuquerque, USA	HPB 1000	_	5700	0.05
Dispersant	Allied Colloids Ltd, Bradford, England	Dispex A40	46.54% in aqueous solution	1300	_
Distilled water	Made by the merit water still, W4000 Bibby Sterilin Ltd, Staffordshire, UK	_	_	1000	_
Silver paste	Johnson Matthey plc, Royston Herts, UK	M4516	_	_	_

Table 2.2 Ancillary equipment used in the experiments

Equipment Name	Mode / brand	Supplier	Application	Specifications
Analytical balance	ADA 102LE	Adam Equipment, Inc. New Milford, USA	Determination of mass	Resolution is 0.1mg
Ultrasonic probe	U200S, Control	IKA Works, Inc. Staufen, Germany	Mixing and dissolution	20 kHz
Oven	_	Gallenkamp plc, Loughborough, UK	Drying	Maximum temperature 300°C
Sample vial	_	Nalge Ltd, Hereford, UK	Ink containers	Capacity: 75ml. Polyethylene vials.
Cylinder	MBL	Bibby Sterilin Ltd, Staffordshire, UK	Determination of volume	Capacity:10ml, divided in 0.2 ml
Test Tube	PYREX	Bibby Sterilin Ltd, Staffordshire, UK	Sedimentation experiment	Capacity:10ml, divided in 0.2 ml
Crucibles	_	Haldenwanger, Berlin, Germany	Loss on ignition experiment	Maximum temperature: 1200°C
96-micro well plate	_	Nalge Nunc International Rochester, USA	Ink containers	0.5ml / well. Round-bottom
Pipette	_	Samco scientific corporation, San Fernando, U.S.A	Aspirate inks.	_
Press	_	Bradley & Turton, Kidderminster, UK	Compaction of powder	_
Calliper	_	Mitutoyo UK ltd, Hampshire, UK	Measure the geometry of ceramics	Resolution is 0.02mm
Micrometer	_	RS Components Ltd, Northants, UK	Measure the geometry of ceramics	Resolution is 0.01mm
The high temperature wire	FLHT	RS Components Ltd, Northants, UK	Wiring of equipment	Operating temperature -55°C to +200°C. Conductor diameter 1.5 mm.

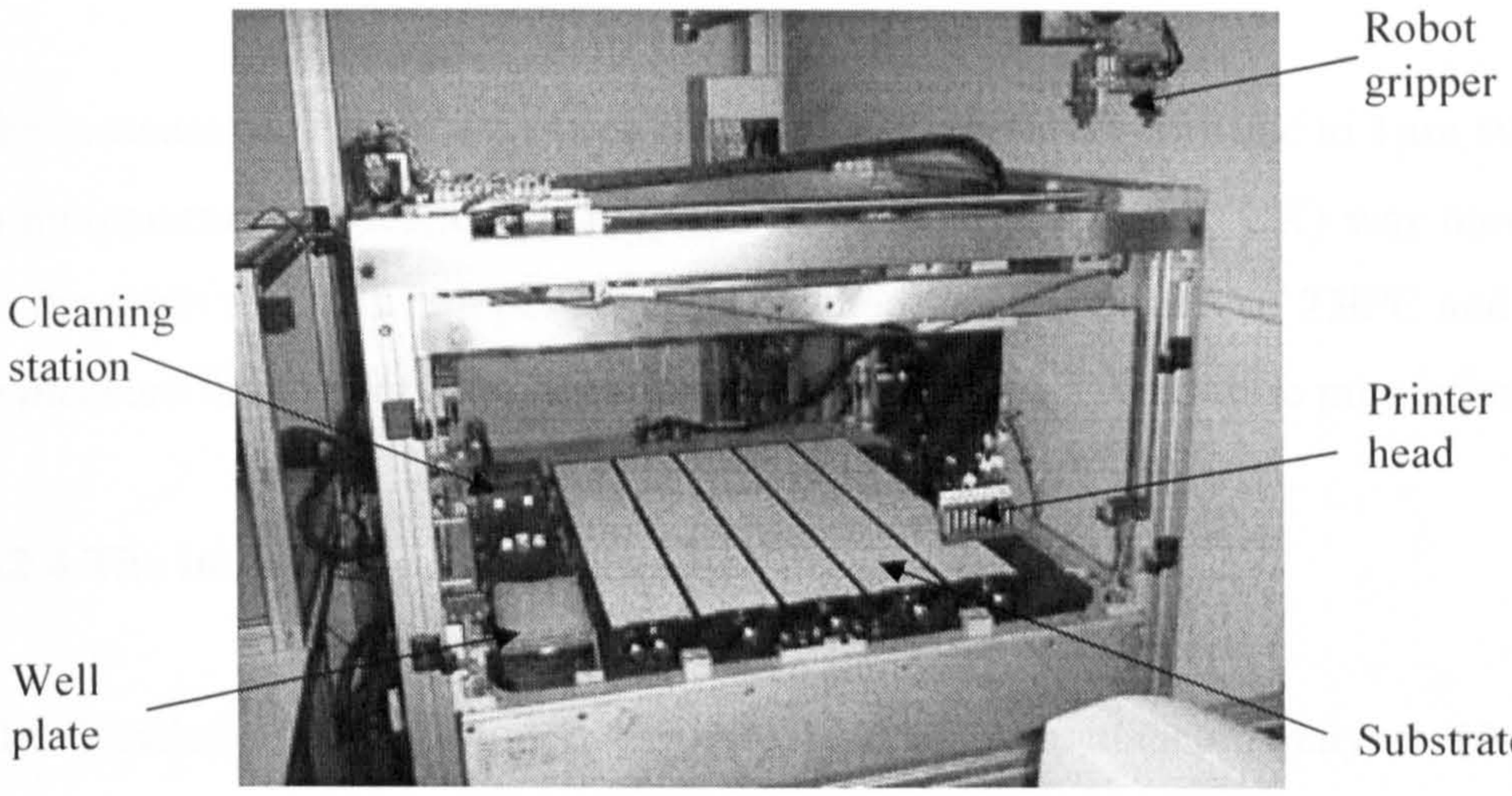

Figure 2.1 ProSys 4510 printer integrated with a large-scale combinatorial robot

2.2.2 The furnace

The furnace was manufactured by Elite Thermal Systems Ltd, Leicestershire, UK and is shown in Figure 2.2. The furnace has four chambers, individually heated and controlled. The maximum operating temperature of the furnace was 1600°C. The top half of the furnace can be raised into the vertical position to allow the robot to transfer samples into the furnace for densification and to relocate the samples after firing.

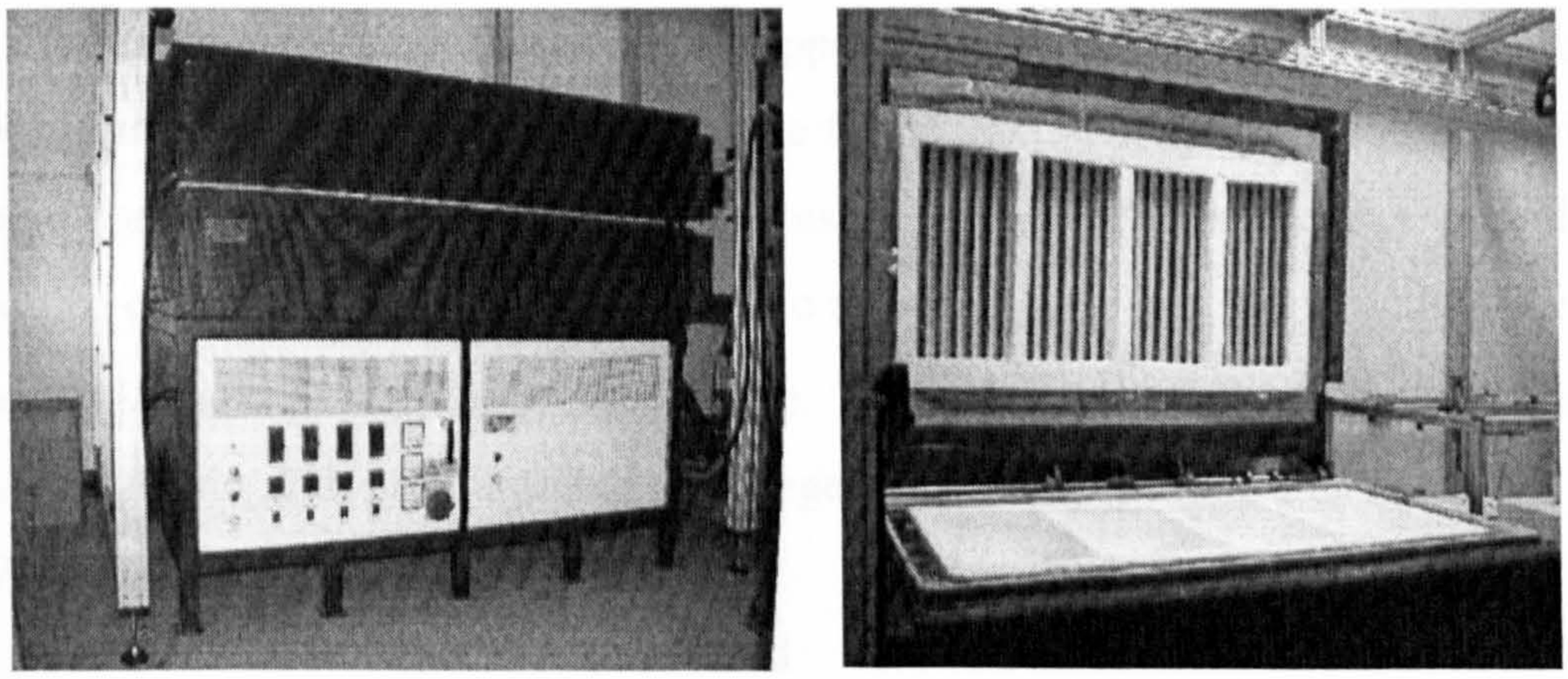

Figure 2.2 The furnace used in the combinatorial experiments

2.2.3 The measurement table and hotplate

The measurement table measures 500mm × 600mm and is precise to 1μm subject to temperature fluctuation. A hotplate (Elmatic Ltd, Cardiff, UK) was mounted on the table and was independently controlled to a maximum of 250°C and used to measure the temperature dependence of, for example, dielectric properties.

2.2.4 The impedance analyzer and its accessories

The Hewlett-Packard Model 4294A (HP4294) Impedance Analyser (Agilent Technologies UK Ltd, West Lothian, Scotland) was used to measure dielectric constants of the samples. The technique of permittivity measurement is based on the auto balancing bridge method described in section 1.4.4. The impedance analyser can measure dielectric properties of samples at one specified frequency or across a range of frequencies (i.e. any range between 40 Hz to 110 MHz). Two types of probe were used in the experiments. One is the probe provided by Agilent, a model 16074A test fixture that covers a frequency range from DC to 13MHz. The other is a user-designed robotic probe as described in section 2.7.

2.2.5 The robot

The printer, the furnace and the hotplate are all contained within a robotic gantry as shown in Figure 2.3. The robotic gripper can pick up each substrate from the printer table and move it from one stage to the next. The robot is manufactured by Labman Automation Limited, Stokesley, UK. The manufacturer provided source codes that can move the gripper to a specified x-y-z position with 100 μ m resolution and pick up or release a slide. The source code is implemented using Visual basic 6.0 programming language and running in a PC (Pentium 3, Windows 2000).

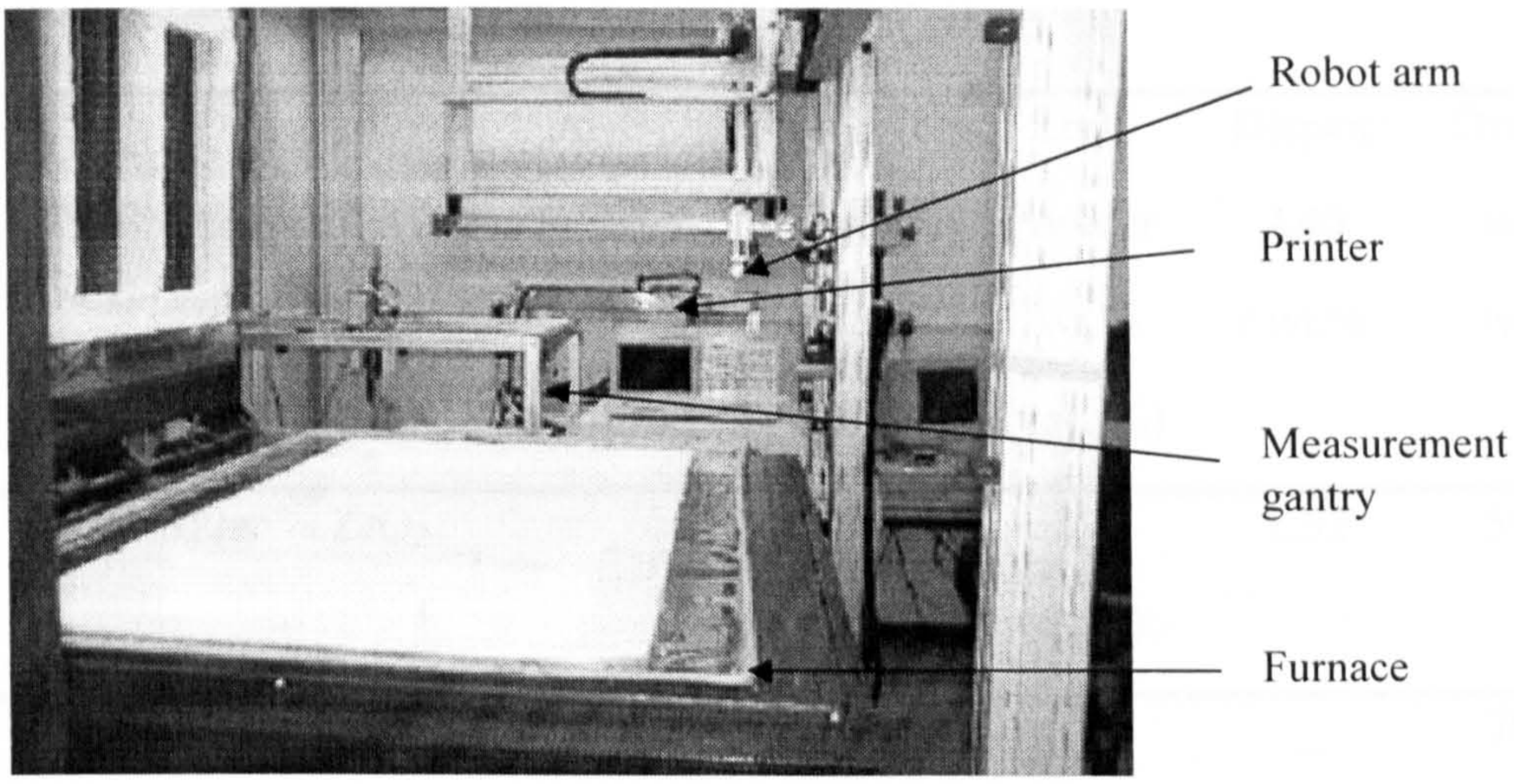

Figure 2.3 The printer, the furnace and the measurement table are all within a robotic gantry.

2.3 Ceramic ink preparation

Table 2.3 gives the compositions of all inks used in this thesis. The common procedure for creating ZrO_2, Al_2O_3 and TiO_2 inks was: after weighing using the analytical balance, powder, distilled water and Dispex A40 (Dispex A40 was only used in ZrO_2 and Al_2O_3 ink) were transferred to a 75ml polyethylene sample vial. The vial containing the mixture was subjected to ultrasonic disruption by the ultrasonic probe pulsed at duty cycle 0.5 and 75% amplitude for 1ks.

A sample of 50 wt% $BaTiO_3$, 15 wt% Dispex A40 and 35 wt% distilled water were weighed and transferred into the sample vial. The vial containing the mixture was subjected to ultrasonic disruption pulsed at duty cycle 0.5 and 75% amplitude for 1ks. The mixture was left for sedimentation for 5 minutes. The liquid mixture was transferred into a tube and the sediment left in the sample vial. The inks in the tube were used as $BaTiO_3$ ink whose composition was worked out from Loss on Ignition experiments as described in section 2.5.2. The ink contains 53.88 wt% $BaTiO_3$, 7.7 wt% Dispex and 38.42wt% distilled water.

Table 2.3 Master table of ceramic ink compositions.

Ink ID *	Designed Composition	Al_2O_3 Powder / wt.% (vol. %)	TiO_2 Powder /wt.% (vol. %)	ZrO_2 Powder /wt.% (vol. %)	Dispex A40 / wt.%	Distilled water /wt.%
A	100wt% ZrO_2	_	_	38.83 (9.99)	1.52	59.65
B	100wt% TiO_2	_	29.93 (9.99)	_	_	70.07
C	100wt% Al_2O_3	30.46 (9..92)	_	_	0.77	68.77
D	$Al_2O_3$50-ZrO_2 50	17.07	_	17.07	1.1	64.76
D'	$Al_2O_3$50-ZrO_2 50	17.07	_	17.07	_	64.76+1.1
E	$Al_2O_3$50-TiO_2 50	15.1	15.1	_	0.38	69.42
F	TiO_2 50-ZrO_2 50	_	16.9	16.9	0.66	65.54
F'	TiO_2 50-ZrO_2 50	_	16.9	16.9	-	65.54+0.6
G	Al_2O_3 25-TiO_2 25- ZrO_2 50	8.49	8.49	16.98	0.88	65.16
H	$Al_2O_3$50-ZrO_2 50	17.07	-	17.07	10	55.86
I	$TiO_2$50- ZrO_2 50	-	16.9	16.9	10	56.2
J	Al_2O_3 25-TiO_2 25- ZrO_2 50	8.49	8.49	16.98	10	56.04

* Ink A, B and C are named as ZrO_2 ink, TiO_2 ink and Al_2O_3ink respectively through the thesis.

2.4 Substrate preparation

The printer was used to print combinatorial libraries on platinum-coated 99.8% α-alumina substrates (Advanced Ceramics Ltd, Stafford, UK). Two approaches to platinum coating were explored.

(a) Evaporation of Platinum

Alumina substrates were first cleaned by submersing in chromic acid (concentrated sulphuric plus CrO_3) for 43.2ks in order to clean the surface of organic contamination. The cleaned substrates were transferred to a vacuum coating unit (Edwards High Vacuum Ltd, West Sussex, England). 100mm platinum wire with diameter 0.2mm (99.95% pure, Agar scientific, Essex, England) was mounted onto the tungsten filament. There was approximately 100mm distance between the tungsten filament and alumina substrates. The wire was evaporated using a high DC current supply. The coating process was repeated twenty times to achieve sufficient thickness and conductance.

(b) Coating with Platinum Ink

Platinum ink (64021001, Ferro Corporation, Hanau, Germany) was painted on alumina substrates using a small brush. The painted substrates were dried in the oven at 60 °C for 0.9ks and then fired in the furnace for 2.4ks at 1400°C.

To study loss of platinum during firing, the platinum-coated substrates produced by both approaches were fired at 1600 °C for 7.2ks. The sheet resistance of the platinum coating layer was measured using a multi-meter (Model: IDM63, ISO-TECH, Southport, England) illustrated as Figure 2.4. The wetting characteristics of platinum coated substrates were also studied by depositing $BaTiO_3$ inks using a pipette to examine whether inks can form a confined drop or spread.

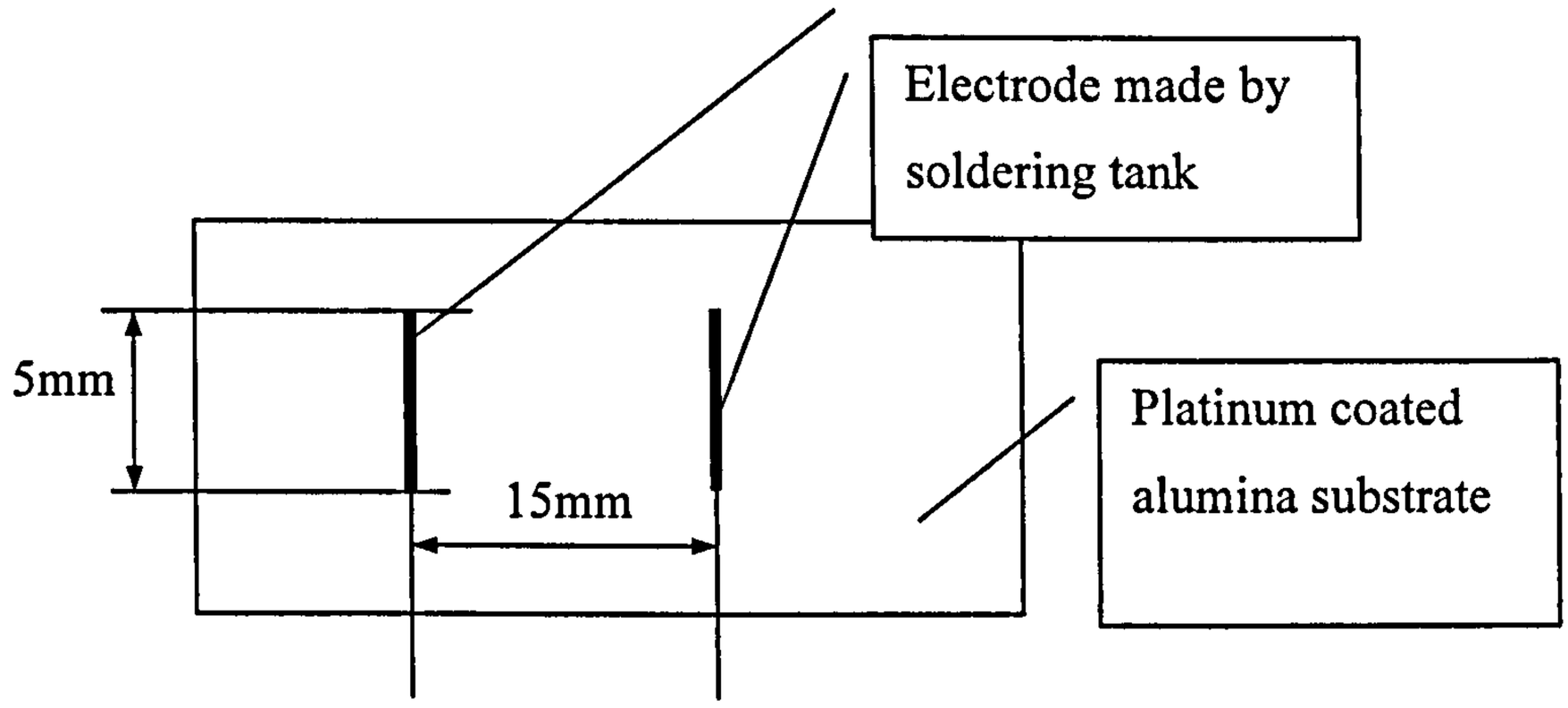

Figure 2.4 The measurement of sheet resistance of the platinum coating.

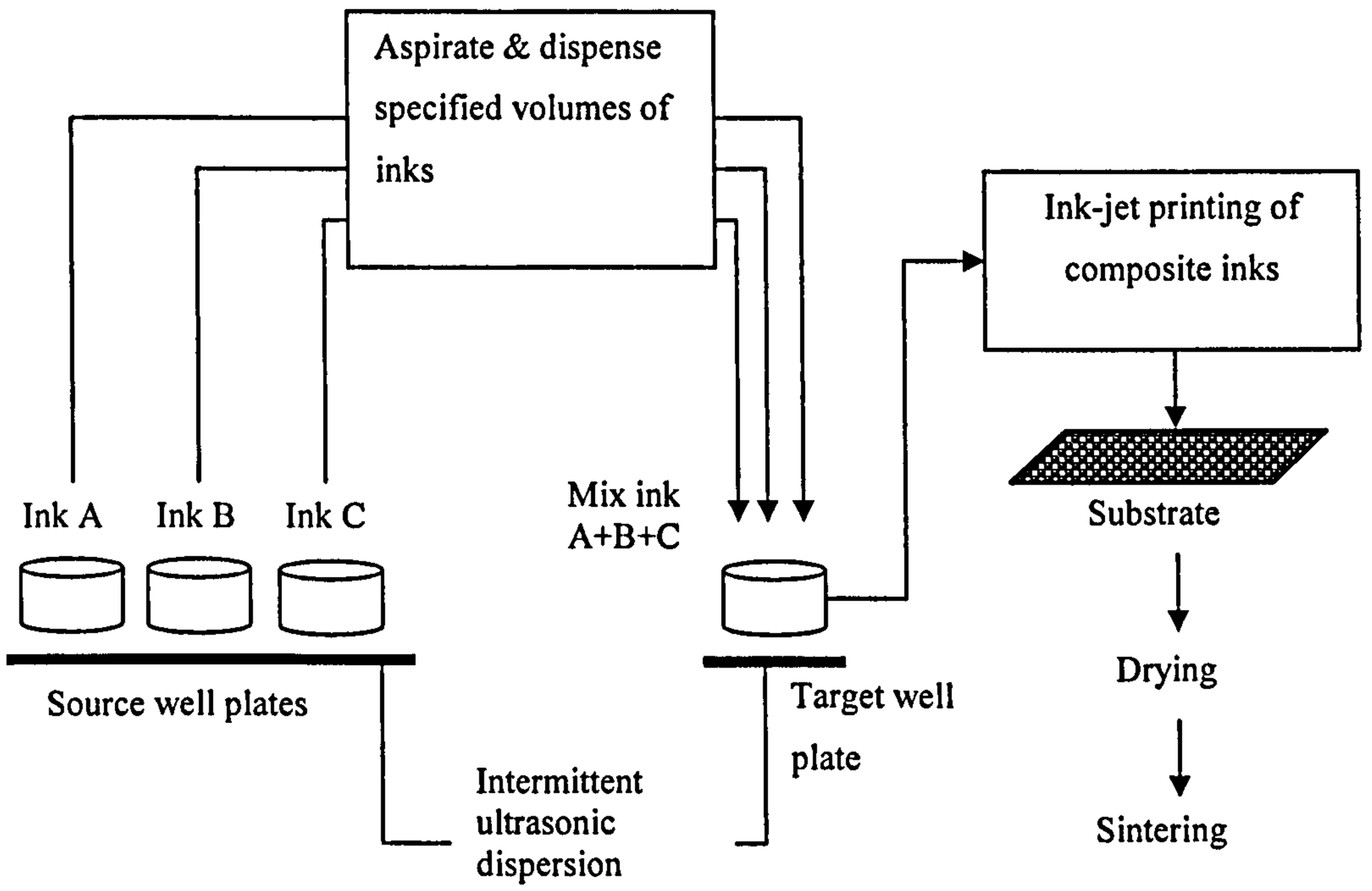

Figure 2.5 The process of preparing ceramic mixtures using an aspirating-dispensing printer.

2.5 Compositional calibration of the ink-jet printer

As reviewed in section 1.6, the conventional way of preparing ceramic mixtures involves: calculation and weighing of powders; milling (dry or wet); drying if using wet milling; calcining; milling; shape forming and finally densification. A new approach, creating ceramic compositions using an aspirating-dispensing printer, was developed and explored in this research. Basically, the printer can transfer specified volumes of several ceramic inks into a well to build a target composite ink as illustrated in Figure. 2.5. The motivation behind this new approach is not only to fulfil the automation requirement of combinatorial methods but also to explore a more efficient and possibly better way of assembling ceramic mixtures and forming functional gradients.

The following example describes the procedure for creating ceramic mixtures using the aspirating-dispensing printer. Suppose the aim is to create a ceramic composition consisting of 50 wt. % Al_2O_3 and 50 wt. % TiO_2:

Step1: Ink preparation. Prepare 10 vol. % water-based Al_2O_3 and 10 vol. % water-based TiO_2 ceramic inks.

Step2: Calculation of transfer volumes. Equations 2.1 and 2.2 give the general formulae for calculation of transfer volumes,

$$V_a + V_b = V_{total}, \tag{2.1}$$

$$\frac{V_a \times Avol.\% \times \rho_a}{V_a \times Avol.\% \times \rho_a + V_b \times Bvol.\% \times \rho_b} \times 100\% = Awt.\%, \tag{2.2}$$

Where V_a and V_b are the volumes of transferred inks A and B, respectively; V_{total} is the volume of the composite ink; A vol. % and B vol. % are the volume percentage of ceramic powders in inks A and B, respectively; ρ_a and ρ_b are the densities of powders A and B, respectively; A wt. % is the weight percentage of A in the ceramic composition. Suppose the aim is to make

0.3ml composite ink. The density of Al_2O_3 powder is 3987 kgm^{-3}. The density of TiO_2 powder is 3850 kgm^{-3}. Thus the equation 2.1 and 2.2 becomes,

$$V_{Al_2O_3} + V_{TiO_2} = 0.3ml\,, \tag{2.3}$$

$$\frac{V_{Al_2O_3} \times 10vol.\% \times 3987kgm^{-3}}{V_{Al_2O_3} \times 10vol.\% \times 3987kgm^{-3} + V_{TiO_2} \times 10vol.\% \times 3850kgm^{-3}} \times 100\% = 50wt.\% \tag{2.4}$$

From equations 2.3 and 2.4, the transfer volume of Al_2O_3 ink is 0.1474ml; the transfer volume of TiO_2 ink is 0.1526ml.

Step 3: Programming the printer to mix inks. The pseudocode code is,

```
Start.
Loop 10 times.
{
    Aspirate 16 µl  TiO2 ink from source well plate.
    Loop 152 times /* Dispense 0.0152ml TiO2 ink */.
    {
        Dispense 0.1 µl  TiO2 ink into a well on the mix well plate.
    }
    Clean the nozzle and channel.

    Aspirate 16ul Al2O3 ink from the source well plate.
    Loop 147 times /* Dispense 0.0147ml TiO2 ink */.
    {
        Dispense 0.1 µl  Al2O3 ink into the well of mix well plate.
    }
    Clean the nozzle and channel.
}
```

Aspirate 2 μl TiO_2 ink from source well plate.

Loop 6 times / Dispense 0.0006ml TiO_2 ink */.*

{

Dispense 0.1 μl TiO_2 ink into the well of mix well plate.

}

Clean the nozzle and channel.

Aspirate 2 μl Al_2O_3 ink from the source well plate.

Loop 4 times / Dispense 0.0004ml Al_2O_3 ink */.*

{

Dispense 0.1 μl Al_2O_3 ink into the well of mix well plate.

}

Clean the nozzle and channel.

Aspirate specified volume of mixed ink from the mix well plate.

Print the composite ink on the target substrates in required pattern.

Clean the nozzle and channel.

Finish.

A volume of 0.1 *μl* was set as the base dispensing unit in order to control the dispensing error since the accuracy of printer dispensing varies with dispensing volume as described in Table 1.4. Using a ten times loop to complete transfer 0.152ml (0.0152 ml×10) TiO_2 ink and 0.147 ml (0.0147ml×10) Al_2O_3 ink rather than completing transfer at one time is intended to mix inks on small volume basis achieving homogeneous mixed ink with the help of ultrasonic disruption (as shown in Figure 2.5). To maintain the consistency of printer programs, transfer of ink is always done as two steps: (1) a ten times loop completes the main part of the transfer inks, (2) and then remaining part is transferred (e.g. 0.0006ml TiO_2 ink and 0.0004ml Al_2O_3 ink).

Step 4 Run the printer program.

Step 5 Dry printed samples on the substrates.

Step 6 Fire the printed samples.

The success of building composites using ProSys 4510 printer relies on: (1) Stable and homogenous ceramic inks that provided the correct base for step 2 calculation; (2) Dispensing technology that allows transfer of nanolitre volumes; (3) Achievement of homogenous liquid mixtures in the well plate though mixing processes by the printer and ultrasonic disruption. The dried ceramic mixtures after ink-jet deposition from the printer mixed composite inks should have uniform distribution of powder as the planned composition.

By building four compositions in the Al_2O_3-TiO_2-ZrO_2 system illustrated in Figure 2.6 as examples, a group of experiments was conducted to examine the accuracy of mixing ink compositions using the printer (Table 2.4). The remaining part of this section gives the details of these experiments.

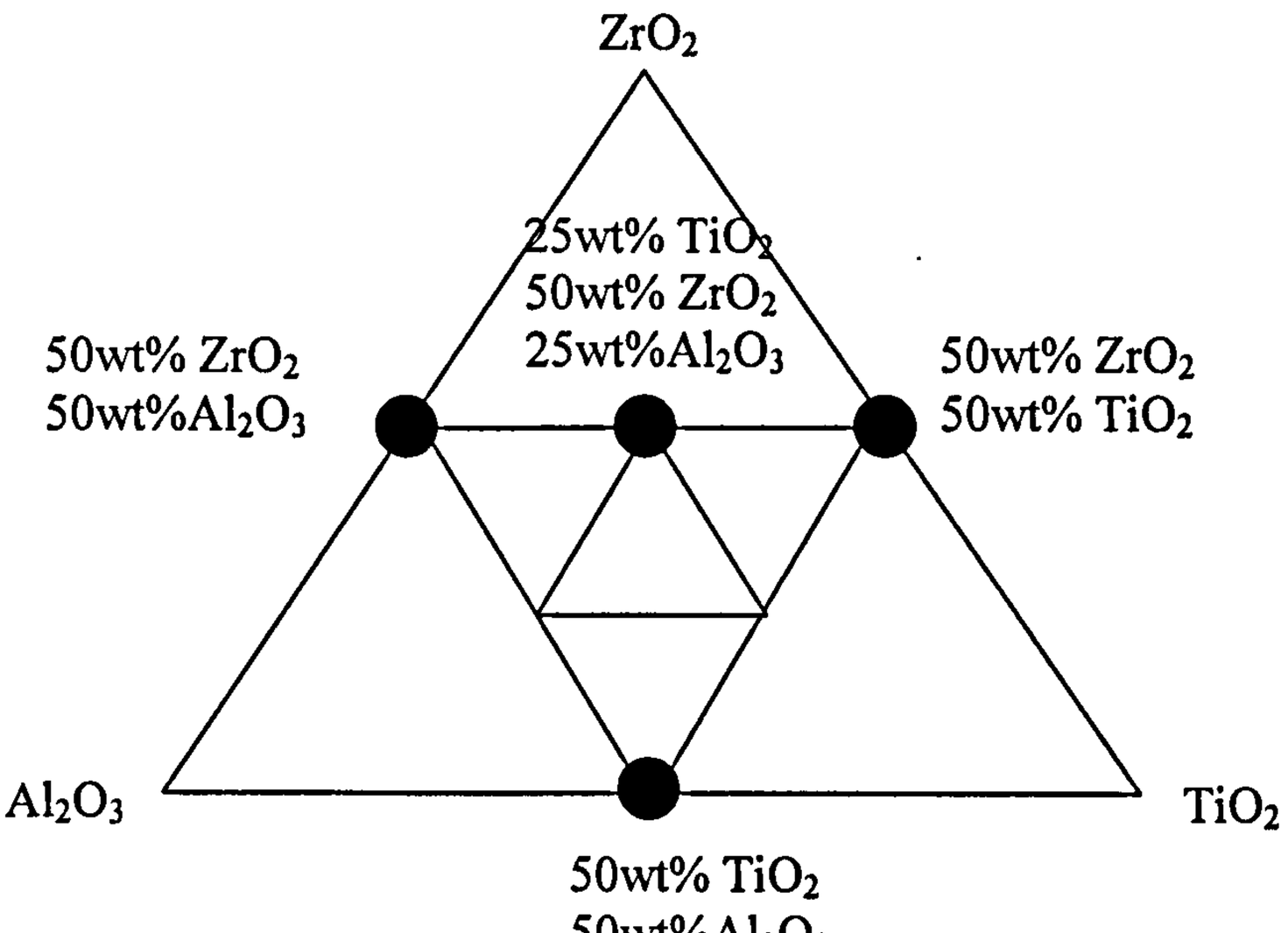

Figure 2.6 Four compositions in the Al_2O_3-TiO_2-ZrO_2 system used in compositional calibration of the ink-jet printer

Table 2.4 Summary of a group of experiments to examine the performance of preparing compositions using the ProSys 4510 printer.

Name	Description	Objective
Sedimentation	Study the sedimentation behaviour of Al_2O_3, ZrO_2 and TiO_2 ceramic inks.	To ensure these inks can be stable for sufficient time for use in later experiments.
Loss on ignition	Loss on ignition of water-based Al_2O_3, ZrO_2 and TiO_2 ceramic inks.	To confirm the mixing of powder and vehicles, so that the weight of powder can be calculated from volume of ink.
Evaporation	Study the evaporative loss of water-based ZrO_2 ink in the well plate as a function of time.	To examine how evaporative losses change the weight percentage of ceramic in water-based ink in the well plate as a function of time
Loss on ignition of transferred inks.	The printer transferred specified volumes of different inks into different crucibles, loss of ignition of these transferred inks was conducted.	To examine whether the printer can bring the supposed amount of each powder into a composite ink.
Suspension stability in the well plate	Build four ink mixtures in the Al_2O_3-TiO_2-ZrO_2 system using the printer. Observe these mixed inks for sedimentation behaviour.	To examine whether there are sediments in the mixed well plate after building composite inks, perhaps due to interaction of particles or dispersants.
Analysis of the printed ceramic samples	Examine two types of four composites in Al_2O_3-TiO_2-ZrO_2 system using EDX protocol. First type was manually-prepared composites. Second were printer-built composites.	To examine whether printed composites are what the user wanted to produce, compare the results with other mixing routes.

2.5.1 Sedimentation Testing

The objective was to study the sedimentation behaviour of Al_2O_3, ZrO_2 and TiO_2 inks as a function of time to ensure these inks were stable for sufficient time for use in printing experiments. Three 10ml samples Al_2O_3, ZrO_2 and TiO_2 inks were transferred to Pyrex test tubes. The test tubes were stoppered, sealed and the inks were left undisturbed to settle through the period of study. The sedimentation behaviour of inks was recorded as a function of time. Further, sedimentation tests were conducted by gently aspirating inks from well plates as described below.

2.5.2 Loss on ignition

The aim was to confirm that water-based ceramic inks were homogenous mixtures so that the weight of the suspended powder can be calculated from the volume of ink. Three 30g ZrO_2 ceramic ink samples were created. Five 2ml samples of ZrO_2 ink were placed in a weighed crucible and then weighed on the analytical balance. The volumes of inks were measured by the 10ml cylinders. The crucibles holding samples were transferred to the oven at 60 °C for two hours. After drying, the crucibles were weighed and put into the furnace at 700 °C for five minutes to remove dispersant. Upon ashing, the crucibles were weighed again. The weight percentage residues of five samples of ink were calculated. The same procedure of loss on ignition was carried for Al_2O_3 and TiO_2 inks as well.

2.5.3 Evaporation

The objective was to study how evaporative loss changes the weight percentage of water-based ink in the well plate as a function of time. 10g ZrO_2 ink was created. One well of the 96 well micro plate was filled with ZrO_2 ink and then weighed on the analytical balance. A paper cover was put on the well plate after filling inks. The cover was hand-made from silicone release paper as illustrated in Figure 2.7. There is a 2mm diameter circular opening in the cover that allows the printer nozzles to penetrate it. The well plate with the cover was previously weighed so that the weight of transferred ink can be calculated. The room

temperature was 26°C. The evaporative loss of inks from the well plate was recorded as a function of time.

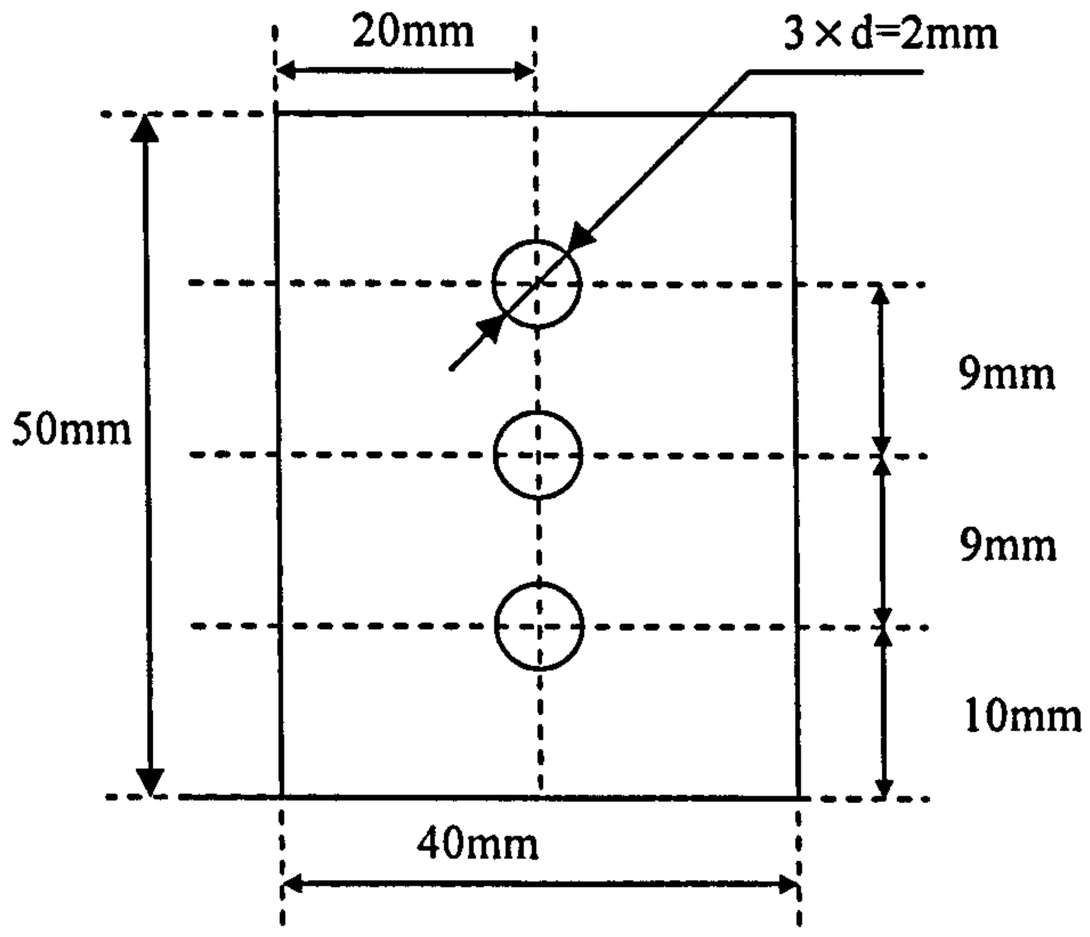

Figure 2.7 A paper cover of the 96-well micro plate

2.5.4 Loss on ignition of transferred inks

The specifications of the printer (Table 1.4) state there is finite accuracy of the printer transfer volumes. This experiment was intended to examine the overall performance of the printer used in ceramic applications by examining whether the printer can transfer a specified amount of powder that is dispersed in the ink into the target well plate. In section 2.5.6, the four compositions in the Al_2O_3-TiO_2-ZrO_2 system that were ink jetted from the mixed inks by the printer were subjected to Energy-dispersive X-ray spectrophotometry (EDS) analysis. Here, the question is whether their corresponding mixed inks (if there are no sediments) contained the correct amounts of each powder.

Three 10g stocks of Al_2O_3, ZrO_2 and TiO_2 ink were created. Table 2.5 gives the calculated transfer volumes of inks for each composition. Based on calculations described in section 2.5, for all the four compositions, the volume of the composite ink is 0.45ml. Appendix 1 gives the pseudocode used in the experiments, in which the printer transferred the calculated volumes of inks from the source well plate into crucibles. After running the printer programs, the

transferred inks in crucibles were subjected to loss on ignition following the procedure of section 2.5.2. Thus the weights of transferred powders were obtained and compared to the planned values in table 2.5. Each program was run three times to build an assessment of confidence limits.

Table 2.5 The programmed transfer volumes of inks for four compositions in the Al_2O_3-TiO_2-ZrO_2 system to build 0.45mL composite inks.

§ Composition	The programmed transfer volumes of ZrO_2 ink (The weight of ZrO_2 powder in inks)	The programmed transfer volumes of Al_2O_3 ink (The weight of Al_2O_3 powder in inks)	The programmed transfer volumes of TiO_2 ink (The weight of TiO_2 powder in inks)
50wt% ZrO_2 50wt%Al_2O_3	0.1835mL (0.1054g)	0.2665mL (0.1054g)	_
50wt% TiO_2 50wt%Al_2O_3	_	0.2219mL (0.0878g)	0.2281mL (0.0877g)
50wt% ZrO_2 50wt% TiO_2	0.1805mL (0.1037g)	_	0.2695mL (0.1037g)
25wt% TiO_2 50wt% ZrO_2 25wt%Al_2O_3	0.182mL (0.1045g)	0.1323mL (0.0523g)	0.1357mL (0.0522g)

§ In this table, the error in weight percentages of compositions caused by rounding the limitation of weighing accuracy to match the calculation was below 0.1%.

The weight of ZrO_2 powder in ink = volume of ink $\times 9.99vol\% \times 5750kgm^{-3}$

The weight of Al_2O_3 powder in ink = volume of ink $\times 9.92vol\% \times 3987\ kgm^{-3}$

The weight of TiO_2 powder in ink = volume of ink $\times 9.99vol\% \times 3850\ kgm^{-3}$

(The volume percentage of ceramic powders in each ink is from Table 2.3. the density of each powder is from Table 2.1)

2.5.5 Observation of composite inks

This section examines whether there are sediments in the mixed well plate after building composite inks, perhaps due to interaction of particles or dispersants. Three 10g stocks of Al_2O_3, ZrO_2 and TiO_2 ink were created. Table 2.5 gives the

calculated transfer volumes of inks for each composition. Appendix 1 gives the pseudocode used in the experiments, in which the printer reformatted the well plate to build composites inks. After running printer programs, the mixed inks in the well were gently aspirated using the pipette. The well was inspected for residues.

2.5.6 EDS Protocol

The aim of the EDS scans was to examine the dried ceramic mixtures after ink-jet deposition from the printer-mixed composite inks. These should be homogenous mixtures having the planned compositions. These results were subsequently compared with the results for manually mixed and deposited ceramic mixtures. This work uses the four compositions in the Al_2O_3-TiO_2-ZrO_2 system (Figure 2.6) as calibration cases.

The printer-built ceramic mixtures

Three 10g stocks of Al_2O_3, ZrO_2 and TiO_2 ink were created. Table 2.5 gives the calculated transfer volumes of inks for each composition. The part of the pseudocode for building composite ink samples is the same as the pseudocode used in section 2.5.5. After building composite inks, the printer aspirated them and dispensed $5\,\mu l$ inks onto the silicone release paper (Sterling Coated Materials, Cheshire UK) to form an ink-jet printed sample. After printing, the samples were left in air for 3.6ks and taken from the silicone release paper for EDS protocol without firing.

The manually prepared ceramic mixtures

Table 2.3 (ink D, E, F and G) give compositions of ceramic liquid mixture for the four compositions. These inks were prepared to give the same compositions as those produced by mixing the single component inks (i.e. Ink A, B and C) in Table 2.3. It was intended to compare EDS results of two types of ceramic mixture (i.e., the printer-built and the manually prepared) in the same base

because different amounts of Dispex A40 and distilled water may have different effects to the drying process of the composites.

After weighing, powders were mixed with half the amount of water first in a 75ml polyethylene sample vial and then dispersant was mixed with the other half of water and then added. The vial containing the mixture was subjected to ultrasonic disruption by the ultrasonic probe pulsed at cycle 0.5 and 75% amplitude for 1ks. For each composition, 10g ceramic liquid mixture was prepared. After ultrasonic mixing, the mixtures were deposited on the silicone release paper using a fine copper wire and left in air for 3.6ks. After drying, they were lifted from the silicone release paper and subjected to the EDS protocol, so that nominally identical printer-built and manually-prepared identical compositions could be directly compared.

EDS Analysis

Both the dried printer-built samples and the manually prepared samples had a bulk radius of ~ 1mm. The top surfaces, the bottom surfaces and the cross-sections were analysed as illustrated in Figure 2.8. The samples were coated with carbon and studied using scanning electron microscopy (SEM; Model 6300, JEOL, Tokyo, Japan) equipped with an EDS system (Model eXL II, Oxford Instruments, Bucks, UK). Measurement was taken over an area approximately 150 μm × 150 μm for the surface and 50 μm × 50 μm for the cross section for a period of 100s. The conditions were 20kV acceleration voltage and 15mm working distance. The data were corrected using INCA software (Oxford Instruments). Cobalt was used as a standard for calibration of the analyzer.

Viscosity and surface tension measurement of suspensions

It is useful to know the viscosity and surface tension of ceramic suspensions when studying the EDS result of the ceramic mixtures. The viscosity and surface tensions of ink D, H, F and I (Table 2.3) were measured at 25 °C using a reverse flow U-Tube viscometer following BS 188:1977 and the du Noüy ring detachment method, respectively. The U-tube was previous calibrated using

standard viscosity calibration oil (Poulten Selfe & Lee Ltd, Essex, England). The ring method was calibrated using both distilled water and ethanol.

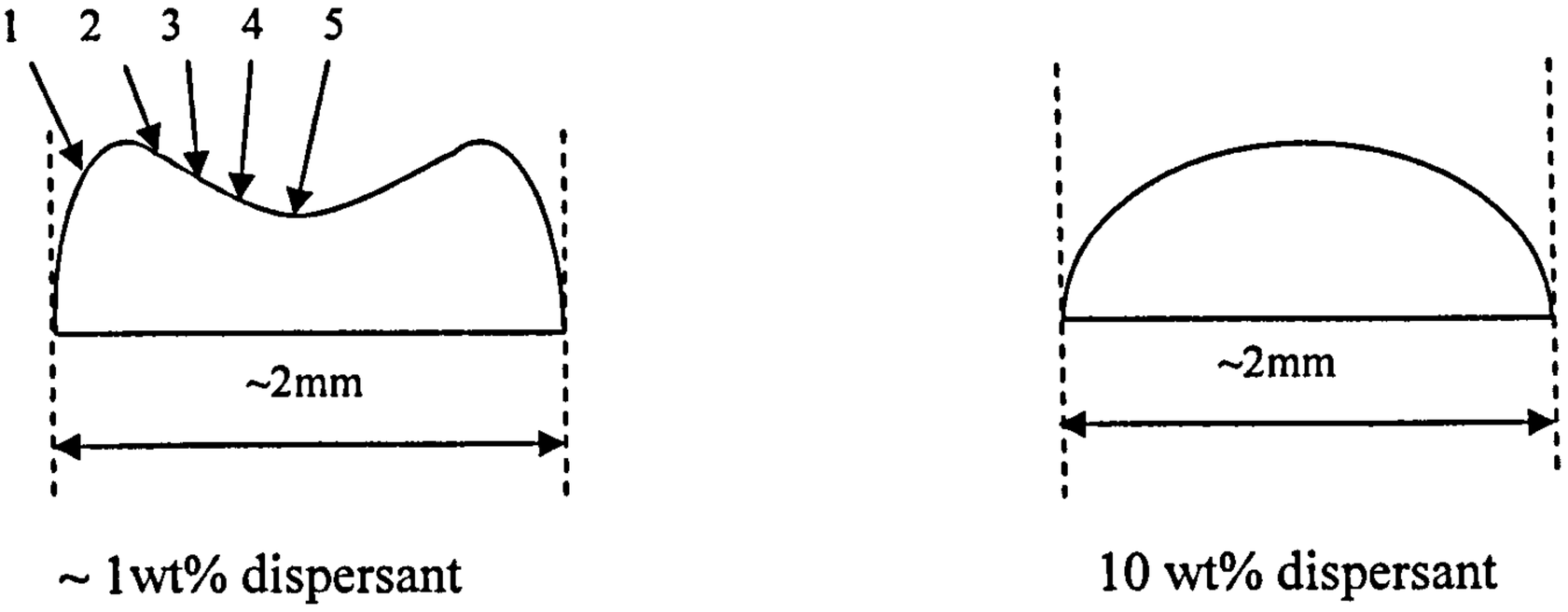

(a) Dried sample profiles

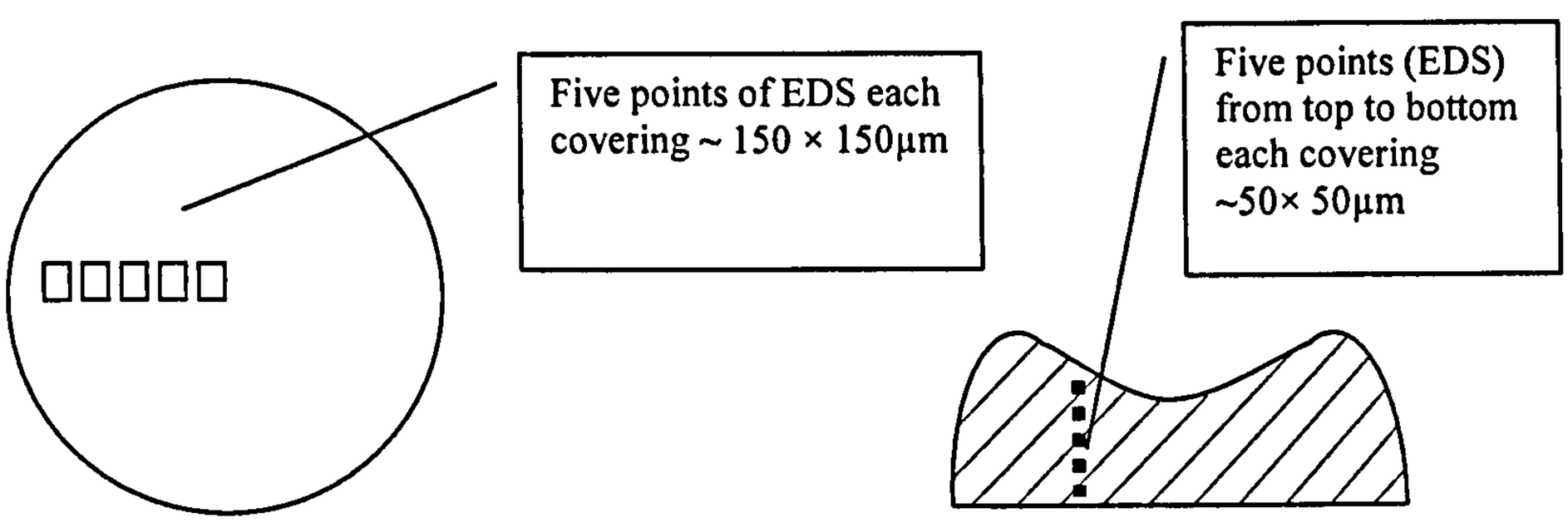

(b) Upper sample surface

(c)The cross-section of the sample

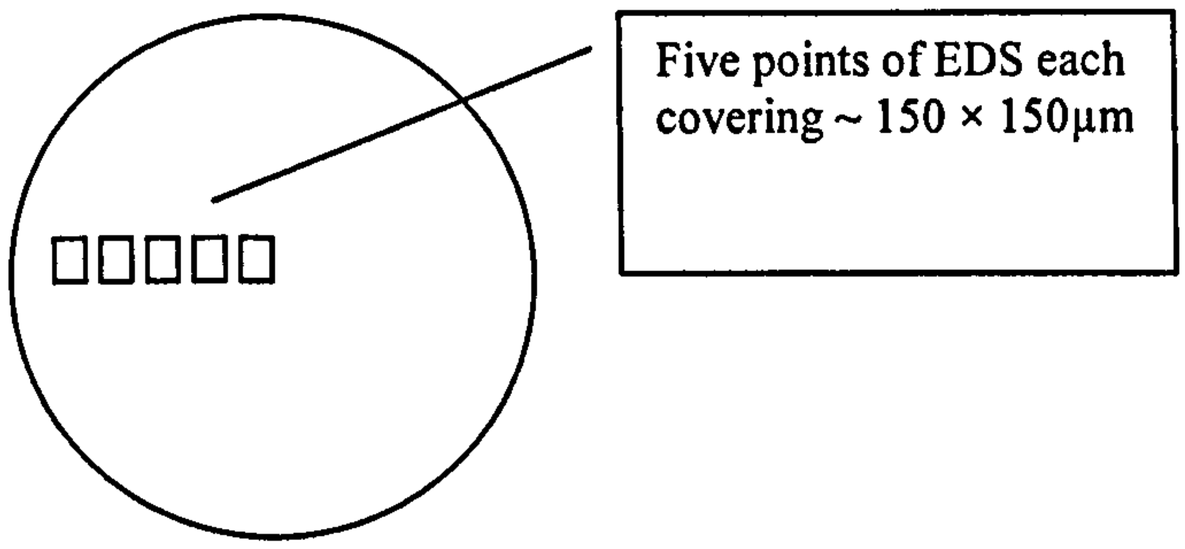

(d) Lower sample surface

Figure 2.8 EDS measurement were made along the top and bottom surfaces and through the cross-section of the samples.

2.6 Drying behaviour of droplets of mixed powder suspensions

Members of the combinatorial library are formed from dried ceramic ink droplets. It is important to study drying behaviour of a sessile droplet of mixed powder suspensions because both compositional distribution and residue shape are established during drying. As discussed in section 1.9.3, the drying behaviour of a droplet deposited on a horizontal non-porous substrate is affected by (1) the wetting characteristics of the substrate (2) the temperature and atmospheric conditions, and (3) the properties of the droplet itself.

All inks (table 2.3) were mixed manually by weighing and deposited manually from a wire knib at room temperature and and ambient air conditions (31% R.H). Each drop was approximately 5μl. The substrate was silicone release paper having a surface free energy of 20 mNm^{-1}. The drying was observed by optical microscopy and classified. Several examples of drying were imaged as a function of time by a video camera (model 4540, Eastman Kodak Co., San Diego, USA). The contact angle θ, contact diameter D, and height of droplets H, were computed from the images as illustrated in Figure 2.9.

The mass loss from droplets was measured at 20 °C and 31 % RH on the analytical balance. The initial masses of droplets were controlled as 11mg, being approximately 8μl. The mass change was recorded at every 180s over a period of 3.6 ks. The mass loss experiments were performed on both The ZrO_2- Al_2O_3 system (Inks D, D'and H) and the TiO_2-ZrO_2 system (Ink F, F' and I).

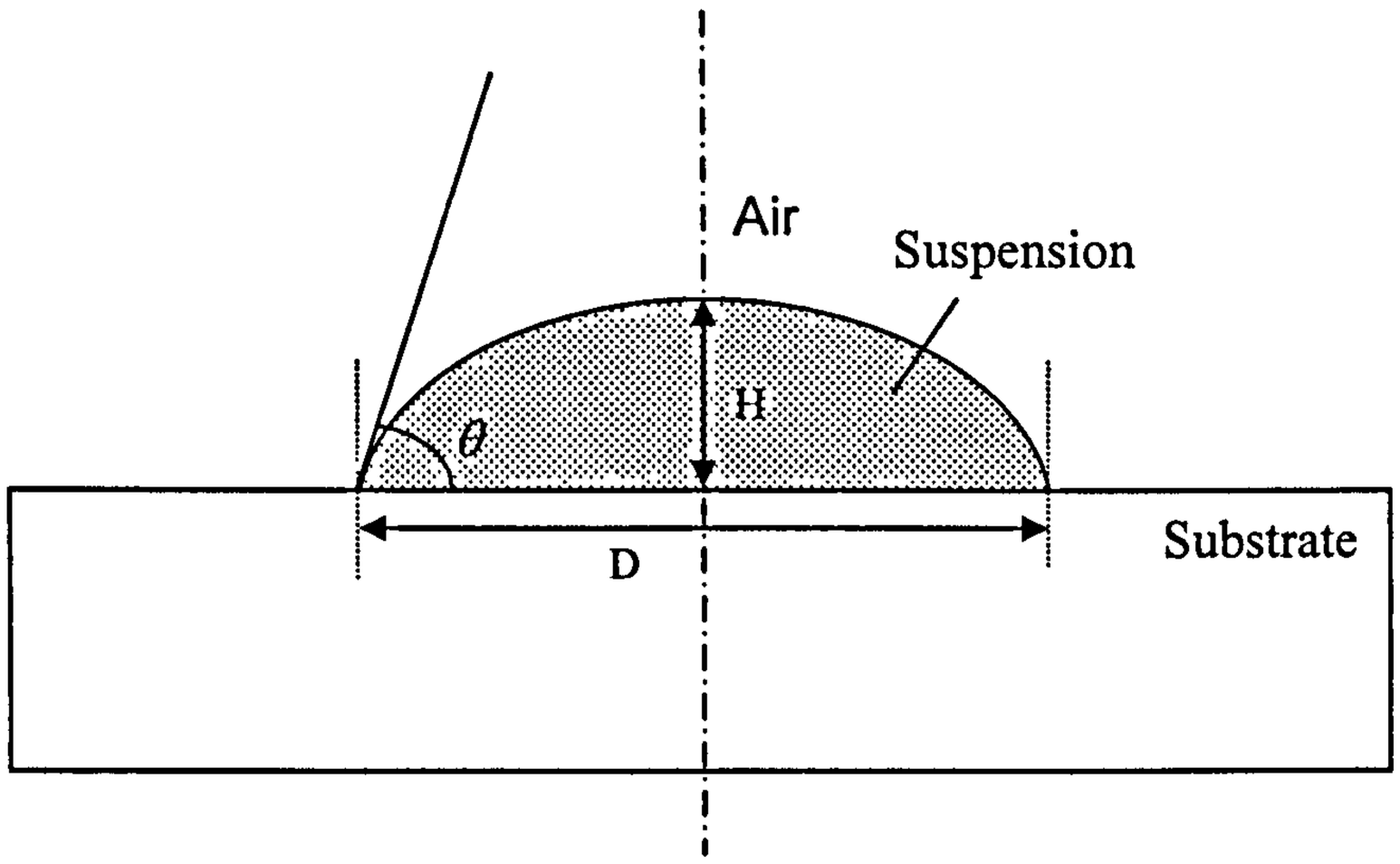

Figure 2.9 Schematic representation of a sessile drop of ceramic suspension

2.7 Calibration of dielectric measurement in the combinatorial method

The combinatorial method reported in this thesis was used to measure relative permittivity of ceramics as a function of temperature or frequency. Figure 2.10 illustrates the procedure. The ink-jet printer printed combinatorial libraries on platinum-coated alumina substrates. After firing, the substrates were robotically placed on a hotplate. Each sample was then stamped by one copper electrode which had been inked with the silver paste. The libraries were then returned to the furnace for a second firing at 800°C for 20 min. After firing; the substrates were relocated on the hotplate. The robotic dielectric probe visited each sample in the libraries and the computer collected experimental data from a HP4294 impendence analyzer, which processed these data, calculated relative permittivity from capacitance and stored information in the database. Table 2.6 lists a group of experiments that were used to calibrate the combinatorial dielectric measurement. In all experiments, relative permittivity k' was calculated from the formula 1.13 in section 1.4.4.

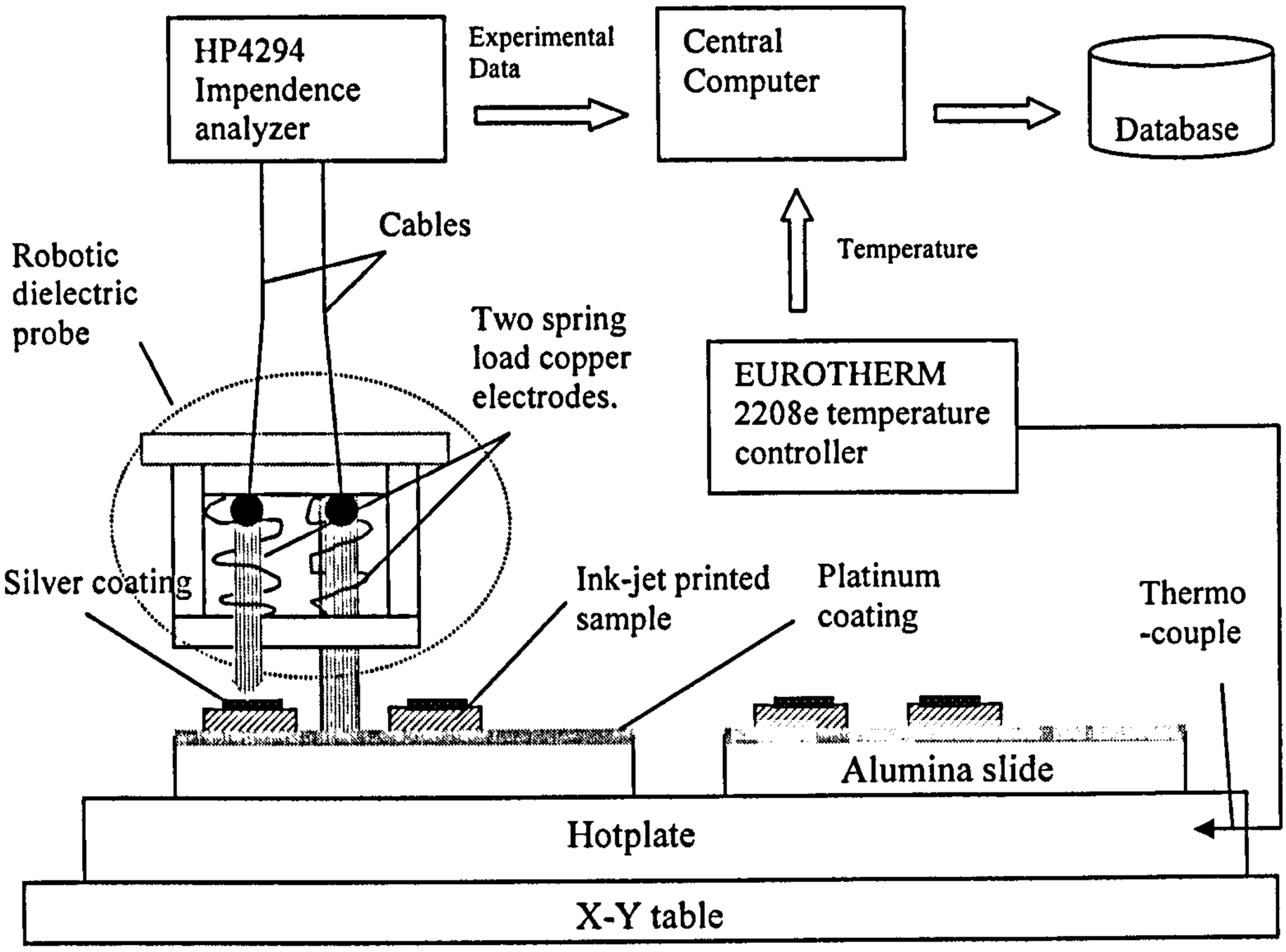

Figure 2.10 The experimental arrangement for combinatorial dielectric measurement.

Table 2.6 A group of experiments to calibrate the combinatorial dielectric measurement method.

ξ Name	Description	Objective
Calibration of HP4294 impedance analyzer	Calibrate the HP4294 impedance analyser using standard capacitors.	To demonstrate the impedance analyser can give accurate readings of capacitance.
Dielectric properties of $BaTiO_3$	Measure relative permittivity of ceramic (i.e.$BaTiO_3$) as a function of temperature or frequency using HP4294 impedance analyzer.	To demonstrate the impedance analyser providing accurate results for a well-known dielectric and provide references for later experiments.
Dielectric properties of ink-jet printed ceramics	Measure relative permittivity of ink-jet thick film ceramic (i.e., $BaTiO_3$) as a function of temperature or frequency.	To study dielectric properties of direct ink-jet thick film ceramics, compare the results with ceramics that were produced in conventional ways.
Calibration of Robotic dielectric probe	Apply the combinatorial method to study dielectric properties of ink-jet thick film ceramic (i.e., $BaTiO_3$).	To calibrate the dielectric measurement of the combinatorial method.

ξ Each experiment described in the table was repeated at least three times to check reproducibility.

2.7.1 Calibration of the HP4294 impedance analyser

Standard capacitors (Table 2.7) were measured using the HP4294 impedance analyser with the 16074A test fixture (reference page 67) at 1kHz and room temperature. All these capacitors were purchased from RS components, Derby, UK. The capacitance values of capacitors were selected to be in the same range of dielectric measurement as that used in later experiments. These capacitors also were applied to calibrate the measurement cell described below when extensions between the test fixture and the sample were implemented.

Table 2.7 The description of capacitors used to calibrate HP4294 impedance analyser

No	Type	Capacitance	Tolerance
1	Ceramic - Surface Mount	1pF	±5%
2	Ceramic - Surface Mount	4.7pF	±5%
3	Miniature plate ceramic	56pF	±2%
4	Polypropylene-Radial	0.01μF	1%
5	Polypropylene-Radial	0.022μF	1%
6	Polypropylene-Radial	0.033μF	1%

2.7.2 Dielectric properties of compacted and sintered samples from $BaTiO_3$ powder

Validity of the impedance analysis procedure was assessed by preparing conventional pressed and sintered discs of materials for which there are sound published measurements. A sample of 5g $BaTiO_3$ powder was weighed and pressed at 350 MPa into a pellet. The pressed pellet was sintered at 1400°C for 7.2ks in air and then abraded to give flat parallel sides. Sintered density was measured by Archimedes method. The geometry of the abraded plate was measured using the vernier calliper. The abraded plate was metalised using silver paste to form a parallel plate capacitor. Both temperature dependency (i.e., from room temperature to 180 °C at 1 kHz) and frequency dependency (i.e., from

100 Hz to 1 MHz at room temperature) of capacitance were measured by the HP4294 Impedance Analyzer. The measurement arrangement was illustrated in Figure 2.11. A SEM picture of the $BaTiO_3$ prepared by the same procedure was taken to study the microstructure. Formula 1.13 is used to calculate the dielectric constant of the sample from its capacitance. The procedure for metalising was: the two parallel surfaces of the samples were painted with silver paste, dried in the oven at 75°C for 1.8ks then fired at furnace at 800°C for 30s in air.

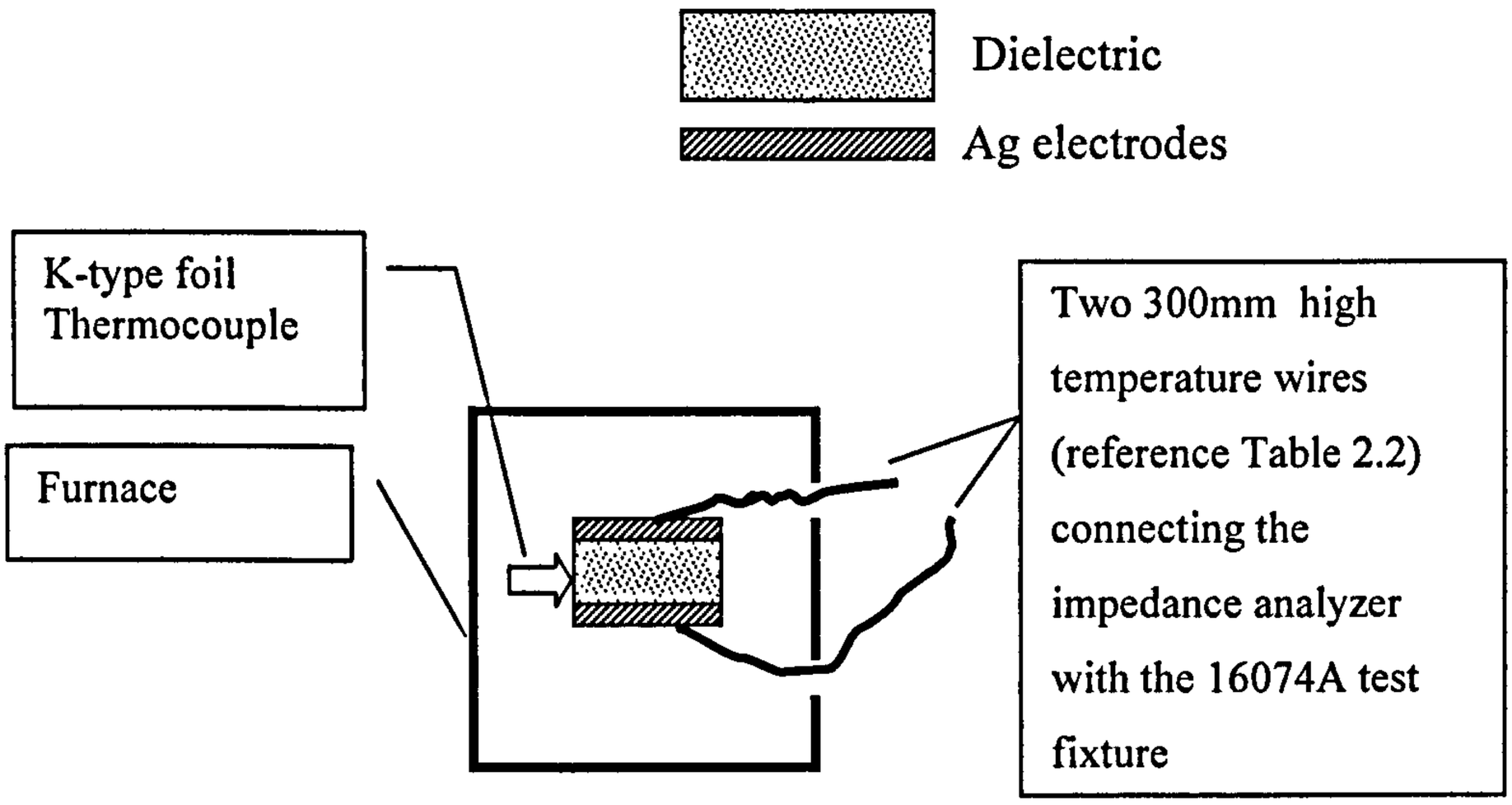

Figure 2.11 The experimental arrangement for measuring dielectric properties of pellets compacted and sintered from $BaTiO_3$ powder.

2.7.3 Dielectric properties of ink-jet printed $BaTiO_3$ samples

Stocks of 10g of $BaTiO_3$ ink were created and then filled into the well plate. The printer aspirated from the well plate and dispensed 150 µl inks on a rectangular recess that was made with the silicon release paper. The inks were dried in air for 3.6ks. After drying, the sample of $BaTiO_3$ was fired at 1400°C for 7.6ks in air. The measurement procedures for geometry and dielectric properties were the same as described in Section 2.7.2. The measurement of dielectric properties was arranged as illustrated in Figure 2.12. SEM images of the fired ink-jet printed ceramic were taken.

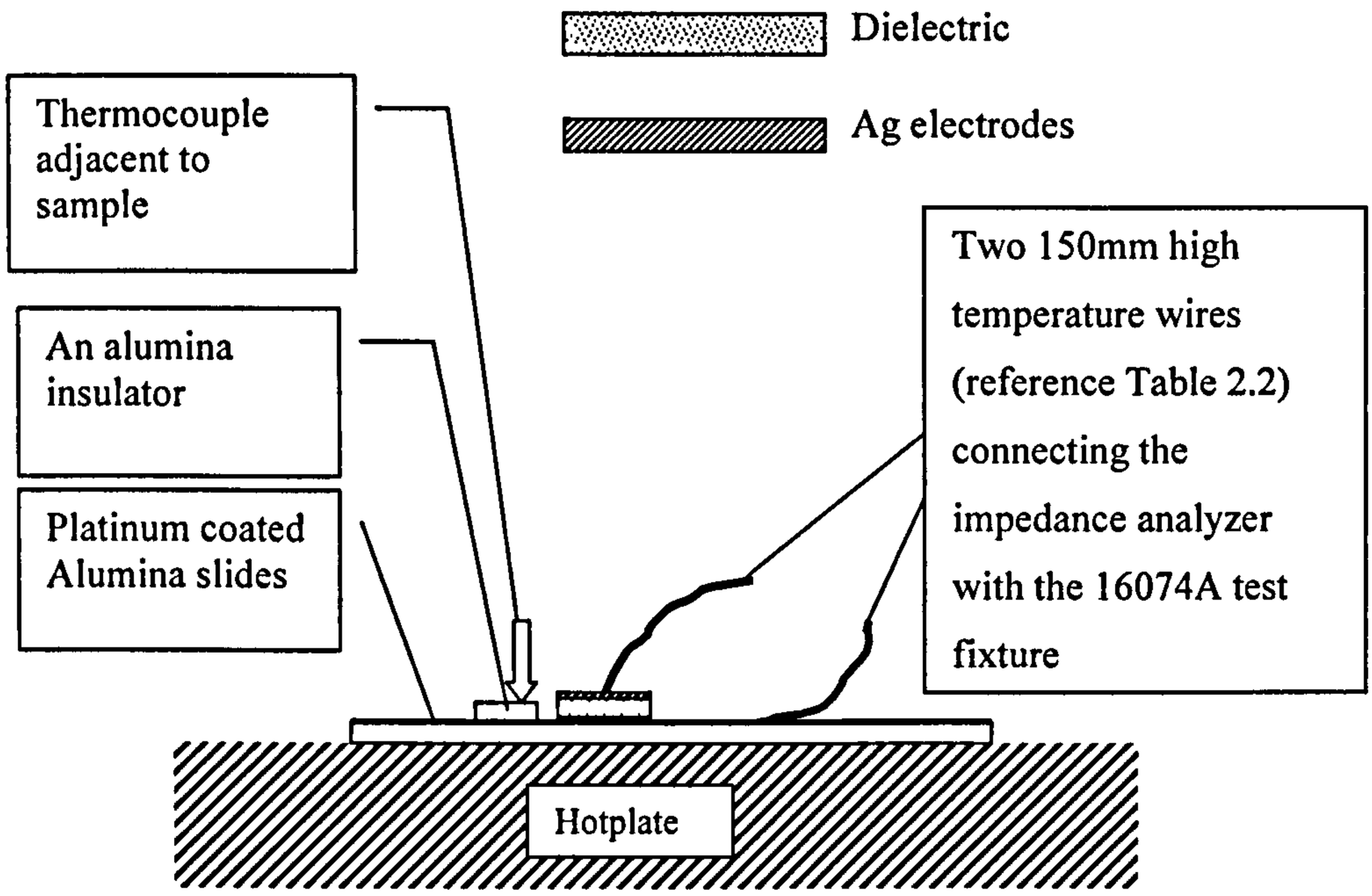

Figure 2.12 The experimental arrangement for measuring dielectric properties of ink jet printed ceramic.

2.7.4 Calibration of combinatorial dielectric measurement

The source well plate was charged with $BaTiO_3$ ink. The operator instructed the system to start a sequence automatically as follows:

Step 1. Ink-jet printing samples - the printer aspirated and dispensed 8.5 μL $BaTiO_3$ drops onto the platinum coated alumina substrate. Figure 2.13 is a photograph of the printer depositing samples on the substrate.

Step 2. Firing - after finishing the printer program, the robot transferred the substrate from the printer to the furnace, where the sample was fired at 1400°C for 7.2ks in air. Figure 2.14 is a photograph of the robot picking up the substrate from the printer to transfer it to the furnace (The robotic gripper can be seen top centre).

Step 3. Metalising - After completing the sintering program, the robot repositioned the substrate to the x-y table, where the probe deposited silver paste on the sample by stamping. The robot then took the substrate back to the furnace, where the samples were fired at 800°C for 5 minutes.

Step 4. Screening – After step 3, the robot replaced the substrate on the x-y table. The robotic dielectric probe touched the sample as pictured in Figure 2.15. The frequency dependence of capacitance from 100 Hz to 1 MHz at room temperature was measured by the HP4294 Impedance Analyzer. The hotplate then raised the temperature. The temperature dependence of capacitance was then measured by the Impedance Analyzer from room temperature to 180 °C at 1 kHz. The impedance analyser transferred data to the central control computer.

Step 5. Data processing- The measured data were then available to be processed as a user might require. The data were converted to database data structure and stored in the database.

The Pt-coated substrates used in the experiment were produced using the platinum ink approach as described in 2.4. Another layer of the platinum ink was then painted on the platinum coated alumina substrates and dried in the oven at 60°C for 15 min but not fired. The $BaTiO_3$ inks were printed on this dried platinum ink. The reasons for using this procedure are described in section 3.2.

A temperature calibration map of the hotplate was prepared as follows. Each location of the substrate on the hotplate was recorded by the robot computer. A foil thermocouple was placed on the substrates. Both the hotplate's temperature and the substrate's temperature were recorded simultaneously in advance at each position. These data were stored in a database. When measuring the temperature dependencies of dielectric properties, the temperature of the sample can be automatically converted from the hotplate temperature by the computer. In the above step 4 "Screening", after the robot measured the frequency dependence of capacitance, a thermocouple was manually placed adjacent to the sample; the

temperature dependence of capacitance of the sample was then recorded manually. The implementation of automation is described in section 3.9.

Figure 2.16 describes how the values of thickness D and area of the electrode of the capacitor, A, as used in formula 1.13 were determined. The sample diameter was kept above 2mm to allow the electroded region to approximate to a parallel plate configuration. The thickness of fired samples, D, was measured by the micrometer.

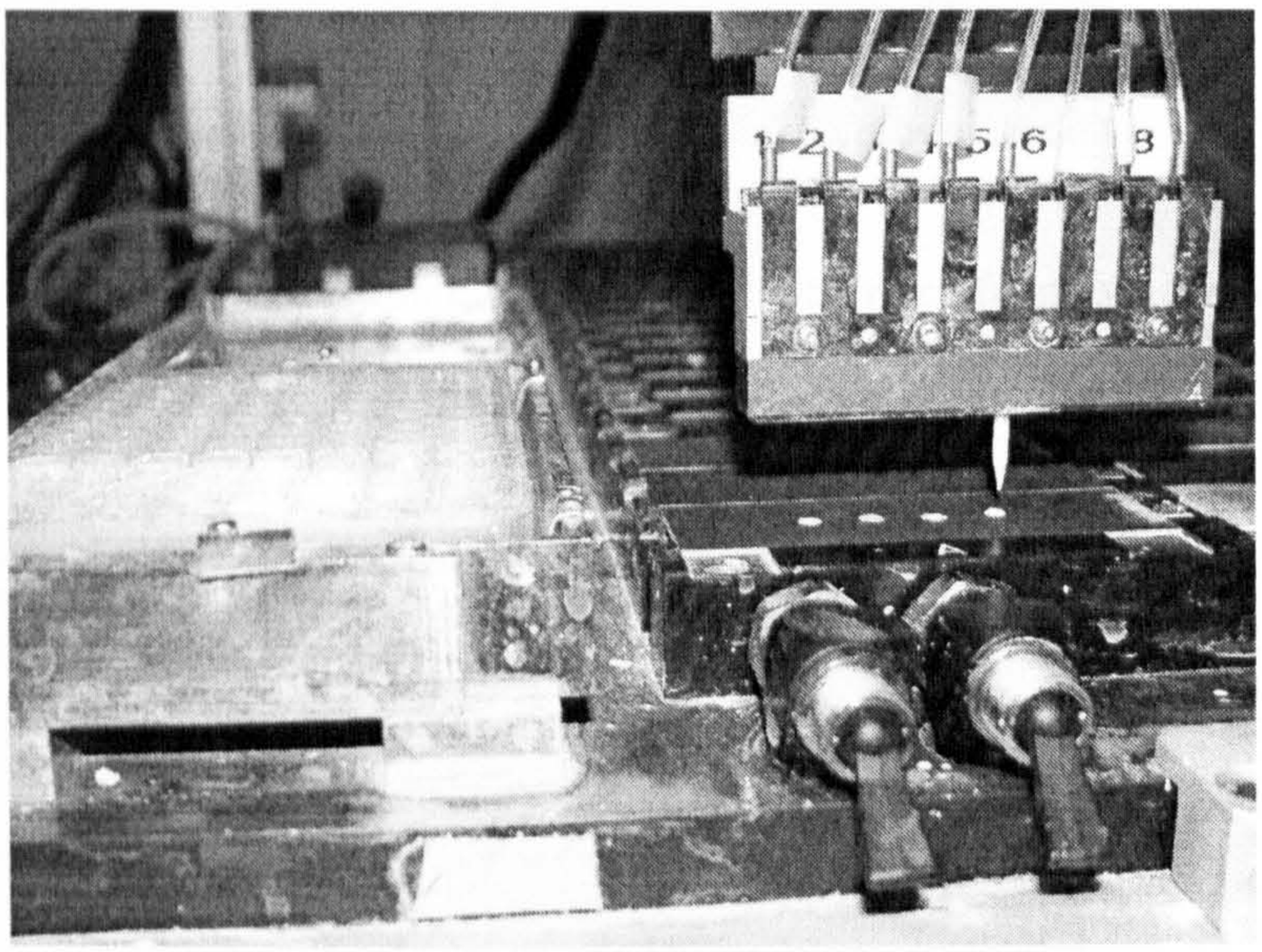

Figure 2.13 Ink-jet printing $BaTiO_3$ on the platinum-coated alumina substrate

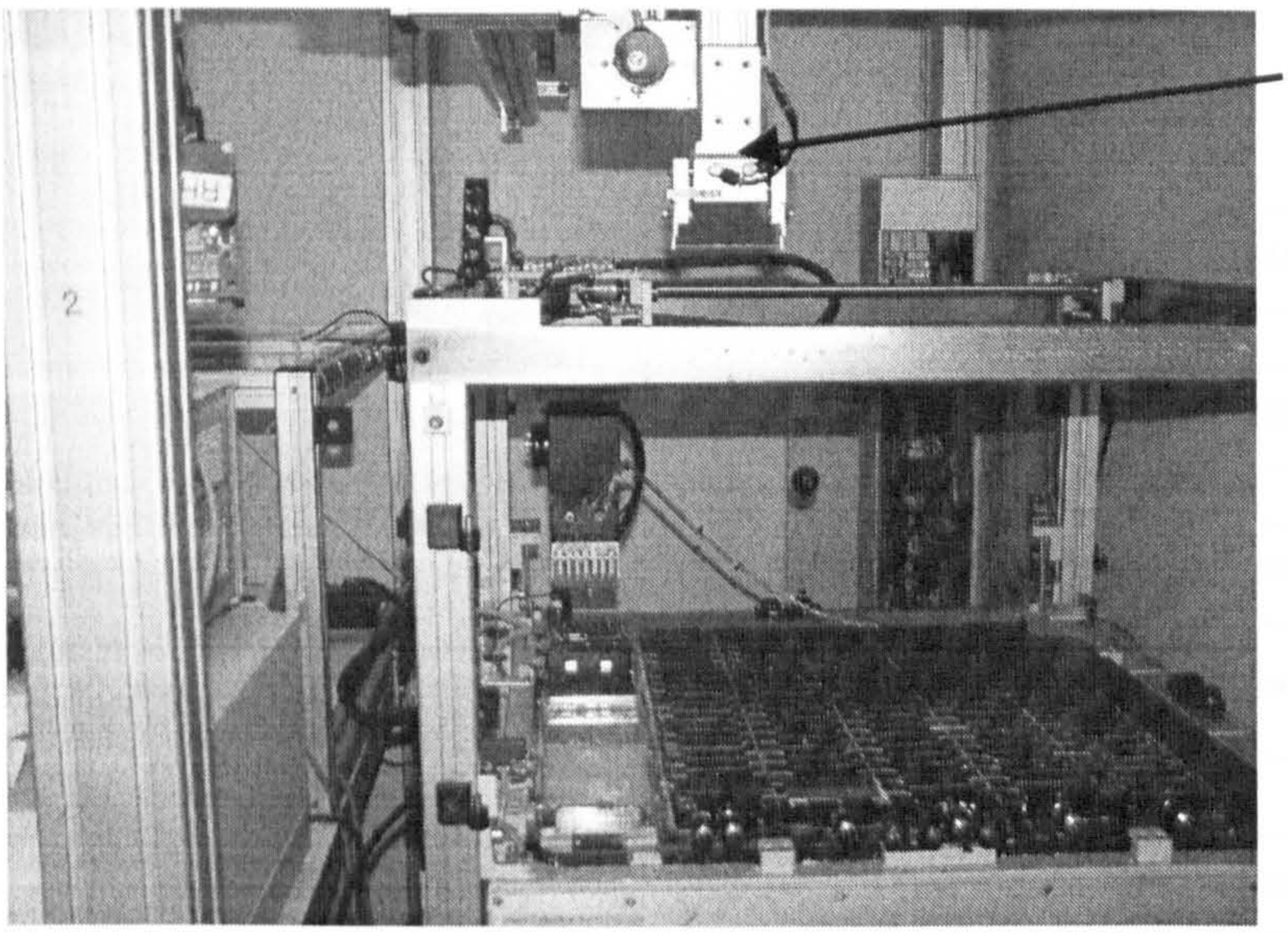

Figure 2.14 The robot can pick up and place substrates from any position inside the robot gantry.

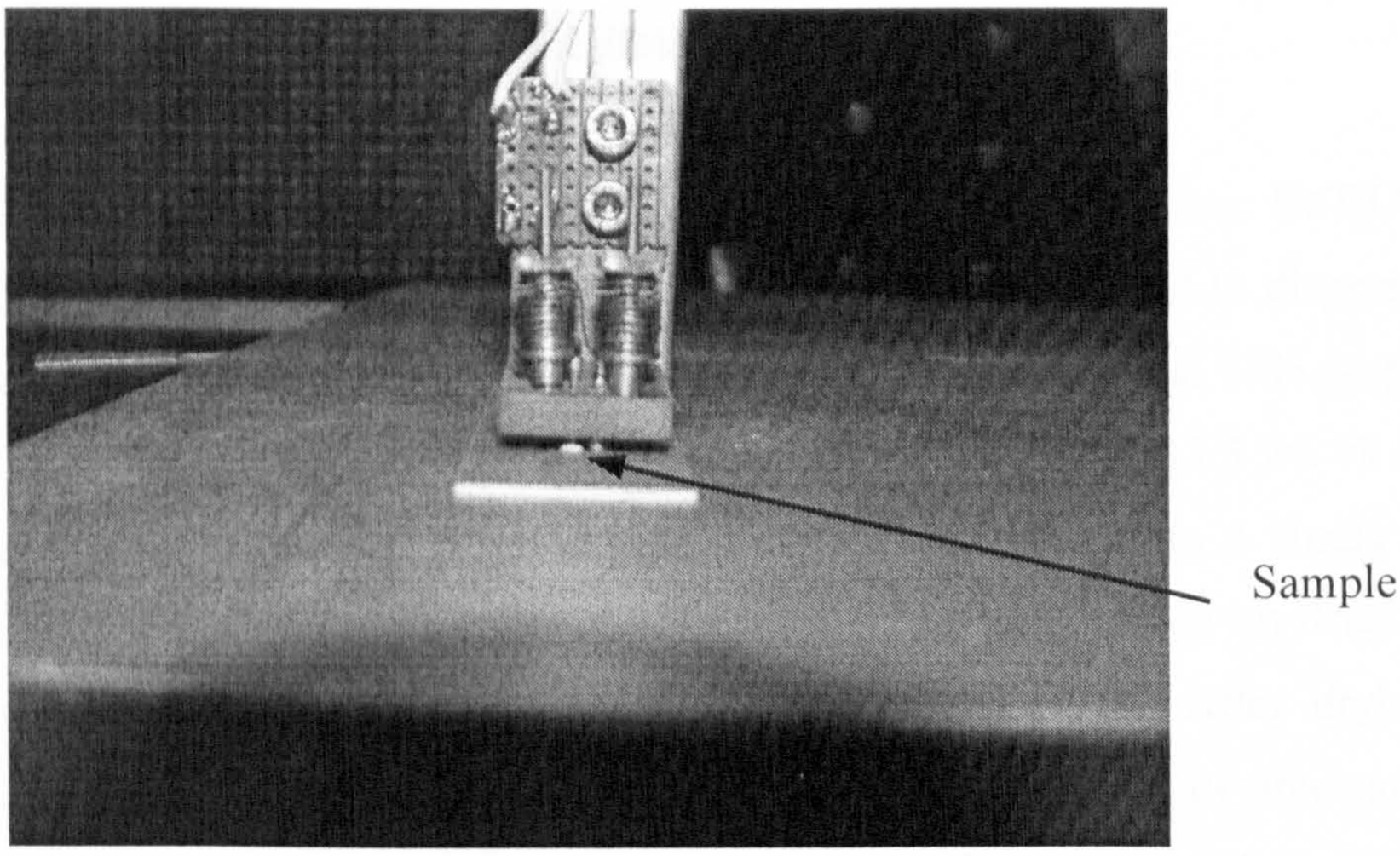

Figure 2.15 The dielectric probe contacts the sample and measures data.

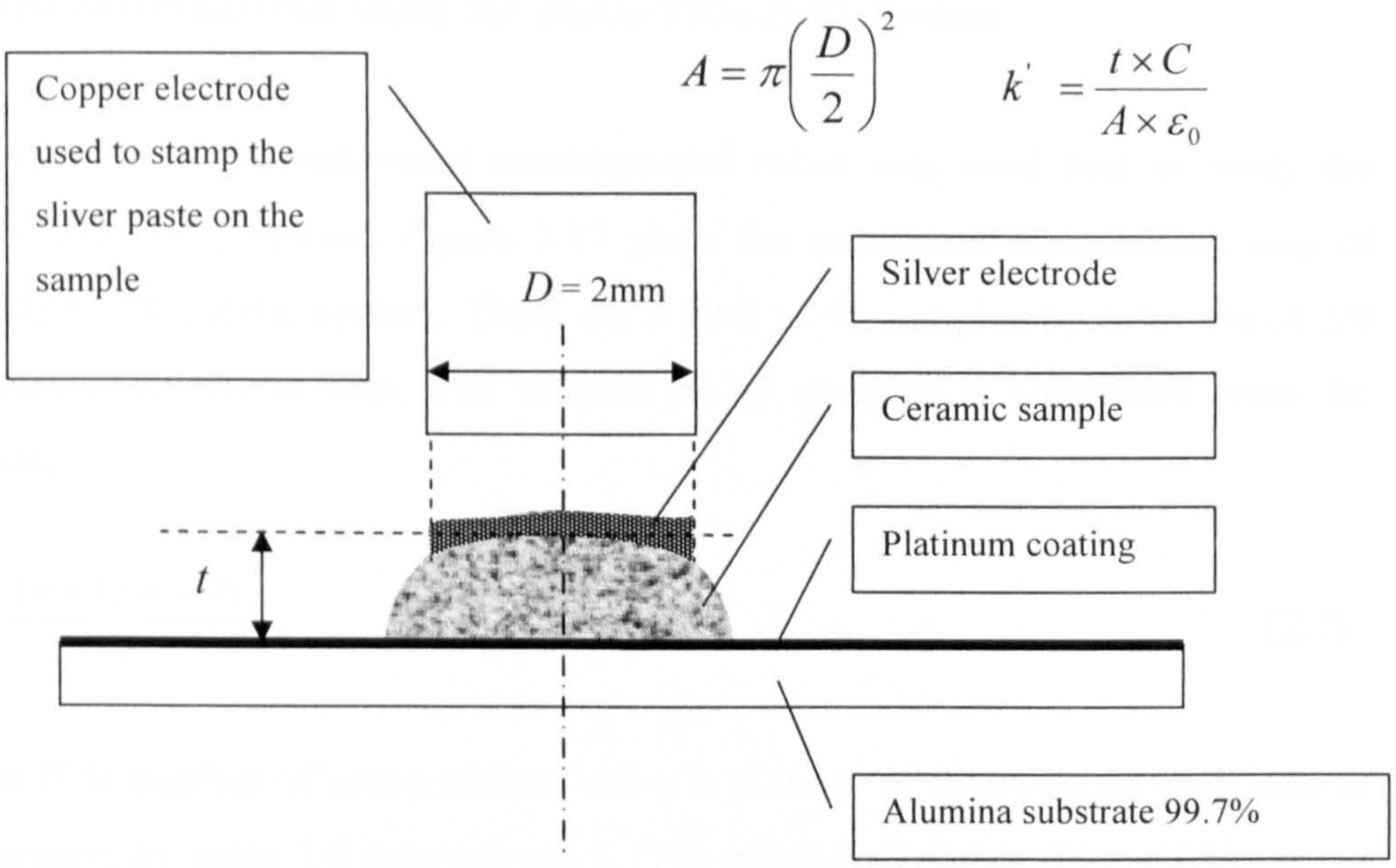

Figure 2.16 The geometry of fired ink jet ceramic on the platinum-coated substrates.

2.7.5 Study of combinatorial dielectric measurement

The combinatorial dielectric measurement was studied further. $BaTiO_3$ powder was mixed with distilled water and dispersant and subjected to dispersion using ultrasound under the ultrasonic probe pulsed at cycle 0.5 and 75% amplitude for 300s. The ink composition contained 44.9 wt. % $BaTiO_3$, 13.3 wt. % dispersant and 41.8 wt. % but to get different sample thickness from a single drop, the composition was varied. Droplets of suspension were placed on dried platinum inks painted on the alumina substrates using pipettes. After drying in air, samples were fired at 1400 °C in air for 7.2ks. The thickness of fired samples was recorded using the micrometer. The upper surfaces of samples were stamped with silver paste using polished steel rods with different diameters. They were fired at 800 °C for 300s. The area of the upper electrode was computed with a microscope (Model: BX60F, Olympus Ltd, Japan). The microscope is equipped with software used to measure a flat geometry, Image-Pro Process, which was previously calibrated using a stage micrometer (Graticules Ltd, Kent, England, 100×0.01 =1mm). The room temperature capacitance at 1 kHz was measured with the impedance analyser.

2.8 The combinatorial study for Al_2O_3-TiO_2-ZrO_2 system

The developed and calibrated combinatorial robot was used first to study the Al_2O_3-TiO_2-ZrO_2 system. Figure 2.17 gives the numbered composition map of the Al_2O_3-TiO_2-ZrO_2 system. There are a total of 45 samples by intervals of 1/8 on each composition axis. The number of 45 samples is calculated from the formula

$$N = \frac{(n+1)(n+2)}{2} \quad , \tag{2.5}$$

where N is number of compositions and n is number of intervals on each side of the ternary, by using 1/8 interval, n = 8. The numbered compositions are mapped to the 96-well plate as described in Figure 2.18 so that each well was assigned for one mixed ink with a planned composition. For example, well A-2 holds mixed ink with planned composition number 2, whose composition can be found in Figure 2.17, as 87.5 wt.% TiO_2 (weight fraction 7/8) and 12.5 wt.% ZrO_2 (weight fraction 1/8).

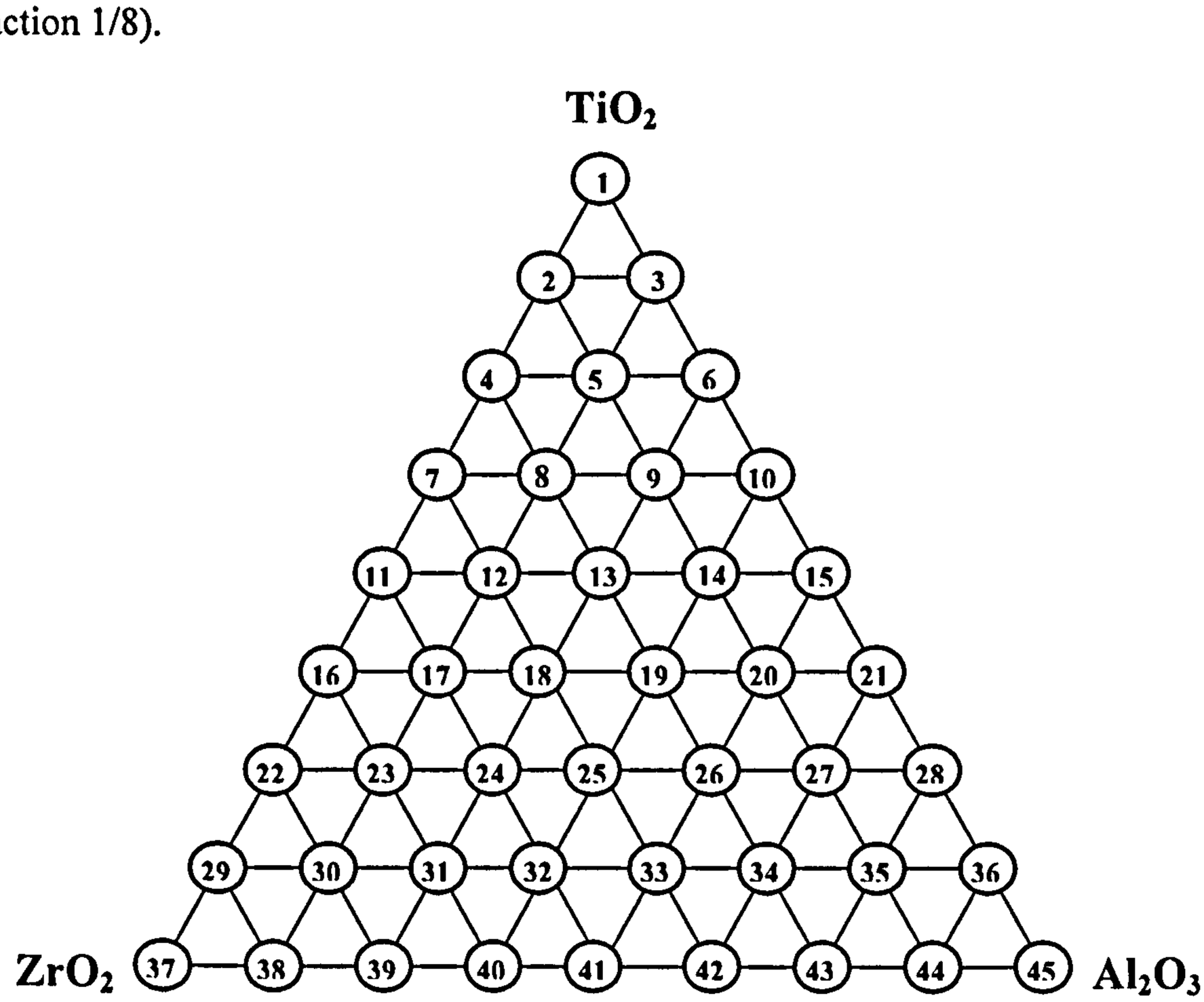

Figure 2.17 A numbered composition map of the Al_2O_3-TiO_2-ZrO_2 system.

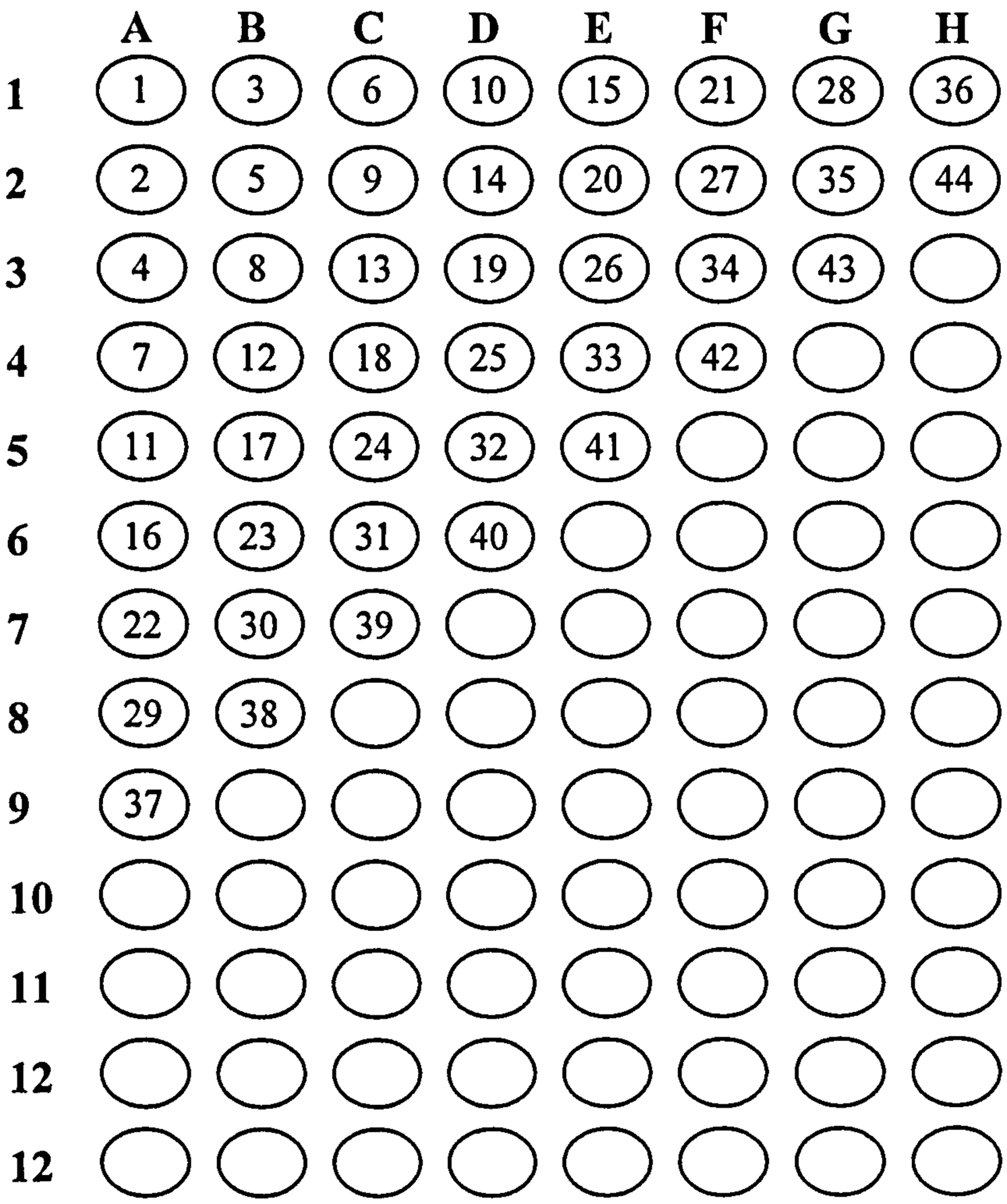

Figure 2.18 Mapping the compositional array of the Al_2O_3-TiO_2-ZrO_2 system to a 96 well-plate.

The pseudocode of the printer program for creating this library is given as follows:

Start

Set rows of well plate =X, columns of well plate =Y, dispense volume =V, control variables = Z and W. Planned mass of ceramic mixture = M.

W =1/8× the volume of TiO_2 ink containing M gram powder, Z=8, V=W;

while (Z≤2)

```
{
        X= Z, Y=1;
        For (i=0; i< Z, i++)
        {
                Aspirating TiO2 ink from source well plate
                Dispensing V to the X, Y of well plate
                X--, Y++;
        }
        Z--, V= V +W;
}

W =1/8× the volume of ZrO2 ink containing M gram powder, Z=8, V=W, X=2;
while (X ≤8)
{
        Y=1.
        For (i=0; i< Z, i++)
        {
        Aspirating ZrO2 ink from source well plate
        Dispensing V to the X, Y of well plate
        Y++;
        }
        X++, Z--, V= V +W;
}

W =1/8× the volume of Al2O3 ink containing M gram powder, Z=8, V=W, Y=2;
while (Y ≤ 8)
{
X=1.
For (i=0; i< Z, i++)
{
Aspirating Al2O3 ink from source well plate
Dispensing V to the X, Y of well plate
X++;
}
```

Y++, Z--, V= V +W;

}

End

In the above, the planned mass of ceramic mixture 'M' is set as 0.2g in this experiment.

The volume of transferred TiO_2 ink = (M ÷ 3850 kgm^{-3}) ÷ 9.99vol%

The volume of transferred ZrO_2 ink = (M ÷ 5750 kgm^{-3}) ÷ 9.99vol%

The volume of transferred Al_2O_3 ink = (M ÷ 3987 kgm^{-3}) ÷ 9.92vol%

The volume percentage of ceramic powder in each ink is taken from Table 2.3.

The density of each powder is taken from Table 2.1

The basic idea of the pseudocode to create this library is as follows. As shown in Figure 2.17, assuming unit mass of ceramic mixture, for the TiO_2 end, numbers 2 and 3 contain 7/8 TiO_2, numbers 4, 5, and 6 contain 6/8 TiO_2, numbers 7, 8, 9, 10 contain 5/8 TiO_2, and so on until number 29-36 containing 1/8 TiO_2. For the ZrO_2 end, numbers 29 and 38 contain 7/8 ZrO_2, number 22, 30 and 39 contain 6/8 ZrO_2, and so on until numbers 2, 5, 9, 14, 20, 27, 35 and 44 which contain 1/8 ZrO_2. For the Al_2O_3 end, numbers 44 and 36 containing 7/8 Al_2O_3, and so on until numbers 3, 5, 8, 12, 17, 23, 30 and 38 which contain 1/8 Al_2O_3. By using the pseducode, the printer transfers the specified mass of each powder into the target well (Figure 2.18) to get the planned mixtures.

In section 2.5, one essential step of the printer in creating ceramic mixtures is to work out the transfer volumes of each component inks for each ceramic mixture using equations [2.1] and [2.2]. By using the above pseducode, a ternary system can be easily implemented without working out transferred volumes of each component ink for each mixture. Here, the 1/8 interval is implemented, but there is no reason why 1/10, 1/16 or any other interval cannot be implemented by mapping the composition array to one well plate or several well plates.

After building composite inks in the target well plate, the printer aspirated composite inks from each well and dispensed 15μl inks onto the porous cellulose

nitrate membranes (Whatmen plc, England), after 900s, the dried samples were removed from membranes and fired at 1450 °C for 2h in the furnace. After firing, the geometry of flat disc shape samples was measured using vernier callipers. Both surfaces of samples were metallized using silver paste as described in section 2.7.2. The capacitances of samples were measured using HP4294 Impedance analysis at 25°C and 1kHz. Formula 1.13 was used to calculate the dielectric constant of sample from its capacitance.

Chapter 3 Results and Discussion

3.1 Characterisation of materials

Figures 3.1, 3.2 and 3.3 are SEM pictures of the individual TiO_2, Al_2O_3 and ZrO_2 powders. These images were obtained from the deposition of single component inks. Clearly, the TiO_2 powder is the finest with ultimate particles in the region 100nm- 200nm. The alumina particles are in the region 0.1-1 μm. The zirconia is a wide size distribution powder but the loose packing is evidence of considerable agglomeration. The ultimate particles are 0.3-2 μm in diameter.

The particle size distributions of powders were measured using Sedigraph (5100, Micromeritics Instrument corporation, Norcross, USA) which detects particles in the range of 100nm to 300 μm. Three 10g batches of Al_2O_3, ZrO_2 and TiO_2 inks were made. Each ink was diluted using 50mL distilled water to reduce the concentration of powder to fit the requirement of the Sedigraph. Table 3.1 describes particle size distributions for the three powders. The specific surface area of powders are ZrO_2 (15.2 m^2/g), Al_2O_3 (9.3 m^2/g) and TiO_2 (8.8 m^2/g) measured by nitrogen absorption BET method.

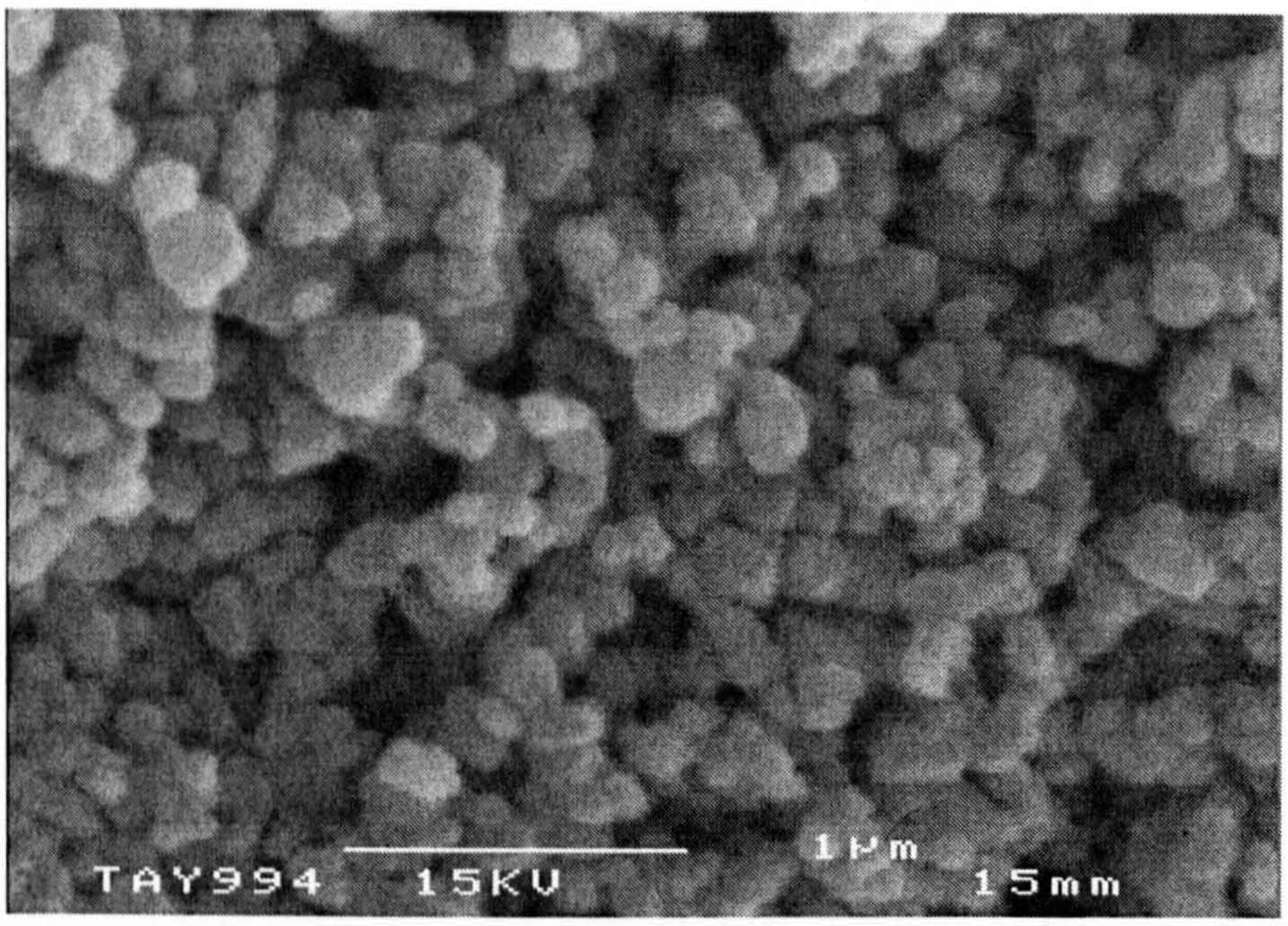

Figure 3.1 SEM picture of TiO_2 powder prepared from single component TiO_2 ink.

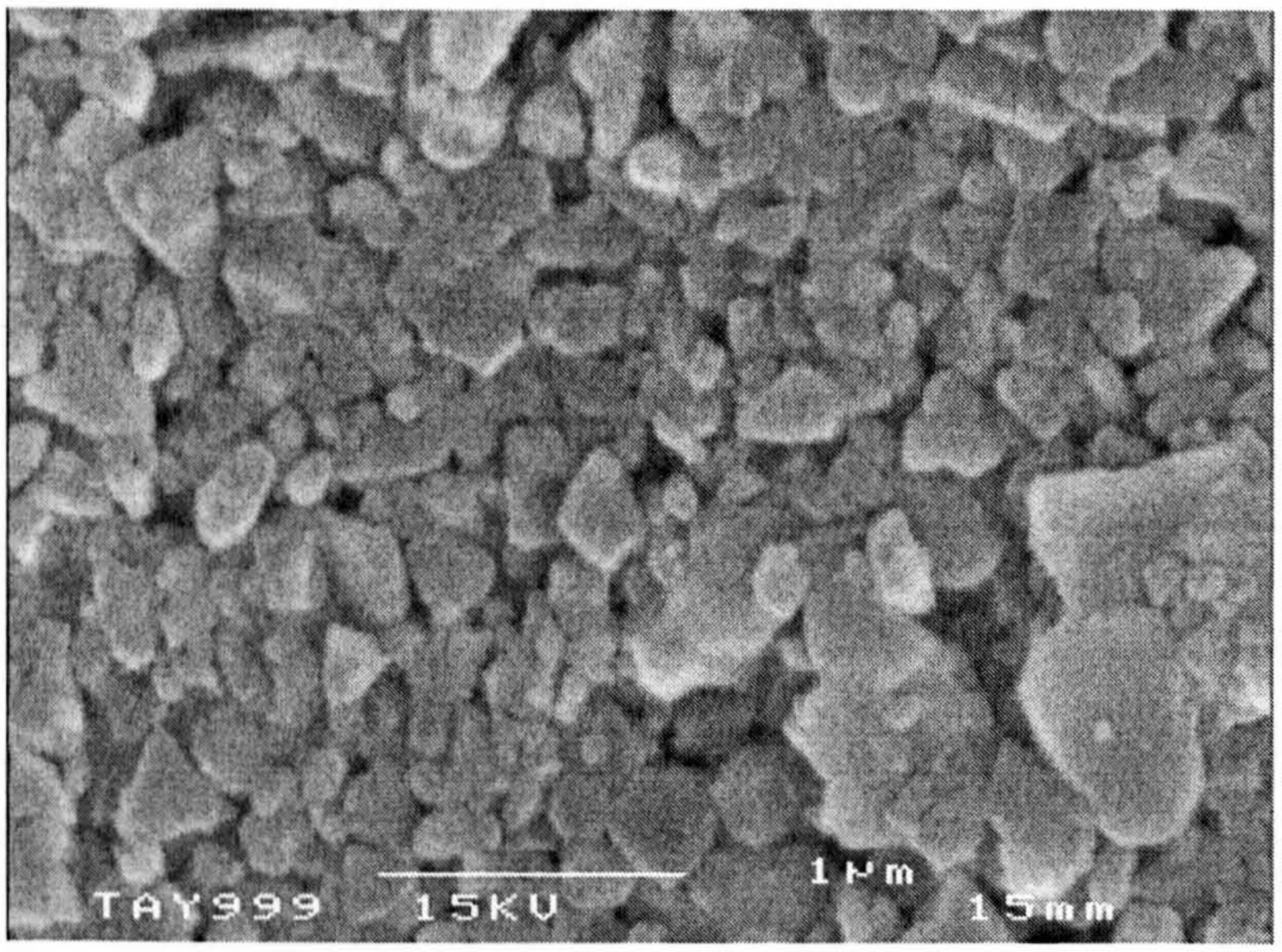

Figure 3.2 SEM picture of Al_2O_3 powder prepared from single component Al_2O_3 ink.

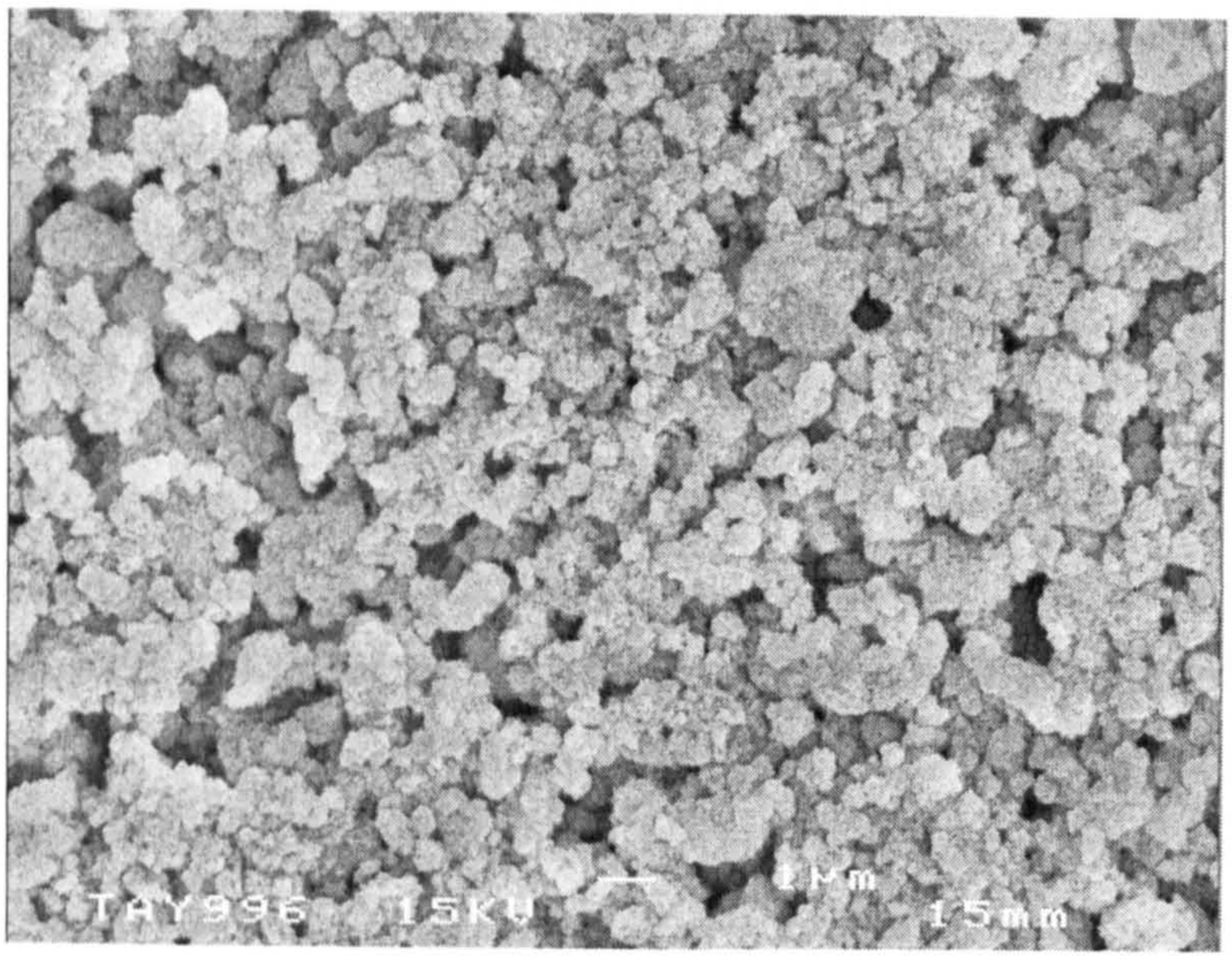

Figure 3.3 SEM picture of ZrO_2 powder prepared from single component ZrO_2 ink.

Table 3.1 Particle size distributions for the three powders

Low Diameter (μm)	Cumulative mass coarser (%)		
	ZrO_2	Al_2O_3	TiO_2
3	1.2	3.7	0.0
0.7	47.0	20.6	2.7
0.4	63.8	45.0	23.9
0.3	70.1	60.4	46.5
0.2	76.9	77.7	73.3
0.1	85.5	91.2	92.4

3.2 Substrate preparation

The sheet resistance of platinum coated substrates using the platinum wire approach was 8 ohm per square after 20 repeated coatings using the vacuum coating unit. After firing at 1600°C for 2 hours, Platinum coatings were all evaporated and beyond the range of resistance the multi-meter can detect. Therefore this approach was abandoned.

The sheet resistance of platinum coated substrates using the platinum ink approach was 0.3 ohm per square before and after firing. The problem with the fired platinum paste was that when water-based inks (e.g., $BaTiO_3$ inks) were deposited on it, the droplets spread giving a thin coating, thus losing the spatial specification. To overcome this problem, a second layer of platinum ink was painted on the fired platinum-coated substrates but not fired. Water-based inks such as $BaTiO_3$ then formed non-spreading drops on the dried platinum ink. This approach was adopted for use in the combinatorial method. Figure 3.4 and figure 3.5 give SEM pictures of 99.8% α-alumina substrates and platinum coating on the α-alumina substrate using the platinum ink approach, respectively.

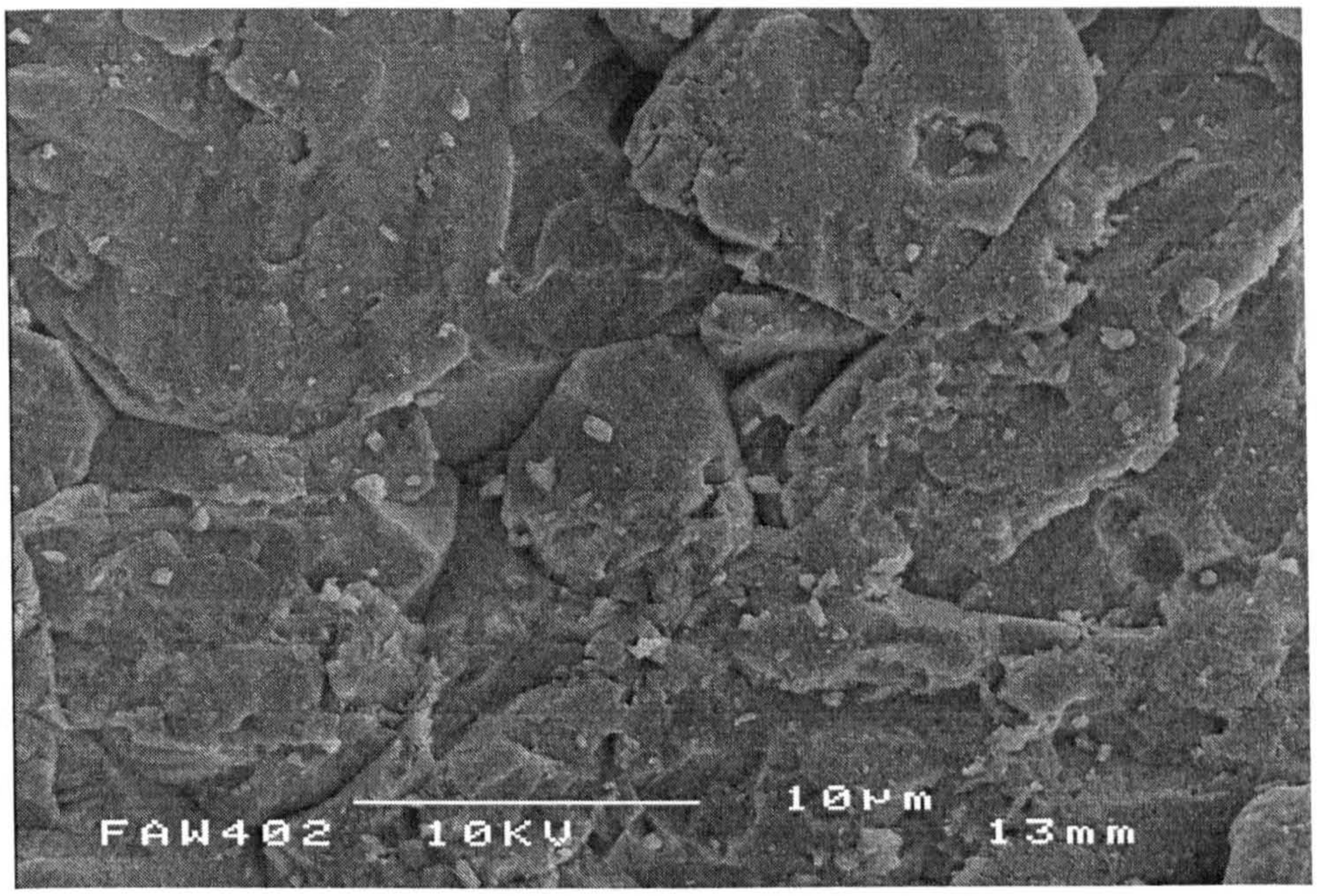

Figure 3.4 SEM picture of a 99.8% α-alumina substrate.

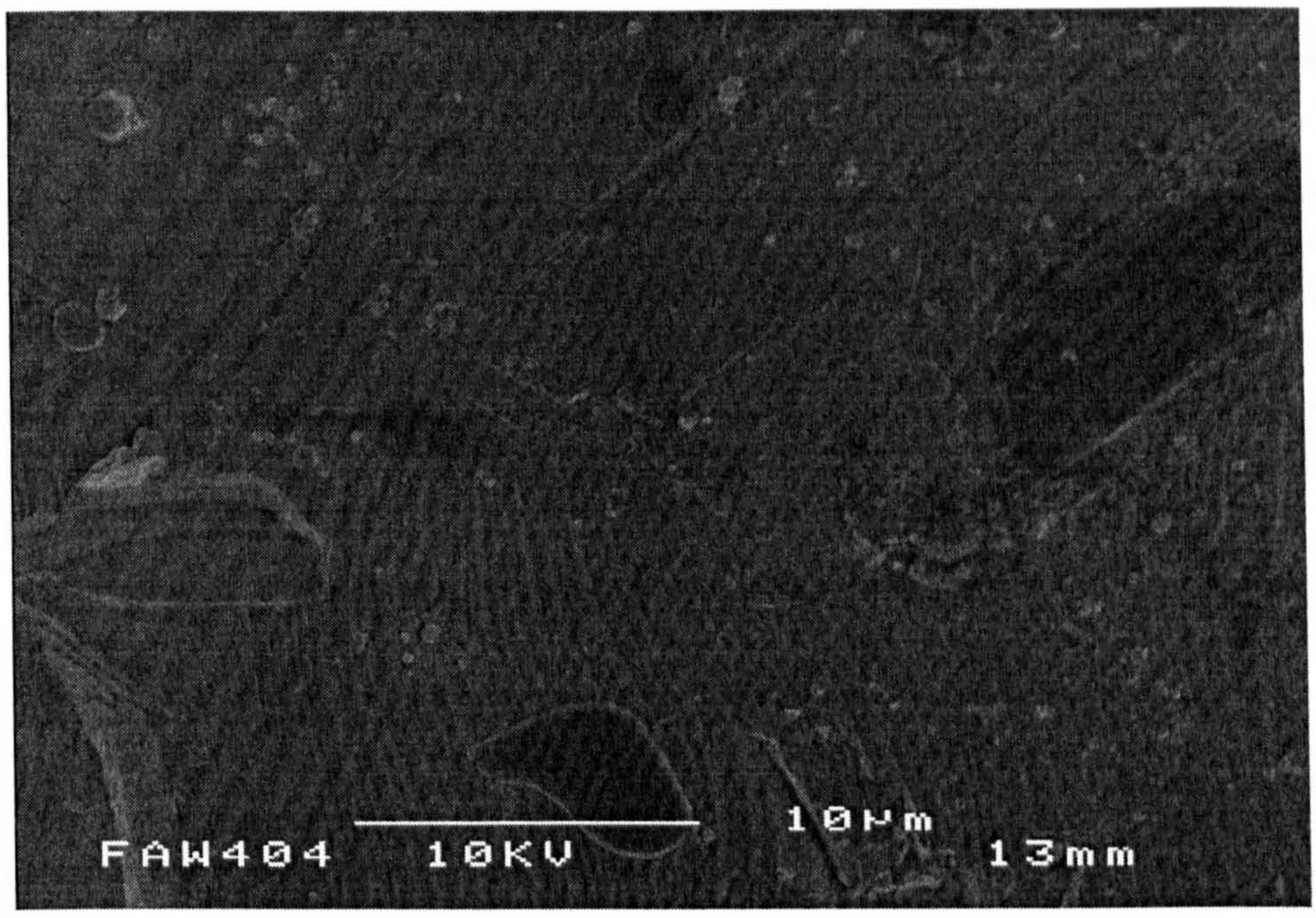

Figure 3.5 SEM pictures of platinum coated on the 99.8% α-alumina substrates using the platinum ink approach.

3.3 Compositional calibration of the ink-jet printer

3.3.1 Sedimentation

Table 3.2 describes the sedimentation behaviour of Al_2O_3, ZrO_2 and TiO_2 inks as a function of time. These results show that Al_2O_3, ZrO_2 and TiO_2 inks were stable at least for 7.2ks after preparation. These inks were used in the experiments on compositional calibration of the printer. Because no printer programs run for more than 7.2ks (i.e., 2 hours) and the well plate holding these inks is subject to intermittent ultrasonic dispersion, these inks have adequate stability during the running of a printing program.

Table 3.2 Sedimentation behaviour of water-based ceramic inks

Time /ks	t= 7.2	t = 14.4	t= 43.2	t = 86.4
TiO_2 Ink	Stable	Stable	Top cloudy liquid; Homogenous mixture below. No sediment.	Top cloudy liquid; Homogenous mixture below. Sediment was found.
ZrO_2 Ink	Stable	Homogenous mixture above. Sediments was thrown.	Top cloudy liquid; Homogenous mixture below. Sediment was thrown.	Appeared same as t=43.2ks
Al_2O_3 Ink	Stable	Cloudy liquid above homogenous mixture. Sediment was thrown.	Appeared same as t= 14.4 ks	Appeared same as t=43.2 ks

3.3.2 Loss on ignition

Table 3.3 presents the results of loss on ignition of ZrO_2, TiO_2 and Al_2O_3 ink. The target ZrO_2, TiO_2 and Al_2O_3 ink contents were 38.83 wt. %, 29.93 wt. % and 30.46 wt. % as described in Table 2.3. The deviations in weight percentages for five individual samples of three inks were each below 1%. These errors can be attributed to the measurement method. The overall deviations can be attributed to evaporation during mixing as discussed in section 3.3.3 below. The conclusion is that the water-based ceramic inks provide a homogenous mixture at this sampling level so it is possible to know the weight of dispersed powder from volume of ink.

Table 3.3 Loss on ignition of water based ceramic inks

Sample No$^{\xi}$	ZrO_2 ink		TiO_2 ink		Al_2O_3 ink	
	ZrO_2 wt. %	Error %	TiO_2 wt. %	Error %	Al_2O_3 wt. %	Error %
1	38.97	0.36	30.11	0.6	30.36	0.33
2	38.99	0.41	30.05	0.4	30.51	0.16
3	38.93	0.26	30.05	0.4	30.68	0.72
4	38.95	0.31	30.04	0.37	30.20	0.85
5	39.01	0.46	30.06	0.43	30.24	0.72
Mean*	38.97 ± 0.04		30.06 ± 0.04		30.40 ± 0.28	

* This row gives the mean value of five samples with 95% confidence limit.

ξ In the table, Error % = 100% × (Experimental powder weight % - Target powder weight %) / Target powder weight %

3.3.3 Evaporation

Table 3.4 describes the evaporative loss of ink in the covered 96 well plate (reference to page 77) as a function of time. To control evaporation of inks, the well plate should be refilled with fresh ink at every 1.8ks (i.e., 30 minutes) during the operation in order to keep the error in weight percentage of ceramic within 1%.

Table 3.4 Evaporative loss of ZrO_2 ink in the covered 96 well plate

Time / ks	t=0*	t= 1.8	t = 3.6	t=4.8	t=7.2
Mass of ink in one well /g	0.5149	0.5112	0.5068	0.5036	0.5005
Evaporation loss /g	0	0.0037	0.0081	0.0113	0.0144
Weight percentage of ZrO_2 powder in the ink **	38.83	39.11	39.45	39.70	39.95
Error in weight percentage	0	0.72	1.6	2.24	2.88

* t=0 once the well was filled with inks and then covered.

** When t=0, the weight percentage of filled ZrO_2 ink was 38.83 wt% as shown in Section 3.3.2 Loss on ignition. After that,

$$ZrO_2 \text{ wt. \% at time t} = \frac{\text{Mass of ink at t=0 (i.e. 0.5149g)} \times 38.83 \text{ wt\%}}{\text{Mass of ink in the well plate at time t}}.$$

As explained in section 2.5, the first requirement for processing ink compositions using the printer was the formulation of stable and homogenous ceramic inks that provide the correct base for step 2, calculation of transfer volumes. From the sedimentation results, loss on ignition and evaporation experiments, the Al_2O_3, ZrO_2 and TiO_2 inks developed here can be used as the basis for the preparation of

multiple ceramic compositions by the aspirating-dispensing printer. These experiments make use of two additions to the equipment; ultrasonic actuation on the well-plate holders and well-plate covers. The time limits are 7.2ks for sedimentation loss and 1.8ks for evaporation.

3.3.4 Loss on ignition of transferred inks

Table 3.5 gives loss on ignition of transferred inks for four compositions in the Al_2O_3-TiO_2-ZrO_2 system and hence compares the masses transferred with those programmed. The errors associated with the transferred masses in Table 3.5 are calculated in two ways. The coefficient of variation from the three trials for each composition is given in brackets as a percentage and defines the variation associated with an individual transfer of one component of the mixture. These vary between 0.3 and 1.4%. The final column gives the compositional error in mass% for that mixture based upon the means. The maximum error is 0.3mass%. These errors can be attributed partly to the inaccuracy of printer dispensing. From Table 1.4, there is ±5 error% at 100nL which was the base dispensing unit in all printer programs. In fact the error is considerably less than this using the protocol described. Evaporative loss as described in Table 3.4 also contributes. Finally there is an error associated with the gravimetric measurement.

As mentioned in section 2.5, the second requirement for processing compositions was dispensing technology that allows transfer of nanoliter volumes. Loss on ignition of transferred inks tests the performance of the printer by examining whether it can transfer a specified amount of dispersed powder into the target well plate for which loss on ignition has established the initial composition. The results of loss on ignition of transferred inks demonstrate that the printer can deliver specified amounts of each powder into the target composite inks with a tolerable error of about 1 wt%.

Table 3.5 The results of loss on ignition of transferred inks (Each result is the mean of 3 trials)

Planned transfers /g			Mean Actual transfers /g (CoV%)*			Error Mass% ξ
ZrO_2	Al_2O_3	TiO_2	ZrO_2	Al_2O_3	TiO_2	
0.1054	0.1054	_	0.1057 (0.8)	0.1060 (0.3)	_	0.07
_	0.0878	0.0877	_	0.0868 (0.5)	0.0879 (1.4)	0.3
0.1037	_	0.1037	0.1037 (0.7)	_	0.1029 (1.4)	0.2
0.1045	0.0523	0.0523	0.1042 (0.8)	0.0519 (1.4)	0.0528 (0.3)	0.1/ 0.2 /0.3

* Coefficient of variation.

ξ This is the error in the mass % of oxide in the delivered mixture.

3.3.5 Observation of composite inks

For all four compositions, no sediments were found in the mixed well plate after the composite inks were gently aspirated out. This confirms the bulk sedimentation trials in section 3.3.1 (*vide supra*). In subsequent work, four compositions were printed from the mixed ink wells and subjected to the EDS protocol which tests variation of composition throughout the sample. From the results discussed here, loss on ignition of transferred inks and observation of composite inks established that the corresponding mixed inks contained the correct amount of each powder overall.

3.3.6 EDS Protocol

This stage of the calibration procedure examines the variation of composition throughout each individual printed sample. The EDS analyses of samples (Table

3.6) show that whether the drops were mixed and printed automatically by the combinatorial printer or mixed by manual weighing and deposited using a fine wire, the EDS results for the lower surfaces and cross sections agreed with the planned compositions. For unpolished surfaces the agreement is within the error associated with the analysis method[41]. The top surfaces, on the other hand, were significantly different. Segregation of powders occurred in the upper surface region during drying.

The residues of these droplets formed 'doughnut' shapes and sometimes there was a through-thickness hole (Figure 3.6a). Figure 3.6a is a picture of droplet residue from ink G. Although cracking of the residue sometimes occurred, EDS was only carried out on whole intact samples. The EDS results summarized in Table 3.6 are averaged from a positional array of assays systematically conducted along radial paths on the upper and lower surfaces and along the depth profile in cross sections (Figure. 2.8).

In each mixture, the EDS results at position 1 of the top surface (edge part) were consistently in better agreement with the planned composition than the results at positions 2, 3 and 4, a result which will become relevant when the segregation is interpreted. Tables 3.7 and 3.8 (rows 1) give only two examples of the positional array but this effect was general. The analysis of large area scans of the cross section does not disclose how deep the surface non-uniformity is. Figure 3.7 is a micrograph of the cross-section of a residue prepared from ink F (TiO_2 - ZrO_2 system) with elemental mapping showing ZrO_2 enrichment over 10-20 μm depth. The segregation layer became less thick from the central part to the edge, indeed there is no segregation in the edge region. Figure 3.7 also confirms the position of the segregation layer on the upper surface. The cross-section, indeed the major part of the body of residue shows no obvious excess concentration of a particular powder. Since the EDS analysis of the cross-section is a five point assay at sampling area of 50 × 50 μm it does not disclose the depth profile.

Compositional non-uniformity and the 'doughnut' shape with a possible hole at the centre present serious problems both for thick film combinatorial studies of ceramics and for forming functionally graded products using direct ceramic ink jet printing. Interventions to solve these problems were launched and the interpretation of their results provides an explanation for these effects.

Table 3.6 Analysis by EDS of printer- (P) and manually-prepared (M) ceramic mixtures deposited on silicone release paper.

Ink ID	Planned Composition / wt.%	EDS analysis / wt% [a]					
		Top surface		Lower Surface		Cross section	
		P	M	P	M	P	M
D	ZrO_2 50	83 ± 5	73 ± 9	51 ± 2	52 ± 1	52 ± 3	52 ± 2
	Al_2O_3 50	17 ± 5	27 ± 9	49 ± 2	48 ± 1	48 ± 3	48 ± 2
E	Al_2O_3 50	84 ± 13	81 ± 16	53 ± 3	50 ± 3	51± 3	49 ± 3
	TiO_2 50	16 ± 13	19 ± 16	47 ± 3	50 ± 3	49 ± 3	51 ± 3
F	TiO_2 50	16 ± 19	10 ± 21	47 ± 2	48 ± 1	52 ± 6	47 ± 1
	ZrO_2 50	84 ± 19	90 ± 21	53 ± 2	52 ± 1	48 ± 6	53 ± 1
G	Al_2O_3 25	26 ± 14	12 ± 11	26 ± 1	26 ± 1	28 ± 3	25 ± 2
	TiO_2 25	6 ± 7	9 ± 12	24 ± 2	24 ± 0	24 ± 2	24 ± 2
	ZrO_2 50	67 ± 21	79 ± 22	50 ± 2	50 ± 1	48 ± 3	51 ± 3

[a] Average for five arrays at different positions shown in Figure 2.8 with 95 % confidence limit.

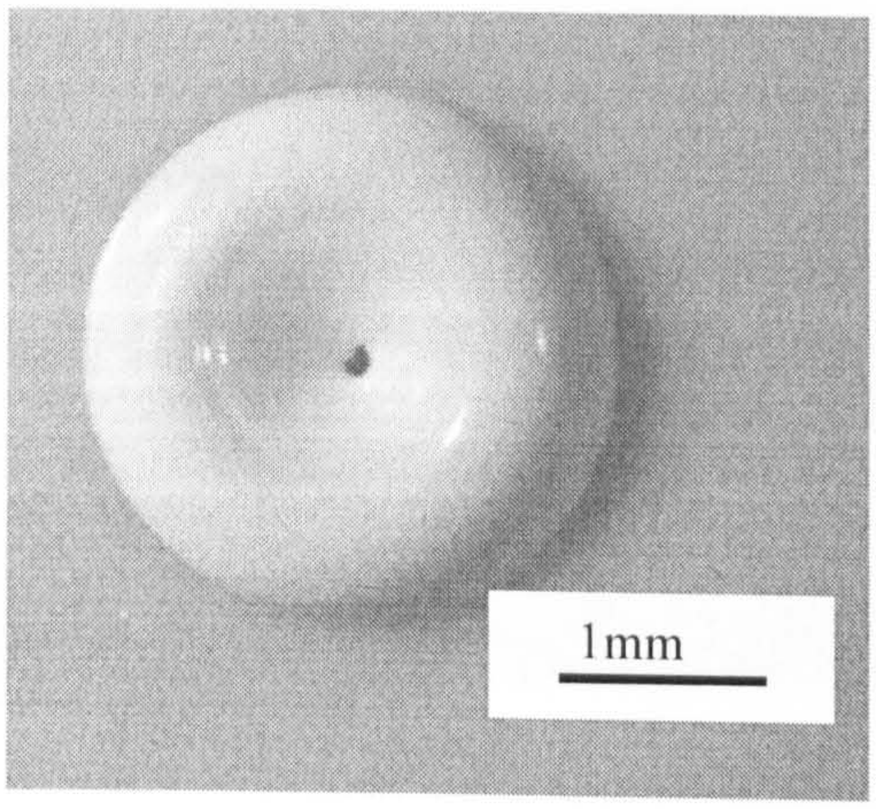

(a)

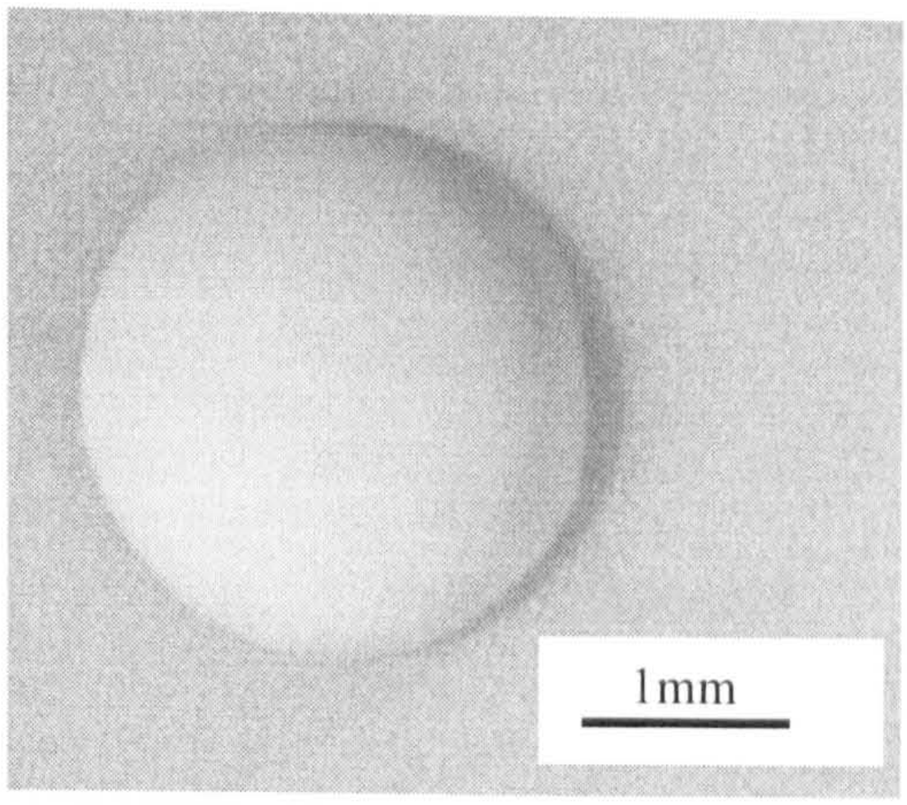

(b)

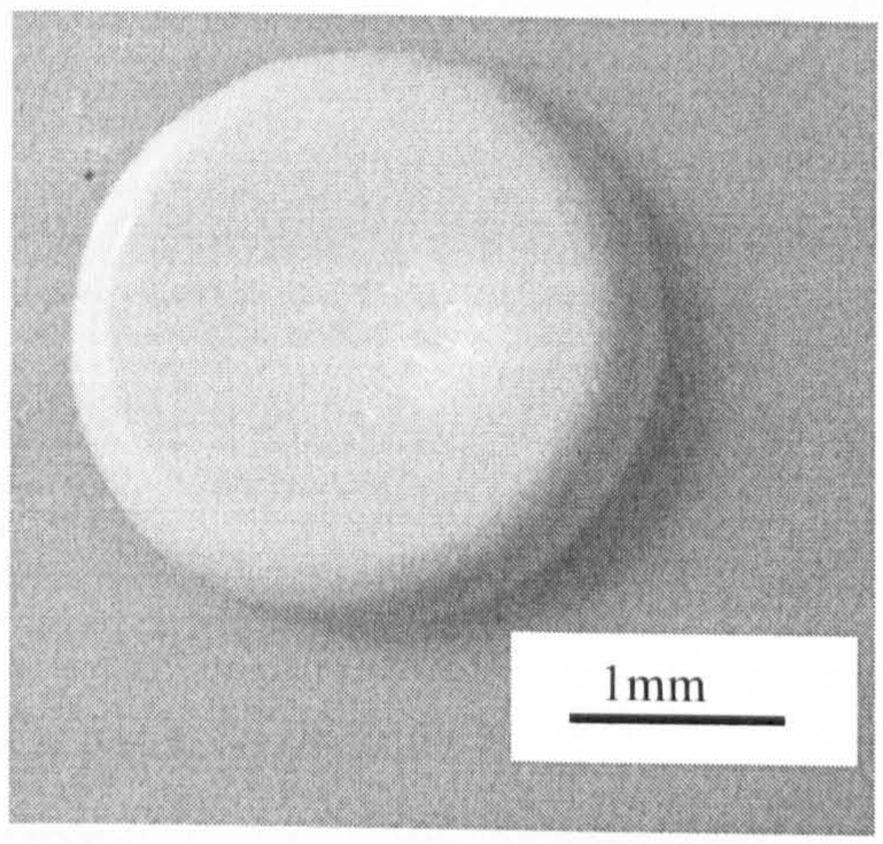

(c)

Figure 3.6 The shape of droplet residues. (a) Colloidal suspension containing around 1 wt% dispersant (Ink G). (b) Colloidal suspension containing excess amount of dispersant. (Ink J) (c) Suspension containing no dispersant (Ink F').

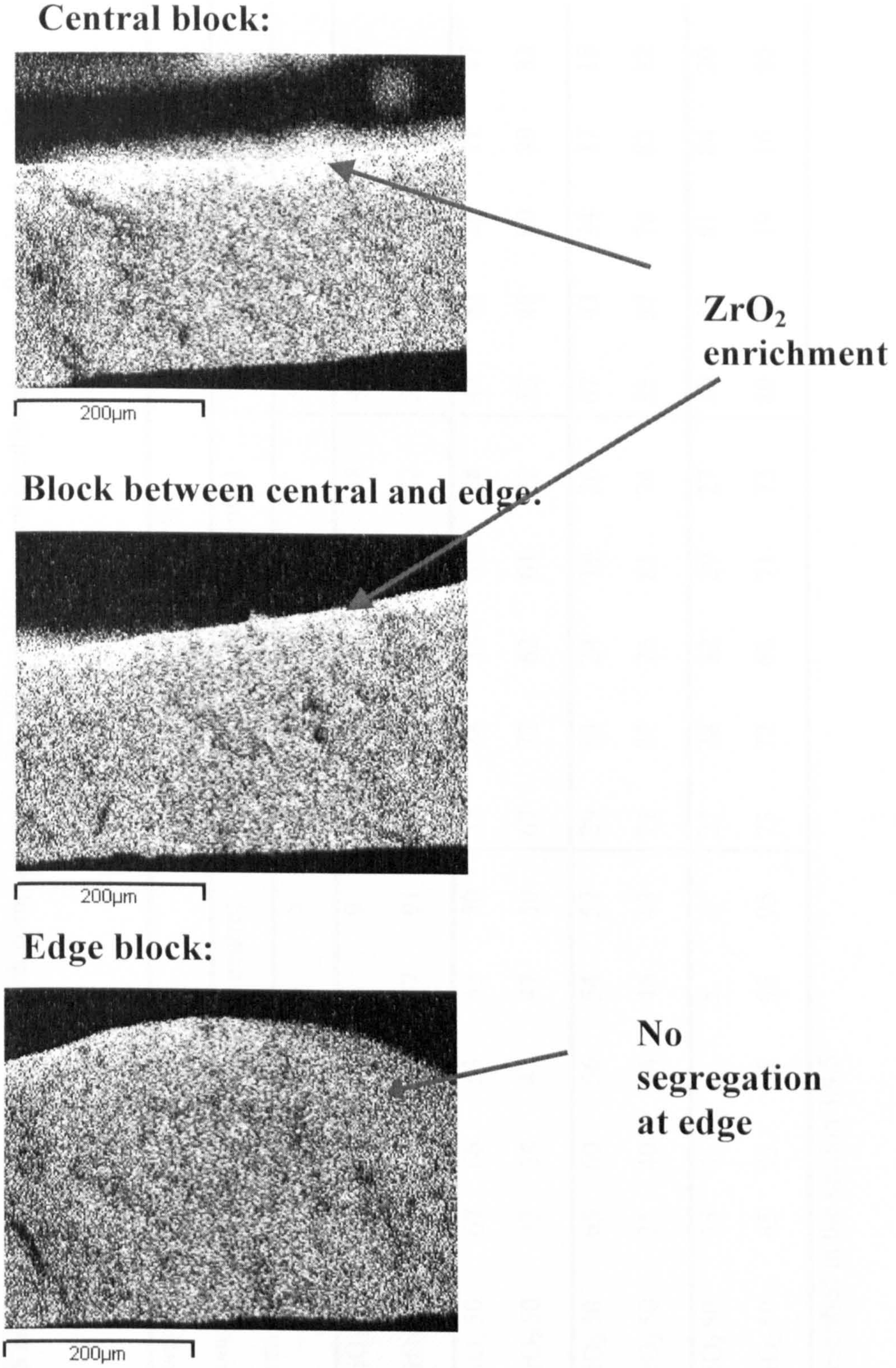

Figure 3.7 Elemental mapping showing the depth of the segregated ZrO_2 layer on the upper surface of residue from ink F.

Table 3.7 EDS analysis for droplet residues of ink composition F with different dispersant conditions, manually placed on silicone release paper.

Ink Designation	Purposed Composition /wt%	EDS analysis / wt%														
		Top surface (Edge to centre)					Lower Surface (Edge to centre)					Cross section (Top to bottom)				
		1	2	3	4	5	1'	2'	3'	4'	5'	A	B	C	D	E
F with dispersant	TiO_2 50	36	1	1	3	9	47	48	49	49	48	46	47	48	48	47
	ZrO_2 50	64	99	99	97	91	53	52	51	51	52	54	53	52	52	53
F without Dispersant	TiO_2 50	67	66	53	53	50	33	28	38	39	28	47	52	20	11	17
	ZrO_2 50	33	34	47	47	50	67	72	62	61	72	53	48	80	89	83
Dispersant on TiO_2 *	TiO_2 50	65	60	56	54	57	29	13	24	19	26	67	43	24	17	18
	ZrO_2 50	35	40	44	46	43	71	87	76	81	74	33	57	76	83	82
Dispersant on ZrO_2 *	TiO_2 50	35	5	5	5	5	27	28	32	29	27	20	48	81	84	20
	ZrO_2 50	65	95	95	95	95	73	72	68	71	73	80	52	19	16	80

* Details are described in the section 3.4.5.

Table 3.8 EDS analysis for droplet residues of ink compositions D with different dispersant conditions, manually placed on silicone release paper.

Ink Designation	Purposed Composition / wt%	EDS analysis / wt%														
		Top surface (Edge to centre)					Lower Surface (Edge to centre)					Cross section (Top to bottom)				
		1	2	3	4	5	1'	2'	3'	4'	5'	A	B	C	D	E
D with dispersant	ZrO_2 50	69	75	75	82	65	51	53	52	52	51	52	52	55	51	51
	Al_2O_3 50	31	25	25	18	35	49	47	48	48	49	48	48	45	49	49
D without dispersant	ZrO_2 50	52	51	51	50	51	51	50	51	51	51	52	52	53	52	51
	Al_2O_3 50	48	49	49	50	49	49	50	49	49	49	48	48	47	48	49
Dispersant on Al_2O_3 *	ZrO_2 50	33	18	25	25	26	59	62	62	58	50	23	17	34	82	80
	Al_2O_3 50	67	82	75	75	74	41	38	38	42	50	77	83	66	18	20
Dispersant on ZrO_2 *	ZrO_2 50	42	51	52	52	53	38	47	45	43	42	41	38	37	42	56
	Al_2O_3 50	58	49	48	48	47	62	53	55	57	58	59	62	63	58	44

* Details are described in the section 3.4.5.

3.4 Particle segregation

It is a necessary but not sufficient condition of combinatorial library preparation that the volumetric calibrations described in section 3.2.3 are sound. It is also necessary that ink mixing in the well-plate is thorough. A further requirement is that the inks should remain mixed as each droplet dries.

Initial experiments (section 3.3.6) on mapping the powder concentrations throughout a dried droplet residue on the substrate showed that this is not always the case. Such segregation effects have been noted before in alcohol-based suspension[40].

3.4.1 Deposition on porous substrates

In previous work[40], there was no segregation when droplets were deposited on dried, pre-placed, porous layers of ink. Droplets were therefore manually placed on plaster of Paris which is used in slip casting and provides rapid separation of powder from its suspending fluid. Table 3.9 shows that all regions of these manually-prepared ink mixtures deposited on this porous substrate agreed with the planned composition, although slightly larger errors were encountered for the analysis of the upper surface.

Similar enhancement of compositional uniformity by capillarity was obtained by placing drops on micro-porous cellulose nitrate membranes. Figure 3.8 compares the pore structure of plaster of Paris (Figure 3.8a) with that of cellulose membrane (Figure 3.8b). Drops of inks F and G were mixed and deposited manually onto cellulose nitrate membrane. Samples were also mixed and printed by the printer on cellulose nitrate membranes. The results show that faster drying again improved compositional homogeneity (Table 3.10) allowing the printer to produce planned compositions.

Table 3.9 Average EDS results for ink mixtures manually deposited on plaster of Paris

Ink ID	Planned Composition / wt.%		EDS analysis / wt% [a] Top Surface	Lower Surface	Cross section
G	Al_2O_3	25	22 ± 5	23 ± 1	23 ± 2
	TiO_2	25	25 ± 5	26 ± 0	28 ± 2
	ZrO_2	50	53 ± 10	50 ± 1	49 ± 2

[a] Average for five arrays at different positions shown in Figure 2.8 with 95 % confidence limits.

Table 3.10 Average EDS results for manually-prepared (M) and machine mixed and printed (P) ink mixtures deposited on micro-porous cellulose nitrate membrane

Ink ID	Planned Composition / wt.%		EDS analysis / wt% [a] Top surface		Lower Surface		Cross section	
			P	M	P	M	P	M
F	TiO_2	50	50	48	53	51	49	47
	ZrO_2	50	50	52	47	49	51	53
G	Al_2O_3	25	25	23	27	26	26	25
	TiO_2	25	24	24	26	26	25	22
	ZrO_2	50	51	53	47	48	49	54

[a] Average for three arrays at different positions.

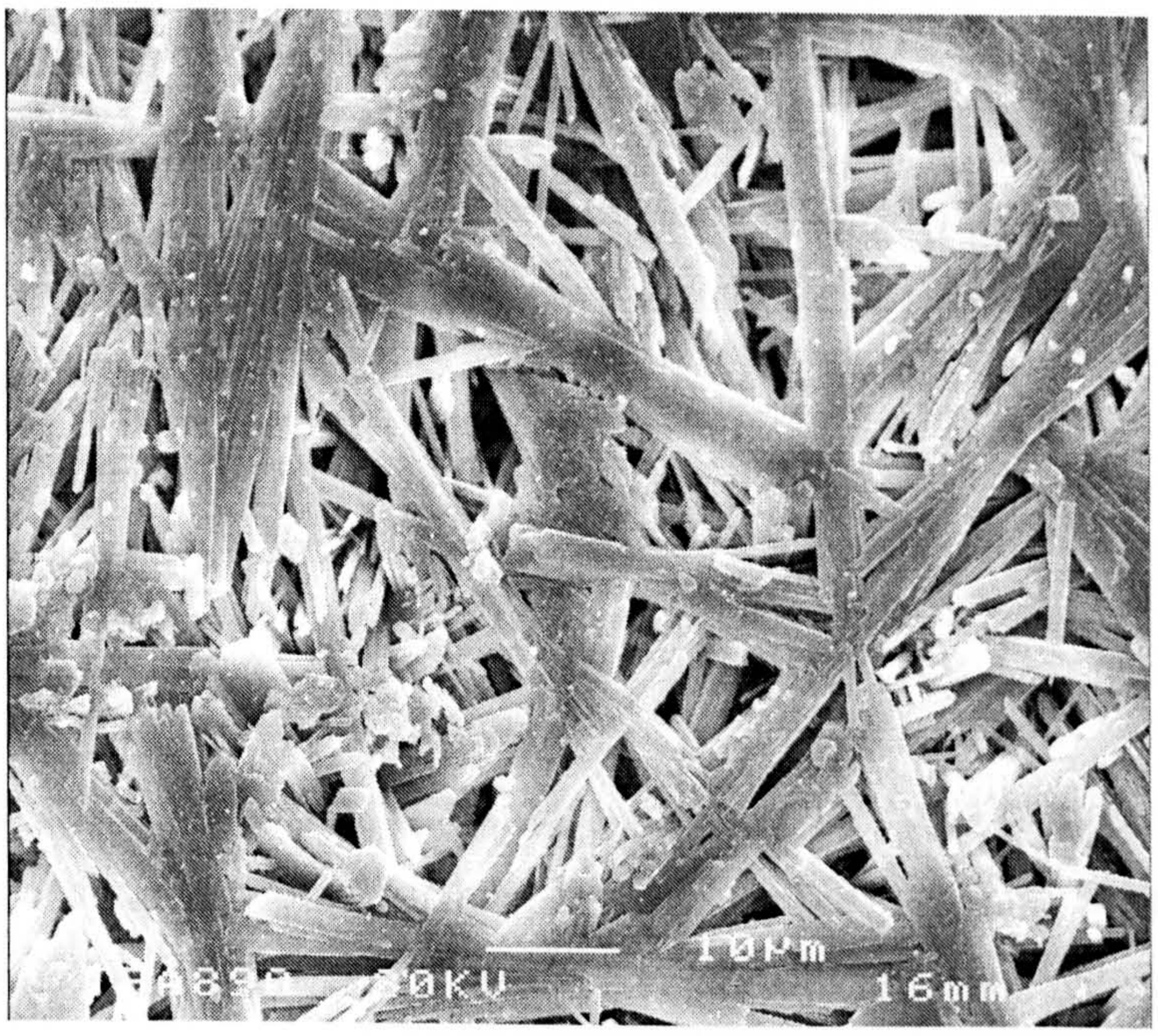

(a) SEM picture of calcium sulphate (Plaster of Paris) substrate

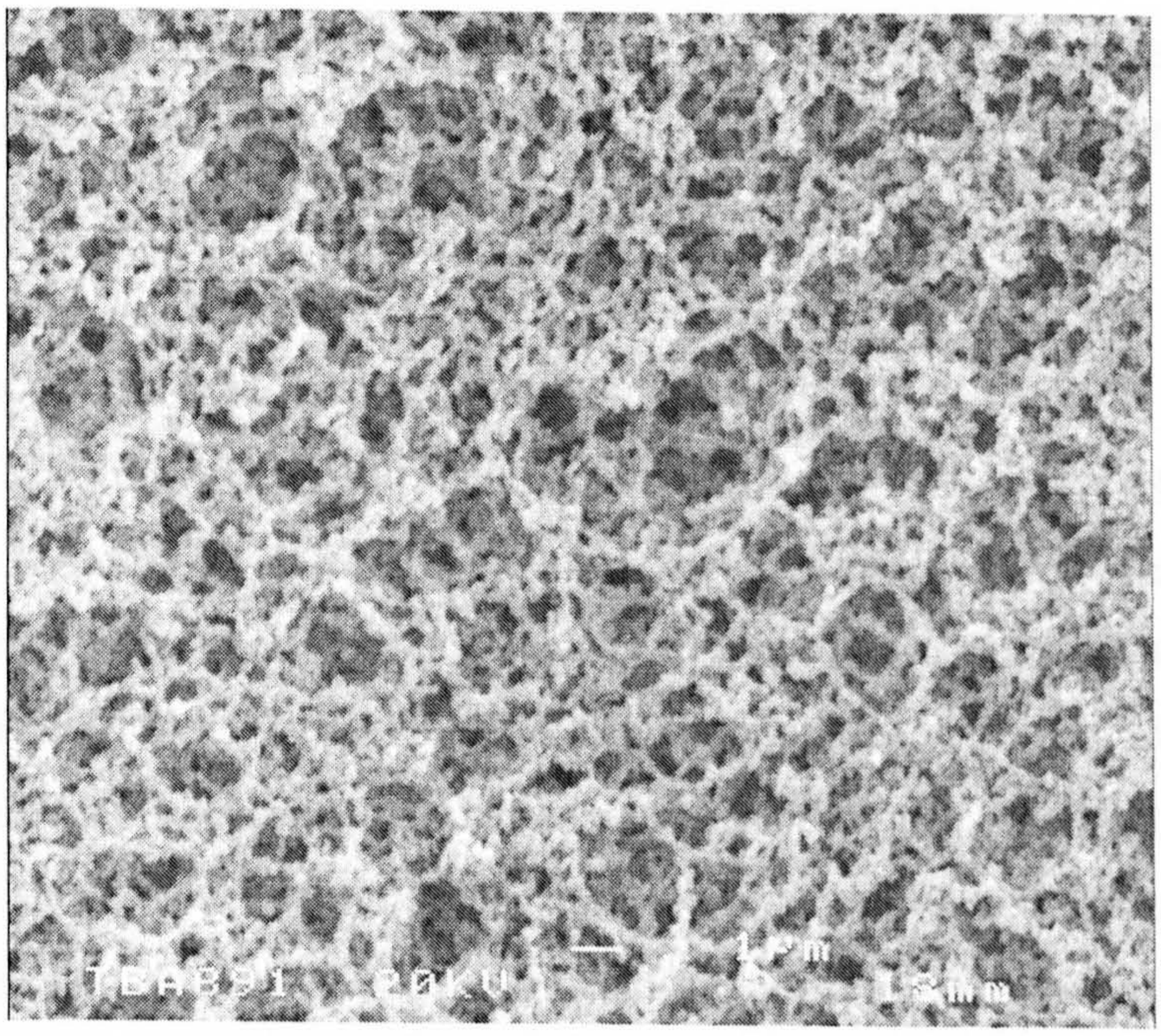

(b) SEM picture of cellulose nitrate membranes

Figure 3.8 Porous substrates used for rapid separation of powder from suspending fluid.

3.4.2 Effects of particle size and density

The simplest explanation for segregation is the selective sedimentation of either larger or more dense particles according to Stoke's law which gives the terminal velocity V_0 as

$$V_0 = \frac{gd^2(\rho - \rho')}{18\eta}, \qquad (3.1)$$

where g is the local acceleration due to gravity (or a centrifugal field), d is the particle diameter, ρ is particle density, ρ' is the fluid density and η is fluid viscosity. As described in Table 2.1, the density and average particle size of powders are ZrO_2 powder (5750 kgm^{-3}, 0.9 μm), Al_2O_3 (3987 kgm^{-3}, 0.5 μm) and TiO_2 (3850 kgm^{-3}, 0.15 μm). However, considering the average particle size and density of powders, it is clear that there is no evidence of preferred sedimentation; indeed there are examples where larger and denser particles ascend to the upper surface (Table 3.6).

Using the particle size distributions shown in Table 3.1, 47% ZrO_2 powder but only 2.7% TiO_2 is greater than 0.7 μm. ZrO_2 also has much higher density (5750 kg m^{-3}) than TiO_2 (3850 kg m^{-3}). For the 50% ZrO_2 - 50%TiO_2 ink, ZrO_2 should be depleted on the upper surface due to preferential sedimentation but as shown by EDS (Table 3.7 row 1), TiO_2 almost disappeared on the upper surface of the residue. This segregation cannot be explained by preferential sedimentation. The same conclusion can be drawn from the other three compositions in Table 3.6. There is no indication of coarser or denser particles settling out.

3.4.3 Effect of dispersant

In order to assess the effects of dispersant, compositions D and F (described in Table 2.3) were prepared without dispersant (which was replaced by the same amount of distilled water). These suspensions (D' and F') were manually prepared and mixed for 1ks with the ultrasonic probe and deposited on silicone release paper.

The results for composition F (TiO_2- ZrO_2 system) with and without dispersant are compared in Table 3.7 rows 1 and 2. The difference in these composition scans is striking. Without dispersant, the upper surface, instead of showing excess zirconia, now presents a slight deficit. No effect of radial distribution can be detected. This implies that the segregation of ZrO_2 to the upper surface seen before, was associated with the presence of dispersant. In contrast, the lower surface is now rich in ZrO_2: an effect that can indeed be attributed to preferential sedimentation. Such sedimentation is clearly seen in the cross section which has a steady increase in ZrO_2 from top to bottom.

The results for ink D (ZrO_2-Al_2O_3 system) with and without dispersant are compared in Table 3.8 rows 1 and 2. In the case of the ink with dispersant, ZrO_2 is richer on the upper surface. Without dispersant, there is no segregation; the upper surfaces, cross-sections and lower surfaces of residues agree well with the planned composition. In this case, there is no preferential sedimentation. This result is further confirmation that segregation on the upper surface is associated with the presence of dispersant.

3.4.4 Order of mixing

It is well known that the order of mixing when preparing colloidal suspensions can affect their properties. Taking two binary compositions in order to demonstrate the generality of the result, three preparation sequences were used. For a composition containing powder A, B, dispersant and water, the sequences

were: (a) powder A was mixed with the full amount of dispersant (i.e., the amount of dispersant described in the Table 2.3) and half the amount of water first, then powder B was mixed with the remaining half of water which was then added. (b) powder A and powder B were mixed with half the water first and then dispersant was mixed with the other half of water and then added; (c) powder B was mixed with the full amount of dispersant and half the amount of water first, then powder A was mixed with the remaining half of water and added. In the above, each mixing was enhanced by ultrasonic probe dispersion.

For the TiO_2- ZrO_2 system as shown in Table 3.11a, the lower surface is unaffected by the order of mixing in each case. The results agreed with the planned composition. The depth profile for sequence (b) also agreed with the planned composition. Sequence (a) and Sequence (c) show similar general trends for the depth profile, which is not consistent with the planned composition. In each case, the top surfaces all show depletion of the fine TiO_2. Considering the extent of depletion of TiO_2 on the upper surface, the order of mixing neither reduces segregation nor offers a route to solution of the problem. It raises more questions about compositional distributions in the depth profile which require a different experiment approach (See section 3.4.5).

The ZrO_2-Al_2O_3 system is shown in Table 3.11b: In each case, the lower surface is slightly rich in ZrO_2: an effect that can be attributed to preferential sedimentation. This is a marginal effect and does not appear definitively in the cross section except in sequence (a) and (b). In each case, the top surface compositions all show depletion of Al_2O_3. Considering the extent of depletion of Al_2O_3 on the upper surface, the sequence of adding dispersant to Al_2O_3 first is more beneficial than the results from the case of adding dispersant to ZrO_2 first. The general conclusion is that the order of mixing does not have a definitive effect on segregation and does not provide a solution.

Table 3.11a Effect of order of mixing on EDS analysis of residues deposited from inks F on silicone release paper

Mixing Sequence	Planned Composition / wt%	EDS analysis / wt%														
		Top surface (Edge to centre)					Bottom Surface (Edge to centre)					Cross section (Top to bottom)				
		1	2	3	4	5	1'	2'	3'	4'	5'	A	B	C	D	E
a)																
Dispersant	TiO_2 50	27	0	0	0	0	54	56	57	54	54	38	62	63	64	63
to ZrO_2 first	ZrO_2 50	73	100	100	100	100	46	44	43	46	46	62	38	37	36	37
b)																
Dispersant to	TiO_2 50	36	1	1	3	9	47	48	49	49	48	46	47	48	48	47
both ZrO_2	ZrO_2 50	64	99	99	97	91	53	52	51	51	52	54	53	52	52	53
and TiO_2																
c)																
Dispersant to	TiO_2 50	41	8	8	8	8	44	51	48	50	47	58	71	64	69	49
TiO_2 first	ZrO_2 50	59	92	92	92	92	56	49	52	50	53	42	29	36	31	51

Table 3.11b Effect of order of mixing on EDS analysis of residues deposited from inks D on silicone release paper

Mixing Sequence	Purposed Composition / wt%	EDS analysis / wt%														
		Top surface (Edge to centre)					Bottom Surface (Edge to centre)					Cross section (Top to bottom)				
		1	2	3	4	5	1'	2'	3'	4'	5'	A	B	C	D	E
a)																
Dispersant to ZrO_2	ZrO_2 50	90	92	93	92	91	56	54	48	51	55	76	39	42	58	77
ZrO_2 first	Al_2O_3 50	10	8	7	8	9	44	46	52	49	45	24	61	58	42	23
b)																
Dispersant to both ZrO_2 and Al_2O_3	ZrO_2 50	69	75	75	82	65	51	53	52	52	51	52	52	55	51	51
	Al_2O_3 50	31	25	25	18	35	49	47	48	48	49	48	48	45	49	49
c)																
Dispersant to Al_2O_3 first	ZrO_2 50	49	67	57	43	74	58	58	57	57	58	43	48	50	54	61
	Al_2O_3 50	51	33	43	57	26	42	42	43	43	42	57	52	50	46	39

3.4.5 Removal of excess dispersant

When dispersant is added to a suspension it tends to adsorb strongly on the solid surface until saturation is reached and the excess remains in solution. The excess can be removed by centrifuging the suspension, removing the supernatant and re-dispersing the powder in the same mass of liquid. The amount of dispersant in solution can be found by drying and weighing.

Using ink F, TiO_2 powder was first mixed with half the amount of water and the full amount of dispersant. The resulting TiO_2 ink contained 1.31wt.% Dispex. After centrifuging for 1.8ks, gravimetric analysis showed that half the dispersant remained in the supernatant and was replaced with the same mass of distilled water. TiO_2 powder was re-dispersed into the replaced water. ZrO_2 powder, mixed with the other half of water without dispersant was then added. This produces a mixed ink with 50 wt.% TiO_2 – 50 wt.% ZrO_2 in which the dispersant is initially adsorbed on the TiO_2. EDS analysis of residues (Table 3.7, row 3) show ZrO_2 depletion on the upper surface and evidence of preferential sedimentation of ZrO_2 in the cross section and on the lower surface.

Again using ink F, ZrO_2 powder was treated with dispersant instead. Excess of dispersant was removed, and this suspension mixed with TiO_2 ink without dispersant. The results (Table 3.7, row 4) show TiO_2 depletion on the upper surface. However preferential sedimentation of ZrO_2 was also found in the lower surface. This combined effect is due to the wider particle size range of the ZrO_2 powder: larger particles are still able to sediment.

This selective procedure was then followed with ink D (50wt% Al_2O_3–50 wt% ZrO_2). Dispersant was first added only to the Al_2O_3 and the excess removed before adding ZrO_2 free from dispersant. The results (Table 3.8 row 3) indicate ZrO_2 depletion on the upper surface and evidence of preferential sedimentation of ZrO_2 on the lower surface and in the cross section.

Again using ink D, dispersant was added to ZrO_2 powder first, excess was removed and Al_2O_3 ink without dispersant added. The results (Table 3.8, row 4) show that for this mixture, the upper surface is close to the as-planned composition with only slight excess of ZrO_2, but there are signs of Al_2O_3 sedimentation on the lower surface not picked up in the large area scans for the cross-section.

Removing excess dispersant does not provide a general solution to the segregation problem but it illustrates the sensitivity of segregation to preferential adsorption on specific powders; an effect that can over-ride preferential sedimentation under Stoke's law. The important observation was that the powder to which dispersant was preferentially attached was always richer on the upper surface of dried droplets and this general observation helps to explain the phenomenon of separation (*vide infra*).

3.4.6 Use of excess dispersant

As described in 3.4.1, one way of solving the segregation problem is to use porous substrates. There are two problems for implementation of this method: (1) the porous substrates still take finite time to remove solvent from the droplet or cannot remove solvent completely from the droplet to stop the drying process. Some segregation still happens. (2) Some applications of direct ceramic ink jet printing require droplets to be deposited on a particular substrate that may not be porous. For example, as described in section 3.5, ceramic ink droplets are deposited on platinum coated alumina substrates. Therefore a general ink formulation solution that is independent of the substrate is preferable.

It may be that there is an optimum level of dispersant to achieve uniformity. The inks used in previous experiments commonly contain around 1 wt.% Dispex; sufficient to achieve stability during the period of printing. In the next step, inks H, I and J (Table 2.3) were prepared with large amounts of dispersant (10 wt.%). These were manually prepared, mixed for 1ks. with the ultrasonic probe and

deposited on silicone release paper. EDS analysis of these residues, described in Table 3.12, show neither sedimentation nor segregation, the whole body of the residues has uniform composition as planned.

Table 3.12 EDS analysis of droplet residues of multi-component ceramic colloids containing excess dispersant showing uniform composition.

Ink No.	Dispex / wt%	Planned Composition / wt%	EDS analysis / wt% [a]		
			Top surface	Lower Surface	Cross section
H	10	Al_2O_3 50	50 ± 3	52 ± 1	51 ± 2
		ZrO_2 50	50 ± 3	48 ± 1	49 ± 2
I	10	TiO_2 50	50 ± 4	46 ± 1	47 ± 2
		ZrO_2 50	50 ± 4	54 ±1	53 ± 2
J	10	Al_2O_3 25	25 ± 1	26 ± 0	24 ± 1
		TiO_2 25	25 ± 1	23 ± 0	24 ± 1
		ZrO_2 50	50 ± 1	51 ± 0	52 ± 1

[a] Average for five arrays at different positions shown in Figure 2.8 with 95% confidence limits.

These inks presented another difference. The residues of ink H, I, J retained a dome shape (Figure 3.6 b). Figure 3.6 b is a picture of residue from ink J. No cracking was found in such residues. The dome shape may imply that particle movement to the periphery of the droplets is restricted and a uniform hemispherical drop ends up as a uniform dome-shaped residue, unlike previous segregation cases when a uniform hemispherical drop ends as a doughnut shape of residue.

For inks H, I, J which contain 10wt% Dispex, the volume fraction of powder in the residue from the droplets is near 76% so that the assembly of particles can sinter to full density. Although the large amount of dispersant increased the kinematic viscosity of these inks (Table 3.13), inks H, I and J could be ink jet printed by the printer. So, adding a larger amount of dispersant provides a generally sound solution to the segregation problem based on formulation rather than substrate selection achieving a uniform residue of the planned composition. Furthermore, the shape of residue was a simple guide to compositional uniformity.

Table 3.13 Surface tensions and viscosities of suspensions

	Ink ID	Wt.% dispersant in the suspension	Surface tension /mNm^{-1}	Kinematic viscosity /mm^2s^{-1}
Al_2O_3-ZrO_2 system	D	1.1	73.4	1.5
	H	10	62.5	3.7
TiO_2-ZrO_2 system	F	0.66	71.7	1.4
	I	10	66.6	11.4

3.4.7 Mechanism of segregation

The final compositional distribution in residues is set up during drying. For a particle in a droplet of ceramic suspension, there are at least four types of particle motion: i) sedimentation due to gravity, ii) Brownian motion due to collisions with fluid molecules, iii) lateral migration of particles to form a 'foot' at the periphery of the drop and iv) fast recirculation flows that occur in the remaining liquid part of the drop which can easily be seen in the optical microscope. These movements can be restricted by surrounding particles, by dispersant and by flocculation behaviour. The details of the droplet drying process have been described in section 1.9.3. On the basis of iii) and iv), the mechanism of segregation can be interpreted and both the shape and the segregation effects are accounted for here.

From the particle size distributions in Table 3.1, the particle size increases for the series TiO_2, Al_2O_3 and ZrO_2. Table 3.6 indicates that in the Al_2O_3-TiO_2, ZrO_2-TiO_2, Al_2O_3- ZrO_2 and TiO_2- Al_2O_3- ZrO_2 systems, powder with the larger particle size is concentrated on the upper surface. Preferential sedimentation fails to explain the segregations seen on the upper surfaces in these experiments.

In a well-dispersed suspension, particles participate in the radial flow, piling up at the periphery and forming a foot which grows as drying proceeds and leaving a hollow central region which may even produce a hole. A similar situation prevails in the spay drying of ceramic slurries; discrete droplets from well-dispersed slurries in which particles retain mobility during drying, form irregular shaped agglomerates with a central hole. Suspensions with a tendency to flocculate, form dense spherical agglomerates[124]. In the present work, the use of large amounts of dispersant increases viscosity and is likely to impede particle mobility by chain entanglement effects. Sessile drops from these inks dry to leave dome shapes (Figure 3.6 b) with uniform planned composition.

For droplets from suspensions containing ~1wt% dispersant (Inks D, E, F and G), particles have high mobility in the suspension. Visual observation of reflectivity, transparency and the appearance of a discontinuity in the surface, suggest that a higher packing density of powder builds up at the three phase boundary as generally observed[129-131, 133]. The suspension on the rim continues drying as liquid migrates from interior regions to the periphery under capillary forces, eventually forming a 'doughnut' shape in which the centre is depleted and sometimes leaving a hole. The process is illustrated as Figure 3.9.

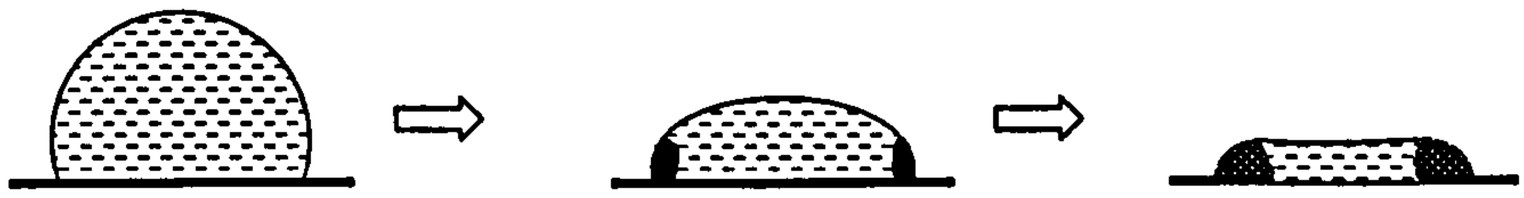

(a) Droplet of uniform composition as deposited

(b) Triple junction is pinned and curvation varies across the surface

(c) Accumulation of powder at the rim

(d) Final shape of residue

(d') In some cases, a hole in the middle of the dried sample can be formed

Figure 3.9 Schematic representation of the observed drying process for droplets from suspensions containing ~1wt% dispersant.

This does not explain the segregation effect, which can only be understood by looking also at the liquid region of the sessile drop bounded by the surrounding foot. As described by Haw at al [136], this region contains vigorous recirculation flows. These can be seen in the optical microscope with oblique illumination. These flows are attributed to Marangoni stresses resulting from surface tension gradients and thermal gradients associated with evaporation of liquid and have been modeled[137]. As the drop dries, this region shrinks while the more densely packed 'foot' grows.

A particle in suspension can either join the 'foot' or participate in the recirculation flows in the central pool. It can be argued that the better dispersed particles participate in the flow while the weakly dispersed particles join the 'foot' and in this way, segregation develops on the upper surface where the well-dispersed particles accumulate. The process is shown schematically in Figure 3.10.

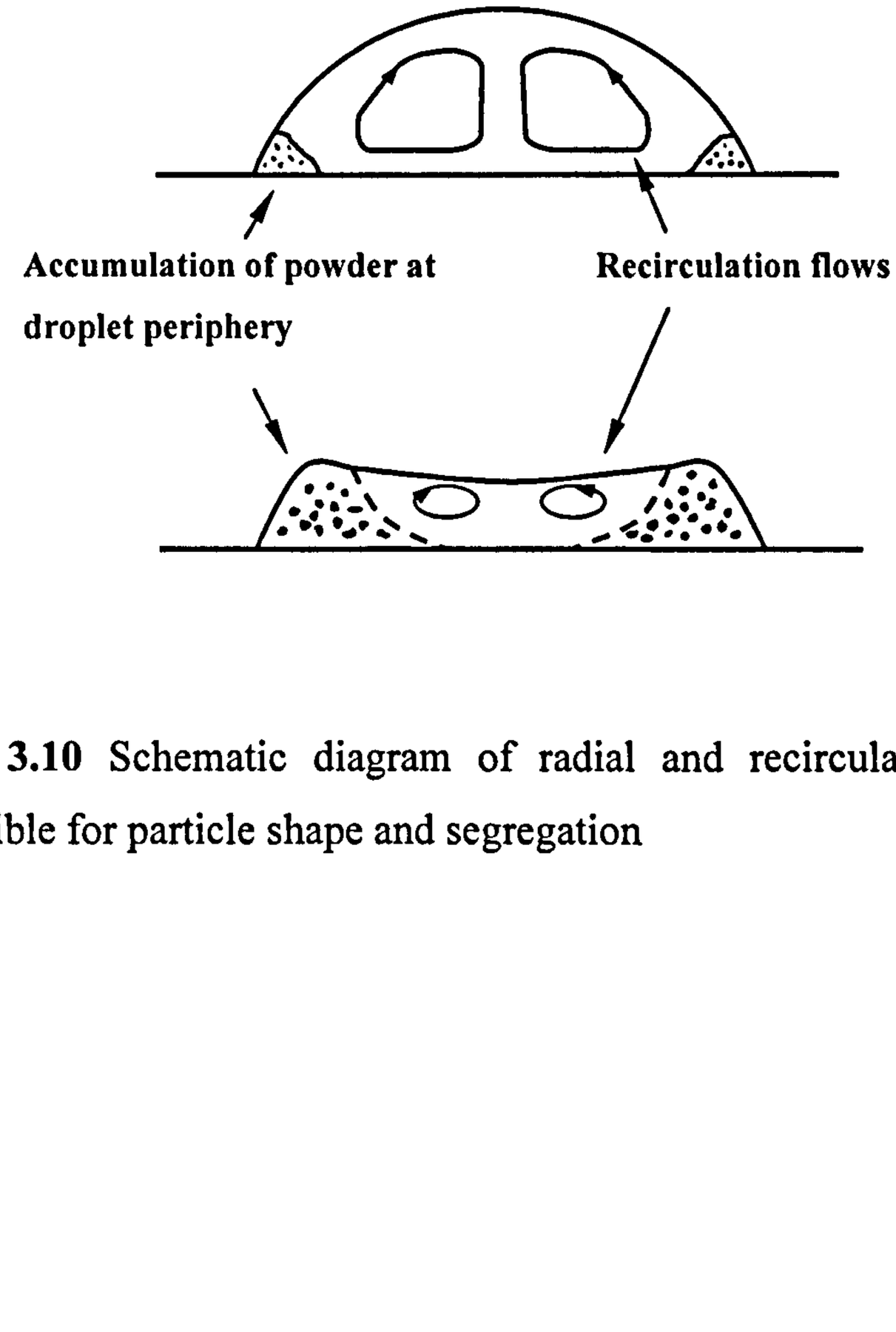

Figure 3.10 Schematic diagram of radial and recirculation flows that are responsible for particle shape and segregation

This explanation is consistent with the geometry of residues and with the observation that at assay position 1 (Tables 3.7 and 3.8 row 1), the composition is closer to that planned than at positions 2-4. Position 1 became isolated from the liquid pool at an earlier stage. The explanation is consistent with the observations that the better dispersed particles always appeared in excess at the top irrespective of their density or particle size. Position 5 is not necessarily worse than position 1 as seen in table 3.8 row 1. When a hole is formed, position 5 is a very thin section from which the final liquid containing well-dispersed particles is drawn laterally by capillary action into position 4 as drying comes to an end.

The behaviour of inks containing no dispersant depended on the particular powders in combination. For the ZrO_2-TiO_2 system, the TiO_2 was a fine powder but the ZrO_2 was a comparatively coarse powder as deduced from SEM images and particle size distributions (Table 3.1). When there was no dispersant, ZrO_2 powder began to sediment, most TiO_2 was still dispersed in the water. These droplets dried to leave a much flatter 'doughnut' shape as shown in Figure. 3.6 (c). After drying, TiO_2 was richer on the upper surface while ZrO_2 powder was preferentially sedimented on the lower surface as evidenced by EDS results (Table 3.7, row 2).

For the Al_2O_3-ZrO_2 system, after the ultrasonic probe was switched off, the powders began to flocculate. The suspension appeared to become more viscous forming a paste rather than a liquid. This is typical of flocculated suspensions[138]. These drops ended as a dome with uniform planned distribution of powder (Table 3.8 rows 2) and it seems reasonable to speculate that this is because a three dimensional flocculated network prevents particles from participating in the two modes of liquid flow. Using flocculation as a means to prevent segregation would provide a solution but it is incompatible with the need to produce suspensions stable against sedimentation.

It is instructive to compare the ZrO_2-TiO_2 system under three conditions: dispersant added to both powders, no dispersant added and dispersant attached only to ZrO_2. When dispersant is attached to both ZrO_2 and TiO_2 powders and excess is left in solution, residues of droplets are 'doughnut' shaped with ZrO_2 powder richer on the upper surface and the lower surface agreeing with the planned composition (Table 3.7, row 1). Without dispersant, the residues of droplets are flatter doughnut shapes with preferential sedimentation of ZrO_2 powder (Table 3.7, row 2). With dispersant attached only to ZrO_2, residues of droplets have both types of segregation; ZrO_2 powder is richer on the upper surface yet preferential sedimentation of larger ZrO_2 particles (Table 3.7 row 4) shows up on the lower surface.

In the Al_2O_3- ZrO_2 system, when dispersant is only attached to ZrO_2 with no excess available for Al_2O_3 in the solution, residues of droplets are 'doughnut' shaped with much more uniform composition (Table 3.8, row 4). The ZrO_2 is slightly denser and coarser than the Al_2O_3 so the effects of sedimentation and ascent in the liquid zone tend to cancel.

3.5 Drying behaviour of droplets of mixed powder suspensions

3.5.1 Droplet profiles during drying

The ceramic suspensions (Table 2.3) used in this thesis can be classified in three types based on the amount of dispersant used. Type I consist of mixtures with large (10%) additions of dispersant, (Inks H, I and J). This is far more than that needed to provide stabilization against sedimentation for several hours to allow printing. Type II are mixtures (Inks A, C, D, E, F and G) containing a smaller amount dispersant (~1 wt. %), though more than enough to preserve stability for the purpose of printing. Type III are mixtures of water and powders without dispersant (Inks B, D' and F').

Droplets from type I suspensions present consistent drying behaviour. As shown in Figure 3.11 using Ink J as the example, the contact angle and height of droplets steadily reduced until a minimum value was reached. The contact diameter was almost unchanged during drying. The droplet that began as a spherical cap completed drying still as a dome as shown in Figure 3.6 (b). As described in section 3.4.5, the residues have uniform planned distribution of powder on both upper and lower surfaces and on cross sections as analyzed by EDS (Table 3.11). Such droplets form ideal combinatorial library members because their shape is suited to testing by electrical or optical probes and composition is consistent.

Droplets of type II suspensions (~1 wt.% dispersant) had a quite different drying behaviour. Using Ink G as the example (Figure 3.12), in the first stage, up to 0.9 ks, the contact angle and height of droplets consistently decreased. In the second stage, at constant contact angle, the height of droplets decreased. In the last stage, both the apparent height of droplets and the contact angle were unchanged but the silhouette imaged against back-illumination does not disclose the pronounced collapse of the central region. The bulk of the ceramic powder, now situated at the rim, subsequently dried. Type II residue therefore ended as a 'doughnut'

shape sometimes with a hole in the centre as shown in Figure 3.6 (a). The drying process has been described in Figure 3.9 and discussed in section 3.4.6.

As described in section 3.3.6, when EDS analysis was performed on these residues, the lower surface and cross-sections agreed with the planned composition but segregation of powders occurred on the upper surface. This variation is to a depth of over 10-20 μm depth. Cracking of the residue could also be found sometimes. These are not suitable for combinatorial work because the shape does not allow access by measurement probes and the composition varies on the upper surface.

For Type III suspensions to which no dispersant was added, the drying patterns depended on the powder. The drying of droplets from Ink D' (Al_2O_3-ZrO_2 system) was similar to Type I suspensions that contained excess dispersant. Both the contact angle and height of droplets consistently reduced until a minimum value was reached. The contact diameter was almost unchanged during drying. The residue also retained a dome and had uniform planned powder distribution as did the residues from the droplets of type I suspensions as shown in Table 3.8 rows 2.

For other type III suspensions, (Ink B; single component TiO_2 ink) and F' (TiO_2-ZrO_2 system without dispersant), the drying was similar to type II inks that contained around 1% dispersant, experiencing three stages as described above. The EDS result of the residue of droplets from Ink F' (Table 3.7 rows 2) shows non-uniform compositional distribution. The resulting residue also had a 'doughnut' shape, as did the type II inks. The residue of droplets from Ink H is shown in Figure 3.6 (c).

Figure 3.13 gives percentage mass loss as a function of time for the ZrO_2- Al_2O_3 system (Inks D, D'and H) and the TiO_2-ZrO_2 system (Inks F, F' and I).

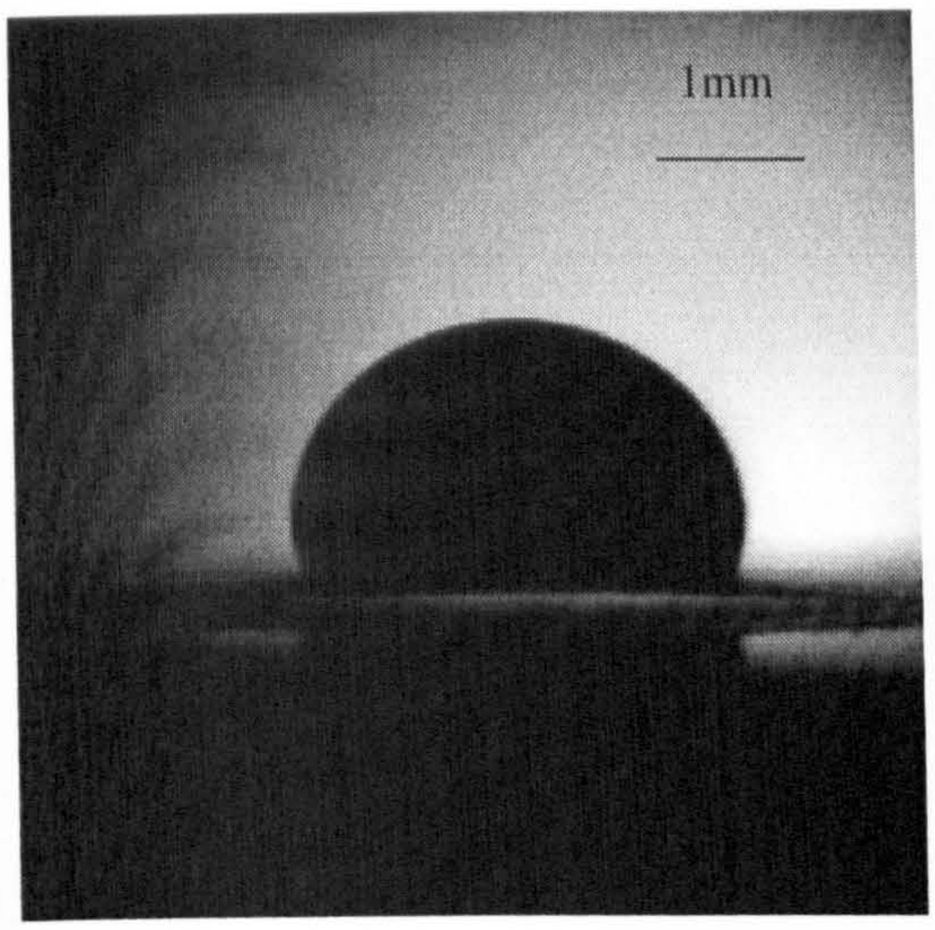

θ = 107°, t = 0s

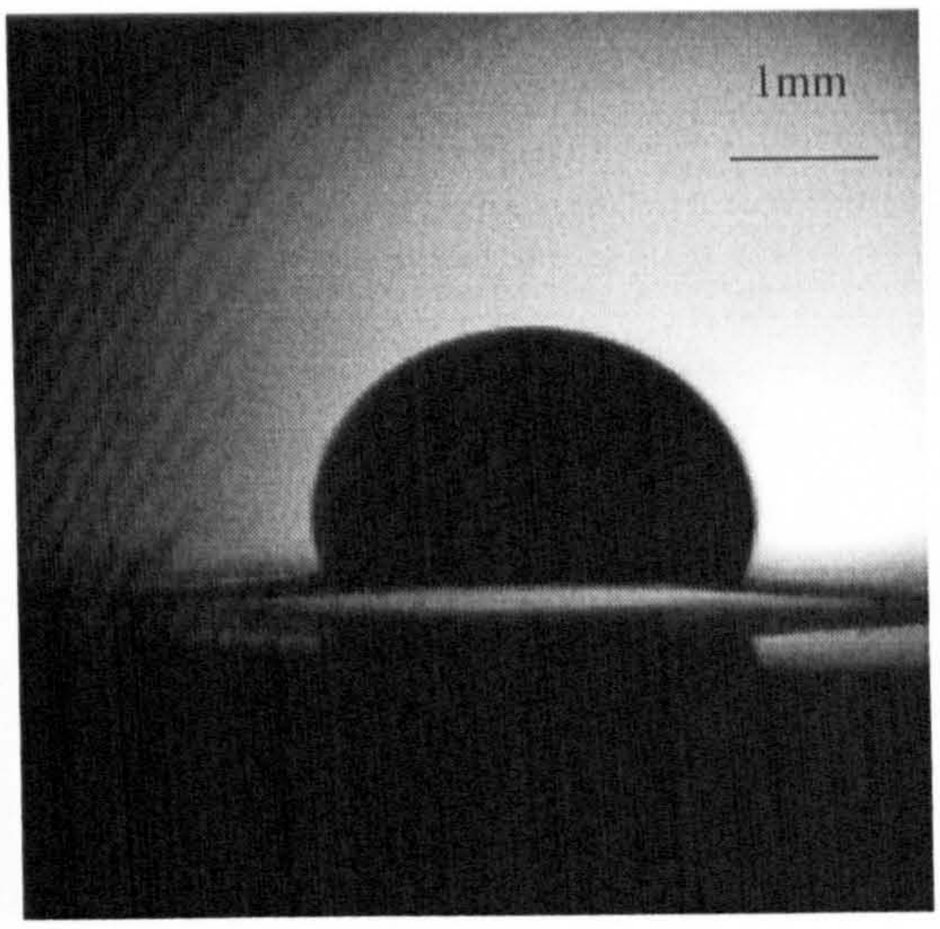

θ = 105°, t = 0.3ks

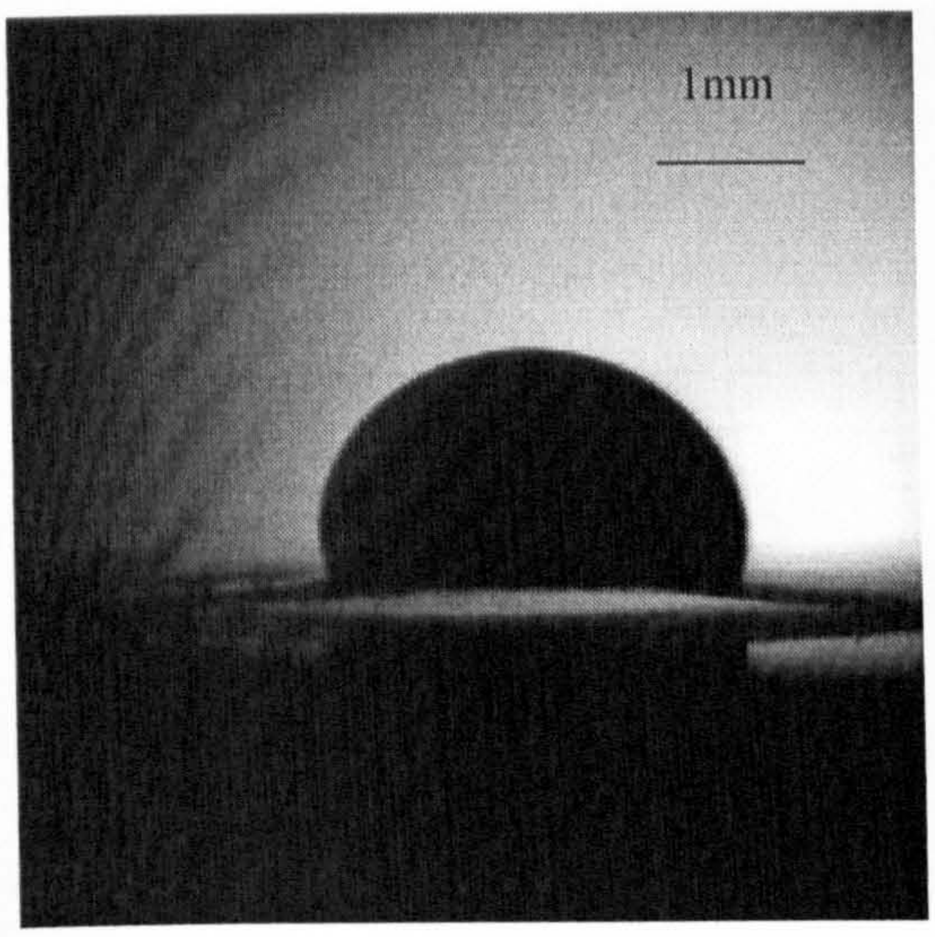

θ =100°, t = 0.6ks

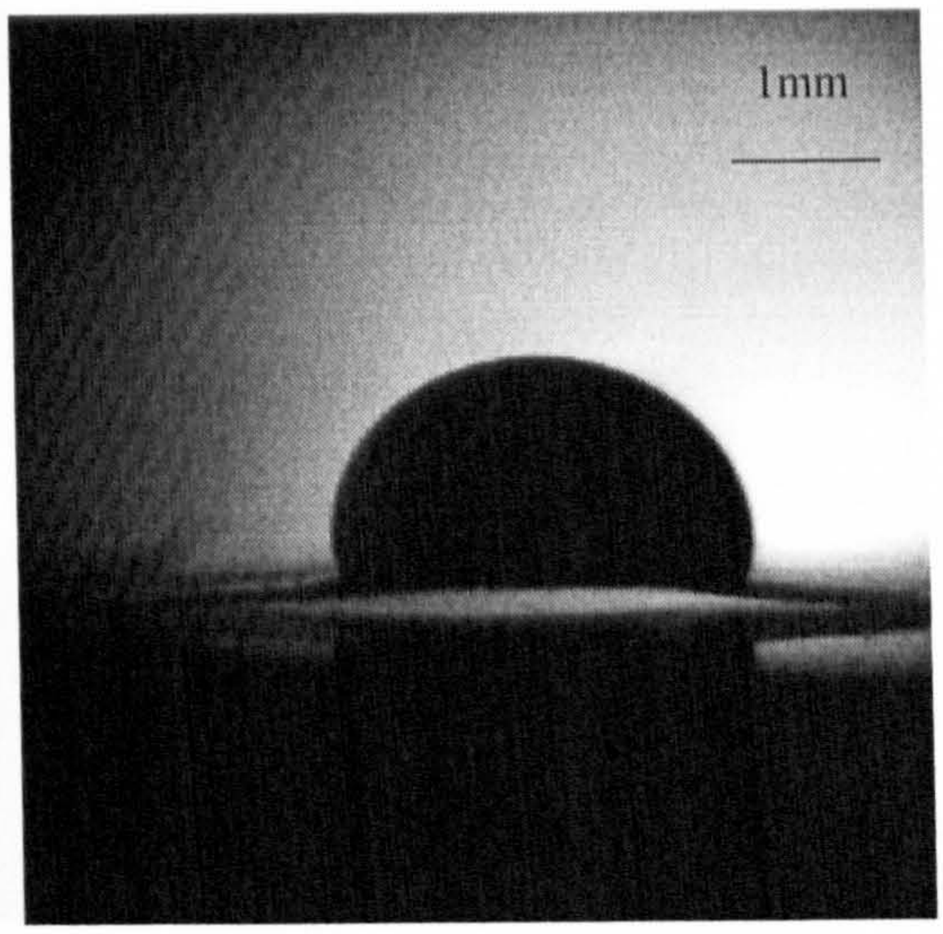

θ =98°, t = 0.9ks

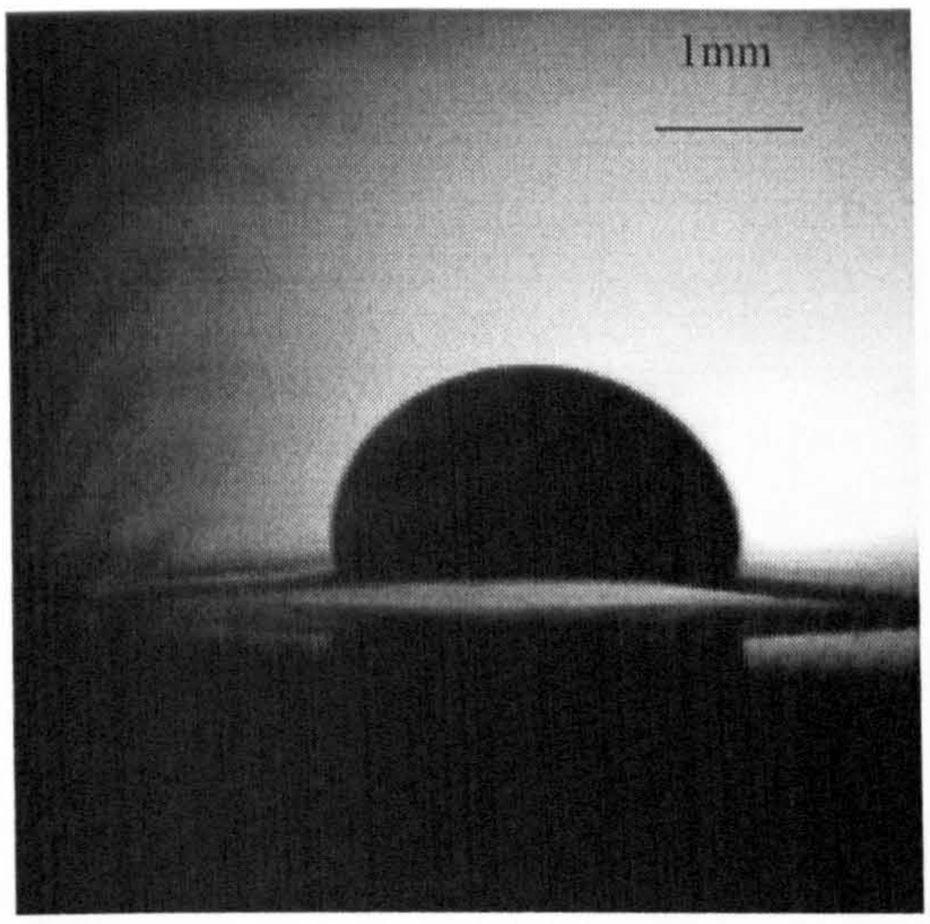

θ = 93°, t =1.2ks

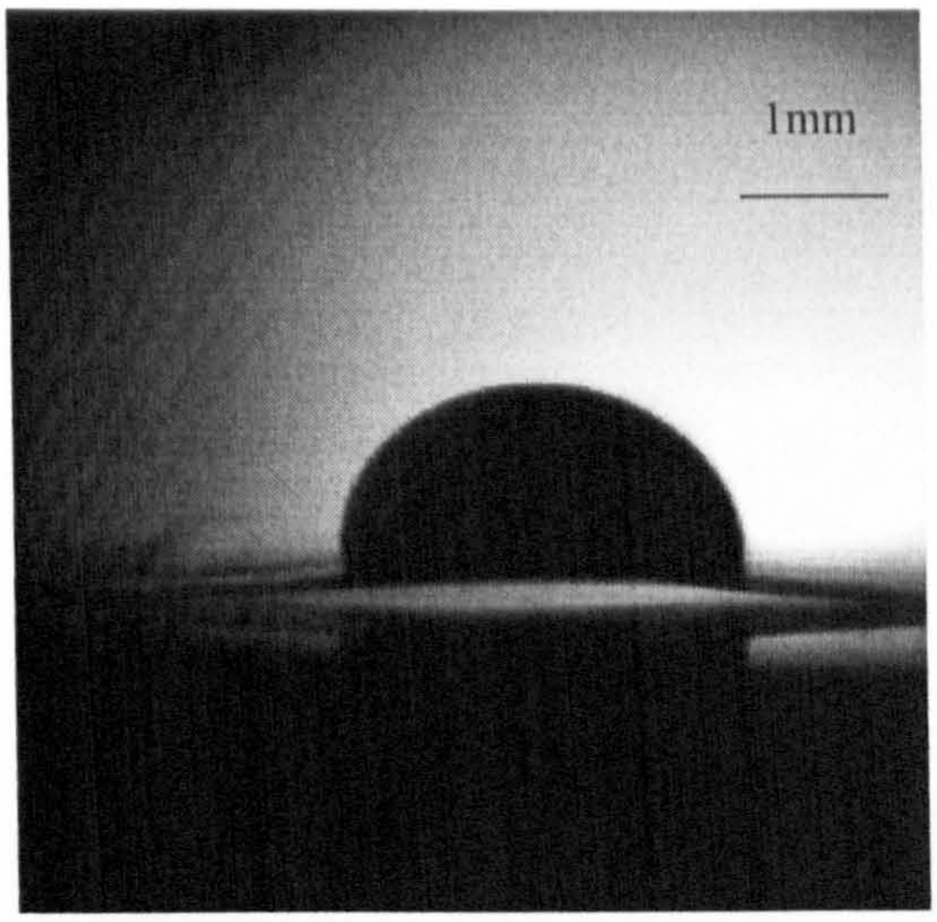

θ = 92°, t =1.5ks

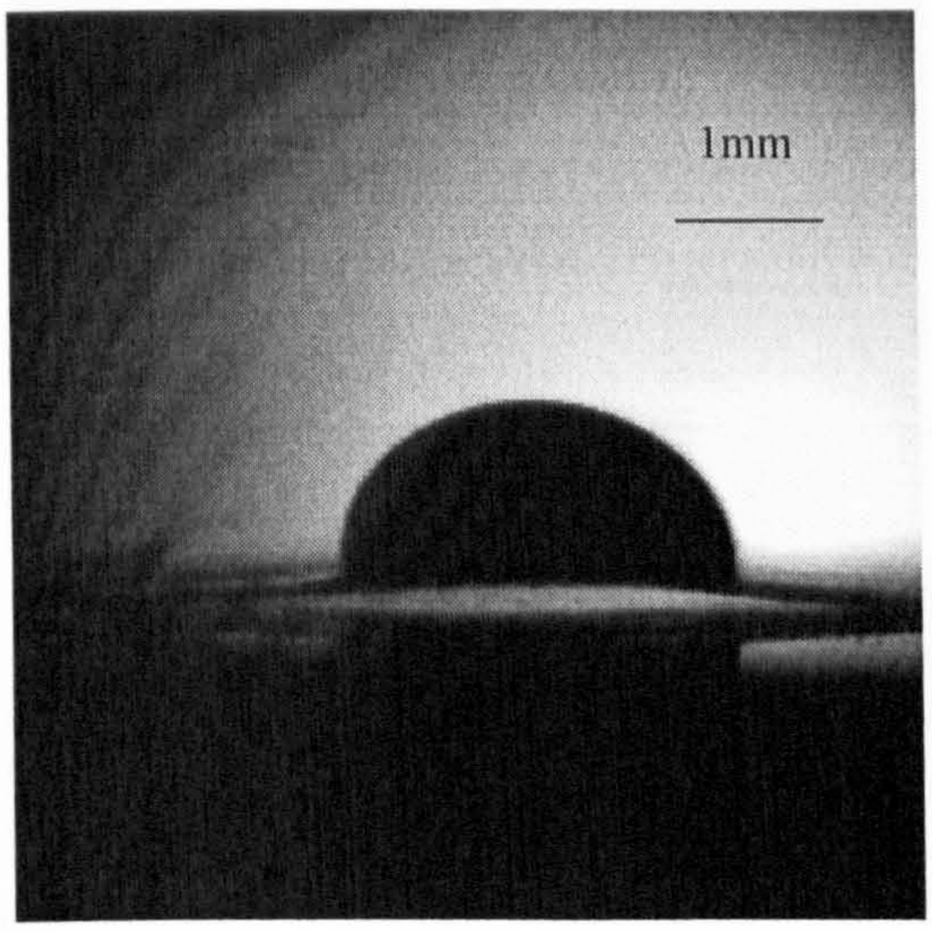

θ = 89°, t =1.8ks

Figure 3.11 The drying process of a droplet of ceramic ink that contains excess amount of dispersant deposited on silicone release paper.

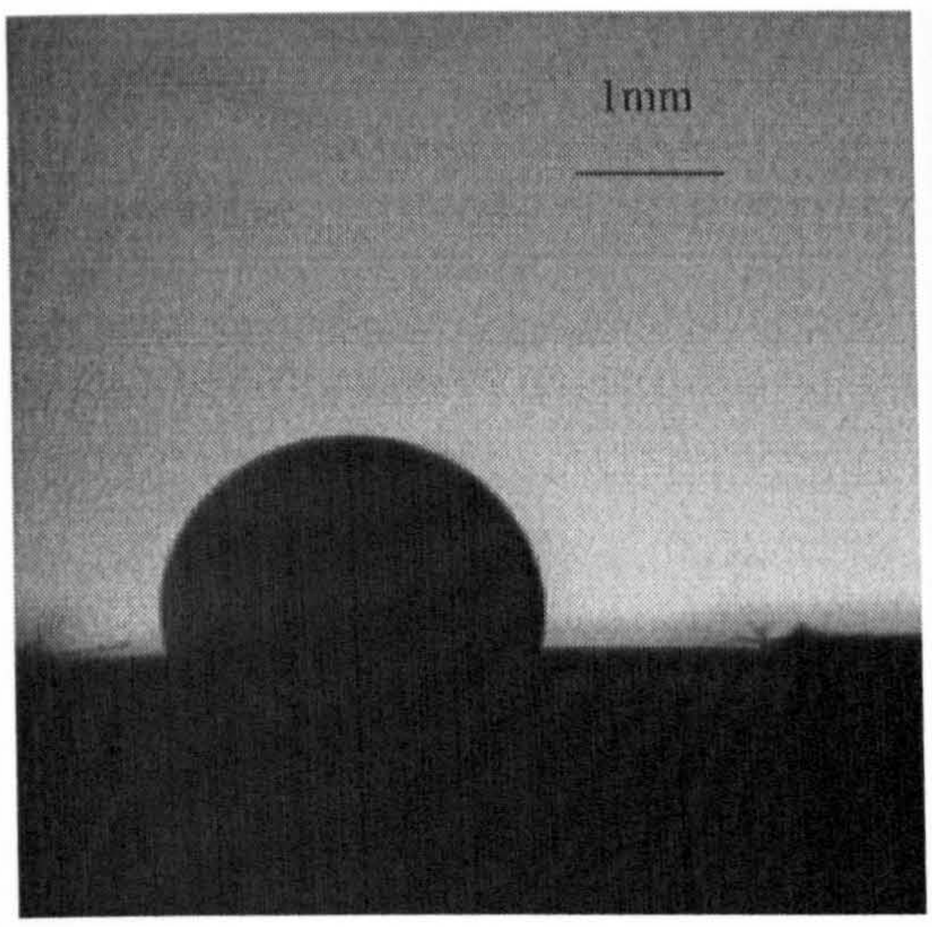

θ = 100°, t = 0s

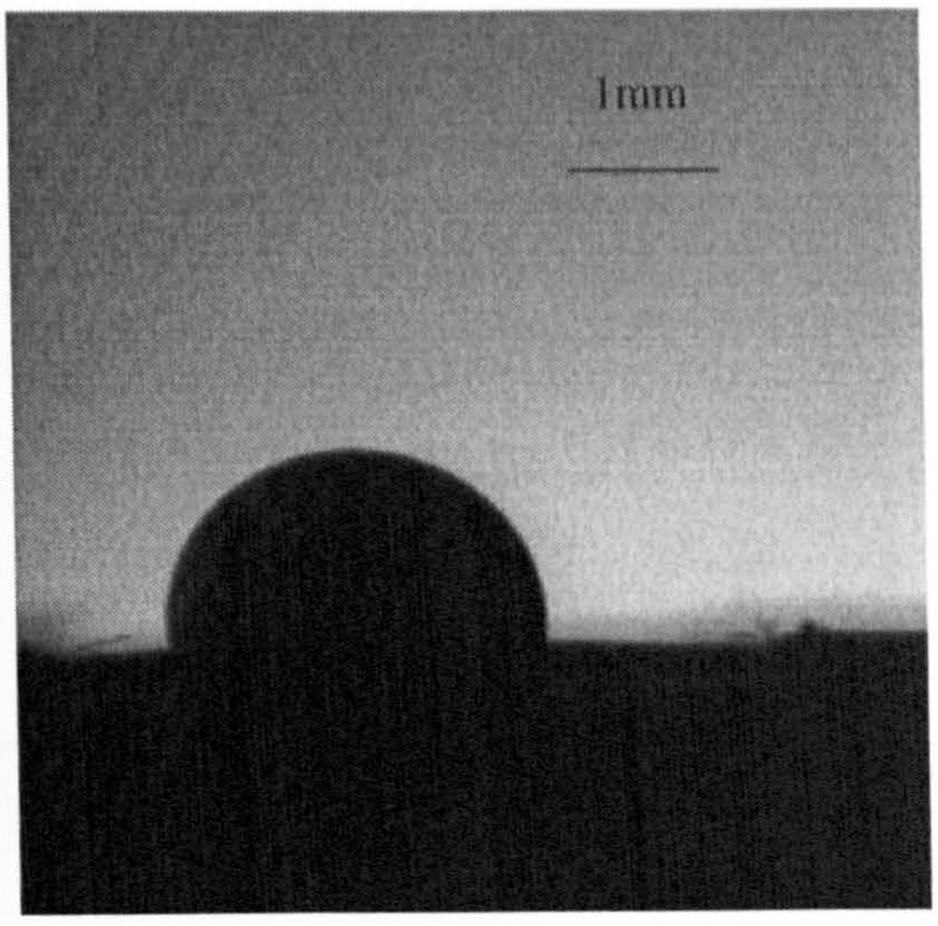

θ = 95°, t = 0.3ks

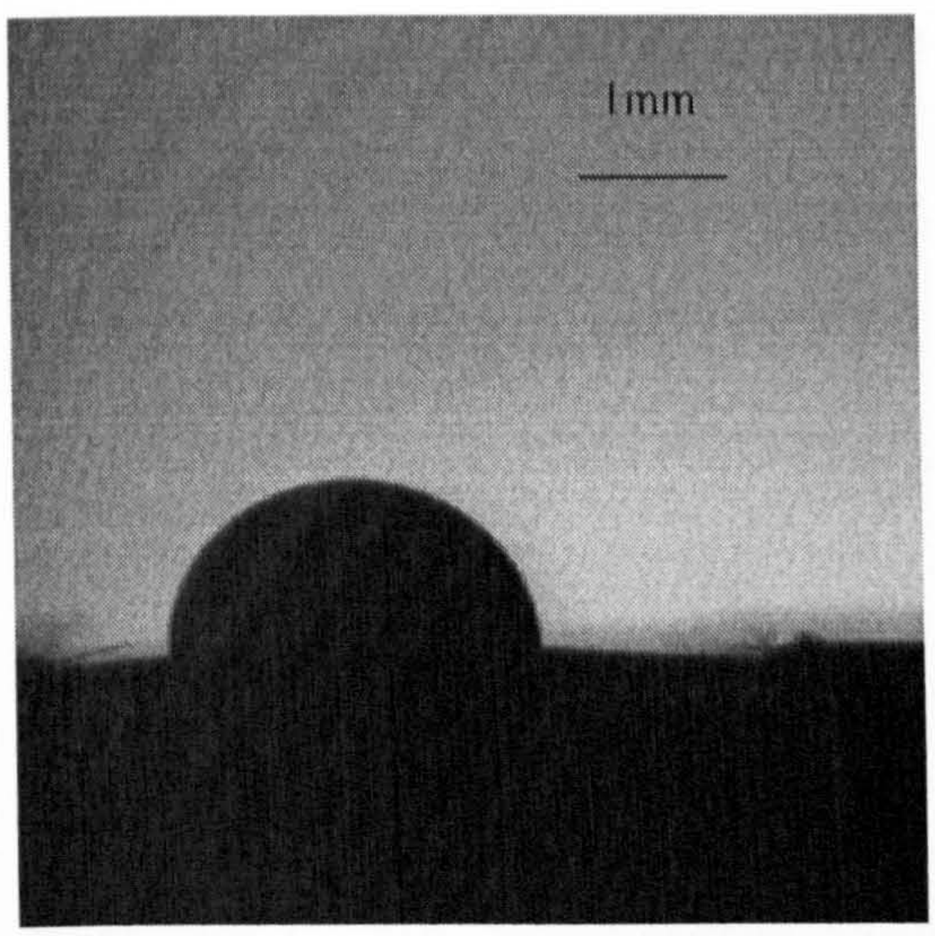

θ = 84°, t =0.6ks

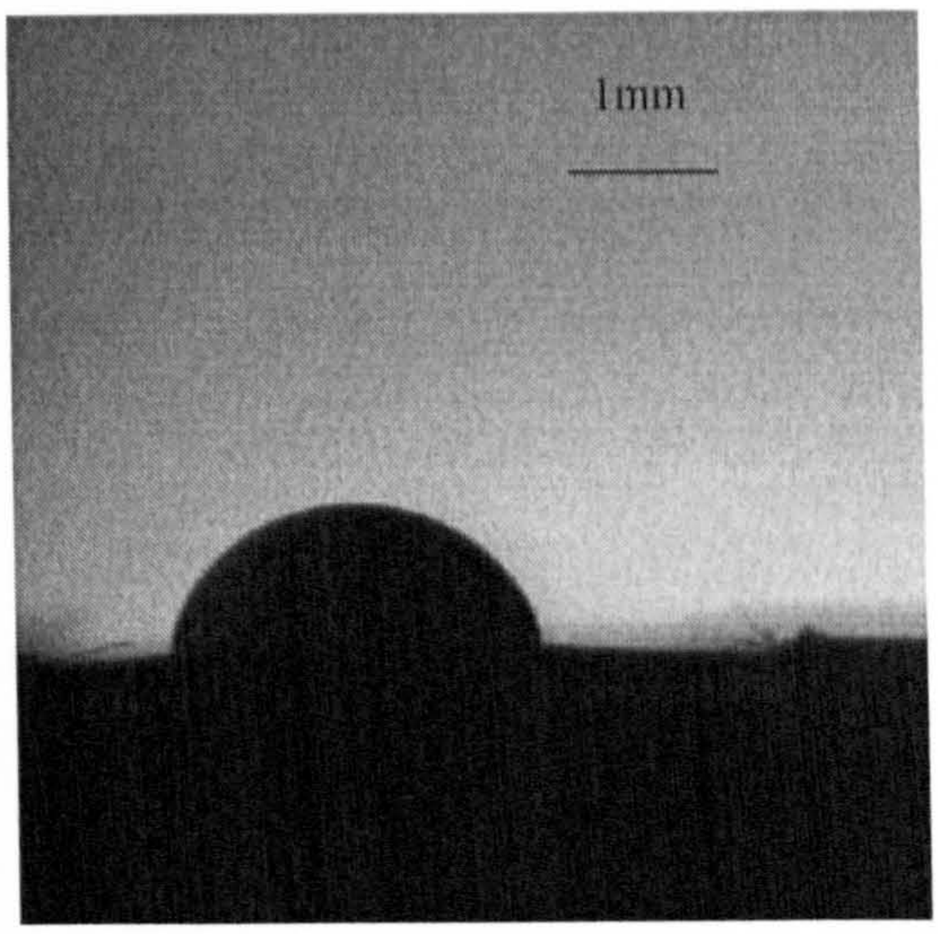

θ = 82°, t =0.9ks

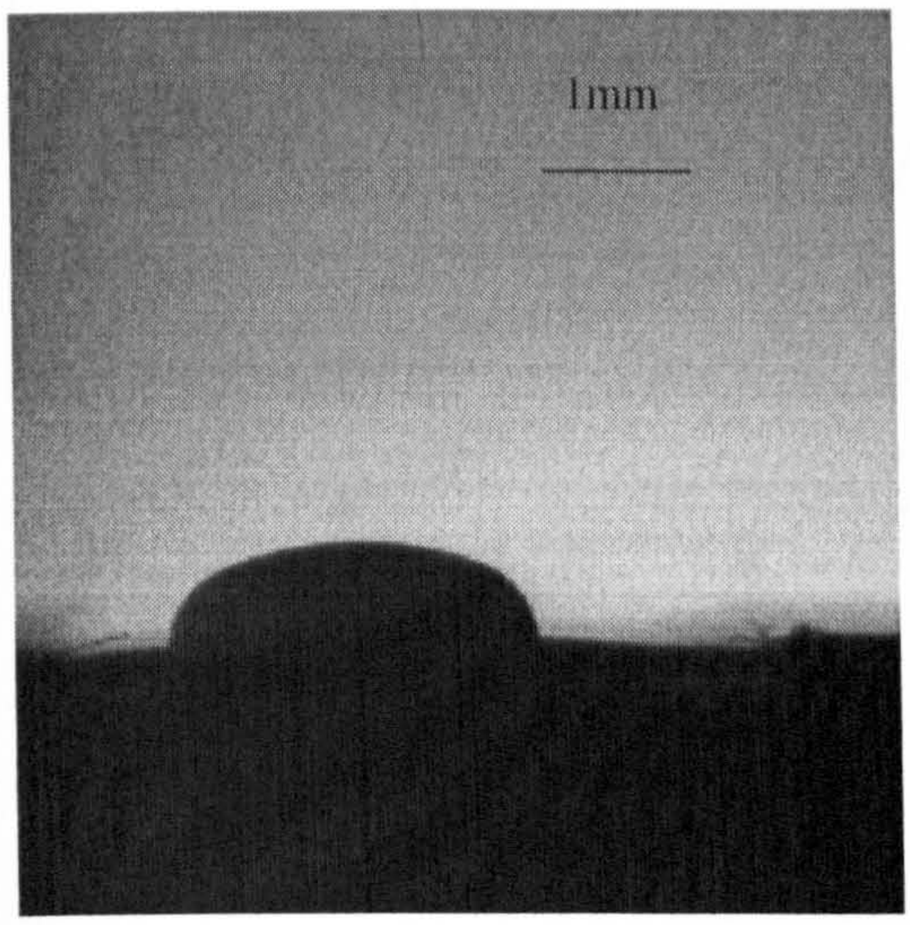

θ = 80°, t =1.2ks

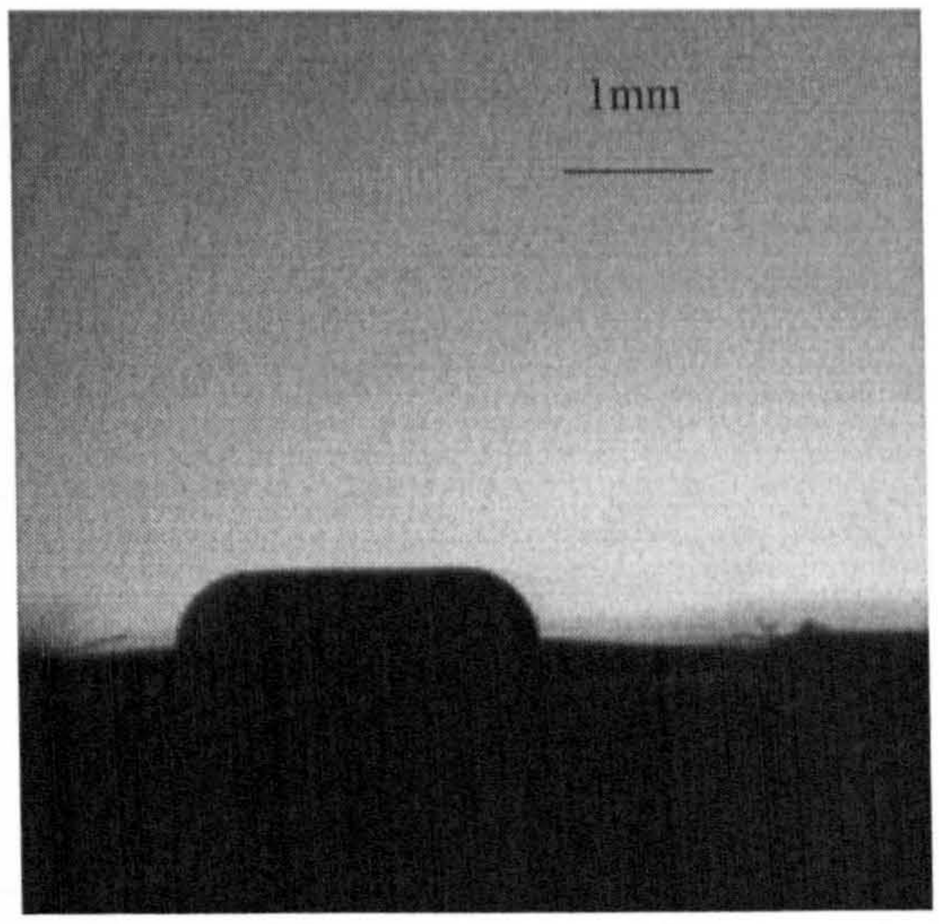

θ = 80°, t =1.5ks

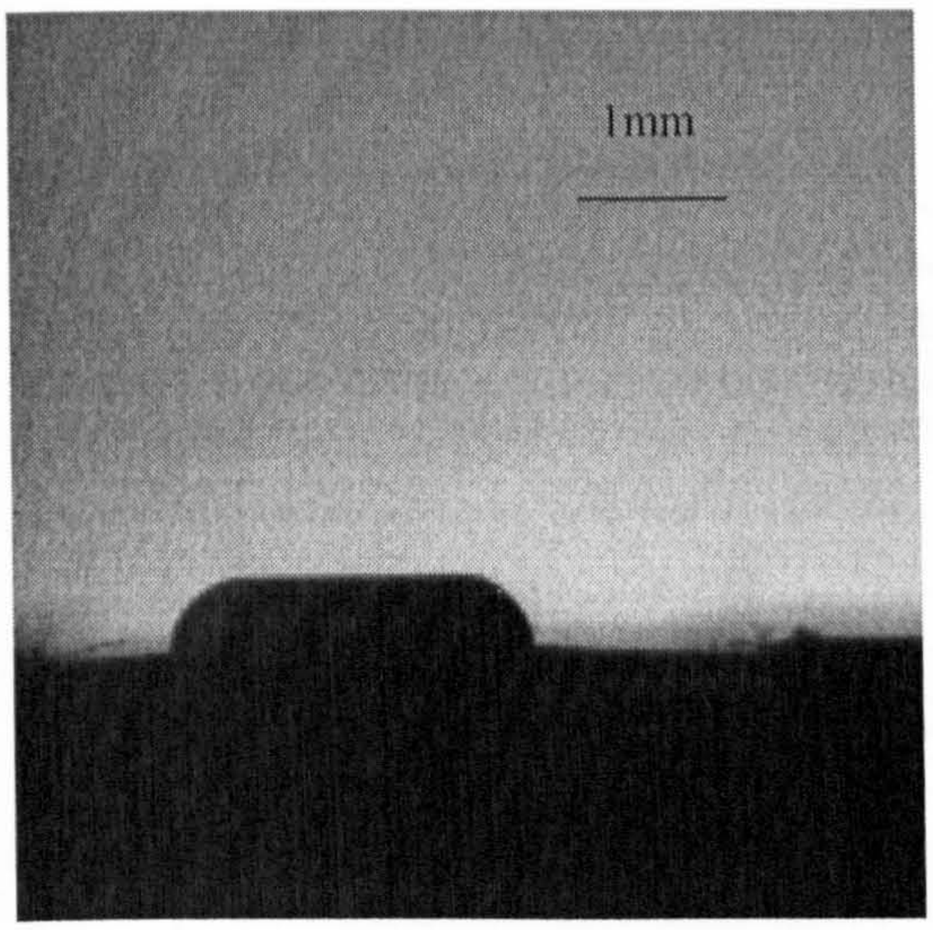

θ = 80°, t =1.8ks

Figure 3.12 The drying process of a droplet of ceramic ink that contains around 1wt% dispersant deposited on silicone release paper.

(a) ZrO_2- Al_2O_3 System

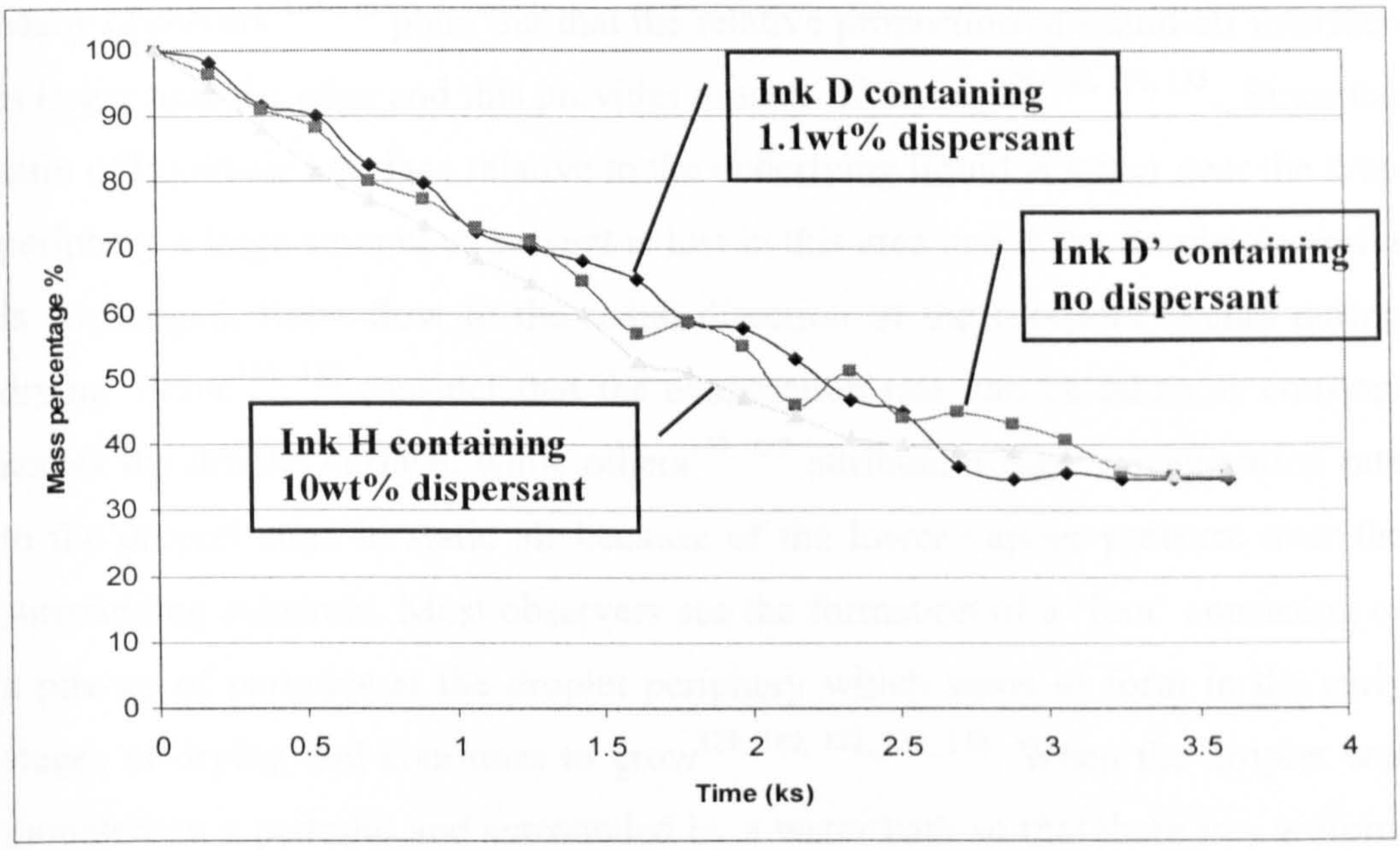

(b) TiO_2-ZrO_2 system

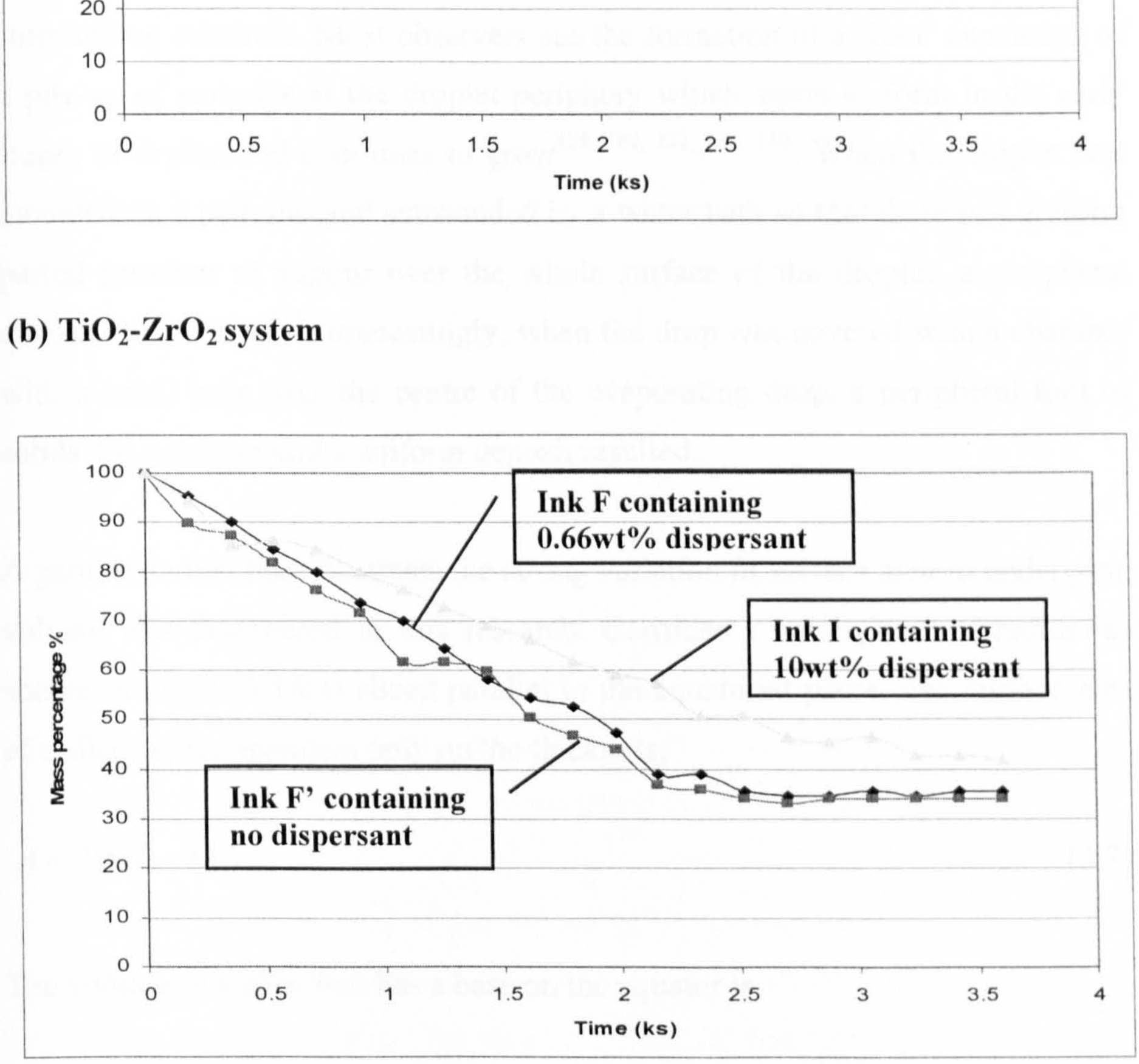

Figure 3.13 The percentage mass loss as a function of time for a droplet of mixed powder suspension placed on the silicone release paper.

3.5.2 Discussion of the drying process

Many observers [134-136] point out that the relative proportion of liquid-air interface is larger near the edge and this provides models of drying[129, 130, 134, 135]. Since the ratio of liquid-air interface relative to the underlying liquid is larger near the drop periphery a large amount of solvent is lost in this area and if the droplet footprint is unchanged, finite flow in the radial direction of the footprint occurs during drying. Some[134, 135] consider that the evaporation rate can be taken as constant across the droplet surface, while others[129, 139] attribute a higher evaporation rate to the droplet edge in static air because of the lower vapour pressure over the surrounding substrate. Most observers see the formation of a 'foot' consisting of a pile-up of particles at the droplet periphery which starts to form in the early stages of drying and continues to grow[129, 130, 132, 134, 136]. When the droplet was mounted on a pedestal and surrounded by a water bath so that there is a uniform partial pressure of vapour over the whole surface of the droplet, a peripheral deposit still formed[129]. Interestingly, when the drop was covered with a chamber with a small hole over the centre of the evaporating drop, a peripheral foot of solids did not form and a uniform deposit resulted.

A geometric fact that illustrates the strong variation in surface area to underlying volume was discovered in this research. Consider a hemisphere of radius r as shown in Figure 3.14(a) sliced parallel to the equatorial plane. The surface area of a slice, A, is dependant only on the thickness;

$$A = 2\pi r(r-h), \tag{3.2}$$

The volume of a slice that has a base on the equator is

$$V_s = \frac{\pi}{3}(2r^3 - 3rh^2 + h^3). \tag{3.3}$$

The volume of the cylinder inside the slice is

$$V_c = \pi x^2 (r - h), \tag{3.4}$$

But since $x^2 = 2rh - h^2$ (x is shown in Figure 5a),

$$V_c = \pi(2r^2 h - 3rh^2 + h^3) \tag{3.5}$$

The volume of the rim is $V_R = V_s - V_c$ and from equation (2) and (3) is

$$V_R = \frac{\pi}{3}(2r^3 + 6rh^2 - 6r^2 h - 2h^3) \tag{3.6}$$

From equations (1) and (5), the ratio of surface area A to volume of rim V_R is,

$$\frac{A}{V_R} = \frac{3r}{(r-h)^2}, \tag{3.7}$$

Equation (3.7) is plotted for r=1 in Figure 3.14(b) showing how the ratio of surface area to volume increases towards the periphery of drop for the case of a 90° contact angle. Obviously a ratio of 3 is obtained for the hemisphere at h=0. This does not address the more complex flow paths that occur during drying but does show that a strong component of flow must occur in the radial direction of the droplet footprint even if drying is uniform over the liquid surface.

Droplets placed on silicone release paper start with a contact angle greater than 90° and, as evaporation proceeds, the contact angle reduces to 90° (hemisphere), as the edge region dries first. The droplet curve is no longer spherical because the contact diameter stays the same. Neither is the curvature continuous because solids pile up at the periphery. The final droplet shape therefore depends on the extent to which powder participates in this flow.

(a)

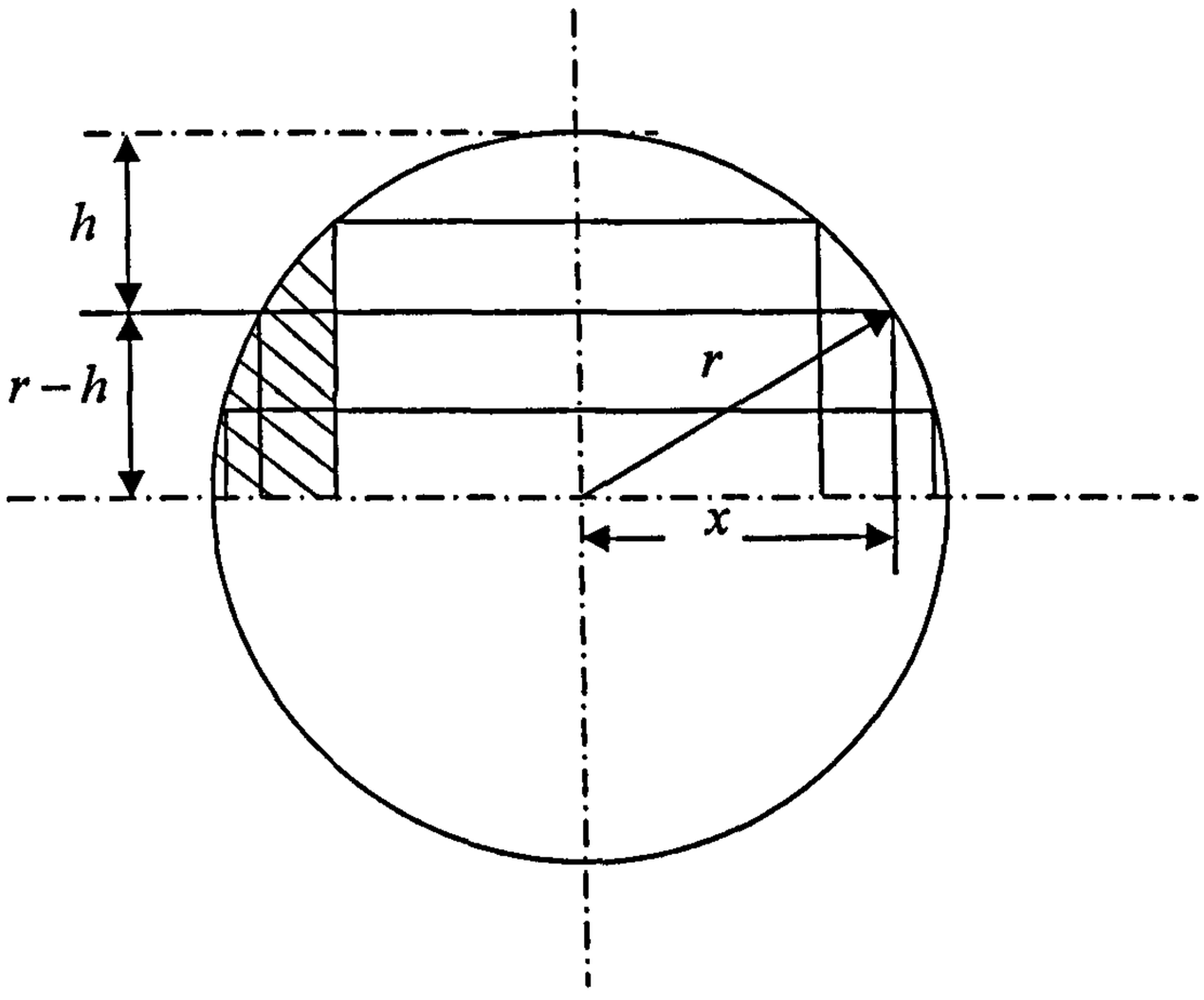

(b)

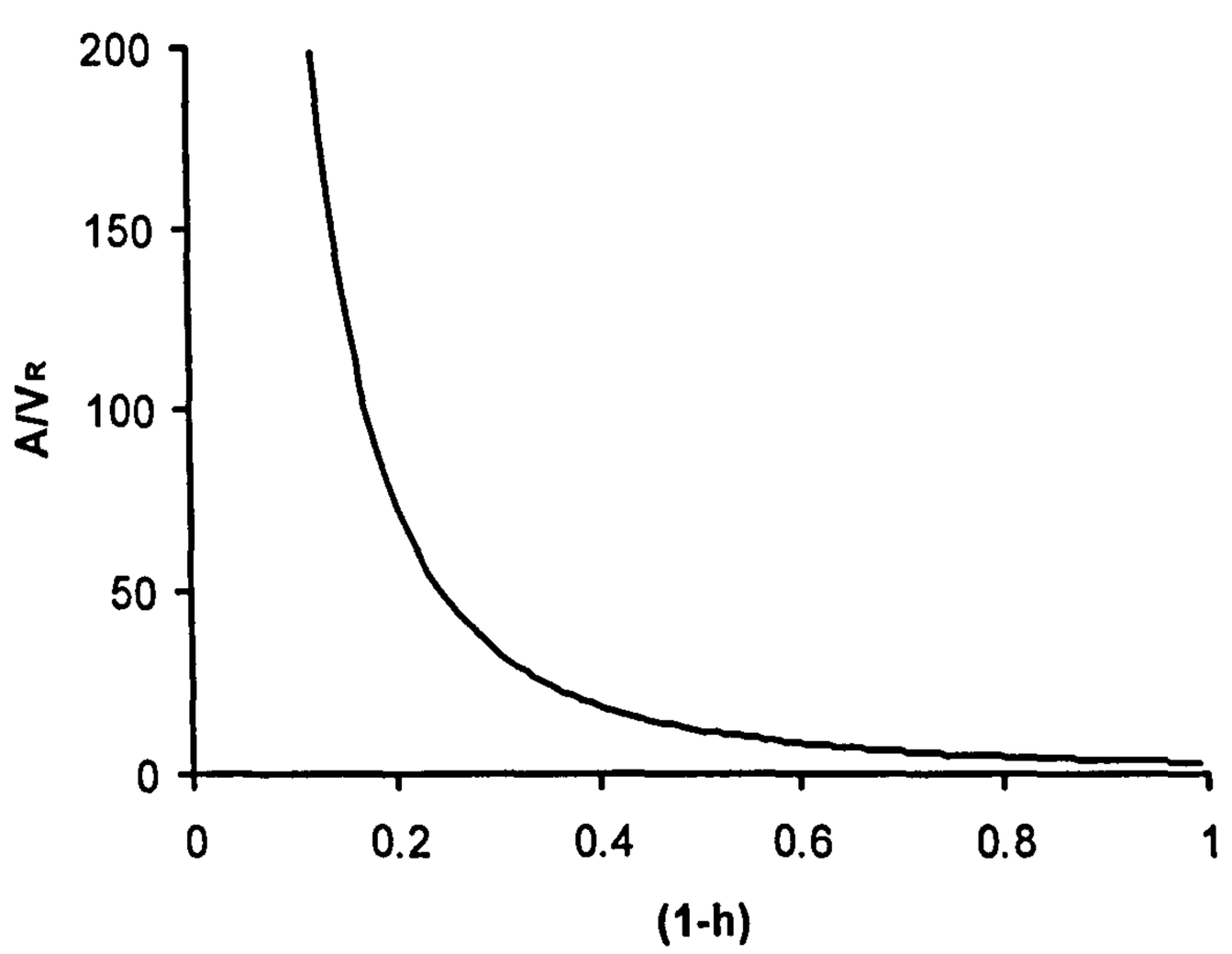

Figure 3.14 (a) Model of a hemispherical cap showing droplet edge as shaded, (b) surface area /volume ratio as a function of *(1-h)* for r=1.

This research proposes that the geometry and compositional distribution of residues of droplets are both related to the movement of particles during drying but to different types of flow. Thus non-uniform composition and droplet residue shape are related to the mobility of particles in the drop. The question is, why, when the edge dried first in all ceramic ink droplets, do droplets of Type I suspension retain a dome shape and do not show segregation in the residue whereas droplets of type II suspension end as a 'doughnut' shape with segregation of powders of the residues? Two possible reasons stand out: (1) flocculation induced by entanglement of excess dispersant molecules inhibits particles from participating in flow during drying; (2) increased liquid viscosity due to excess dispersant prevents movement of particles in the suspension. There is a striking parallel with the morphological development of residues from spherical spray dried ceramic agglomerates; droplets from well-dispersed slurries in which particles retain mobility during drying, form irregular shaped agglomerates with a central hole. Suspensions with a tendency to flocculate, form dense spherical agglomerates[124].

Careful observation of Type II droplets during drying shows that early in the process, a high packing density of powder builds up at the periphery of the drop. The three dimensional network of particles that forms here is well-known (*vide supra*). The rim of the drop accumulates powder and becomes larger forming a solid-like ring that can be observed on the drop periphery as a discontinuity of curvature seen in Figure 3.12 (t = 1.2ks) and shown schematically in Figure 3.9. Eventually a 'doughnut' shape forms in which the centre is depleted in powder, sometimes leaving a hole. Clearly particle motion to the periphery accompanies radial liquid flow in the case of these drops. This flow explains the droplet shape but not the segregation effects.

The second type of flow is the recirculation currents observed by Haw et al.[136] and modeled in terms of Marangoni flows by Hu and Larson[137]. This liquid region has the shape delineated by the dashed region in Figure 3.9 and within it circulation flows persist, driven by Marangoni stresses that result from

temperature gradients and in turn, surface energy gradients, due to evaporation. These dramatic recirculation currents can be seen in an optical microscope fitted with oblique illumination.

As discussed in detail in section 3.4.6, as some particles become immobilized in the peripheral 'foot' the recirculation region contains an excess of the particles that are best dispersed and therefore least able to join the 'foot' which they do by a flocculation mechanism. The upper surface within the peripheral foot is thus the last to 'solidify' and this is precisely the region where segregation effects are observed. In all experiments it is the powder that is better dispersed that resides in excess on this part of the upper surface. It may also be possible for fine powders to filter through denser packed regions of coarse particles to the surface as radial liquid flow occurs but the preferred segregation of coarse particles suggests this is a secondary effect.

For droplets of type III suspensions which are dispersant-free, the drying behaviour and compositional distribution varied with the powder characteristics. For the Al_2O_3-ZrO_2 system (suspension D'), there was a noticeable, but not measured, increase in viscosity without dispersant. This is typical of flocculated suspensions[138]. A three dimensional flocculated network prevents particles from participating the liquid flow. The spherical cap shape and homogenous mixture end as a dome with uniform planned distribution of powder.

On the other hand, Ink B (single component TiO_2 ink) and suspension H (TiO_2-ZrO_2 system without dispersant) do shown three stage drying and show evidence of preferential sedimentation of ZrO_2. TiO_2 is a fine powder that disperses well in water even without addition of dispersant. ZrO_2 is a comparatively coarse powder as deduced from SEM images.

In summary, the edge dries first when a sessile drop retains its three phase boundary and this is common to all ceramic ink drops. If powder can be dispersed in water such that it is de-flocculated and particle mobility is high,

three stages drying and a doughnut shape result (e.g. Ink B, Ink F' and Type II inks). If powders mobility is not high due to flocculation and, or increased liquid viscosity, then the sample that began as a spherical cap completed drying still as a dome shape (e.g., Ink D', and Type I inks).

For the ZrO_2-Al_2O_3 system, inks D, D'and H have dried mass percentages of 34.65wt%, 34.14wt% and 38.79wt% (calculated from Table 2.3), respectively. As shown in Figure 3.14 (a) at 3.5ks, the three types of inks' droplets completed drying at the same time. For the TiO_2-ZrO_2 system, ink F, F' and I have dried mass percentages of 34.11wt%, 34.14wt% and 38.79wt% (calculated from Table 2.3), respectively. As shown in Figure 3.14 (b) at 3.5ks, inks F and F' droplets completed drying but droplets from ink I that contain 10wt% dispersant dried slower. Overall, three types of inks' droplets have similar mass loss pattern.

3.6 Calibration of combinatorial dielectric measurement

This assessment has four stages. In the first stage, the HP4294 impedance analyser was calibrated using standard capacitors. In the second stage, $BaTiO_3$ was selected because there is an established literature basis for its dielectric properties. A conventional pressed sample was prepared using the same powder as that printed. In the third stage, a sample of ink was printed in a rectangular recess that was made by the silicon release paper and dried to produce a small disc. Its dielectric properties were measured after metalised using silver paste, Finally, a sample was printed onto dried platinum ink and tested using the combinatorial robot. Table 3.14 describes the measured values for standard capacitors. It proves the HP4294 impedance analyser gives accurate readings of capacitance.

Table 3.14 Calibration of the measurement cell using standard capacitors

No	Capacitance of standard capacitors	The measured capacitance	Error %
1	1pF	1.03pF	3%
2	4.7pF	4.73pF	0.64%
3	56pF	56.52pF	0.93%
4	0.01μF	0.0100171 μF	0.17 %
5	0.022μF	0.0219951 μF	0.02 %
6	0.033μF	0.0331363 μF	0.41 %

Figure 3.15 gives a picture of the pressed $BaTiO_3$ sample, the free-standing ink-jet printed $BaTiO_3$ sample and ink-jet printed $BaTiO_3$ samples on platinum coated alumina substrates. In the picture, all samples were electroded. The thickness of the pressed sample, the ink-jet sample separated from silicone release paper and ink-jet printed sample on platinum-coated alumina substrates were 2.13 mm, 0.8mm and 0.36mm respectively. Figure 3.16 describes temperature and frequency dependency of dielectric constants of $BaTiO_3$.

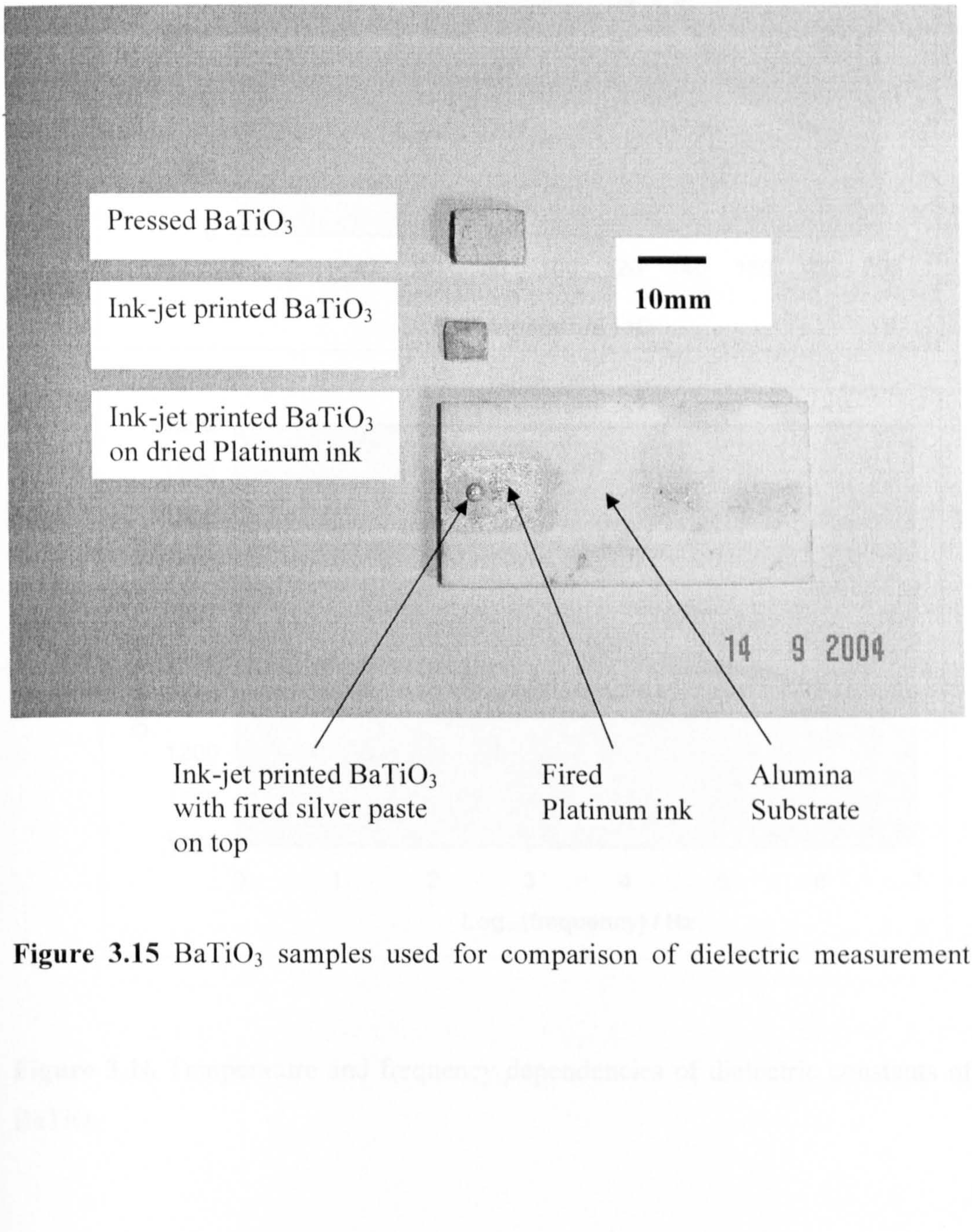

Figure 3.15 $BaTiO_3$ samples used for comparison of dielectric measurement

Pressed $BaTiO_3$

Ink-jet $BaTiO_3$ ink dried in a mould

Ink-jet printed $BaTiO_3$ on platinum coated substrates measured by the dielectric probe in the combinatorial robot.

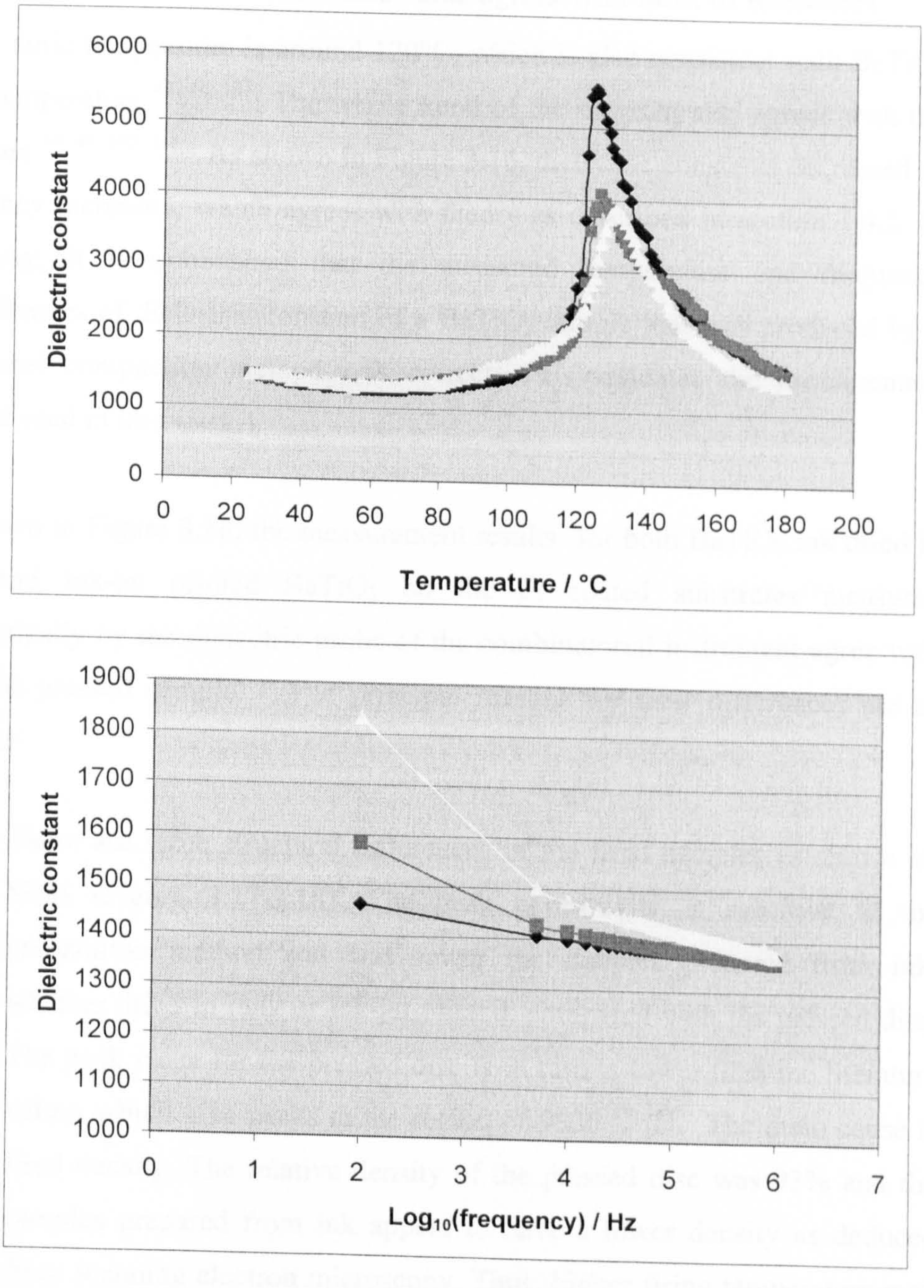

Figure 3.16 Temperature and frequency dependencies of dielectric constants of $BaTiO_3$

The measured value of dielectric constants of $BaTiO_3$ are affected not only by frequency and temperature, but also grain size, porosity and purity of samples.[44, 78,140] The method of measurement can influence the values recorded as described in section 1.3. As shown in Figure 3.16, the pressed $BaTiO_3$ sample has $\varepsilon_r = 1450$ at 25 °C and 1 kHz. This value agrees with most of references [43, 44, 141]. Its curie temperature is around 120°C, which is also consistent with $BaTiO_3$ curie temperature [43, 44, 141]. The whole trend of the diagram also agrees with the literature [43, 44, 140, 141]. As shown in Figure 3.16, dielectric constants decreased as frequency increased, which agrees with theory as described in section 1.4.2. In this way, it is established that the measured temperature and frequency dependencies of dielectric constant of a $BaTiO_3$ sample that was produced by a traditional compaction method was correct. This validates the measurement method used in this work.

As shown in Figure 3.16, the measurement results for both $BaTiO_3$ ink dried in bulk and ink-jet printed $BaTiO_3$ on the Pt coated substrates measured automatically by the dielectric probe of the combinatorial instrument agree well with the pressed sample. The principal reasons for their differences are as follows:

(1) There are some structural differences in the fired samples as shown by SEM (Figure 3.17-3.18). The peak permittivity is sensitive to the preparation method and was lower for samples prepared from ink, whether dried in bulk or ink-jet printed, compared with the pressed disc. The peak value for the pressed disc is in turn is lower than the literature values which give peaks in the region of 9500 [44, 141]. The main cause is fired density. The relative density of the pressed disc was 93% and the samples prepared from ink appear to have a lower density as deduced from scanning electron microscopy. Thus, higher firing temperature may be needed to establish the same density from material prepared in the form of an ink in a combinatorial routine to samples prepared by

conventional compaction with consequences for grain size which is known to influence dielectric properties[78].

(2) As show in Figure 2.10, the cables linking the dielectric probe used in the combinatorial method and test fixture are around 800mm and fasten to the frame of the x-y table. Although screened, they can interfere with each other or with other electromagnetic sources, e.g. the hotplate.

(3) As described in section 2.7.4, there is an error for the calculation of dielectric constant for the ink-jet printed $BaTiO_3$ on platinum coated substrates associated with geometrical factors. Due to finite accuracy of the robot movement, the silver paste electrode on the top of the sample may be displaced away from the centre part of the sample.

(4) As described in section 2.6.3 and 2.6.4, because the ink-jet samples were so thin, the thermocouples were placed adjacent to the samples whereas the thermocouple was in direct contacted with the pressed sample as described in section 2.6.2. There may be differences between the recorded temperature and the actual temperature of samples.

This section establishes the measurement method for dielectric constant and links it to literature values for a well-established dielectric using conventional compaction for sample preparation. It establishes that the same material prepared in the form of an ink, dried and fired as it would be in a combinatorial routine gives similar dielectric measurement.

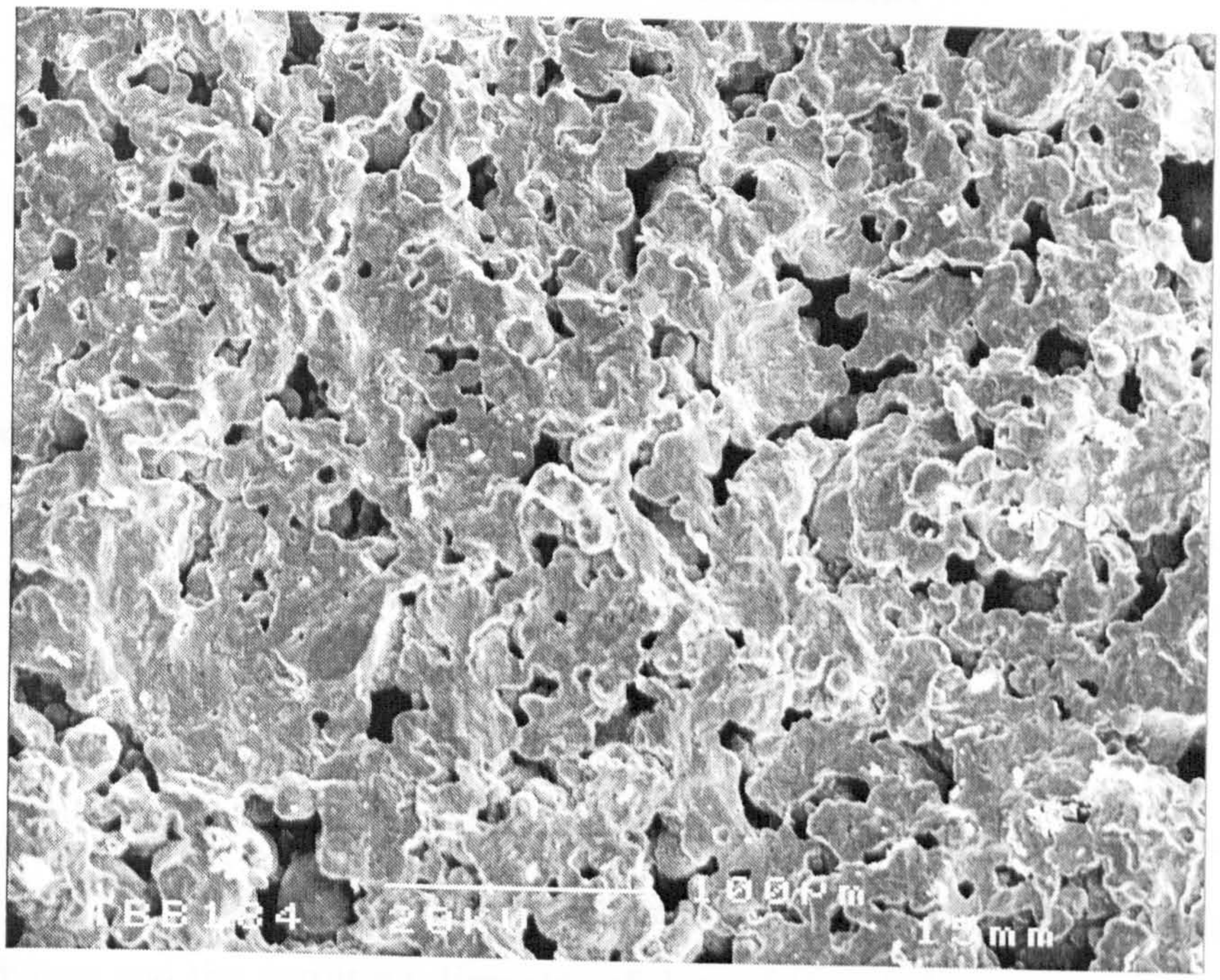

Figure 3.17 SEM picture of ink-jet printed $BaTiO_3$ fired at 1400 °C for 2 hours.

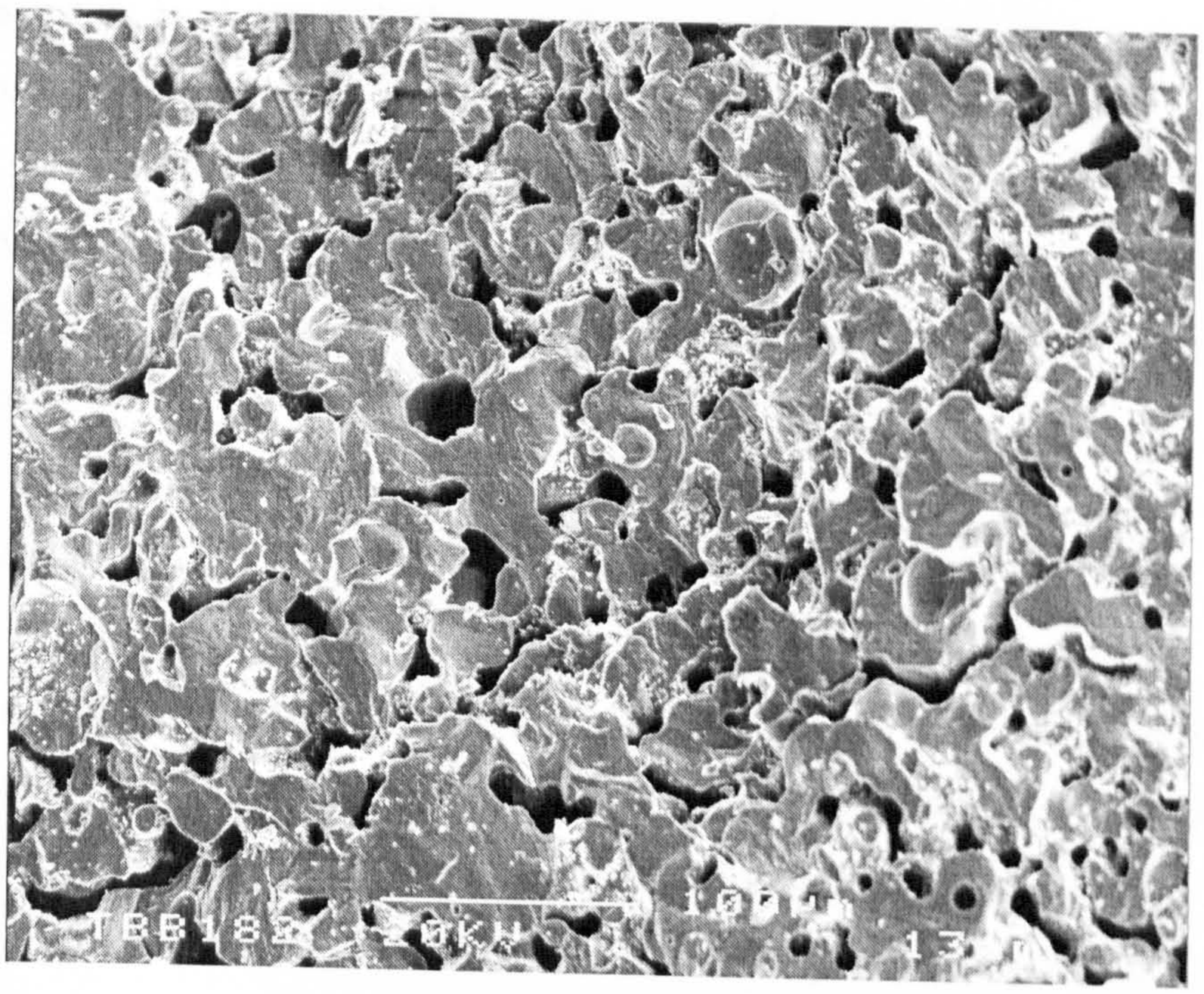

Figure 3.18 The SEM picture of pressed $BaTiO_3$ fired at 1400 °C for 2 hours.

3.7 Study of combinatorial dielectric measurement

ASTM designation D150-87 (1989 section 10) specifies the conditions for measuring dielectric constant and dissipation factor. For high accuracy, the guarded electrode method is preferred but for routine work, the unshielded two-electrode system is accepted and is used here. In combinatorial work there is necessarily a trade-off between accuracy and miniaturisation for high throughput. The greatest error is regarded as lying in the measurement of dimensions. The 'unequal electrodes' method given in Table 1 of the ASTM designation was used (i.e., smaller electrode area is 'A' used in equation 1.13).

The library density is a function of the contact angle of drops on the substrate. If the droplets spread, repeated prints are needed to develop sufficient sample thickness and the resulting diameter of drops is large. If a small radius is needed, the substrate must be pre-treated to provide a high contact angle or to prevent spreading. The result is a high curvature in the upper surface of the sample. When this is electroded, the sample can no longer be treated as a parallel plate capacitor. The purpose of this section is to calibrate the dielectric measurement for dome-shaped samples on a common ground electrode with an upper metallised electrode by measuring the capacitance with an impedance analyzer and establishing the corrections needed to obtain dielectric constant of the sample.

Theory

Using the geometry of Figure 3.19, a top electrode of radius r_e is deposited by contact printing centrally onto the sample whose thickness t_0 can be measured and logged using a displacement transducer or measured with a micrometer gauge as in this case. The thickness of the sample t, at any radius r, is given by the equation for a circle as:

$$t = t_0 - R + \sqrt{R^2 - r^2} \tag{3.8}$$

where t_0 is the measured thickness of the sample. Hence the capacitance of a thin cylindrical shell between 0 and r_e is:

$$\delta C = \frac{2\pi\varepsilon_0\varepsilon_r r dr}{t} \tag{3.9}$$

The capacitance of the capacitor formed by the upper curved electrode and the ground electrode directly below it is thus:

$$C = 2\pi\varepsilon_0\varepsilon_r \int_0^{re} \frac{r}{t} dr \tag{3.10}$$

In fact, the field lines are not strictly parallel near the periphery of the capacitor and fringe effects are discussed below. Expressing the capacitance as:

$$C = 2\pi\varepsilon_0\varepsilon_r \int_0^{re} \frac{r}{t_0 - R + \sqrt{R^2 - r^2}} dr \tag{3.11}$$

and making the substitutions, $U = R^2 - r^2$, $A = t_0 - R$

$$\int \frac{1}{A + \sqrt{U}} dU = 2\sqrt{U} - 2A\ln(\sqrt{U} + A) \tag{3.12}$$

this gives for capacitance C;

$$C = 2\pi\varepsilon_0\varepsilon_r[(t_0 - R)\ln(\sqrt{R^2 - r^2} + t_0 - R) - \sqrt{R^2 - r^2}]\Big|_{r=0}^{r=r_e} \tag{3.13}$$

$$C = 2\pi\varepsilon_0\varepsilon_r\left[(t_0 - R)\ln\frac{\sqrt{R^2 - r_e^{\,2}} + t_0 - R}{t_0} - \sqrt{R^2 - r_e^{\,2}} + R\right] \tag{3.14}$$

Noting that $R = \dfrac{t_0^2 + r_0^2}{2t_0}$

$$C = \frac{\pi\varepsilon_0\varepsilon_r}{t_0}\left[\left(t_0^2 - r_0^2\right)\ln\frac{\sqrt{\left(t_0^2 + r_0^2\right)^2 - 4t_0^2 r_e^{\,2}} + t_0^2 - r_0^2}{2t_0^2} - \sqrt{\left(t_0^2 + r_0^2\right)^2 - 4t_0^2 r_e^{\,2}} + \left(t_0^2 + r_0^2\right)\right] = \frac{\varepsilon_0\varepsilon_r}{t_0}S'$$

(3.15)

where

$$S' = \pi\left[\left(t_0^2 - r_0^2\right)\ln\frac{\sqrt{\left(t_0^2 + r_0^2\right)^2 - 4t_0^2 r_e^{\,2}} + t_0^2 - r_0^2}{2t_0^2} - \sqrt{\left(t_0^2 + r_0^2\right)^2 - 4t_0^2 r_e^{\,2}} + \left(t_0^2 + r_0^2\right)\right]$$

equivalent to plate area of a parallel plate capacitor with plate separation distance of t_0. Thus, two equations for the permittivity of ceramics calculated from capacitance can be applied to the samples. For the sample approximating to a parallel plate: formula 1.13 (i.e., implemented as Figure 2.16) is used, and for samples with a pronounced curvature of the upper electrode:

$$\varepsilon_r = \frac{t_0 C}{\varepsilon_0 S'} \tag{3.16}$$

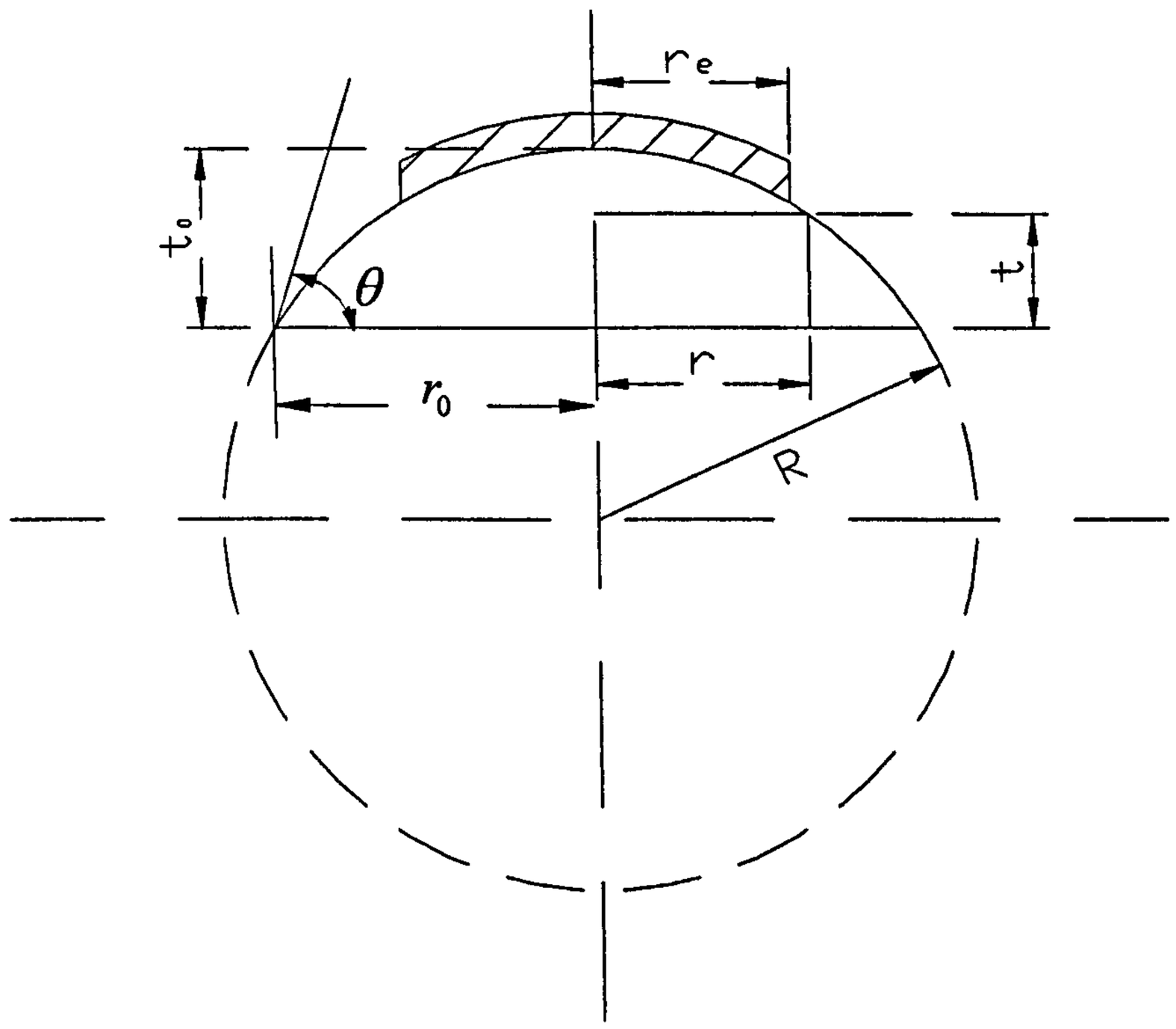

Figure 3.19 Geometry for calculation of dielectric constant from capacitance measured from a pronounced curvature of the upper electrode.

Experimental results and discussion

The experiment detail was described in section 2.7.5. Figure 3.20 gives the picture of samples. Both formula 1.13 and equation 3.16 are applied to calculate dielectric constant of each sample from its geometry and measured capacitance. The results for a range of values of electrode radius and sample thick are given in Table 3.15.

(1) Literature values[43, 44, 140, 141] for the dielectric constant of $BaTiO_3$ at room temperature and 1 khz are about 1600. In fact, this may range from 2000 down to 1200 depending on grain size, porosity and other factors. As discussed in section 3.6, the permittivity of the pressed disc measured in the conventional way was 1450. Scanning electron microscopy of both the pressed disc of $BaTiO_3$ and $BaTiO_3$ from the ceramic suspension is shown in

Figure 3.17 and 3.18. There is substantial porosity in both which accounts for the lower value. Samples No 1 to 9 in Table 3.15 give dielectric constants from 2861 to 4796. The reason for the much higher dielectric constant calculated from the curved $BaTiO_3$ samples cannot be explained by a difference of grain size, porosity or other structural factors. These curved samples have contact angles ranging from 54 to 88° and r_e/r_0 from 0.36 to 0.63. Geometrical factors gave significant error of permittivity calculated from these curved plate capacitance values showing that there are geometrical constraints that must be observed when preparing combinatorial libraries for the measurement of dielectric constant by a capacitance method.

(2) Samples No 10 to 13 in Table 3.15 have dielectric constant from 1488 to 1806, which gives more sound permittivity values compared with Samples 1 to 9. These samples also have high contact angle values ranging from 80 to 85°. The reason for the more accurate result is that as r_e/r_0 increased (i.e., ranged from 0.72 to 0.79), the upper and lower electrodes of samples are more near to the parallel configuration.

(3) The equation 3.16 tends to give smaller values than the dielectric constant calculated by equation 1.13 but fails to fully account for the geometrical variability. Equation 3.16 is obtained from treating a curved plate capacitor as an integration of parallel capacitors. In fact, the field lines are not strictly parallel near the periphery of the capacitor and fringe effects for each parallel capacitor need to be included. This is not pursued further in this research; these results are used to argue that combinatorial libraries for capacitance measurement must be designed close to the parallel plate model.

As described in section 2.7.4, $BaTiO_3$ samples obtained from printing $BaTiO_3$ ink drops gave a parallel configuration when measuring capacitance. The permittivity of these samples kept consistency with the result from the pressed disc $BaTiO_3$ at 1 kHz and room temperature (Figure 3.16). As discussed in section 3.4.6, by using excess dispersant in ceramic inks, the residue from a

single droplet has dome shape with uniform planned composition and is considered as an ideal member of combinatorial libraries. The problem that arises in this section, when measuring permittivity, is that the curved geometry can give significant error. Two possible solutions are available: one is using an analytical formula as given in equation 3.16 but this fails to give a satisfactory correction. Actually, what is needed is a much flatter dome shape and r_e/r_0 should be larger (e.g. about 0.75) to get close to a flat disc configuration. Then using the conventional equation 1.13 gets permittivity from capacitance with negligible error.

There is an alternative way learned from section 3.4.1: by printing ceramic inks on a porous substrate, the dried sample when separated from the substrate, gives a flat shape with uniform planned composition. When querying permittivity on these flat samples, the geometrical factor can be excluded. This approach is implemented in the following a combinatorial study of Al_2O_3-TiO_2-ZrO_2 system.

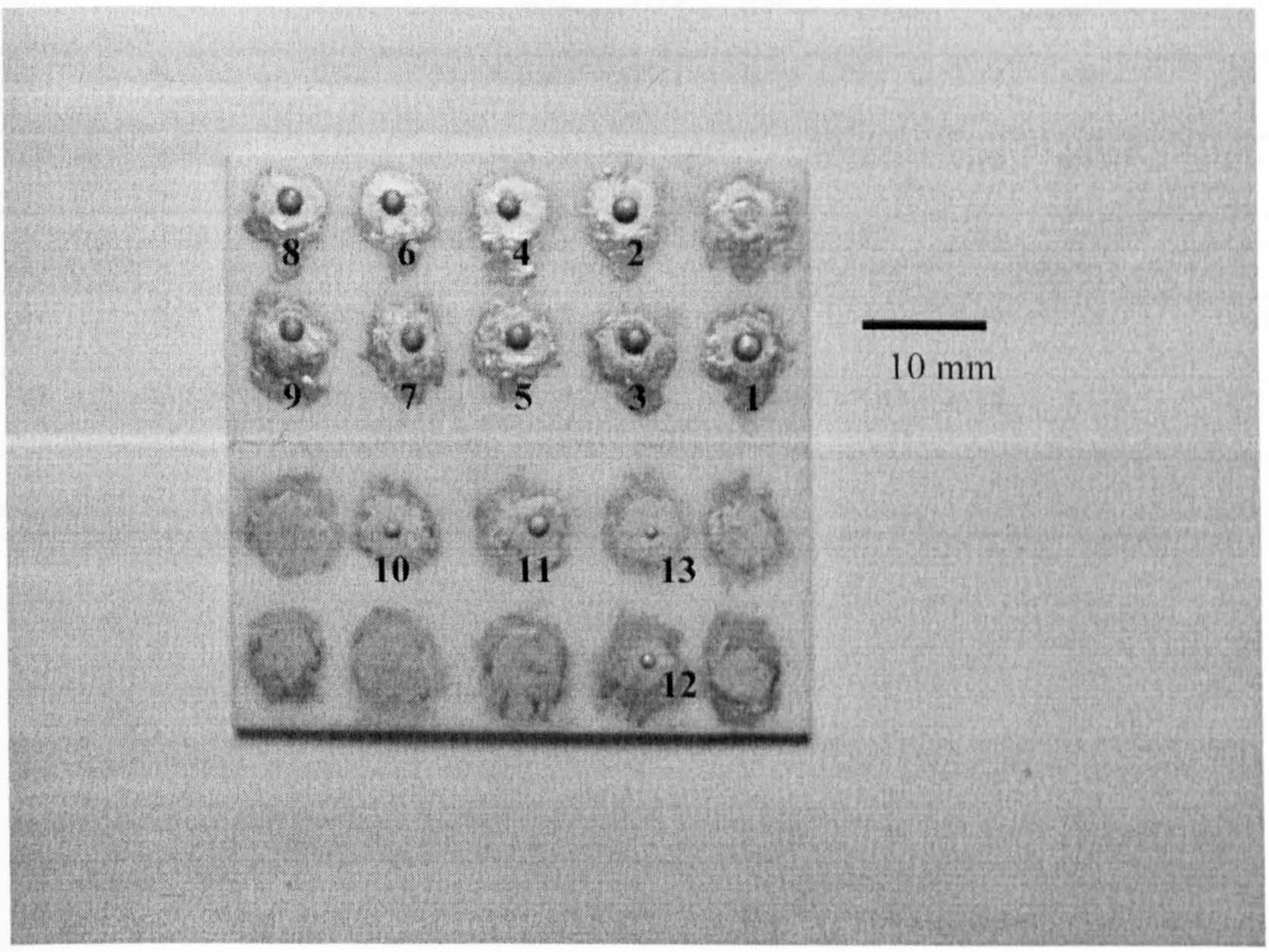

Figure 3.20 Curved $BaTiO_3$ samples prepared from single drop of $BaTiO_3$ inks.

Table 3.15 Measurement of dielectric constant of $BaTiO_3$ from curved plate capacitors.

Sample No.	Electrode stamp radius /mm	A* /mm²	θ § /°	r_e # /mm	r_0 /mm	t_0 /mm	C_m /pf	r_e/r_0	ε_r	
									Using equation 1.13	Using equation 3.16
1	1	2.11	87	0.82	1.33	1.4	64	0.62	4796	4308
2	0.75	1.64	87	0.72	1.15	1.09	42	0.63	3152	2806
3	0.75	1.33	88	0.65	1.19	1.14	28	0.55	2710	2486
4	0.625	1.19	85	0.62	1.02	1.11	26	0.61	2739	2446
5	0.625	0.89	86	0.53	1.11	1.18	26	0.48	3893	3703
6	0.5	0.79	64	0.5	1.05	0.65	33	0.48	3067	2815
7	0.5	0.78	86	0.5	1	0.93	30	0.5	4040	3723
8	0.41	0.53	56	0.41	1.15	0.61	30	0.36	3900	3713
9	0.41	0.54	54	0.41	1.11	0.57	24	0.37	2861	2762
10	0.625	1.03	80	0.57	0.73	0.61	27	0.78	1806	1415
11	0.75	1.6	82	0.71	0.95	0.83	29	0.75	1699	1387
12	0.5	0.86	85	0.52	0.66	0.61	25	0.79	2003	1605
13	0.285	0.51	82	0.40	0.55	0.48	14	0.72	1488	1239

* In this table, 'A' is the area of electrode, θ, r_e, r_0 and t_0 are described in Figure 3.20.

$r_e = \sqrt{\frac{A}{\pi}}$

§ $\theta = Sin^{-1}\frac{2t_0r_0}{t_0^2 + r_0^2}$

3.8 A combinatorial study in the Al_2O_3-TiO_2-ZrO_2 system

As described in section 3.3, Al_2O_3, TiO_2 and ZrO_2 inks were used for calibration of the printer. The instrument can assemble ceramic mixtures with compositional accuracy of 1-3 wt%. Therefore, the first combinatorial study was applied to the Al_2O_3-TiO_2-ZrO_2 system.

The combinatorial samples have flat-disc shape (Figure 3.21). These samples were obtained from printing inks on the cellulose nitrate membrane (reference page 97). Thus the geometrical constraints for dielectric constant measurement described in section 3.7 are excluded. The thicknesses of samples were approximate 0.3mm. The individual samples were accurately measured with a micrometer screw gauge before electroding. The dielectric properties of the library are described in Table 3.16.

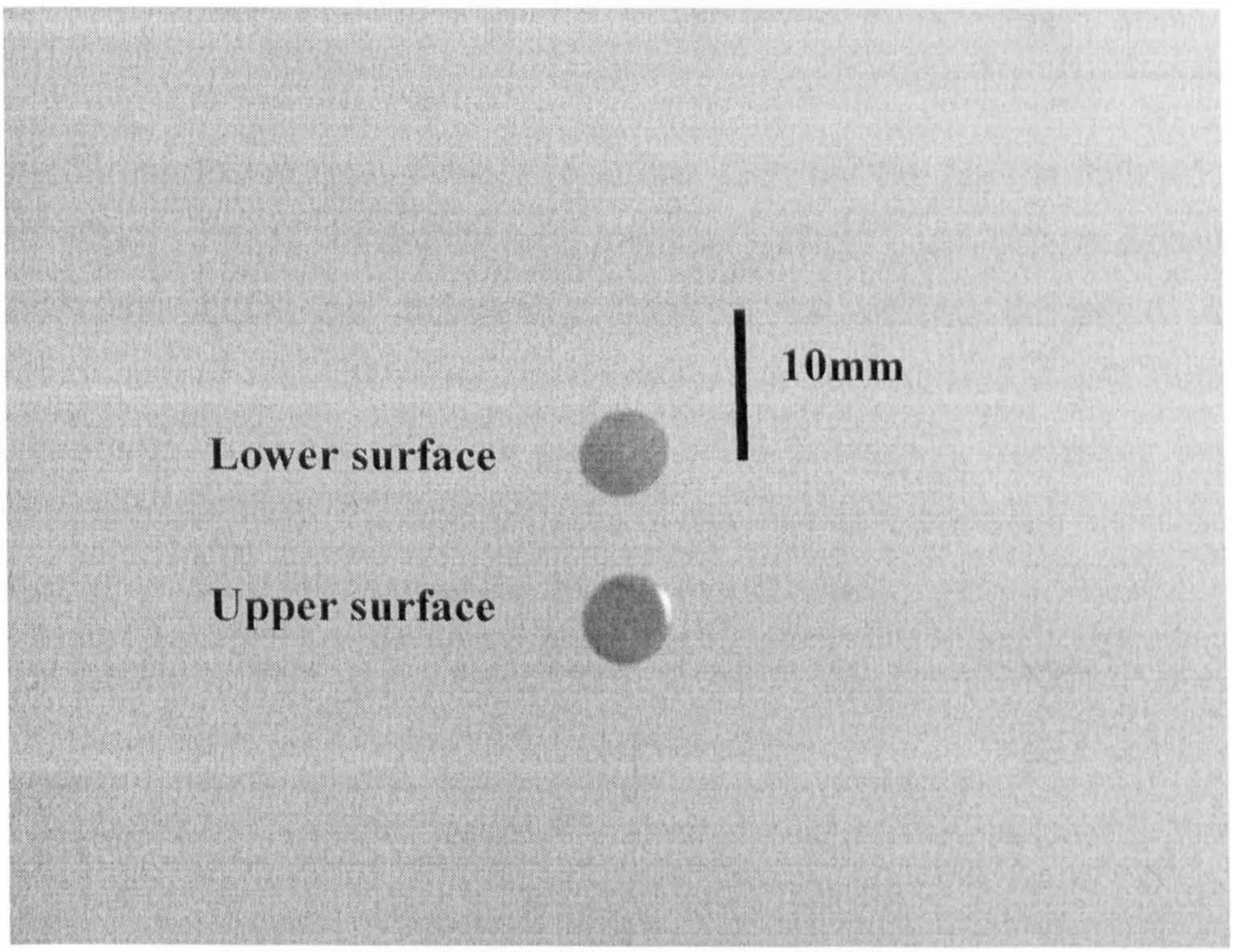

Figure 3.21 Example of a combinatorial sample in the Al_2O_3-TiO_2-ZrO_2 system (the sample in the picture is 100 wt%TiO_2).

Table 3.16 Dielectric constant measurement in the Al_2O_3-TiO_2-ZrO_2 system

Composition Number in Section 2.8	Composition / wt%			Dielectric constants
	TiO_2	ZrO_2	Al_2O_3	
1	100	0	0	116
2	87.5	12.5	0	47
3	87.5	0	12.5	34
5	75	12.5	12.5	27
6	75	0	25	19
9	62.5	12.5	25	25
11	50	50	0	17
12	50	37.5	12.5	18
21	37.5	0	62.5	24

The general conclusion from Table 3.16 is that TiO_2 has the highest dielectric constant whose value is consistence with literature value[43,44]. As TiO_2 is diluted with ZrO_2 and Al_2O_3, the dielectric constant of the mixture decreased. A permittivity map of the Al_2O_3-TiO_2-ZrO_2 system can be generated if data from all compositions in Figure 2.17 are given. This is potentially interesting but requires more time. Here, the combinatorial library was developed and dielectric properties of specified members of the library were accessed.

3.9 A robot system for combinatorial study of new functional oxides

One feature of this combinatorial method is that the ceramic libraries can be printed, sintered, tested and analysed by robot. In this section, the robot system is documented.

3.9.1 The initial plan

Figure 3.22 describes the system. Libraries are developed by the printer and then transferred to the furnace where they are sintered under different conditions. After firing, the libraries were transferred to a measurement table. The range of measurement methods that can be applied is open–ended such as dielectric property measurement using impedance analyser, a colour measurement using luminescence spectrometer or mechanical testing using an indentation method. The measurement data are stored in an Oracle database on a SGI Origin 3200 computer for subsequent mining and analysis. The system is connected to Reality-Grid[142, 143], the EPSRC's e-science programme so that it can be steered and interrogated remotely.

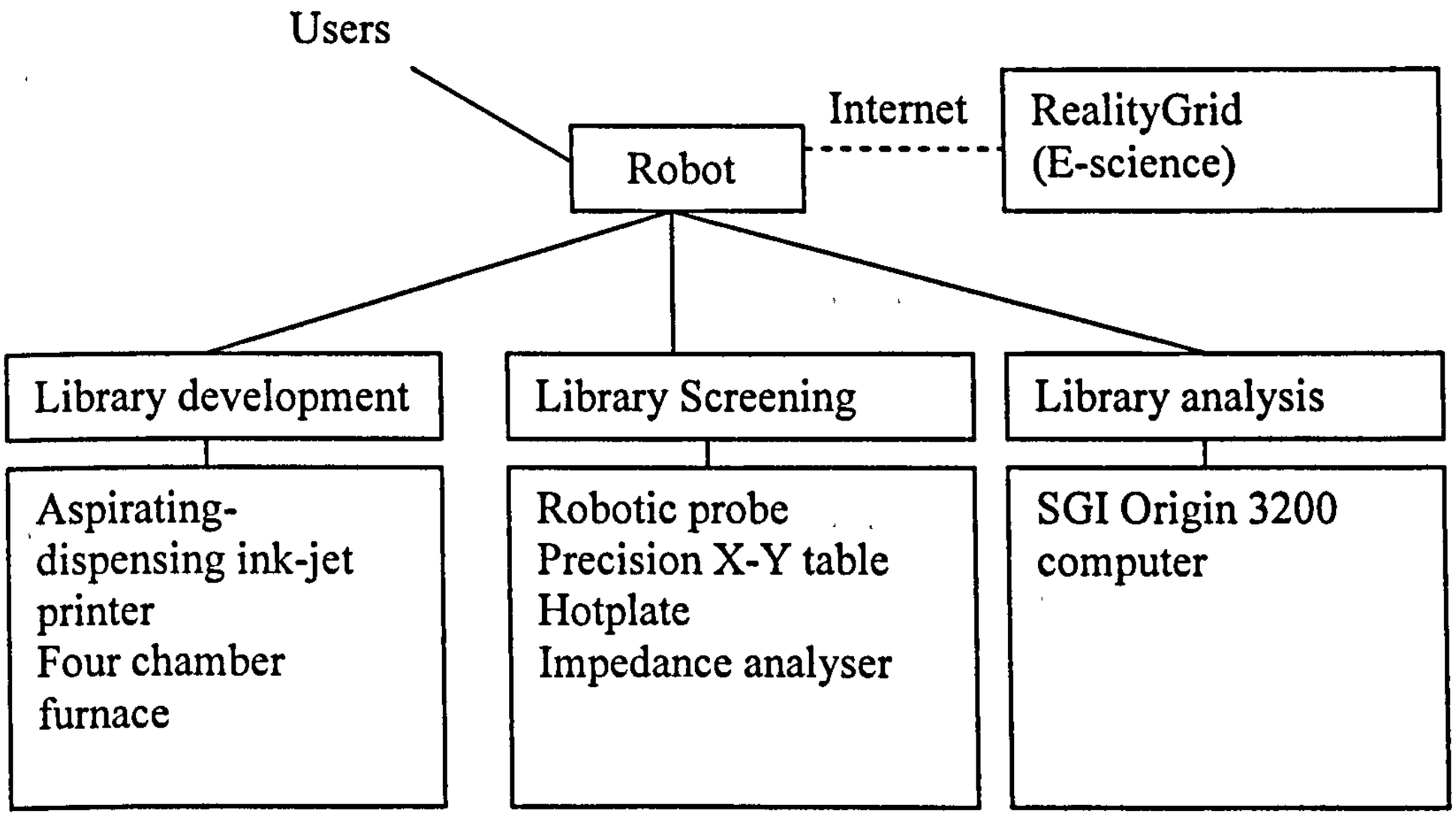

Figure 3.22 Schematic diagram of the combinatorial robot system

3.9.2 Requirements specification

Functional requirement 1: Start of a combinatorial trial

The user inputs the details of one combinatorial trial that includes the library construction, firing, screening and analysis. The robot checks the validity of information. If the information is not correct, an error message with corresponding information is given; otherwise the robot records the information of the trial and acknowledges the user.

Functional requirement 2: Generate the printer programs

The user-input information for library construction includes: the identification of the library, the composition of each sample in the library, the geometrical shape requirement of samples and density of the library. The robot creates a library development plan that includes:

(1) The identification of the library is converted into a form of identification code (e.g. bar code) that will be printed on a particular location of the substrate.

(2) The well-plate reformation algorithm is worked out according to the compositional distribution in the library.

(3) The volume of printed mixed inks is worked out so that each sample meets the geometrical requirement of the sample.

(4) The space location of each sample on the substrate is specified according to the requirements from the density of the library and the geometrical shape of samples.

The library-development-plan is converted to programs that can be run by the printer.

Functional requirement 3: The robot triggers the printer

The robot sends a signal to the printer. If the printer receives the signal and is ready to work, the printer is informed, otherwise, the robot gives an error message to the user.

Functional requirement 4: The printer produces libraries

The robot instructs the printer to run the programs to create libraries. Once the libraries are constructed, the printer informs the robot. If any problem occurs, the printer informs the robot, and the robot backs the error-message to the user.

Functional requirement 5: The robot processes the information on firing conditions.

The robot processes the user-input information for library firing. The firing program of each chamber of furnace is worked out. Each substrate is located to a specified location in the chamber.

Functional requirement 6: The robot transfers libraries to the furnace.

Once the robot gets the message from the printer that libraries are ready, the robot informs the furnace door to open and uses the gripping device to transfer each substrate from the printer platform to the specified location in the furnace.

Functional requirement 7: Firing libraries

After the libraries are transferred to the furnace, the robot instructs the furnace to close door and run firing programs. Once the firing finished, the furnace informs the robot.

Functional requirement 8: Transfer substrates from the furnace to the x-y table

After firing, the robot instructs the furnace door to open and uses gripping device to transfer substrates from the furnace to the x-y table.

Functional requirement 9: Robotic stamping of silver paste to form the top electrode.

Once substrates are placed to the x-y table, the robot paints silver paste on top of each sample by a stamping action. A pool of silver paste is available for the robot probe repeat action: picking up silver paste from the pool and stamping it to the sample.

Functional requirement 10: Transfer of substrates from the x-y table to the furnace

After the libraries are painted by silver paste, the robot transfers them to the furnace.

Functional requirement 11: Second firing.

The robot instructs the furnace door to close and runs a standard firing program to metalise silver paste. Once finished, the furnace informs the robot.

Functional requirement 12: Transfer substrates to the x-y table for measurement.

Once the second firing finished, the robot instructs the furnace door open and uses the gripping device to transfer the substrates from the furnace to the x-y table.

Functional requirement 13: The robot sets up the measurement equipment

The robot sets up the conditions of measurement equipment (e.g., the impedance analysis) based on the user-input information for library screening.

Functional requirement 14: Library screening

The robot synchronises the measurement probe, the x-y table, and measurement equipment so that the properties of each sample in the library are accessed according to the user-specified information on libraries screening. The robot records the measurement data.

Functional requirement 15: Store the measurement data of libraries into the database.

The robot converts the measurement data of libraries into the database structures and stores these into SGI Origin 3200 computer.

Functional requirement 16: The collection of substrates after libraries screening.

The robot picks up the substrates from the x-y table and places onto the stock area.

Functional requirement 17: Data mining and analysis

Data mining and analysis programs are open-end implemented. For example, the experimental data can be compared to the result from either machine learning algorithms such as those provided by artificial neural networks or developing predicate theories. Each application will have its own software engineering process.

Functional requirement 18: System status feedback

During the combinatorial trials, the robot must give system feedback to the user such as "The printer is printing libraries", "The libraries are transferring from the printer to the furnace", etc. If anything goes wrong, error messages should be given.

Functional requirement 19: Report generation

A report of the combinatorial trail should be generated for the user. The report must include the detailed information of libraries, the measurement results and analysis data. The content and format of report might be allowed to be user specified.

Database requirement: A database must be developed and implemented in SGI Origin 3200 computer. The database must record and maintain the details of combinatorial libraries. The database must be expandable and can be integrated with other applications such as data-mining and analysis programs. A distributed database is required as the system will be internet-linked.

User interface requirement: The interfaces between users and robot should be windows-based. The information of library construction, firing, screening and analysis must be categories and standardised so that user can select these from the menu.

Safety requirements: during the robot transfer of substrates inside the robot gantry, the robot must not crash with any equipment such as the printer and the furnace. The furnace door can only be opened when chambers' temperature is below 50°C in case heat from the furnace damages equipment or users. A password protection must be implemented so that the system is only available for authorised users.

3.9.3 System design

Equipment making up the system has been described in section 2.2. These items of equipment are sourced from different manufacturers each having a stand-alone system. Thus the first task is making each part function. The second job is integrating all parts to work as a system. The functioning of each part (i.e., the printer, the furnace, the robot and the impedance analysis) has been described in

the previous section. The connection among these separate items of equipment relies on a local area network (Queen Mary, university network) as described in Figure 3.23. The benefits of this design are that the system can share the university network resource and save connection costs but still keep as a private network.

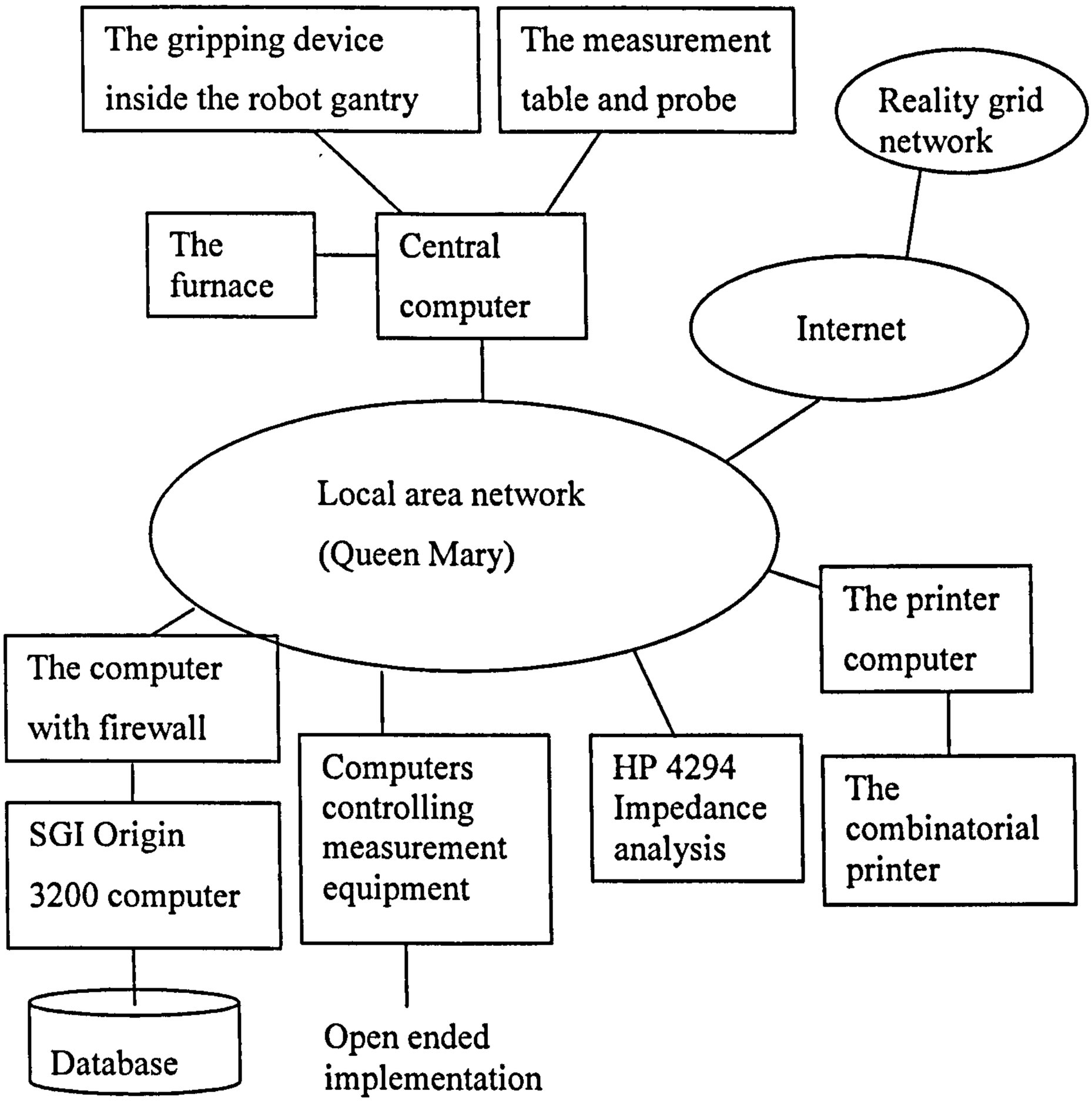

Figure 3.23 The combinatorial robot system lying on a local area network

The robot computer is used as the central control computer. The control programs are implemented using Visual basic 6.0 and integrated with the codes provided by Labman Automation Limited. The control program directly controls the operations of the measurement table, the measurement probe, the furnace and the gripping device inside the robot gantry. This is important because these

operations are real-time and can't rely on the network communication which takes time and is relatively unstable. The control program has four other functions: (1) Providing an interface between users and the system; (2) Converting user-input information into operations of combinatorial trial. (3) Communication with the printer, the measurement equipment (e.g. impedance analysis) and the SGI computer. (4) Communication outside the system (e.g. Internet).

A library containing various standard procedures of the printer is developed using AxSys^{TM} software. The printer programs are built from these procedures. A specification for the printer procedures should be developed but this is not addressed in this research. An application program is implemented in the printer computer using Visual basic 6.0. The program has three functions: (1) Communication with the central computer via implemented TCP connection; (2) Communication with the printer via Active X control to AxSys^{TM} software; (3) Development of the printer program from the library-development-plan that was passed from the central computer.

HP 4294 impedance analysis has LAN (Local area network) port and can be assign an IP address. The central computer controls the operation of HP4294 impedance analysis using GPIB command via LAN.

Entity relationship (ER)[144,145] model is a common tool used in relational database design. Figure 3.24 gives the ER schema diagram for the system database. Oracle is a popular commercial relational database management system (RDMS)[145,146]. The database is implemented using Oracle running on a SGI Origin 3200 computer equipped with 1 Gbyte of memory. A personal computer is acting as a bridge between the LAN and SGI. The computer is installed with a firewall that acts against any unauthorised access of the SGI.

Entity: an object with a conceptual existence (e.g. a company, a job).

Attributes: Each entity has attributes- the particular properties describe it.

Key attributes: an attribute can unique identify the entity.

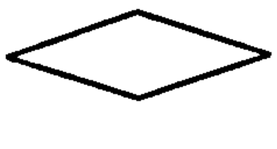

Relationship between entities

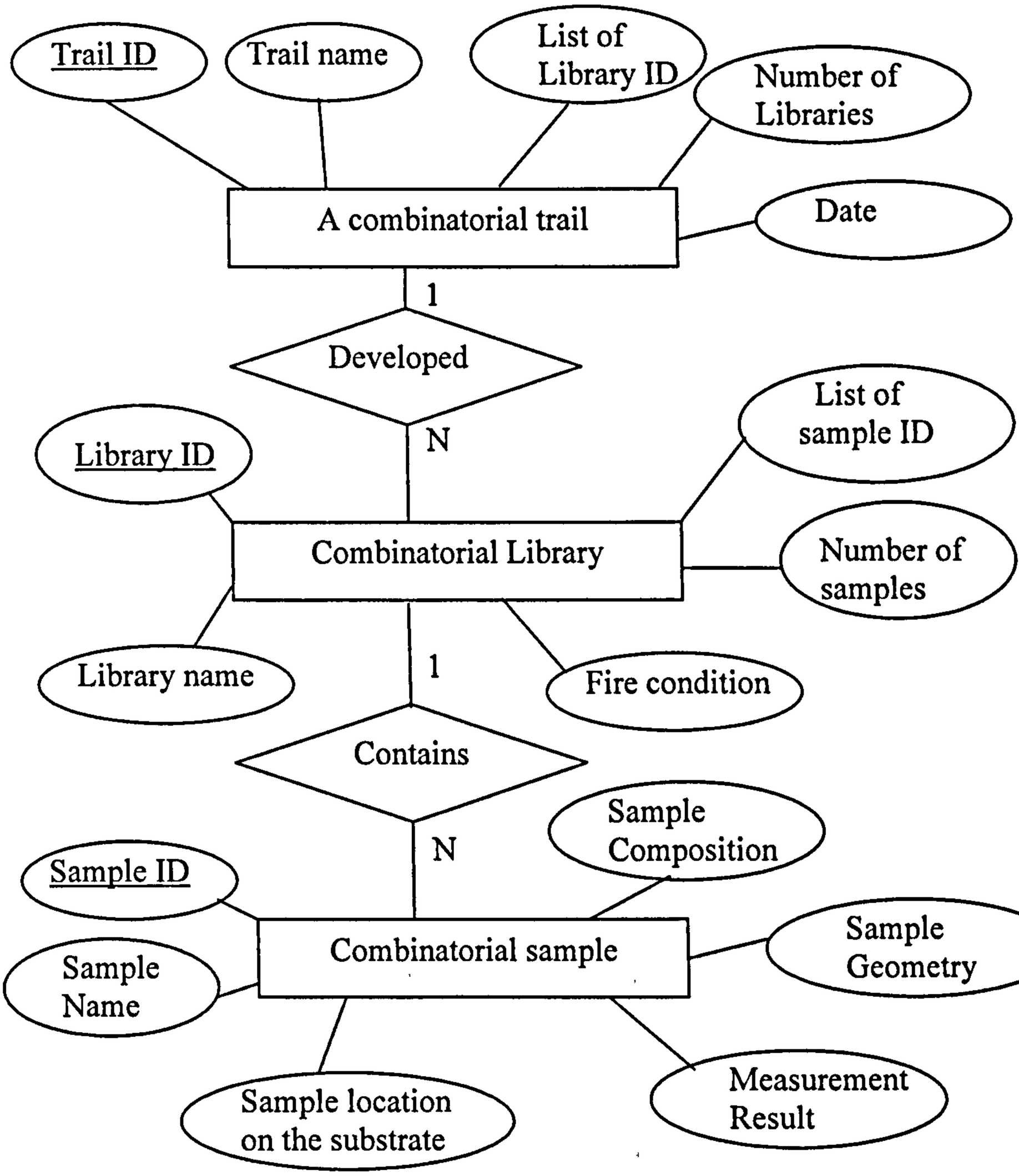

Figure 3.24 The ER schema diagram for the database of combinatorial robot system

3.9.4 System implementation

The requirement specification was not fully implemented due to limited time. In this section, the system implementation is described in two parts. First the users-interfaces of the system are described. Second the system functions are documented.

Figure 3.25-3.27 gives the user interfaces of the system. The basic process of running the system: The user selects a list of robot operations that implements a combinatorial trial via a user-interface (Figure 3.25). The list of operations is recorded by the system and appears in the main user-interface (Figure 3.26). While these operations are proceeding, the status of the running system are also displayed and keep updating. The measurement data from the HP4294 impedance analysis is given in another user-interface (Figure 3.27).

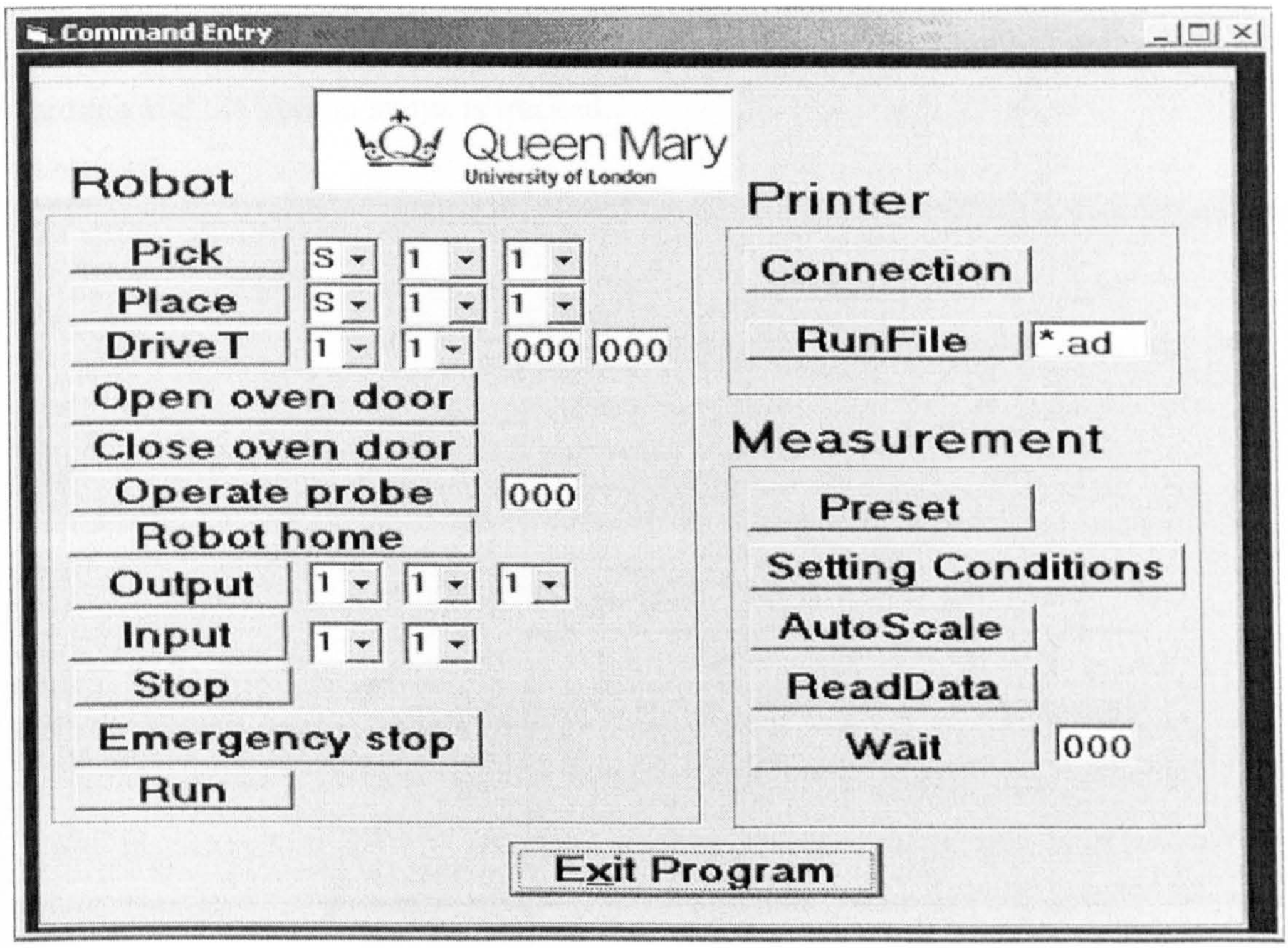

Figure 3.25 The user-interface where the user creates a list of robot operations that implement a combinatorial trial.

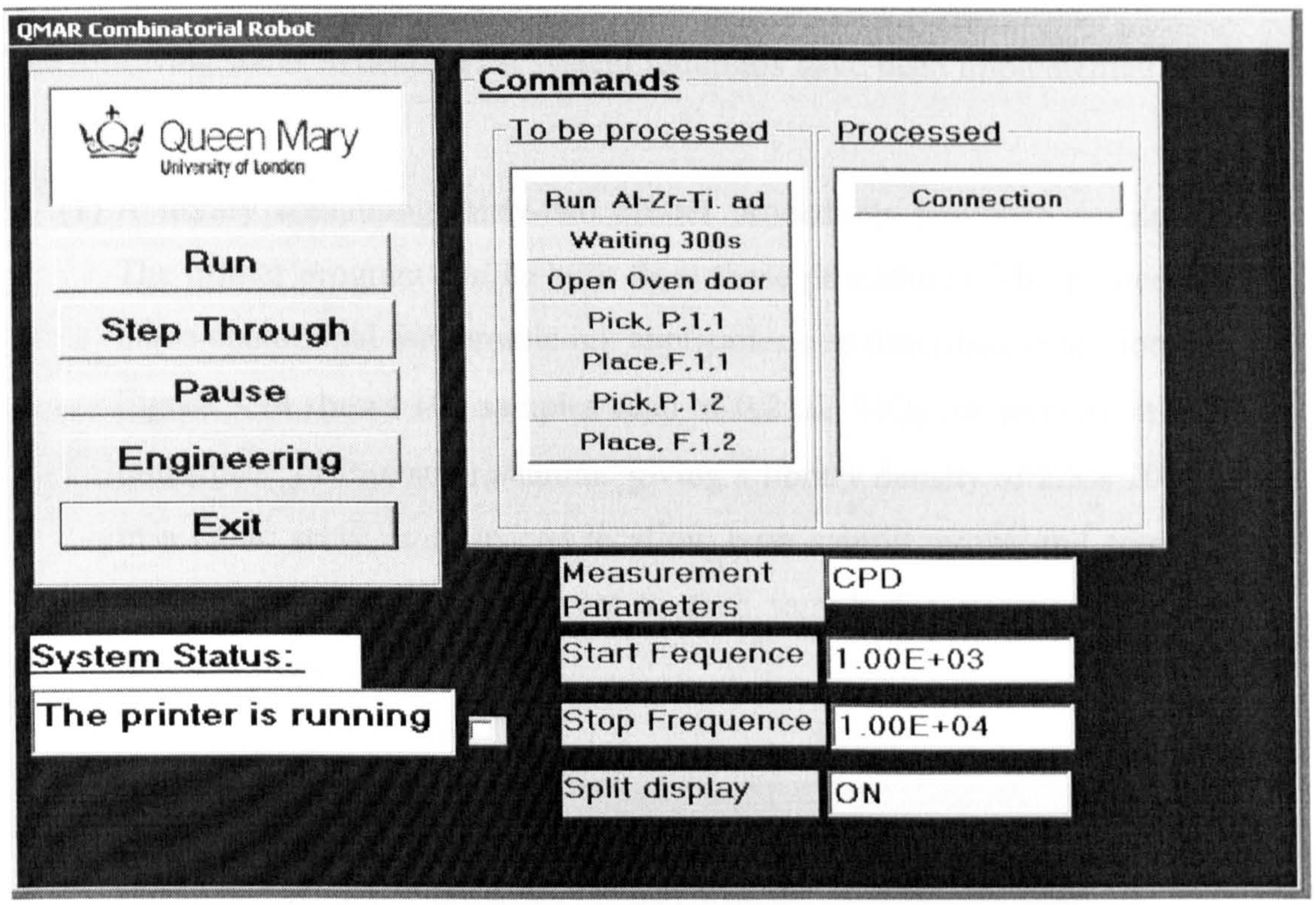

Figure 3.26 The main user-interface where a list of robot operations is going through and the system status is tracked.

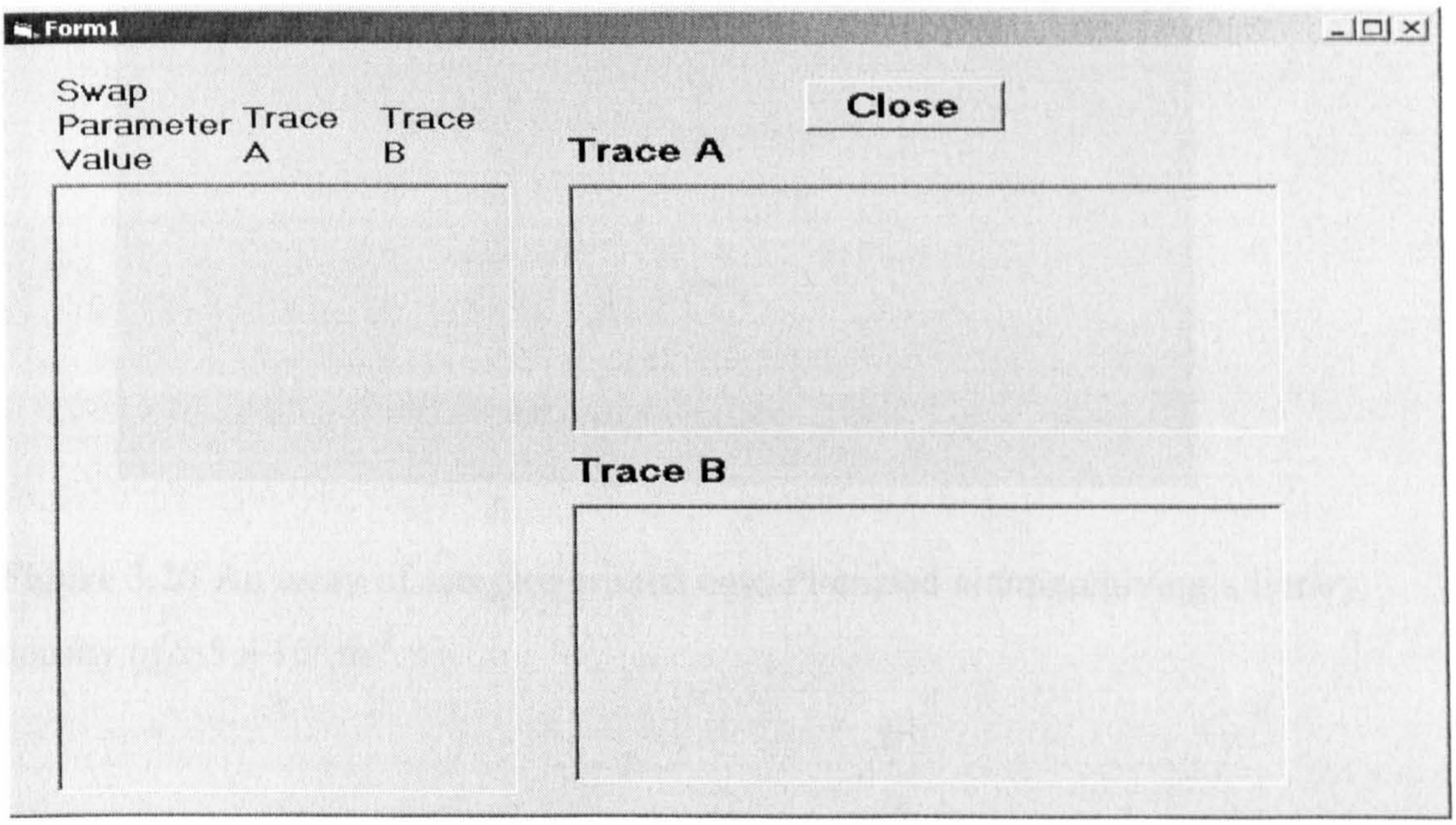

Figure 3.27 The user-interface which displays the measurement results from the HP4294 impedance analysis.

The following states in detail what system functions have been implemented.

(1) A library containing thirty-two printer procedures has been developed. The printer program can be built from these procedures. The printer was made operational for ceramic ink applications as described in section 2.5. Figure 3.28 shows 100 samples each of 0.2 μL TiO_2 ink printed on a 20 mm square of Pt-coated alumina, giving a library density of 2.5×10^5 m^{-2} in a cubic array. It is spaced to allow both sample probe and common electrode probe contact adjacent to each sample for electrical property measurement.

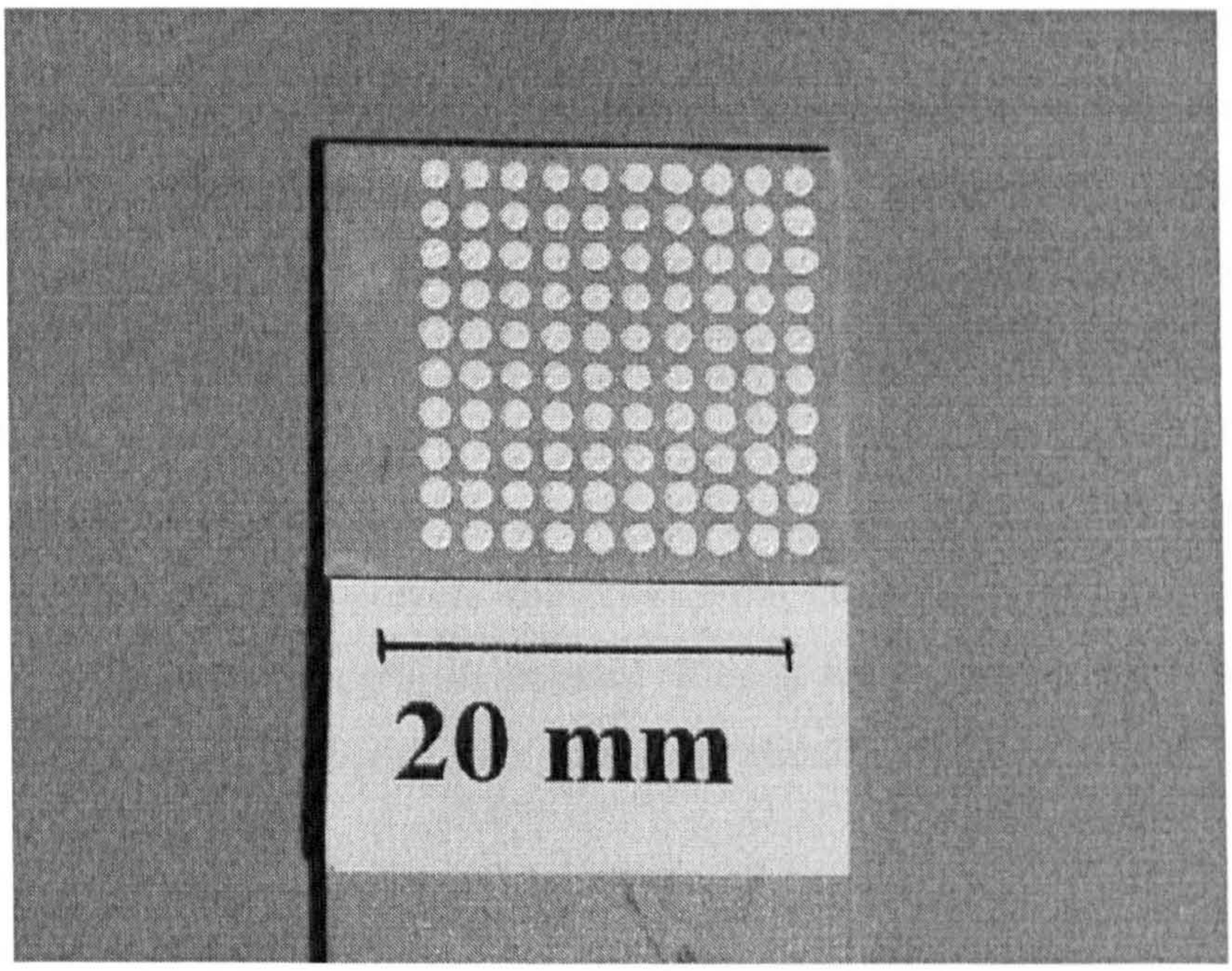

Figure 3.28 An array of samples printed onto Pt-coated alumina giving a library density of 2.5×10^5 m^{-2}.

(2) The printer was integrated with the robot so that the robot can open a specified printer program, run, stop, and know execution status.

(3) The robot can instruct the furnace door to open, close and run a firing program and know the status of the furnace door (i.e., open or closed). The physical integration of the furnace and robot was done by Labman Automation Limited. The software implementation was done in this research.

(4) The robotic probe was developed and integrated with the impedance analyser and proved to function as described in section 3.6.

(5) The impedance analyser and the robotic probe were integrated with the robot. Thus the robot can synchronise the probe contact with the sample, setting a specified measurement condition of the impedance analyser and reading data from the impedance analyser into the robot computer.

(6) The robot gripper can pick up and place substrates on any top-cleared position inside the robot gantry. Various security procedures have been implemented to prevent the robot from crashing with other equipment. For example, unless the furnace door is fully opened, the robot gripper can't move. The time lock was used when the furnace door is opening or closing.

Table 3.7 gives the performance of automation process described in the section 2.7.4. The conclusion is: the nucleus part of the combinatorial system has been developed so that the combinatorial library can be printed, fired and screened automatically.

Table 3.17 The automation of the process for calibration of dielectric measurement in the combinatorial method.

Automation Sequence	Time used	Note
Ink jet printing samples	15 minutes	The printer aspirated $BaTiO_3$ ink and printed it on dried platinum ink that was painted on the alumina substrate.
Firing	48 hours	It takes 54 seconds for the robot gripper to transfer one substrate from the printer to the furnace and go back to home position. It takes around 6 hours for the furnace firing samples at 1400 °C for 2 hours. the other time is used to naturally cool down the furnace to 50 °C. Then the operator instructed the robot the furnace can be safely open.
Metalising	24 hours	It takes 41 seconds for the robot to transfer one substrate from the furnace to the hotplate and vice verse. The silver paste was manually painted as one electrode in advance although it is possible to automatically ink the electrode in a pool of silver paste. It takes 2 hours for the furnace program to metalise the sample at 800 °C for 5 minutes. The other time is used to naturally cool down the furnace to 50 °C. Then the furnace can be safely opened.
Screening	5 minutes	It takes 45 seconds for the robot gripper to pick up one substrate from the furnace and place it on the hotplate and position it under the robotic probe. The setting of measurement conditions, measuring capacitance as a function of frequency and reading data from impedance analyser to the computer were all done in real time.

3.9.5 Discussion of the combinatorial robot system

In the above section, the robot system was documented in a software engineering approach[147,148] with necessary simplification to make it widely accessible. Due to limited time, the system is not fully implemented. There is also much room for improvement for the documentation of the system itself. Considering the scope of the system, truly it requires a team rather than single person (i.e., the author) to design and implement this type of system. In fact, the system has been implemented and proved to function. A general formula for the approximate time (in seconds) used in the combinatorial method is:

$$t = [t_P(N,S) + t_F(X \times 54, Y) + t_M(X \times 45 + S \times 20 + 86.4 \times 10^3) + t_S + t_A + 360] \times n \quad (3.16)$$

where, t_P is the time for the printer to reformat the well-plate and print samples on the substrate. This is a function of the number of compositions created N, and the number of printed samples, S, n is the number of cycles. One composition may be printed as several copies to allow firing at different temperatures in order to explore processing as well as compositional parameters or to provide an assessment of error by replication. This base time depends on the number of components in the system and the sequence chosen for mixing and printing. It can be reduced by, for example, printing in flight and the printer has this ability. t_F is a function of the number of printed library substrates, X, and the firing program Y. The robot takes around 54 s to transfer one substrate from the printer to the furnace and return to its home position. The firing program, Y, varies as the experiment requires and provides the greatest time penalty. t_M is the time required for printing metallised electrodes; it takes around 45 s for the robot to replace a substrate from the furnace to the hotplate and vice verse. It takes around 30 s to deposit silver paste on the top of each sample and 86.4 ks for the furnace to fire the metallised samples to 800 °C for 300s and to cool naturally to 50 °C. t_S and t_A are the times spent screening the library and analysing the library, respectively, which are both experiment dependent. During one cycle,

the furnace door closes and opens twice, which costs 360 s. The time required for ink preparation is excluded; it is assumed inks are available from stock. On this basis, the times given are not sensitive to the oxide types.

The whole system can perform unlimited operations with minimum human intervention. The system is a unique instrument and therefore it is desirable to make it available through e-science networks. The evolving paradigm for sharing computational and experimental resources over the Internet is the Grid. RealityGrid is a leading UK e-science project that has as one of its aims the integration of the system into the Grid. Thus alongside molecular modelling and the associated visualisation methods which are presently being grid-enabled, we may begin to envisage combinatorial laboratories in which geographically diffuse operators steer searches on the basis of their own computer-assisted analysis of the emerging data.

Clearly a range of machine learning algorithms such as those provided by artificial neural networks (weak methods) to those capable of specifying the nature of connections (strong methods) are becoming available. Thus when informatics are combined with combinatorial methods, it then becomes necessary to distinguish the terms 'high throughput screening' from 'combinatorial' methods. The former implies a screen or mesh through which unwanted (not optimised) compositions pass to waste while the latter implies that all data are collected, stored and assessed for the creation of wider and more general knowledge. These important issues are discussed in greater depth in current texts[149,150]. A controversy surrounds the application of informatics to scientific discovery; it is claimed by some that hypothesis-free experiments from which 'in silico' or machine learning can generate new theory can never be conducted. One can discern the fallacy of converse accident in this criticism. It is rarely the intention, and may not be a possibility, to conduct hypothesis-free experiments. The choice of starting materials and even the measurement methods are 'theory laden' and the perceived uses of these methods should be seen, and are being used as, a way of speeding up what is often already an empirical approach to

scientific discovery in areas where predictive theory is inadequate, rather than the complete exclusion of human intervention.

Chapter 4 Conclusions and Suggested Future Work

4.1 Conclusions

The conclusions of this research are described following as five parts.

Compositional calibration of the ink-jet printer

1. A procedure for preparing thick film combinatorial ceramic libraries by an aspirating-dispensing ink-jet printer is developed.

2. Three water-based ceramic inks (i.e., Al_2O_3, ZrO_2 and TiO_2 inks) were developed. The sedimentation behaviours of these inks were reported. These results show that these inks were stable at least for 7.2ks after preparation.

3. Loss on ignition experiments confirmed these water-based ceramic inks (i.e., Al_2O_3, ZrO_2 and TiO_2 inks) were homogenous mixtures so it is possible to know the weight of dissolved powder from volume of ink.

4. The evaporative loss of ZrO_2 inks in the covered 96 well plate was reported. To control evaporation of inks, the well plate should be refilled with fresh ink at every 1.8ks during the operation in order to keep the error in weight percentage of ceramic within 1%.

5. The loss on ignition of transferred inks demonstrated that the printer can deliver specified amounts of each powder into the target composite inks with a tolerable error about 1wt%.

6. Inspection of the target well plates after each composite ink was gently aspirated out found no evidence of sediment, confirming the bulk

sedimentation trials and indicating the interaction of ink constituents did not promote flocculation.

7. By changing the amount of dispersant used in the inks or by printing onto a porous substrate, the geometry of residues from dried ceramic ink droplets can be modified to facilitate property measurements and uniform composition, as planned, can be achieved.

8. The printer can assemble ceramic mixtures with compositional accuracy throughout the entire sample as mapped by EDS of 1-3wt%, when precautions are taken to establish stability against sedimentation, evaporation of vehicle, and particle segregation on drying. This is comparable to accuracy of the EDS measurement method itself as applied to unpolished surfaces.

Particle segregation

1. When multi-component ceramic suspensions are deposited in the form of small drops (~ 5μl), particle segregation can occur on drying so that the upper surface of the powder residue does not match that of bulk composition.

2. A micrograph of the cross-section of a residue prepared from ink F (TiO_2-ZrO_2 system) with elemental mapping showed ZrO_2 enrichment over 10-20μm depth. The segregation layer became less thick from the central part to the edge, indeed there is no segregation in the edge region. The figure also confirms the position of the segregation layer on the upper surface.

3. Droplets were placed on porous substrates (i.e., both plaster of pairs and micro-porous cellulose nitrate membranes) which provide rapid separation of powder from its suspending fluid. The EDS results on

droplet residues show that fast drying by liquid capillarity improves compositional homogeneity; segregation is associated with slow drying by evaporation.

4. The segregation cannot be explained by preferential sedimentation unless dispersant addition is restricted.

5. In order to assess the effects of dispersants, inks D and F(described in Table 2.3) were prepared without dispersants, The EDS results on droplet residues from these inks confirm that segregation on the upper surface is associated with the presence of dispersant.

6. The order of mixing components of ceramic inks does not have a definitive effect on the segregation and does not provide a solution to the problem of segregation.

7. By centrifuging a discrete suspension, removing the supernatant and re-dispensing the powder in the same mass of liquid, it is possible to obtain mixtures in which only one type of powder is treated with dispersant. This experimental method was invented in this research and is named "Removing excess dispersant".

8. Removing excess dispersant does not provide a general solution to the segregation problem but it illustrates the sensitivity of segregation to preferential adsorption on specific powders; an effect that can over-ride preferential sedimentation under Stokes' law. The important observation was that the powder to which dispersant was preferentially attached was always richer on the upper surface of dried droplets.

9. Adding a larger amount of dispersant (i.e., 10wt% in the inks) increases viscosity and is likely to impede particle mobility by chain entanglement effects. Sessile drops from these inks dry to leave dome shapes with

uniform planned composition. So, adding a larger amount of dispersant provides a generally sound solution to the segregation problem based on formulation rather than substrate selection.

10. The segregation is attributable to the partitioning of particles between the growing peripheral 'foot' that develops during drying and the diminishing liquid pool which contains vigorous recirculation flows. Better dispersed particles remain in the pool and hence are found in excess on the upper surface of residues. Less well dispersed particles join the 'foot' earlier in the drying process.

Drying behavior of sessile droplets of mixed powder suspensions

1. For droplets of suspension in which there is limited particle mobility either due to excessive loadings of dispersant or because of absence of dispersant, the contact angle and height of droplets consistently reduced until a minimum value was reached. The contact diameter was almost unchanged during drying. Droplet residues retained a dome shape with uniform planned distribution of powder.

2. Droplets of suspension in which particles are mobile, such as those containing around 1wt% dispersant or fine powder that disperses well in water without the addition of dispersant, have three stages of drying and a 'doughnut' shape of residue sometimes with a central hole resulted. Either segregation of powders on the upper surface or preferential sedimentation on the lower surface occurs.

3. The conclusions (i.e., above 1 and 2) are striking by similar to the morphological development of residues from spherical spray dried ceramic agglomerates; droplets from well-dispersed slurries in which particles retain mobility during drying, form irregular shaped

agglomerates with a central hole. Suspensions with a tendency to flocculate, form dense spherical agglomerates.

4. A geometrical fact that illustrates the strong variation in surface area to underlying volume for a hemispherical drop is discovered in this research. This does not address the more complex flow paths that occur during drying but does show that a strong component of flow must occur in the radial direction of the droplet footprint even if drying is uniform over the liquid surface.

Combinatorial dielectric measurement

1. Two approaches, Evaporation of platinum wire and coating with platinum ink, are used to coat platinum on alumina substrates. By using the platinum ink approach, 0.3 ohm per square (i.e., sheet resistance) after 1600°C for 2h was measured. The platinum ink approach was chosen to facilitate combinatorial dielectric measurement.

2. The combinatorial dielectric measurement method was developed. The measurement results for both $BaTiO_3$ ink dried in bulk and ink-jet printed $BaTiO_3$ on the Pt coated substrates measured automatically by the dielectric probe of the combinatorial instrument agree well with both the pressed sample and literature values.

3. The capacitance measurement for dome-shaped $BaTiO_3$ samples on a common ground electrode with an upper metallised electrode was studied. The results show the geometry factor can bring significant error of dielectric constant calculated from the measured capacitance using conventional equation 1.13. As the upper and lower electrode of samples are closer to a parallel configuration, the dielectric constant calculated from the capacitance become more reasonable.

4. A formula for calculation dielectric constant from capacitance measured from a pronounced curvature of the upper electrode was developed, but the current form of the formula failed to account for geometrical effects probably due to the influence of edge effects.

The combinatorial robot system

1. The combinatorial robot system was designed, documented and implemented so that combinatorial libraries can be printed, fired and screened automatically.

2. A library of Al_2O_3-TiO_2-ZrO_2 system was developed using the developed combinatorial method. Dielectric properties of the library were accessed.

4.2 Suggested future work

There are seven suggestions for future work.

1. A new generation of combinatorial ink-jet printers needs to be developed. The relationship between ink properties (e.g., the volume percentage of powder, viscosity) and the aspirating and dispensing ability of printer should be cleared. An ideal printer should be able to aspirate and dispense these inks that have high volume percentage of powder and viscosity.

2. More ceramic inks which have sound properties (i.e., being compatible with the printer and applications) need to be developed.

3. Considering the cost of platinum, using platinum-coated substrates in the combinatorial method is not an economic approach. An alternative way needs to be researched.

4. The mechanism of segregation and its solutions (i.e., using porous substrate or using excess dispersant in the inks) needs to be further studied so that a quantitive explanation can be given.

5. The relationship among the amount of dispersant used in the inks, the geometry of droplet's residue and the powders' characterises needs to be further studied. The aim is to use an optimal amount of dispersant to get the required geometry of droplet' residue with uniform planned composition.

6. More combinatorial measurement such as measuring electric conductivity, mechanical properties and colour measurement of samples can be developed in the light of the developing combinatorial dielectric measurement method. The thinking is increasing the measurement accuracy without losing the advantage of the high thoughput approach.

7. The combinatorial robot system needs to be further developed as discussed in section 3.9.

Appendix 1: Program sequence for formatting well plates with calibration inks.

Start.

Loop 10 times.

{Aspirate X ×1.5 μl ink A from source well plate.

Loop X times

{Dispense 0.1 μl ink A into the target position. }

Clean the nozzle and channel.

Aspirate Y ×1.5 μl ink B from the source well plate.

Loop Y times

{Dispense 0.1 μl ink B into the target position}

Clean the nozzle and channel.}

Aspirate X' × 1.5 μl ink A from source well plate

Loop X' times

{Dispense 0.1 μl ink A into the target position}

Clean the nozzle and channel.

Aspirate Y'× 1.5 μl ink B from the source well plate

Loop Y' times

{Dispense 0.1 μl ink B into the target position }

Clean the nozzle and channel.

Aspirate specified volume of mixed ink from the mix well plate.

Print the composite ink on the target substrates in required pattern.

Clean the nozzle and channel.

Finish.

In the above, (X + X') × 0.1 μl is the required transfer volume of ink A; (Y + Y') × 0.1 μl is the required transfer volume of ink B. The target position can be one of wells of the mixed well plate or crucibles as experiment specified.

References

1. http://groups.iop.org/DG/home/dielectrics.html Copyright: Institute of Physics and IOP Publishing Ltd, 2000 – 2002.
2. D. Guo, Y.L. Wang, J.T. Xia, C. Nan, and L.T. Li: Investigation of $BaTiO_3$ formulation: an artificial neural network (ANN) method. *J. European. Ceram. Soc.* **22**, 1867 (2002).
3. Z.X. Xiong, X.J. Zhou, W.Z. Zen, K.Z. Baba-Kishi, and S.T. Chen: Development of ferroelectric ceramics with high dielectric constant and low dissipation factor for high-voltage capacitors. *J. Electrocream.* **3**, 239 (1999).
4. D.L. Zhang, G.A. Weng, S.P. Gong, and D.X. Zhou: Computer simulation of grain growth of intermediate-and final-stage sintering and Ostwald ripening of $BaTiO_3$-based PTCR ceramics. *Mater. Sci. Eng. B-Solid State Mater. Adv. Technol.* **99**, 428 (2003).
5. J.R.G. Evans, M.J. Edirisinghe, P. Coveney, and J. Eames: Combinatorial Searches of Inorganic Materials using the ink-jet Printer: science, philosophy and technology. *J. European. Ceram. Soc.* **21**, 2291 (2001).
6. J.C. Meredith, A. Karim, and E.J. Amis: Combinatorial Methods for Investigations in Polymer Materials Science. *Mater. Res. Bull.* **27**, 330 (2002).
7. H. Koinuma and I. Takeuchi: Combinatorial solid-state chemistry of inorganic materials. *Nat. Mater.* **3**, 429 (2004).
8. F. Bellamy: High throughput synthesis (combinatorial chemistry) in the pharmaceutical industry, a technique that has reached maturity. *Actual. Chimique.* **9**, 4 (2000).

9. I. Muegge: Selection criteria for drug-like compounds. *Med. Res. Rev.* **23,** 302 (2000).

10. S.Y. Yang and J.R.G. Evans: Device for preparing combinatorial libraries in powder metallurgy. *J. Comb. Chem.* **6,** 549 (2004).

11. M.A.R. Meier, R. Hoogenboom, and U.S. Schubert: Combinatorial methods, automated synthesis and high-throughput screening in polymer research: The evolution continues. *Macromol. Rapid. Commun.* **25,** 21 (2004).

12. S.R Hall and M.R Harrison: The search for new superconductors. *Chem. Brit.* **30,** 739 (1994).

13. T.P. Beales, W.G. Freeman, S.R. Hall, M.R. Harrison, and J.M. Parberry: Synthesis and properties of a series of layered copper oxide superconductors with a (Pb0.5Cd0.5) rock-salt dopant layer. *Physica. C.* **205,** 383 (1993).

14. X.D. Xiang, X.D. Sun, G. Briceno, Y.L. Lou, K.A. Wang, H.Y. Chang, W.G. Wallacefreedman, S.W. Chen, and P.G. Schultz: A combinatorial approach to materials discovery. *Science.* **268,** 1738 (1995).

15. E.J. Amis, X.D. Xiang, and J.C.L. Zhao: Combinatorial materials science: What's new since Edison? *Mater. Res. Bull.* **27,** 295 (2002).

16. Y.K. Yoo and X.D. Xiang: Combinatorial material preparation. *J. Phys. - Condes. Matter.* **14,** R49 (2002).

17. X.D. Xiang: High throughput synthesis and screening for functional materials. *Appl. Surf. Sci.* **223,** 54 (2004).

18. X.D. Xiang: Combinatorial materials synthesis and high-throughput screening: An integrated materials chip approach to mapping phase diagrams and discovery and optimization of functional materials. *Biotechnol. Bioeng.* **61,** 227 (1999).

19. R.B. Van Dover, L.D. Schneemeyer, and R.M. Fleming: Discovery of a useful thin-film dielectric using a composition-spread approach. *Nature.* **392,** 162 (1998).

20. R.B. Van Dover and L.F. Schneemeyer: The codeposited composition spread approach to high-throughput discovery/exploration of inorganic materials. *Macromol. Rapid Commun.* **25,** 150 (2004).

21. I. Takeuchi I., R.B. Van Dover, and H. Koinuma: Combinatorial synthesis and evaluation of functional inorganic materials using thin-film techniques. *MRS. Bull.* **27,** 301 (2002).

22. R.B. Van Dover, L.D. Schneemeyer, R.M. Flaming, and H.A. Huggins: A high-throughput search for electronic materials thin-film dielectrics. *Biotechnol. Bioeng.* **61,** 217 (1999).

23. R. Cremer, K. Reichert, and D. Neuschutz: A composition spread approach to the optimization of (Ti,Al) N hard coatings deposited by DC and bipolar pulsed magnetron sputtering. *Surf. Coat. Technol.* **142,** 642 (2001).

24. T.X. Sun and G.E. Jabbour: Combinatorial screening and optimization of luminescent materials and organic light-emitting devices. *MRS. Bull.* **27,** 309 (2002).

25. T.X. Sun: Combinatorial search for advanced luminescence materials *Biotechnol. Bioeng.* **61,**193 (1999).

26. I. Yanase, T. Ohtaki, and M. Watanabe: Combinatorial study on nano-particle mixture prepared by robot system. *Appl. Surf. Sci.* **189**, 292 (2002).

27. H.M. Reichenbach and P.J. McGinn: Combinatorial solution synthesis and characterization of complex oxide catalyst powders based on the $LaMO_3$ system. *Appl. Catal. A-Gen.* **244**, 101 (2003).

28. H.M. Reichenbach and P.J. McGinn: Combinatorial synthesis of oxide powders. *J. Mater. Res.* **16**, 967 (2001).

29. M.A. Gulgun, M.H. Nguyen, and W.M. Kriven: Polymerized organic-inorganic synthesis of mixed oxides. *J. Am. Ceram. Soc.* **82**, 556 (1999).

30. A.V. Lemmo, D.J Rose, and T.C. Tisone: Inkjet dispensing technology: applications in drug discovery. *Curr. Opin. Biotech.* **9**, 615 (1998).

31. A.V. Lemmo, J.T. Fisher, H.M. Geysen, and D.J. Rose: Characterization of an inkjet chemical microdispenser for combinatorial library synthesis. *Anal. Chem.* **69**, 543 (1997).

32. J.F. Cargill and M. Lebl: New methods in combinatorial chemistry - robotics and parallel synthesis. *Curr. Opin. Chem. Biol.* **1**, 67 (1997).

33. B.J. de Gans and U.S. Schubert: Inkjet printing of polymer micro-arrays and libraries: Instrumentation, requirements, and perspectives. *Macromol. Rapid. Comm.* **24**, 659 (2003).

34. A.R. Bhatti, M. Mott, J.R.G. Evans, and M.J. Edirisinghe: PZT pillars for 1-3 composites prepared by ink-jet printing. *J. Mater. Sci. Lett.* **20**, 1245 (2001).

35. X. Zhao, J.R.G. Evans, M.J. Edirisinghe, and J.H. Song: Ink-jet printing of ceramic pillar arrays. *J. Mater. Sci.* **37,** 1987 (2002)

36. X. Zhao, J.R.G. Evans, M.J. Edirisinghe, and J.H. Song: Direct ink-jet printing of vertical walls. *J. Am. Ceram. Soc.* **85,** 2113 (2002).

37. M. Mott and J.R.G Evans: Zirconia/alumina functionally graded material made by ceramic ink jet printing. *Mat. Sci. Eng. A*-Struct. **271,** 344 (1999).

38. S. Okamura, R. Takeuchi, and T. Shiosaki: Fabrication of ferroelectric Pb(ZrTi)O-3 thin films with various Zr/Ti ratios by ink-jet printing. *Jpn. J. Appl. Phys.* **41,** 6714 (2002).

39. M.M. Mohebi and J.R.G. Evans: A drop-on-demand ink-jet printer for combinatorial libraries and functionally graded ceramics. *J. Comb. Chem.* **4,** 267 (2002).

40. M.M. Mohebi and J.R.G. Evans: Combinatorial ink-jet printer for ceramics: calibration. *J. Am. Ceram. Soc.* **86,** 1654 (2003).

41. V.D. Scott, G. Love, and S.J.B. Reed: *Quantitative Electron-Probe Microanalysis* (Ellis Horwood, London, U.K., 1995), p. 93.

42. A.R. Von Hippel: Dielectric Materials and Applications (Chapman & Hall, London, U.K., 1954), pp. 1-10.

43. D.W. Richerson: Modern Ceramic Engineering, Second edition. (Marcel Dekker, New York, U.S.A., 1992), pp. 251-262.

44. A.J. Moulson and J.M. Herbert: Electroceramics Materials-Properties-Application (Chapman & Hall, London, U.K., 1997), pp.182-241, 265.

45. P.M.B Walker: Dictionary of Science and Technology (Larousse plc, 1995), pp. 255, 272, 812, 828.

46. J.C. Anderson: Dielectrics (Chapman & Hall, London, U.K., 1964), pp. 1-19, 49-55, 121-125.

47. http://energy21.freeservers.com/dielectrics.htm Copyright: G. Egel, Loxton South Australia, Australia.

48. J. Nowotny: Electronic Ceramic Materials (Trans Tech, Switzerland, 1992), pp. 48-61.

49. L. Solymar and D.Walsh: Lectures on the electrical properties of materials. Fifth edition, (Oxford University Press, U.K., 1993), pp. 269-296.

50. Technical Brochure (NOVACP Ltd, Valencia, U.S.A), Section A through O.

51. M.W. Barsoum: Fundamentals of Ceramics (McGraw-Hill, New York, U.S.A., 1997). pp. 513-549.

52. J. Munoz-Saldana, M.J. Hoffmann, and G.A. Schneider: Ferroelectric domains in coarse-grained lead zirconate titanate ceramics characterized by scanning force microscopy. *J. Mater. Res.* **18,** 1777 (2003).

53. W.L. Luan, L. Gao, H. Kawaoka, T. Sekino, and K. Niihara: Fabrication and characteristics of fine-grained $BaTiO_3$ ceramics by spark plasma sintering. *Ceram. Int.* 30, 405 (2004).

54. Agilent Technologies Impedence Measurement handbook, Second edition. (Agilent Technologies Co. Ltd, Tokyo, Japan, 2000) pp. 2-4 to 2-7.

55. H. Edward and I.M. Smith: Hughes electrical technology, Seventh edition. (Addison Wesley Longman, London, U.K., 1995), pp. 266-275.

56. J.M. Durand and P.Y. Guillon: New method for complex permittivity measurement of dielectric materials. *Electron. Lett.* **22**, 63 (1986).

57. http://www.gamry.com/App_Notes/EIS_Primer/EIS_Primer.htm Electrochemical Impedance spectroscopy theory: A Primer. Copyrights: 1997-2005. GAMRY instruments, Warminster, USA.

58. Accessories Selection Guide for impedance measurements (Aglient Technologies Co. Ltd, Tokyo, Japan, 2001), p. 41.

59. ASTM Standard, D150, 1989, Standard Test methods for A-C Loss characteristics and permittivity(Dielectric constant) of solid Electrical insulating materials.

60. Y. Suyama and T. Yamaguchi: Products for advanced ceramics: characterisation and synthesis. in *Fundamentals of ceramic Engineering.* P. Vincenzini, ed.; Elsevier Science Ltd., Essex, U.K., 1991, pp.121-151.

61. J.B. Birks: Modern Dielectric Materials (Heywood, London, U.K., 1960), pp. 164 -196.

62. S. Saito: Advanced Ceramics (Oxford university press, Oxford, U.K., 1998), pp. 184-200.

63. http://www.eia.org Copyright: 2001-2003 Electronic Industries Alliance.

64. Y. Yuan, S.R. Zhang, and W.N. You: Preparation of $BaTiO_3$-based X7R ceramics with high dielectric constant by nanometer oxides doping method. *Mater. Lett.* **58**, 1959 (2004).

65. J.S. Kim, C.I. Cheon, T.R. Park, and H.S. Shim: Dielectric properties and crystal structure of Ba6-3x(Nd, M)(8+2x)Ti18O54 (M = La, Bi, Y) microwave ceramics. *J. Mater. Sci.***35**, 1487 (2000).

66. V.V. Mitic and I. Mitrovic: The influence of Nb_2O_5 on $BaTiO_3$ ceramics dielectric properties. *J. European. Ceram. Soc.* **21**, 2693 (2001).

67. J.Q. Qi, Z.L. Gui, W. Li, Y.L. Wang, Y.J. Wu, and L.T. Li: Temperature stable Ba1-xCdxTiO3 dielectrics. *Mater. Lett.* **56,** 507(2002).

68. J. Bernard, R. William, J.R. Cook, and J. Hans: Piezoelectric Ceramics (Academic Press, London, U.K., 1971), pp. 271-279.

69. J.F. Scott and C.A. Araujo: Ferroelectric Memories. *Science*. **24,** 1400 (1989).

70. X. Kornmann and C. Huber: Microstructure and mechanical properties of PZT fibres. *J. European. Ceram. Soc.* **24,** 1987 (2004).

71. G.H. Haertling: Ferroelectric ceramics: History and technology. *J. Am. Ceram. Soc.* **82,** 797 (1999).

72. R. Jain, V. Gupta, A. Mansingh, and K. Sreenivas: Ferroelectric and piezoelectric properties of non-stoichiometric $Sr_{1-x}Bi_{2+2x/3}Ta_2O_9$ ceramics prepared from sol–gel derived powders. *Mater. Sci. Eng. B-Solid State Mater. Adv. Technol.* **112,** 54 (2004).

73. H.X. Fu and R.E. Cohen: Polarization rotation mechanism for ultrahigh electromechanical response in single-crystal piezoelectrics. *Nature.* **403**, 281 (2000).

74. A.M. George, J. Iniguez, and L. Bellaiche: Anomalous properties in ferroelectrics induced by atomic ordering. *Nature.* **413**, 54 (2001).

75. H.J. Lee, H.M. Park, Y.K. Cho, H. Ryu, J.H. Paik, S. Nahm, and J.D Byun: Dielectric and structural characteristics in barium lanthanum magnesium niobate. *J. Am. Ceram. Soc.* **83**, 937 (2000).

76. Y.S. Cho, S.M. Pilgrim, H. Giesche, and K. Bridger: Dielectric and electromechanical properties of chemically modified PMN-PT-BT ceramics. *J. Am. Ceram. Soc.* **83**, 2473 (2000).

77. X.X. Wang, H.L.W. Chan, and C.L. Choy: (Bi1/2Na1/2)TiO3-Ba(Cu1/2W1/2)O-3 lead-free piezoelectric ceramics. *J. Am. Ceram. Soc.* **86**, 1809 (2003).

78. X.H. Wang, R.Z. Chen, Z.L. Gui, and L.T. Li: The grain size effect on dielectric properties of $BaTiO_3$ based ceramics. *Mater. Sci. Eng. B-Solid State Mater. Adv. Technol.* **99**, 199 (2003).

79. H.R. Xu and L. Gao: Hydrothennal synthesis of high-purity $BaTiO_3$ powders: control of powder phase and size, sintering density, and dielectric properties. *Mater. Lett.* **58**, 1582 (2004).

80. H.S. Potdar, S.B. Deshpande, and S.K. Date: Chemical coprecipitation of mixed (Ba+Ti) oxalates precursor leading to $BaTiO_3$ powders. *Mater. Chem. Phys.* **58**, 121 (1999).

81. O. Harizanov, A. Harizanova, and T. Ivanova: Formation and characterization of sol–gel barium titanate. *Mater. Sci. Eng. B-Solid State Mater. Adv. Technol.* **106**, (191) 2004.

82. K.M. Hung, W.D. Yang, and C.C. Huang: Preparation of nanometer-sized barium titanate powders by a sol-precipitation process with surfactants. *J. European. Ceram. Soc.* **23**, 1901 (2003).

83. X. Kornmann and C. Huber: Microstructure and mechanical properties of PZT fibres. *J. European. Ceram. Soc.* **24**, 1987 (2004).

84. S.M. Olhero and J.M.F. Ferreira: Particle segregation phenomena occurring during the slip casting process. *Ceram. Int.* **28**, 377 (2002)

85. J.G. Yeo, Y.G. Jung, and S.C. Choi: Design and microstructure of ZrO_2/SUS316 functionally graded materials by tape casting. *Mater. Lett.* 37, 304 (1998).

86. A.V. Zinchuk, M.P. Mullarney, and B.C. Hancock: Simulation of roller compaction using a laboratory scale compaction simulator. *Int. J. Pharm.* **269**, 403 (2004).

87. E.S. Thiele, D. Damjanovic, and N. Setter: Processing and properties of screen-printed lead zirconate titanate piezoelectric thick films on electroded silicon. *J. Am. Ceram. Soc.* **84**, 2863 (2001).

88. N. Frage, L. Levin, and M. P. Dariel: The effect of the sintering atmosphere on the densification of B_4C ceramics. *J. Solid State Chem.* **177**, 410 (2004).

89. M.S. Jogad, M. Goswami, A. Sarkar, T. Mirza, L.A. Udachan, and G.P. Kothiyal: Dielectric measurement on magnesium aluminum silicate glass–ceramics prepared by different routes. *Mater. Lett.* **57**, 619 (2002).

90. S. Kirihara, Y. Miyamoto, K. Takenaga, and M.W. Takeda: Fabrication of electromagnetic crystals with a complete diamond structure by stereolithography. *Solid State Commun.* **121**, 435 (2002).

91. http://home.att.net/~castleisland/rp_int.htm Copyright: Castle Island Co.

92. http://cybercut.berkeley.edu/mas2/html/processes/stereolith/more.html Berkeley Manufacturing Institute.

93. http://www.azom.com/details.asp?ArticleID=1649 CERAM Research Ltd.

94. I. Grida and J.R.G. Evans: Extrusion freeforming of ceramics through fine nozzles. *J. European. Ceram. Soc.* **23**, 629 (2003).

95. R.C. Pennington, N.L. Hoekstra, and J.L. Newcomer: Significant factors in the dimensional accuracy of fused deposition modelling. *Proc. Inst. Mech. Eng. Part E-J. Process Mech. Eng.* **219**, 89 (2005).

96. J.C. Lorrison, K.W. Dalgarno, and D.J. Wood: Processing of an apatite-mullite glass-ceramic and an hydroxyapatite/phosphate glass composite by selective laser sintering. *J. Mater. Sci.-Mater. Med.* **16**, 775 (2005)

97. P.K. Bai, J. Cheng, and B. Liu: Selective laser sintering of polymer-coated Al_2O_3/ZrO_2/TiC ceramic powder. *Trans. Nonferrous Met. Soc. China* **15.** 261 (2005).

98. S. Yang and J.R.G. Evans: Acoustic initiation of powder flow in capillaries. *Chem. Eng. Sci.* **60,** 413(2005).

99. A. Das, G. Madras, N. Dasgupta, and A.M. Umarji: Binder removal studies in ceramic thick shapes made by laminated object manufacturing. *J. European. Ceram. Soc.* **23**, 1013 (2003).

100. X.M. Cui, S. Ouyang, Z.Y. Yu, and C.G. Wang, and Y.A. Huang: A study on green tapes for LOM with water-based tape casting processing. *Mater. Lett.* **57,** 1300 (2003).

101. L.Weisensel, N. Travitzky, H. Sieber, and P. Greil: Laminated object manufacturing (LOM) of SiSiC composites. *Adv. Eng. Mater.* **6**, 899 (2004).

102. M. Lee, J.C.Y. Dunn, and B.M. Wu: Scaffold fabrication by indirect three-dimensional printing. *Biomaterials*. **26**, 4281 (2005).

103. B.J. de Gans, P.C. Duineveld, and U.S. Schubert: Inkjet printing of polymers: State of the art and future developments. *Adv. Mater.* **16**, 203 (2004).

104. S. Upcraft and R. Fletcher: The rapid prototyping technologies. *Assem. Autom.* **23**, 318 (2003).

105. J. Moon, A.C. Caballero, L. Hozer, Y.M. Chiang, and M.J. Cima: Fabrication of functionally graded reaction infiltrated SiC-Si composite by three-dimensional printing (3DP (TM)) process. *Mat. Sci. Eng. A*-Struct. **298**, 110 (2001).

106. H.P Le: Progress and trends in ink-jet printing technology. *J. Imaging Sci. Technol.* **42**, 49 (1998).

107. B.Y. Tay: Continuous direct ink-jet printing, PhD thesis, 2001, Queen Mary, University of London.

108. M. M. Mohebi: An ink-jet printer for ceramic combinatorial libraries and functional gradients, PhD thesis, 2004, Queen Mary, University of London.

109. Cartesian technologies, Prosys^{TM} GANTRY SYSTEM, System operating manual version 1.0, June 2000, Huntingdon, U.K.

110. D.J. Shaw: Introduction to colloid and surface chemistry, fourth edition. (Butterworth-Heinemann, Oxford, U.K., 1996), pp. 1-20, 169-173, 244-26.

111. J.A. Lewis: Colloidal processing of ceramics. *J. Am. Ceram. Soc.* **83**, 2341 (2000).

112. S.H. Bell and V.T. Crowl: Assessment of the state of dispersion. In *Dispersion of powders in liquids.* G.D. Parfitt, ed., Applied Science Publishers., London, 1973, pp.267-307.

113. W.D. Teng and M.J. Edirisinghe: Development of ceramic inks for direct continuous jet printing. *J. Am. Ceram. Soc.* **81,** 1033 (1998).

114. B. Jirgensons and M. E. Straumanis: A Short Textbook of Colloid Chemistry. (Pergamon Press Limited, London, U.K., 1954), pp. 121-125.

115. D.H. Napper: Polymeric Stabilisation of Colloidal Dispersions (Academic press, London, U.K., 1983), pp.4-13.

116. J. Ma, R. Zhang, C.H. Liang, and L. Weng: Colloidal characterization and electrophoretic deposition of PZT. *Mater. Lett.* **57,** 4648 (2003).

117. J. Widegren and L. Bergstrom: The effect of acids and bases on the dispersion and stabilization of ceramic particles in ethanol. *J. European. Ceram. Soc.* **20,** 659 (2000).

118. V.M.B. Moloney, D. Parris, and M.J. Edirisinghe: Rheology of zirconia suspensions in a nonpolar organic medium. *J. Am. Ceram. Soc.* 78, 3225 (1995).

119. British Standard 188:1977, Methods for determination of the viscosity of liquids.

120. B. Jirgensons and M.E. Straumanis: A short textbook of colloid chemistry(Pergamon Press Ltd, London, U.K., 1954), pp. 56-63.

121. P.C. Hiemenz: Principles of colloid and surface chemistry, Second edition. (Marcel Dekker, New York, 1986), pp. 287-315.

122. J. Wang and J. R. G. Evans: Segregation in multicomponent ceramic colloids during drying of droplets. *Phys. Rev. E.* **73,** 021501 (2006).

123. H.W. Cheong, G.V. Jeffreys, and C.J. Mumford: A receding interface model for the drying of slurry droplets. *AICHE. J.*, **32,** 1334(1986).

124. G.E. Fair and F.F. Lange: Effect of interparticle potential on forming solid, spherical agglomerates during drying. *J. Am. Ceram. Soc.* **87,** 4(2004).

125. T. Elperin and B. Krasovitov: Evaporation of liquid droplets containing small solid particles. *Int. J. Heat Mass Transf.* **38,** 2259 (1995).

126. T.O.K. Audu and G.V. Jeffreys: The drying of drops of particulate slurries. *Trans. Instn. Chem. Engrs.*, **53,** 165 (1975).

127. W.W.Y. Lau and C.M. Burns: Kinetics of spreading - Polystyrene melts on plane glass surfaces. *J. Colloid Interface Sci.* **45,** 295(1973).

128. M.E.R. Shanahan and C. Bourges: Effects of evaporation on contact angles on polymer surfaces. *Int. J. Adhes. Adhes.* **14,** 201 (1994).

129. R.D. Deegan, O. Bakajin, T.F. Dupont, G. Huber, S.R. Nagel, and T.A. Witten: Contact line deposits in an evaporating drop. *Phys. Rev. E.* **62,** 756 (2000).

130. E. Adachi, A.S. Dimitrov, and K. Nagayama: Stripe patterns formed on a glass surface during droplet evaporation. *Langmuir.* **11,** 1057(1995).

131. J.J. Guo and J.A. Lewis: Aggregation effects on the compressive flow properties and drying behavior of colloidal silica suspensions. *J. Am. Ceram. Soc.* **82,** 2345 (1999).

132. F. Parisse and C. Allain: Drying of colloidal suspension droplets: Experimental study and profile renormalization. *Langmuir.* **13,** 3598 (1997).

133. S. Maenosono, C.D. Dushkin, S. Saita, and Y. Yamaguchi: Growth of a semiconductor nanoparticle ring during the drying of a suspension droplet. *Langmuir.* **15,** 957 (1999).

134. E. Ciampi, U. Goerke, J.L. Keddie, and P.J. McDonald: Lateral transport of water during drying of alkyd emulsions. *Langmuir.* **16,** 1057 (2000).

135. A.F. Routh and W.B. Russel: Horizontal drying fronts during solvent evaporation from latex films. *AICHE. J.* **44,** 2088 (1998).

136. M.D. Haw, M. Gillie, and W.C.K. Poon: Effects of phase behaviour on the drying of colloidal suspensions. *Langmuir.* **18,** 1626 (2002).

137. H. Hu and R.G. Larson: Analysis of the effects of Marangoni stresses on the microflow in an evaporating sessile droplet. *Langmuir.* **21,** 3972 (2005).

138. P. C. Hidber, T. J. Graule, and L. J. Gaukler: Citric acid- a dispersant for aqueous alumina suspensions. *J. Am. Ceram. Soc.* **79,** 1857 (1996).

139. R.D. Deegan, O. Bakajin, T.F. Dupont, G. Huber, S.R. Nagel, and T.A. Witten: Capillary flow as the cause of ring stains from dried liquid drops. *Nature.* **389,** 827 (1997).

140. Z. Zhao, V. Buscaglia, M, Viviani, M.T. Buscaglia, L. Mitoseriu, A. Testino, M. Nygren, M. Johnsson, and P. Nanni: Grain-size effects on the ferroelectric behavior of dense nanocrystalline $BaTiO_3$ ceramics. *Phys. Rev. B.* **70.** 024107 (2004).

141. T. Mitsui, R. Abe, Y. Furuhata, K. Gesi, T. Ikeda, K. Kawabe, Y. Makita, M. Marutake, E. Nakamura, S. Nomura, E. Sawaguchi, Y. Shiozaki, I. Tatsuzaki, K. Toyoda, Numerical data and functional relationships in science and technology, Group III, Volume 3: Ferro- and Antiferroelectric substances; Alle.Zeit.Wach Press: Springer-Verlag, Berlin-Heidelberg, New York, 1969, pp 51, 247.

142. P.V. Coveney: Scientific grid computing. *Proc. R. Soc. A-Math. Phys. Eng. Sci.* **363,** 1707 (2005).

143. B.M. Boghosian and P.V Coveney: Scientific applications of grid computing. *Comput. Sci. Eng.* **7,** 10(2005).

144. R. Elmasri and S.B. Navathe: Fundamentals of database systems, third edition. (Addison-Wesley, Essex. England, 2000), pp. 41-72.

145. J.L. Johnson: Database Models, Languages, Design (Oxford university Press, New York, 1997), pp. 21-69.

146. M. Abbey and M. J. Corey: Oracle: A beginner's guide (McGraw-Hill, California, U.S.A., 1995), pp. 3-28.

147. H.V. Vliet: Software Engineering, Principles and Practice (John Wiley & Sons, Chichester, U.K, 1993), pp.1-19, 121-230.

148. I. Sommerville: Software Engineering, fifth edition (Addison-Wesley, Essex, England, 1996), pp. 63-312.

149. D. Farrusseng, C. Mirodatos, Combinatorial Strategies for Speeding up Discovery and Optimization of Heterogeneous Catalysts on the Academic Laboratory Scale: A Case Study of Hydrogeneous Purification for Feeding PEM Fuel Cells. In *High-Throughput Screening in Chemical Catalysis: Technologies, Strategies and Applications;* A. Hagemeyer, P. Strasser, and A.F. Volpe Jr, Wiley-VCH, New York, 2004; pp 239-270.

150. M. Holena, M. Baerns, Artificial Neural Networks in Catalyst Development. In *Experimental Design for Combinatorial and High Throughput Materials Development*; J.N. Cawse, Eds.; John Wiley & Sons Inc.: New York, 2003; pp 163-202.

Publications

1. J. Wang and J. R. G. Evans: London University Search Instrument: A combinatorial robot for high-throughput methods in ceramic science. *J. Comb. Chem.* **7**, 665 (2005).
2. J. Wang and J. R. G. Evans: Library preparation using an aspirating-dispensing ink-jet printer for combinatorial studies in ceramics. *J. Mater. Res.* **20**, 2733 (2005).
3. J. Wang, M. M. Mohebi and J. R. G. Evans: Two methods to generate multiple compositions in combinatorial ink-jet printing of ceramics. *Macromol. Rapid Commun.* **26**, 304 (2005).
4. J. Wang and J. R. G. Evans: Drying behaviour of droplets of mixed powder suspensions. *J. European. Ceram. Soc.* In press.
5. J. Wang and J. R. G. Evans: Segregation in multicomponent ceramic colloids during drying of droplets. *Phys. Rev. E.* **73**, 021501 (2006).

Acknowledgement

The author is grate for EPSRC and Queen Mary, University of London funding this PhD studentship. Thanks Professor Julian R.G. Evans for supervising this work. Thanks Professor Mohan Edirisinghe for various helps and advices.